Application of anti-amyloid beta immunization using encapsulated cell technology in mouse models of Alzheimer's disease

Thèse N° 9751

Présentée le 4 octobre 2019

à la Faculté des sciences de la vie
Laboratoire d'étude sur la neurodégénérescence
Programme doctoral en biotechnologie et génie biologique

pour l'obtention du grade de Docteur ès Sciences

par

Vanessa LAVERSENNE

Acceptée sur proposition du jury

Prof. H. Lashuel, président du jury
Dr. B. Schneider, Prof. P. Aebischer, directeurs de thèse
Prof. L. Buée, rapporteur
Prof. P. Paganetti, rapporteur
Prof. B. McCabe, rapporteur

2019

ÉCOLE POLYTECHNIQUE
FÉDÉRALE DE LAUSANNE

“All models are wrong, but some are useful.”

George Box, statistician

“I hate Mondays”

Garfield, cat

Acknowledgements

For the opportunity and the existence of such a great laboratory with great science, I will start by thanking **Prof. Patrick Aebischer**. The LEN is his achievement and I am glad I had the chance to be part of his team.

Then the person that helped me the most in the realization of this scientific work is **Dr. Bernard Schneider**, my thesis director. He accompanied me during every single steps of my scientific adventure from my master's thesis to my Ph.D. graduation day. He allowed me to become the scientist I am today, and for that I am forever in his debt.

To build up my scientific skills before this Ph.D. thesis, many thanks to **Dr. Justin Boyd** and the **Bertarelli fellowship team**, in particular **Dr. Dietrich Reinhard** at EPFL and **Prof. John Assad** and **Prof. David Corey** at Harvard. They believed in me and allowed me to do my master thesis in Harvard, where I first accounted academic science and decided I wanted to be part of it.

For their involvement and work in the evaluation of my thesis, I already wanted to thank my thesis committee, **Prof. Luc Buée**, **Dr. Paolo Paganetti**, **Prof. Brian McCabe** and **Prof. Hilal Lashuel.**

For scientific advices, many thanks to **Dr. Pamela Valdes** and **Dr. Nathalie Bernard-Marissal**. They helped me grow in the laboratory and developed my scientific mind.

I owe to thank all the technicians of the lab, especially **Philippe Colin**, **Christel Voize** and **Aline Aebi** for the technical support and all the knowledge they provided during these 5 long years. They are the memory of the laboratory for all scientific methods and I would never have learned so much and so fast without them.

Thanks to the **BIOP team** that helped me with the image processing, huge part of my work, especially **Olivier Burri**.

In term of social support and more relaxing time in the laboratory, I thank the entire laboratory for the nice atmosphere. In particular, I want to thank **Dr. Cylia Rochat** for her friendship and support.

Outside the laboratory, I am thanking **my family** of course, even though I am a bit the weird sheep in the flock, spending all my twenties as a student not knowing the real world. **My parents** encouraged me to be and do what I wanted and accept me as I am, and I am very grateful for it.

I thank a thousand times my fellow Ph.D. friends that encouraged me, guided me, listened to me and suffered with me all these years. They almost all became doctors before me and I learnt a lot from their experience, especially **Dr. Cyril Piemontesi**, **Dr. Raphaël Sommer**, **Dr. Jérome Gandar**, **Dr. Julie Scotton**. **Olivier Dubey**, you are the next one! Cyril thanks again, you deserve it twice as I regain faith in my science, thanks to you.

Thank to the others scientists in my life, among them **Dr. Greg Mann** and **Dr. Ed Moraud,** both suggested me they could revise this thesis, which is a great token of friendship.

At last, many thanks to all my non-scientific friends, especially **Elise Périat**, and my **brother** and my **sister** for being outside the EPFL world and keeping me in touch with (almost) normal people. **Ludovica Visciola**, same, even if you are a scientist, you are now far enough from EPFL: your apartment in Zurich has become my safe place!

I have been incredibly well surrounded during my Ph.D. life and I am grateful for it.

Summary

Alzheimer's disease (AD) is the most common form of dementia in the elderly. Unfortunately, there is no cure to stop or slow down the disease. AD is characterized by the deposition of two aggregated proteins: Amyloid beta (Aβ) and hyperphosphorylated tau. In the brain parenchyma, Aβ is present both inside neurons and in the extracellular space, where it accumulates and forms neuritic plaques. Intracellular phosphorylated tau assembles into paired helical filaments, which accumulate and form neurofibrillary tangles. Accumulations of these proteins are thought to be the signature of a pathogenic process causing the loss of neurons and synaptic connections associated with severe cognitive impairments in AD patients. Other important factors are involved in the neurodegeneration occurring in AD, such as neuroinflammation mainly characterized by microglia activation.

In the present thesis work, we are investigating the effects of passive anti-Aβ immunization, a strategy that has recently been tested in clinical trials in order to decrease Aβ burden in AD patients. Passive anti-Aβ immunization consists in the delivery of antibodies targeting Aβ, with the aim to prevent its accumulation and promote the removal of pathological amyloid species. Although the treatment has been shown to clear amyloid pathology in the brain of AD patients, it has so far failed to prevent or slow down cognitive decline. Hence, it is important to determine the effects of anti-Aβ immunization when administered either before or during Aβ deposition, and explore how the treatment affects the Alzheimer's manifestations in mouse models combining Aβ and tau pathologies.

In order to continuously deliver antibodies in AD mouse models, we used encapsulated cell technology (ECT) to implant myoblasts genetically engineered and secrete the recombinant mAb11 mouse IgG2a antibody directed against aggregated forms of Aβ. Using this approach, we investigated the following three topics of research:

1) We examined the effect of *a preventive administration of anti-Aβ antibodies* in a slowly progressing mouse model with both Aβ and tau (P301L)

pathologies. We demonstrated that delivery of anti-Aβ antibodies before the onset of the disease dramatically reduces Aβ pathology. We also found that the treatment decreases hyperphosphorylated tau accumulation and recruits microglial around Aβ plaques.

2) We next assessed the effects of passive anti-Aβ immunization in another AD mouse model overexpressing both Aβ and wild-type (WT) tau. In this second study, *we administered the anti-Aβ antibodies when both Aβ and tau pathologies were already established*. In the hippocampal formation, we showed that WT tau overexpression might affect the microglial response to ongoing pathology by reducing the tight interaction of these cells with the amyloid plaques. This effect, however, is counteracted by passive anti-Aβ immunization, which was found to redirect microglia towards Aβ deposits. In addition, passive anti-Aβ immunization decreases tau spreading throughout the hippocampus, but fails to prevent neither tau phosphorylation, nor the hippocampal degeneration induced by local tau overexpression.
3) In parallel, we developed a human myoblast cell line secreting anti-Aβ antibodies for translation of our ECT towards human application. Using C2C12 mouse myoblasts, our flat-sheet device allowed for long-term continuous antibody delivery in the plasma of subcutaneously implanted mice. We were able to generate antibody-secreting *human cells* using the immortalized C25 cell line. It was possible to differentiate these cells into myotubes and adapt them to long-term survival inside the capsules maintained *in vitro*. However, when implanted in the subcutaneous tissue of immunocompromised mice, myoblasts survived in the ECT device as a thin layer of cells and were not able to secrete recombinant antibodies in sufficient amounts to be considered for therapeutic purposes.

Keywords

Alzheimer's disease, tau, amyloid beta, microglia, passive immunization, encapsulated cell technology.

Résumé

La maladie d'Alzheimer est la forme de démence la plus commune chez les personnes âgées. Malheureusement, aucun remède n'existe pour arrêter ou ralentir la maladie. Alzheimer est caractérisée par l'accumulation de deux protéines sous forme agrégées : Amyloïde beta (Aβ) et tau hyperphosphorylé. Dans le parenchyme du cerveau, Aβ est présent à l'intérieur et à l'extérieur de l'espace cellulaire où il s'accumule et forme de plaques neuritiques. Tau phosphorylé, quant à lui, forme des filaments hélicaux qui s'assemblent en inclusions intracellulaires appelées enchevêtrements neurofibrillaires. L'accumulation de ces protéines semble être à l'origine des mécanismes provoquant la perte de connections synaptiques et de neurones responsable de la perte de cognition observée chez les patients atteints d'Alzheimer. D'autres facteurs sont également impliqués dans la neurodégénérescence responsable de la maladie, notamment la neuroinflammation principalement due à l'activation de microglies.

Dans cette thèse, nous avons étudié l'immunisation passive contre Aβ, une stratégie thérapeutique récemment testée dans plusieurs essais cliniques afin de réduire l'accumulation d'Aβ. Lors de l'immunisation passive contre Aβ, des anticorps sont administrés afin de reduire les dépôts cérébraux d'Aβ. Bien qu'il ait été démontré que l'immunisation passive réduis l'accumulation de plaque Aβ chez les patient, les derniers essais cliniques testant l'efficacité de divers anticorps contre Aβ n'ont pas eu d'effets sur le déclin cognitif associé à Alzheimer. C'est pourquoi il est important de déterminer les effets de l'immunisation passive contre Aβ, administrée avant et pendant accumulation d'Aβ, et d'explorer les effets du traitement sur les modèles animaux de la maladie d'Alzheimer exprimant Aβ et tau

Afin de pouvoir distribuer l'anticorps de manière continue lors de nos expériences, nous avons utilisé la technologie d'encapsulation cellulaire (ECT). Il s'agit d'un implant contenant des myoblastes modifiés génétiquement pour sécréter l'anticorps de souris recombinant mAb11 IgG2a qui cible les formes

agrégées de Aβ. En utilisant cette approche, nous avons étudié trois axes de recherche en lien avec l'immunisation passive contre Aβ :

1) Nous avons évalué *les effets de l'immunisation passive contre Aβ de manière préventive* dans un modèle murin développant lentement les pathologies Aβ et P301L tau. Nous avons démontré que l'administration préventive d'anticorps réduit de manière spectaculaire la pathologie Aβ. De plus, nous avons également observé que le traitement diminue tau hyperphosphorylé et recrute les microglies autours des plaques.
2) Nous avons ensuite étudié l'influence de l'immunisation passive contre Aβ sur un autre modèle murin de la maladie d'Alzheimer développant Aβ et tau non-muté. Dans cette seconde étude*, nous avons administré l'anticorps après la consolidation des pathologies Aβ et tau*. Dans l'hippocampe, nous avons démontré que l'expression de tau altérait le fonctionnement des microglies en réduisant leur interaction avec les plaques. Cet effet, cependant, est contrebalancé par l'immunisation passive qui semble rediriger les microglies vers Aβ. De plus, nous avons montré que l'immunisation passive diminuait le déploiement de tau dans l'hippocampe mais échouait à diminuer sa phosphorylation ou la dégénérescence de l'hippocampe due à l'expression locale de tau.
3) En parallèle, nous avons développé une *lignée de myoblaste humain* ayant la faculté de secréter des anticorps afin d'appliquer notre ECT chez l'humain. En utilisant des cellules murines, notre dispositif « flat-sheet » est capable de distribuer l'anticorps en sous-cutanée de manière continue à long terme chez la souris. La lignée cellulaire utilisée s'est avérée prometteuse puisqu'il nous a été possible d'obtenir une sécrétion d'anticorps satisfaisante et d'encapsuler les cellules. Malheureusement une fois implantées *in vivo* dans des souris immunosupprimée, les cellules se sont stabilisées sous la forme d'une mince couche tissulaire, insuffisante pour secréter la dose d'anticorps requises pour une application thérapeutique.

Mots clefs

Maladie d'Alzheimer, tau, amyloïde beta, microglies, immunisation passive, technologie d'encapsulation cellulaire.

Table of content

Abbreviations

AAV	Adeno-Associated Virus
Aβ	Amyloid beta
Aβo	Amyloid beta oligomers
AD	Alzheimer's Disease
ADA response	Anti-Drug Antibody response
AICD	Amyloid precursor protein Intracellular Domain
API	Alzheimer's Prevention Initiative
APOE	Apolipoprotein E
APP	Amyloid Precursor Protein
sAPP	secreted Amyloid Precursor Protein ectodomain
ARIA	Amyloid-Related Imaging Abnormalities
BACE	Beta-secretase Enzyme
BBB	Blood Brain Barrier
CSF	CerebroSpinal Fluid
DAPI	4', 6-DiAmidino-2-PhenylIndole
DG	Dentate Gyrus
DIAN-TU	Dominantly Inherited Alzheimer Network Trial Unit
ECT	Encapsulated Cell Technology
ELISA	Enzyme-linked Immunosorbent Assay
Fab	Fragment antigen-binding
Fc	Fragment cristallizable region
FTDP	Frontotemporal dementia and parkinsonism
GFP	Green Fluorescent Protein
GWAS	Genome-Wide Association Study
HE	Hematoxylin and Eosin
IgG	Immunoglobulin G
LAMP	Lysosomal-Associated Membrane Protein
LTD	Long-Term Depression
LTP	Long-Term Potentiation

mAbs	monoclonal Antibodies
MAPT	Microtubule-Associated Protein Tau
MCI	Mild Cognitive Impairment
MT	Masson's Trichrome
NFTs	NeuroFibrillary Tangles
NIH	National Health Institut
NMDA	N-Methyl-D-Aspartate
NOS	Nitric Oxide Synthase
PET	Positron-Emission Tomography
PSD	PostSynaptic Density protein
PSEN	Presenilin
RNA	RiboNucleic Acid
SNP	Single-Nucleotide Polymorphism
TBI	Traumatic Brain Injury
TREM	Triggering Receptor Expressed on Myeloid cell
WT	Wild-Type

List of figures

1

Chapter 1 : Introduction

1.1 Alzheimer's disease and amyloid beta

1.1.1 Alzheimer's disease

Alzheimer's disease is the most common form of dementia in the elderly. According to the American national institute of health, more than 5 millions Americans suffer from the disease with an estimated annual cost exceeding $100 billion for the national health insurance program in the United-State (Medicare). Although the Alzheimer's prevalence steadily increases with age, the disease is not considered to be the consequence of normal brain aging. As many populations are currently aging, the numbers of affected patients is expected to triple by 2050 if no effective disease-modifying treatment is found until then.

Disease course

Alzheimer's disease is a slow progressive disorder, which starts years before the onset of symptoms. Often, the first signs of cognitive impairments are similar to age-related symptoms. These signs involve memory loss of recently learned information and challenge in planning as well as confusion with time and place. Individuals also experience mood and personalities change. However, in Alzheimer's disease, these symptoms worsen over time, slowly leading to the inability to perform daily tasks, and result in progressive loss of independence.

The disease usually starts with mild cognitive impairment (MCI), which consists in a measurable decline in cognitive abilities that can be noticed by the patient himself. However, these cognitive changes do not interfere with daily life and the individual can still live independently. Not all individuals experiencing MCI will develop Alzheimer's disease. Some person with MCI will remain cognitively stable but others will worsen with time and develop dementia.

The second stage of the disease is moderate Alzheimer's disease and is usually the longest stage. During this period, relatives become progressively aware of the symptoms and the disease is generally diagnosed. Severe Alzheimer's disease is the final stage of the disease. Dementia symptoms cause individuals to lose the ability to respond to their environment. At this stage, patients need constant personal care. Due to swallowing difficulties, patients with severe Alzheimer's disease tend to be more vulnerable to infection, especially pneumonia.

Impact on the society

In addition of being a devastating disease for patients and their relatives, Alzheimer's disease is a major burden for the society. Middle stage of Alzheimer's disease can last for many years, while individuals increasingly require assistance. During the late stage, care needs are extensive and constant and often required moving the patient into assisted living facility.

Alzheimer's disease is the most expensive disease in America, with an estimated cost of $290 billion in 2019 according to the American Alzheimer's association. This number includes the cost supported by the different federal U.S government-sponsored programs but also by the families (See Figure 1). It does not include the associated burden for caregivers who provide billions of hours of unpaid care estimated to a value of 234 billions dollars by the *Alzheimer's disease facts and figures 2019* annual report from the Alzheimer's association.

Alzheimer's disease is a worldwide problem. In Switzerland, 151 000 persons are suffering from dementia with a cost that reached 9.7 billion in 2017 according to the Swiss Alzheimer's association (Alzheimer association CH, 2019). Dementia is currently the main reason for care-need in elderly persons in Switzerland and is also expected to increase due to the aging of the population.

Figure 1-1. The cost of dementia in the United States of America

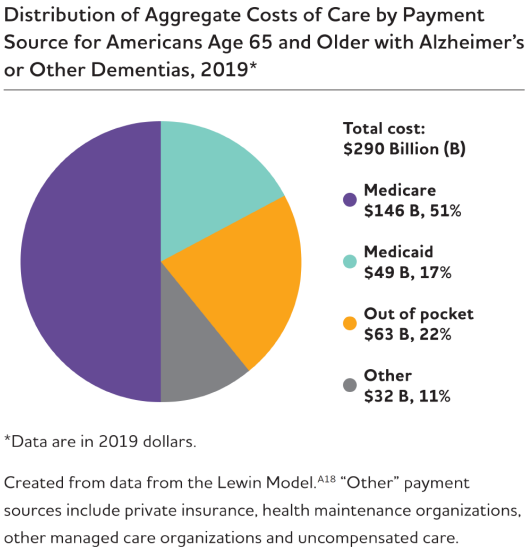

Figure 1: The cost of dementia in the United States of America
Total cost and source of payment in the United State for AD or other dementia in 2019 according to the *Alzheimer's disease facts and figures 2019* annual report. AD is a financial burden for both the patients and the society.

Current treatments

Reducing the impact of Alzheimer's disease is one of the priorities for national health organizations such as the American national institute of health (NIH). NIH funding for Alzheimer's disease research rose every year and reached 2.3 billion in 2019. Nevertheless, there is currently no cure for Alzheimer's disease and no way to slow or stop its progression. The only available options manage some of the symptoms such as anxiety, depression or sleep changes.

Besides finding a treatment to cure the disease, primary prevention is also considered to decrease the incidence of Alzheimer's disease. Numerous studies suggest that a healthy life style could lower the risk of developing the disease. Regular physical exercises, healthy eating, maintaining strong social connection and intense intellectual activity might all be beneficial.

1.1.2 Historical discovery

First description of the disease

Dr. Alois Alzheimer first described Alzheimer's disease (AD) in 1906. He was a senior physician in the hospital for the Mentally Ill and Epileptics in Frankfurt, Germany. Dr. Alois Alzheimer was greatly influenced by Dr. Frank Nissl who also

worked at the institute. The two physicians were conducting researches on the cause of mental diseases by analyzing histological preparation sampled during the autopsy (Tagarelli et al., 2006). Auguste D was admitted in 1901. She was 51 years old and experienced reduced cognitive ability in term of comprehension, memory and speech. She had unpredictable behaviors and paranoia as well as auditory hallucinations (Maurer et al., 1997). Shortly after Auguste D death, Alzheimer published observation about the case. More than 100 years ago, he already highlighted and illustrated all the hallmarks of the disease (See Figure 2) (Graeber and Mehraein, 1999). He described an evenly atrophic brain and striking pathophysiological changes. He emphasized on neurofibrillary tangles (NFTs) and carefully portrayed the different stages of tangles accumulation in neurons as well as neuronal cell death. He pictured the amyloid plaques as deposition of substance in the cortex and noticed glia activation around them (Stelzmann et al., 1995).

Figure 1-2. Original representation of the neuropathologies by Dr. Alois Alzheimer (Alzheimer, 1911)

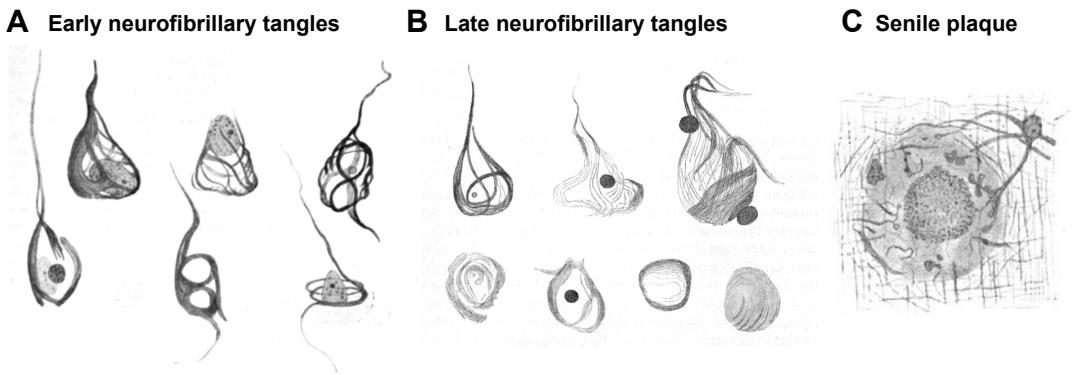

Figure 2: Original representations of the neuropathologies by Dr. Alois Alzheimer
In its second publication on Alzheimer's disease in 1911, Dr. Alois Alzheimer drew representative illustrations of neurofibrillary tangle at (A) an early stage and (B) a late stage of their formation. He also illustrated (C) senile plaques surrounded by activated glia.

Hallmarks of the disease

Today, pathological diagnosis of AD is still based on the presence of neuronal degeneration associated with senile plaques and NFTs. However, we have come to a progressively better understanding of the mechanisms leading to these pathological hallmarks.

The tubulin-binding protein tau was discovered in 1975 by Marc Kirschner when his team investigated the regulation of tubulin self-assembly into microtubules (Weingarten et al., 1975). However, the link between Alzheimer's disease and the tau protein was only made in 1986. At that time, different groups reported the presence of tau protein in NFTs (Brion et al., 1985; Grundke-Iqbal et al., 1986a; Kosik et al., 1986) and that the protein was abnormally phosphorylated in AD (Grundke-Iqbal et al., 1986b).

The composition of senile plaques, initially described as "deposition of substance" in the cortex by Dr. Alois Alzheimer, was elucidated in 1984. Glenner and Wong isolated and purified 40 or 42 amino acids long peptides from the senile plaques associated with AD that was never described before (Glenner and Wong, 1984a). They hypothesized that it was a fragment cleaved from a bigger protein. This was confirmed a year later when the amyloid precursor protein (APP) was discovered (Kang et al., 1987). *APP* gene was mapped on the chromosome 21 and linked to Down Syndrome, explaining the development of amyloid deposits and AD symptoms in patient with trisomy 21 (Glenner and Wong, 1984b).

1.1.3 The amyloid beta cascade hypothesis

APP function and processing

APP is a transmembrane protein abundantly expressed in neurons. Its physiological role is still not elucidated. But studies linked APP to different roles in cell health and growth (Oh et al., 2009) as well as in cognitive function and synaptic density (Meziane et al., 1998; Roch et al., 1994).

APP processing occurs through either the non-amyloidogenic pathway or the amyloidogenic pathway (See Figure 3). Amyloidogenic processing of APP is taking place in the endosomal compartment due to the presence of β-secretase 1 (also called BACE1) which cleaves APP before the γ-secretase. In this pathway, γ-secretase can generate an Aβ peptide of different length; the most common forms are either a 40 amino acid long peptide (Aβ40) or a 42 amino acid long peptide (Aβ42). The resulting Aβ peptide is then secreted in the extracellular space. In addition of the Aβ peptide, processing of APP generates different

intracellular and extracellular fragments such as secreted APP fragment α and β (sAPPα, sAPPβ) and APP intracellular domain (AICD). Each of these fragments has different effects on the neuron biology leading to the various cellular functions of APP processing (Coronel et al., 2018).

Figure 1-3. Amyloid precursor protein (APP) processing

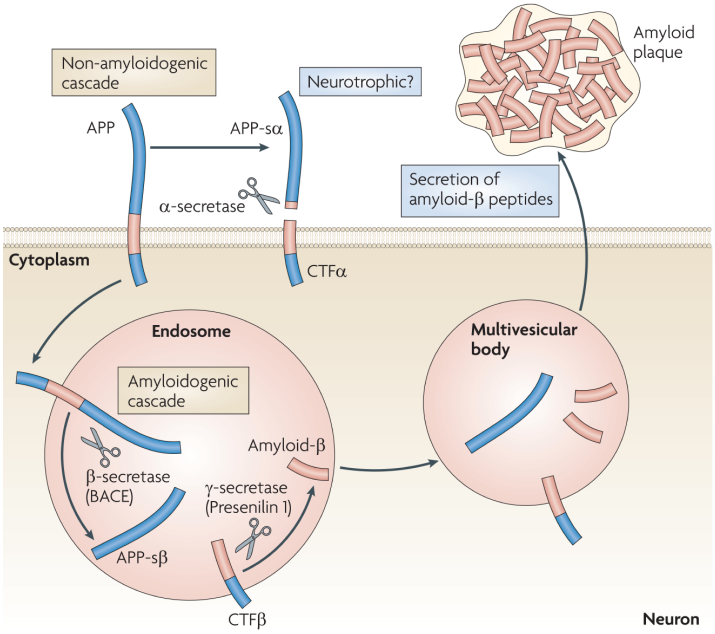

Figure 3: Amyloid precursor protein (APP) processing
APP can enter either a non-amyloidogenic processing or an amyloidogenic processing. The amyloidogenic cascade is taking place in the endosomes due to the presence of BACE that cleaves APP into the APP-sβ fragment. This fragment is then cleaved by the γ-secretase in either Aβ40 or Aβ42 peptides. From the endosomes, Aβ peptides are secreted in the extracellular space where it can aggregate and form Aβ deposits.
Illustration from *Nature Reviews Immunology*, volume 9, pages 429–439 (2009)

The genetic of Alzheimer's disease

Approximately 5% of Alzheimer's disease cases have genetic origin (Tanzi, 2012). Usually these cases have an early-onset as the disease occurs before 60 years old. Sequencing of *APP* revealed pathogenic mutations linked with familial forms of Alzheimer's disease (Goate et al., 1991). Surprisingly at the time, most families with early-onset familial Alzheimer's disease showed no mutations in *APP*. Linkage studies later leaded to the discovery of two other genes involved in the familial disease: *PSEN1* (Sherrington et al., 1995) and *PSEN2* (Levy-Lahad et al., 1995), both involved in APP processing. More than 200 pathological mutations were discovered, 24 in *APP*, 185 in *PSEN1* and 13 in *PSEN2* (Tanzi, 2012). All these mutations, but two, are transmitted in a fully penetrant

autosomal dominant manner. One mutation in PSEN2 shows incomplete penetrance (Sherrington et al., 1996) and one mutation in APP is inherited in an autosomal recessive manner (Di Fede et al., 2009).

Familial AD is closely linked to APP processing and the activity of the γ-secretase enzyme. Presenilin proteins, encoded in *PSEN* genes, are part of the γ-secretase complex. Most pathological mutations in *PSEN* or *APP* enhance the production of Aβ42 versus Aβ40 peptides (O'Brien and Wong, 2011; Scheuner et al., 1996), and therefore lead to higher levels of the most aggregating form of Aβ.

However, it exists other mutations such as the very famous but extremely rare Swedish family mutation that occurs in the *BACE1* cleavage site. The Swedish mutation favors the β-secretase over α-secretase cleavage increasing the activity of the amyloidogenic pathway (Haass et al., 1995). Another rare coding mutation also situated near the *BACE1* cleavage site was discovered in Iceland (Jonsson et al., 2012). This APP variant, however, was protective against AD and cognitive decline in the healthy elderly. This mutation was shown to have the opposite effect of the Swedish mutation and reduces the amyloidogenic processing of APP.

Interestingly, some mutations in the Aβ coding sequence of APP change Aβ oligomerization properties and also causes autosomal dominant familial AD (Gessel et al., 2012). The Artic mutation increases the ability of Aβ to form protofibrils, which might increases its toxicity (Nilsberth et al., 2001). On the other hand, the Flemish mutation blocks the Aβ ability to form protofibrils but increases the presence of large oligomers, also leading to an increased toxicity of the Aβ peptide (Gessel et al., 2012).

Besides being very rare, mutations in the *APP* gene gave very important insight in the mechanisms of AD: First familial AD is a very heterogeneous disease; second increased aggregation of Aβ seems to be a common denominator in the familial form of the disease.

In addition of the familial AD, it exists important genetic factors that significantly increase the risk to develop sporadic AD. *APOE* ε allele polymorphism is the most common of these genetic factors. *APOE* gene have three major variants: ε2, ε3 and ε4. *APOE* ε4 carriers constituted 20 to 25% of the general population and are

more likely to develop the disease (Van Cauwenberghe et al., 2016). Overall 40 to 60% of patients with AD (Fernandez et al., 2019) are *APOE* ε4 carriers. *APOE* ε4 effect is dose-dependent with heterozygous carriers having a 3-fold risk increase of developing the disease and homozygous carriers a 15-fold risk (Corder et al., 1993; Van Cauwenberghe et al., 2016). *APOE* ε2 allele, on the other hand, seems to be protective (Conejero-Goldberg et al., 2014; Corder et al., 1994).

The effect of the variant on APOE protein function has been extensively studies but is still not yet completely understood. According to Thomas Südhof work, APOE protein secreted by glia drives APP transcription in an APOE variant dependent manner. APOE4 protein further increases APP transcription and Aβ peptide production compared to APOE3 and APOE2 proteins. Other studies showed that APOE4 protein increases Aβ42 production as well as synaptic abnormalities in neurons (Lin et al., 2018) but also impact Aβ clearance by microglia (Lin et al., 2018; Ulrich et al., 2018).

The number of genetic risk factors involved in AD keeps increasing with genome-wide association studies (GWAS) of the available genetic data from AD and healthy patients. The latest study was published in January 2019 (Jansen et al., 2019) and will probably leads to the discovery of new mechanisms involved in the disease. We will not discuss all of these risk factors here. But instead, we will focus on the fact that the most common genetic causes of AD are all increasing Aβ production and aggregation.

Formulation of the hypothesis

The central role of Aβ peptide production in familial AD, and in particular the finding that production of the pro-aggregant form Aβ42 is favored in pathogenic processes, lead to the hypothesis that Aβ production and accumulation could be the initial cause of Alzheimer's disease.

This hypothesis was first proposed in the early 90s by Hardy and Selkoe in subsequent publications (Hardy and Higgins, 1992; Selkoe, 1991). The hypothesis stated that the primary influence of AD is the accumulation of Aβ peptide in the brain. The others neuropathological hallmarks of the disease, including tau hyperphosphorylation, tangles formation and neuronal cell death,

were all proposed to be the direct or indirect consequences of Aβ deposition (See Figure 4).

The hypothesis implied that sporadic forms of Alzheimer's disease are also caused by increased Aβ accumulation. This increase might be triggered by aging as well as a combination of environmental and genetic risk factors. All together these factors were though to cause an imbalance between Aβ production and Aβ clearance.

Figure 1-4. The amyloid cascade hypothesis

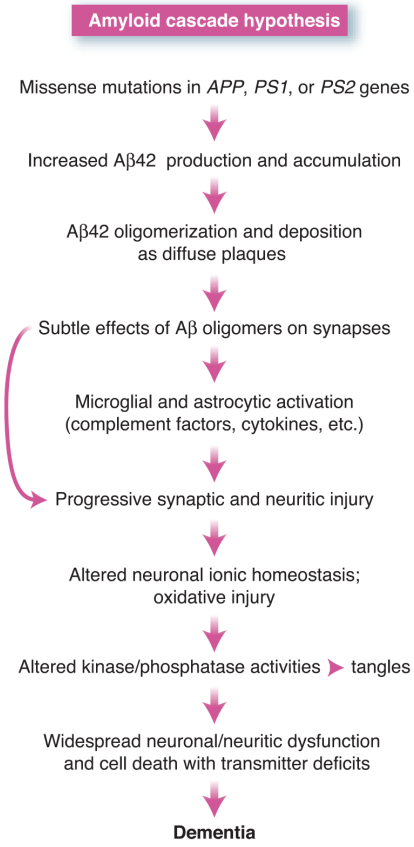

Figure 4: The amyloid cascade hypothesis
Updated version of the amyloid cascade hypothesis by Hardy and Selkoe, 10 years after their inital statement. The reviewed version is including microglia activation and the Aβ oligomers effect on synaptic dysfunction. The arrow illustrates that Aβ oligomers can directly influence synaptic injury.
Illustration from *Science,* 19 Jul 2002: Vol. 297, Issue 5580, pp. 353-356

Aβ normal function

On another hand, there are evidences that soluble Aβ is more than a peptide produced by a pathogenic process and that should be degraded. Indeed, it appears to play a physiological role in the brain. First, APP and Aβ peptides are

present in all vertebrates with more than 90% homology (Tharp and Sarkar, 2013). In addition, the presence of amyloid precursor protein able to generate Aβ like peptides (AβAPP-like) was found in hydra (*hydra magnipapillata*) as well as in cartilaginous ray (*Narke japonica*) (Tharp and Sarkar, 2013). The conservation of the Aβ peptide through vertebrate evolution suggests a role that confers selective advantage. Soluble Aβ is continuously produced in healthy individuals and is thought to have a physiological protective effect.

Furthermore, reducing or depleting APP or Aβ levels have deleterious cognitive effects in mice and rats (Brothers et al., 2018). And it was demonstrated that low dose of Aβ enhances synaptic plasticity and memory in mice (Puzzo and Arancio, 2013). It was suggested that Aβ could act as a chelator or bioflocculant for potentially toxic agents in the extracellular compartment such as metal ions or microbacteria. According to the "bioflocculant hypothesis", Aβ plaques could be protective as they precipitate toxic agents and present them to microglia (Robinson and Bishop, 2002). This hypothesis is reinforced by the antimicrobial properties of the peptide (Soscia et al., 2010). Filamentous Aβ peptide might also have a role in maintaining the integrity of the blood brain barrier and preventing the spread of toxic components in the brain (Atwood et al., 2003).

Furthermore, Aβ peptide accumulates in a matter of hours in the brain of people experiencing traumatic brain injury (TBI). However, these individuals do not exhibit more Aβ plaques in the long-term, suggesting that the accumulation of Aβ plaque is transient after TBI and resolves afterward. Studies in mice also suggest that Aβ accumulation after TBI might help recovery (Brothers et al., 2018). All these studies indicate that both soluble Aβ and Aβ transient aggregation may have an important physiological role during an individual's lifetime.

Aβ toxic species

In addition, it was discovered that the Aβ plaques themselves might not be necessarily toxic. Starting in 1986, David Snowdon conducted a longitudinal study on 678 catholic sisters 75 to 107 years of age in order to evaluate the effect of age on cognition and neuropathology (Snowdon, 2003). He discovered that Aβ plaques load in the brain does not correlate with cognitive impairment in AD (Snowdon, 1997). Some individuals can accumulate Aβ deposition with age to

similar levels as AD patients, and do not show any sign of dementia (Dickson et al., 1992; Snowdon, 1997). When he first described the disease, Dr. Alois Alzheimer also suggested that the plaques were not the cause of the disease but only a consequence (Avila, 2006). He hypothesized that the NFTs were responsible for the brain degeneration.

Since genetic evidence pointed in the Aβ direction, scientists actively searched for the Aβ "toxic species". It was rapidly demonstrated that soluble assembled Aβ forms such as protofibrils or oligomers were more toxic to neurons and synapses than insoluble fibrils *in vitro* (Lorenzo and Yankner, 1994; Pike et al., 1991). In a mouse model overexpressing human APP, it was shown that synaptic loss correlates with the level of soluble Aβ. In the same model, the synapse loss did not correlate with either Aβ deposition or APP transgene expression (Klein et al., 2001).

Aβ oligomers (Aβo) and neuritic plaque formation

It was suggested that Aβ plaques could act as a reservoir for soluble Aβ toxic species such as Aβo (Koffie et al., 2009). The concept was reinforced by the observation that Aβ depositions trigger the formation of neuritic plaques (Cras et al., 1991). Neuritic plaques are constituted of an Aβ core surrounded by swollen dystrophic neurites. These abnormal neurites are likely to be the neuron response to the toxic environment around the Aβ depositions. As a confirmation, it was demonstrated that compaction of Aβ plaques could be protective by reducing Aβo diffusion thus lowering Aβ plaque toxicity (Cohen et al., 2009).

In AD, neurites surrounding Aβ depositions accumulated APP proteins (Cras et al., 1991) as well as neuritic filaments positive for phosphorylated tau and ubiquitin. These filaments are very similar to NFTs (Dickson et al., 1999; Onorato et al., 1989). In addition, dystrophic neurites exhibit synaptic abnormality such as synaptophysin accumulation (Sadleir et al., 2016) as well as synapse loss (Koffie et al., 2009; Spires et al., 2005). The lysosomal pathway is also involved with a resulting accumulation of LAMP1 positive vesicles (Hassiotis et al., 2018).

It was observed that dystrophic neurites containing hyperphosphorylated tau appears later than neurites exhibiting APP, ubiquitin and synaptophysin,

suggesting a maturation of these dystrophies along with the evolution of the disease (Blanchard et al., 2003). In addition, phospho-tau and LAMP1 dystrophies were spatially and morphologically distinct (Boutajangout et al., 2004; Hassiotis et al., 2018), suggesting different kind of dystrophic neurites surrounding.

Non-demented subjects with Aβ usually exhibited diffused Aβ deposition lacking an Aβ core and that exhibit APP and LAMP1 positive dystrophies but not tau positive dystrophies (Cras et al., 1991; Hassiotis et al., 2018).

The architecture of the neuritic plaque in AD is highly complex and will not be assessed in details here. We will focus on the fact that neuritic plaques are toxic to their surrounding due to release of soluble Aβ and that the resulting neuronal dystrophies and synapse dysfunctions are considered an important hallmark of AD.

1.2 Targeting amyloid beta to cure Alzheimer's disease

The amyloid beta cascade hypothesis, strengthened by the genetic evidences and the discovery of soluble toxic Aβo, directed AD research towards the prevention of Aβ accumulation. Treatments can act on Aβ accumulation at two different levels: they can prevent its production by modulating APP processing or they can act directly on Aβ itself to prevent accumulation and aggregation. For the first strategy, modulation of the γ-secretase and inhibition of BACE1 were thoroughly investigated. However, we will not discuss these strategies in this chapter and instead we will focus on targeting Aβ itself. For a summary of the target of the anti- Aβ treatment recently or currently tested in phase III, see Figure 5.

Figure 1-5. Targets of anti-Aβ treatments

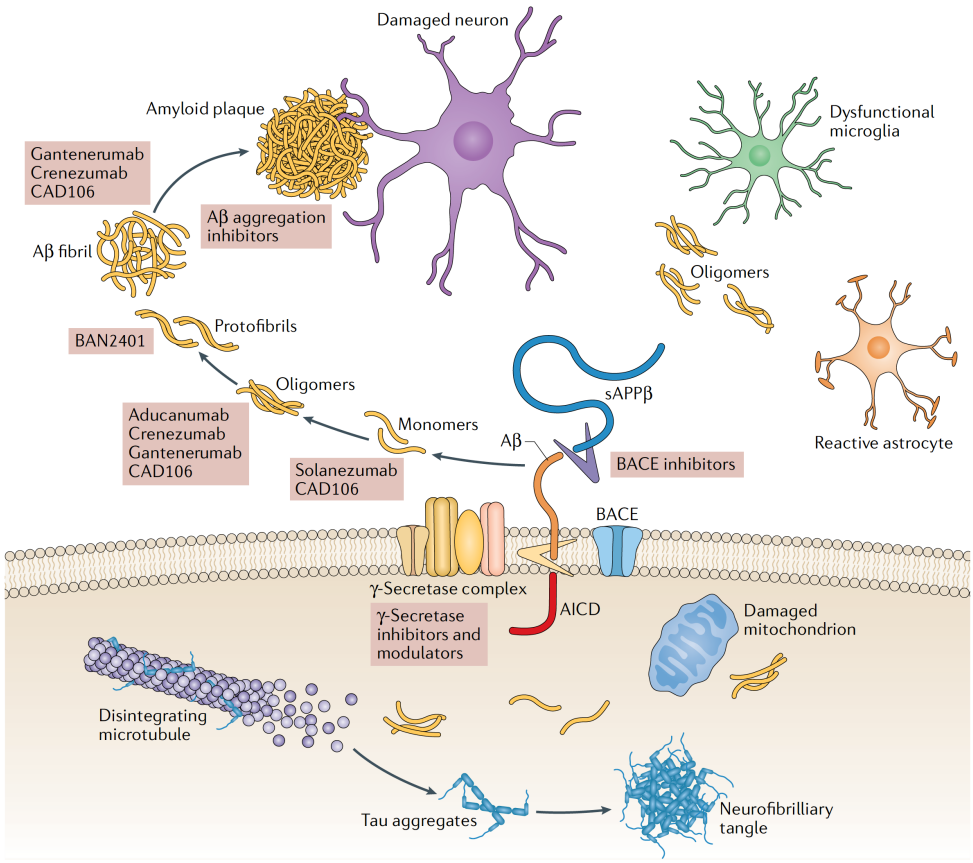

Figure 5: Targets of anti-Aβ treatments
Target of the anti-Aβ approaches tested currently or recently in phase III clinical trials. BACE and γ-secretase inhibitors aim to modulate Aβ processing in order to prevent Aβ production. Whereas passive and active immunization are targeting Aβ after its formation in order to promote its clearance or prevent its aggregation.
Illustration from *Nature Reviews Neurology*, volume 15, pages 73–88 (2019)

1.2.1 Aβ immunization

Active Aβ immunization

The first approach developed to prevent accumulation of Aβ peptide after its processing was active immunization. Active Aβ immunization involved the administration of Aβ antigen with an adjuvant in order to elicit an immune response of the patient against Aβ. The patient will then develop its own anti-Aβ antibodies in order to fight against Aβ accumulation. The first developed vaccine, AN-1792, contained pre-aggregated Aβ42 and an adjuvant.

In pre-clinical studies in the APP mouse model, administration of AN-1792 elicited an immune response resulting in the development of antibody against Aβ42 in all injected mice (Schenk et al., 1999). In young mice, AN-1792 completely prevented the apparition of Aβ deposits. When administrated after the onset of the disease on older mouse, AN-1792 significantly decreased the Aβ burden (Schenk et al., 1999).

AN-1792 was tested on patients with mild to moderate AD. In the phase II clinical trial, 20% of the 300 treated patients developed an adequate anti-Aβ42 response (antibody responders). Unfortunately, the clinical trial was halted for safety reason, when 6% of the 300 treated patient developed meningoencephalitis (Gilman et al., 2005). Long-term postmortem study of the responders showed that AN-1792 was able to considerably reduced Aβ burden (Holmes et al., 2008). Unfortunately the neuropathological analysis showed not improvement in term of neurodegeneration. In addition, there was no evidence of reduction of dementia before death (Holmes et al., 2008).

Safer active Aβ immunization approaches were developed: anti-Aβ vaccine CAD106 is an Aβ antigen made of multiple copies of the Aβ6 fragment coupled with an adjuvant. CAD106 was well tolerated with no case of meningoencephalitis (Farlow et al., 2015; Vandenberghe et al., 2016; Winblad et al., 2012). In phase IIb clinical trial, CAD106 elicited a strong serological response with 80% of the patients responding to the vaccine in the high dose group (Vandenberghe et al., 2016). There was no evidence of decrease of Aβ burden or improvement of cognitive impairment in these studies. At the

opposite, antibody responders tended to score worst at the mini-mental state examination (MMSE) but the difference was not significant (Vandenberghe et al., 2016). CAD106 is currently evaluated in Generation S1 preventive trial on cognitively healthy *APOE* ε4 allele carriers.

In addition of active Aβ immunization, the direct administration of monoclonal anti-Aβ antibodies was investigated. Because passive anti-Aβ immunization does not require the patient to elicit a strong anti-Aβ immune response, it was considered safer.

Monoclonal antibodies as therapeutics

The development of mouse hybridoma technology for monoclonal antibodies (mAbs) production by Kohler and Milstein in 1975 (Köhler and Milstein, 1975) paved the way to the use of mAbs as therapeutics. Antibodies constitute an incredibly versatile toolbox: their structure and function allow infinite tailoring of their properties (Buss et al., 2012). The variable region can be aimed to any target protein and is highly specific. Modulation of the variable region allows the control of the binding affinity. The constant region can be engineered to enable different effector functions including antibody-dependent cytotoxicity, phagocytosis and complement-dependent cytotoxicity. In the context of AD, antibodies can be used to target various forms of Aβ to trigger their removal or prevent their aggregation.

Effect of passive anti-Aβ immunization in mice

Before its translation in humans, the effect of anti-Aβ passive immunization was extensively studied in Aβ mouse models (Jicha, 2009; Wisniewski and Goñi, 2015). It is now established that anti-Aβ antibodies are able to cross the blood brain barrier (BBB) and that peripheral administration triggers Aβ clearance in mice (Bard et al., 2000). In addition, removal of Aβ results in cognitive benefits in Aβ mouse models (Hartman et al., 2005; Lee et al., 2006).

By testing different Aβ epitopes, Bard et al. were able to determine that targeting the N-terminus epitopes of Aβ was important for antibody-mediated clearance of Aβ plaques. Even though it was shown later that targeting central (DeMattos et al., 2001) or C-terminal epitopes (Wilcock et al., 2004a) could also be successful

to reduce Aβ burden. Targeting oligomeric Aβ forms by using specific antibodies that recognize conformational epitopes was also efficient in mice (Lee et al., 2006).

It was demonstrated that mouse immunoglobulin isotype G2b (IgG2a) antibodies (corresponding to IgG1 isotype in human) were more efficient than other isotypes to reduce Aβ burden, suggesting a role for Fc-mediated phagocytosis in mediating the effects of passive immunization (Bard et al., 2003).

Passive anti-Aβ immunization activation of microglia

Wilcock and al. demonstrated in subsequent studies that microglia activation was indeed facilitating Aβ clearance following systemic passive immunization (Morgan et al., 2005; Wilcock et al., 2004a, 2004b). However, it appears that passive immunization can also affect the Aβ pathology via microglia-independent mechanisms (Wilcock et al., 2003), such as plaque disruption (Bacskai et al., 2002) or inhibition of Aβ aggregation (Solomon et al., 1996). Anti-Aβ antibodies administration modulates the microglia activation and it was suggested that the antibodies can polarize microglia towards protective phagocytosis, rather than the destructive mode associated with chronic inflammation (Morgan et al., 2005).

These proof-of-concept studies in mice allowed the translation of passive anti-Aβ immunization in human.

1.2.2 Clinical trials of anti-amyloid beta antibodies

The first generation of clinical trials

Starting in 2007 with bapineuzumab, several antibodies targeting different Aβ species were developed and tested first in clinical trials targeting mild-to-moderate AD and then in prodromal-to-mild AD. There were proven safe but unfortunately none of them showed clinical benefit in phase III trials. Nevertheless, each failure built-up our knowledge about the disease and contributed to today's deeper understanding.

Bapineuzumab

The first anti-Aβ antibody tested was an IgG1 antibody targeting Aβ N-terminal region called Bapineuzumab. Bapineuzumab showed target engagement in phase III trials but little benefit (Salloway et al., 2014). In *APOE* ε4 carriers, a decreased rate of Aβ accumulation was observed using PET analysis as well as a reduction of phospho-tau in the cerebrospinal fluid (CSF). Increase phospho-tau in the CSF is considered a marker of neurodegeneration. However, there was no evidence of cognitive improvement. It was concluded that bapineuzumab might be able to modify Aβ accumulation as well as downstream markers such as phospho-tau in *APOE* ε4 carriers, but this effect was not resulting in a cognitive benefit (Salloway et al., 2014).

In term of adverse effects, bapineuzumab phase II trials brought awareness on a very serious point: a significant portion of the participants enrolled in the clinical trial developed amyloid-related imaging abnormalities (ARIA) (Salloway et al., 2014).

Amyloid-related imaging abnormalities

ARIA appeared as signal abnormalities in MRI and represented accumulation of extravascular fluid. It is thought to be caused either by vasogenic edema (defined as ARIA-E) or microhemorrages (defined as ARIA-H) (Sperling et al., 2012). ARIA was observed mainly in the subjects that received the higher dose of anti-Aβ antibody, as well as in *APOE* ε4 allele carriers (Salloway et al., 2014). Most ARIA events were asymptomatic and resolved by themselves. However, in some cases, ARIA caused clinical symptoms depending on the location where it occurred. Furthermore, ARIA was often observed during the initial phase of the antibody treatment and did not reappear once resolved.

Crenezumab and Solanezumab

Two of the subsequent anti-Aβ antibodies, Crenezumab and Solanezumab, were developed in order to minimize the incidence of ARIA.

Crenezumab was designed as an IgG4 in order to reduce neuroinflammation while preserving the induction of phagocytosis by microglia (Adolfsson et al., 2012). It did show a reduction of ARIA incidence compare to Bapineuzumab

(Cummings et al., 2018). Crenezumab binds to a mid-region of Aβ in both monomers and aggregated forms but had a specifically high affinity for oligomers. Crenezumab prevents Aβ aggregation but also promotes Aβ disaggregation by destabilizing the β-hairpin in the Aβ hydrophobic core (Ultsch et al., 2016).

Crenezumab efficiency was first tested in phase II trials on mild-to-moderate AD in ABBY and BLAZE studies (Cummings et al., 2018; Salloway et al., 2018). Both studies shown a significant increase of Aβ level in the CSF, suggesting target engagement, but failed to show cognitive benefit. In the PET study (BLAZE), there were no evidence of Aβ plaques reduction (Salloway et al., 2018). In both studies, *post hoc* analysis suggested that Crenezumab could have beneficial effects on patients with mild AD. Consequently, phase III studies of Crenezumab (CREAD 1 and 2) were conducted on prodromal-to-mild AD. CREAD studies were both discontinued end of January 2019 based on a futility analysis. It was demonstrated that both clinical trials would not be able to meet their primary end-points. Preliminary data analysis presented in the Alzheimer's Disease/ Parkinson's Disease (ADPD) conference 2019 showed no trends toward any cognitive benefits.

Solanezumab also targets the central region of Aβ but was designed to recognize soluble monomeric Aβ only (Farlow et al., 2012). This strategy also decreased the occurrence of ARIA (Doody et al., 2014). By targeting monomers only, the objective was to clear soluble Aβ forms before they gain their toxic functions. In addition, administration of Solanezumab increased Aβ plasma concentration (Siemers et al., 2010). It was hypothesized that promoting Aβ flow from the central nervous system to the peripheral system could induces Aβ clearance (peripheral sink theory)(Doody et al., 2014; Yamada et al., 2009). In phase III trials, EXPEDITION 1 and 2, Solanezumab showed target engagement by increasing both plasma and CSF Aβ concentrations but failed to show cognitive improvement in mild-to-moderate AD (Doody et al., 2014). Similarly to Crenezumab, the *post hoc* analysis on mild AD suggested a potential cognitive benefit if the treatment was administrated earlier (Willis et al., 2018). EXPEDITION 3, a third phase III trial, was then started on mild AD patients only

(Honig et al., 2018). The study demonstrated that Solanezumab did not reduce Aβ deposit in the brain but the patients performed slightly but significantly better in some cognitive tests such as MMSE. However, this effect was not enough to result in a significant beneficial outcome of the primary cognitive endpoints (Honig et al., 2018).

Earlier intervention on Prodromal AD: Gantenerumab

The failure of the first generation of clinical trials to show cognitive benefit raised a lot question in the scientific community. Most scientists believed that failures were due to late intervention or low dosage. Indeed, subgroup analyses of these first trials commonly proposed that higher dosage were more efficient as well as earlier intervention. Nevertheless, phase III trials on mild AD also failed to improve cognitive impairment. The designs of the clinical trials were also questioned. Indeed, systematic positive amyloid scans were not required to be enrolled in the trials and patients were included based solely on their cognitive scores (Schneider and Sano, 2009).

Consequently, Roche was the first company to test their new antibody gantenerumab on prodromal AD only in a phase II/III called SCarlet RoAD. Early diagnostic for AD was based on the National Institute on Aging guidelines (Sperling et al., 2011). In this study, only patients over 50 with a positive amyloid PET and scoring below average for a selection of memory and cognitive tests were enrolled (Ostrowitzki et al., 2017). The aim was to select a population of patients whose memory deficits, although still mild, were likely due to Alzheimer's pathology. However, it remained uncertain whether these patients would indeed develop AD.

Gantenerumab is an IgG1 antibody that recognizes a conformational epitope of Aβ and binds preferentially to Aβ oligomers and fibrils. Gantenerumab commonly caused ARIA as adverse events (Lasser et al., 2015). It was demonstrated that antibodies with an IgG1 backbone and with an affinity for aggregated forms of Aβ were more prone to trigger ARIA. Indeed, the design of these antibodies is aimed at activating microglia for parenchymal reduction of Aβ but also trigger inflammation and increase deposition of Aβ around the cerebral vasculature (Fuller et al., 2014).

According to the amyloid PET imaging analysis, Gantenerumab decreased Aβ burden in a dose- and time-dependent manner (Ostrowitzki et al., 2017). In addition, it also decreased phospho-tau and total-tau in the CSF. No significant increase of Aβ in the CSF was observed. Beside Gantenerumab effects on AD biomarkers, SCarlet RoAD study was halted in 2014 due to an interim futility analysis. According to the results of the patients that finished the study (50% of the entire cohort), Gantenerumab would not be able to meet the primary endpoint in term of cognitive benefit in prodromal AD (Ostrowitzki et al., 2017). Patients had the possibility to enter an open-label extension study where all patients received a higher dose (1200mg) of Gantenerumab. In order to manage ARIA events, the dose was slowly titrated up (Ostrowitzki et al., 2017).

Preliminary results of the open-label extension study of SCarlet ROad were released at the 2018 Alheimer's Association International Conference. They showed important decrease of Aβ burden using amyloid PET imaging. After two years of high Gantenerumab dose, half of the patient felt below the threshold signal for positivity in amyloid PET.

Successful removal of Aβ depositions

Others antibodies, such as Aducanumab and BAN2401, showed promising abilities to clear Aβ plaques and raised the hope to improve cognitive decline in prodromal AD.

Aducanumab was developed through reverse engineering from a human B-lymphocyte library (Arndt et al., 2018). These B-lymphocyte came from a population of healthy elderly that did not exhibit cognitive decline. The idea was that these elderly might have developed potent human anti-Aβ antibodies by fighting Aβ accumulation during their entire life.

Aducanumab is a fully human IgG1 that binds to aggregated Aβ. In 2015, results of the PRIME phase I study on Aducanumab antibody on prodromal-to-mild AD were released (Sevigny et al., 2016). Aducanumab largely and rapidly reduced Aβ burden and slowed cognitive decline in a dose- and time-dependent manner in a small cohort of AD patients. It was the first evidence that Aβ burden could be decreased using anti-Aβ antibodies and resulted in cognitive improvement in

human, which raised a lot of hope. As expected, it did trigger ARIA-E but it was managed through dose titration (Sevigny et al., 2016).

Despite these promising results, Aducanumab did not live up to the expectations. Unfortunately the PRIME phase I study was statistically underpowered and not designed to show efficiency. Phase III clinical trials, ENGAGE and EMERGE, were discontinued based on interim futility analysis in March 2019, no details about the results were released. The disappointment in the scientific community was immense.

Conclusion of these very recent data is that we are now able to clear Aβ plaques from prodromal AD patients. However, this Aβ decrease does not necessarily translate into positive effects on cognitive benefits.

BAN2401

BAN2401 is another IgG1 antibody that bind selectively to large Aβ protofibrils (Logovinsky et al., 2016). BA2401 was tested in a phase IIb clinical trials on prodromal-to-mild AD that suggested a slowing down of cognitive decline and brain Aβ accumulation in treated-groups. Results were progressively presented in successive conferences end of 2018 and beginning of 2019 but are not yet published. It seems, however, that the efficiency analysis was complicated by an imbalance distribution of *APOE* ε4 carriers. A phase III clinical trial started in March 2019 called clarity AD.

ARIA and Aβ clearance

ARIA was still a major concern associated with IgG1 antibody such as Gantenerumab, Aducanumab and BAN2401. In the SCarlet RoAD open-label study, one-third of the patients developed ARIA-E when the treatment dose was increased.

It was observed that the regions affected by ARIA-E events colocalized with areas showing the highest degree of amyloid plaque clearance (Ostrowitzki et al., 2012). In addition, ARIA occurred at higher dosage that showed the best efficiency at removing Aβ plaques. A link between ARIA and Aβ removal was suggested. ARIA could be a consequence of Aβ clearance by microglia showing target engagement and removal (Ostrowitzki et al., 2012). Recent released data

by Roche at conference ADPD 2019 on the SCarlet RoAD open label study showed that patients with ARIA exhibited high plaque reduction. On the other hand, a significant decrease of Aβ plaques could also be achieved without the incidence of ARIA. Consequently, ARIA might be part of the process but is not necessary for Aβ plaque removal. In any case, the current strategy toward ARIA aims at monitoring and managing this side effect instead of avoiding it.

Preventive trials on familial AD

The notion that anti-Aβ antibodies should be administered at an earlier stage of the disease to be efficient is widely prevalent in the scientific community. Indeed, the progression of AD in the central nervous system of affected individuals is being rampant for many years, even before the prodromal stage of the disease. Once cognitive deficits become detectable, the neurodegenerative process might not be reversible, even when Aβ deposits are efficiently cleared from the affected brain.

In order to tackle this issue, prevention trials on autosomal dominant familial AD were implemented. The dominantly inherited Alzheimer network trials unit (DIAN-TU) and the Alzheimer's prevention initiative (API) trials are aiming to test multiple drugs efficiency to prevent or slow down AD progression in autosomal dominant familial AD (Bateman et al., 2017; Tariot et al., 2018). Solanezumab and Gantenerumab are tested in DIAN-TU and Crenezumab is tested in API. In these trials, we can predict that the subjects will eventually develop AD. It allows the drug trials to start years or even decades before the onset of the disease. These initiatives were also designed to identify possible biomarkers of the disease progression. Success or failure of these trial using anti-Aβ antibodies will shape the future of drug development for AD.

1.3 Alzheimer's Disease: A multifactorial disorder

Despite the hopes to see one of the ongoing prevention trials on familial AD to become successful, it is clear that anti-Aβ treatment did not meet their promises. The successive failures questioned the central role of Aβ in AD. Beside the fact that we might not administrate the treatment early enough, the possibility exists that targeting Aβ only may not be an effective approach.

The three hallmarks of the disease initially described by Dr. Alois Alzheimer did not receive the same attention during the century that followed. Interestingly, Dr. Alzheimer emphasized his own research toward the neurofibrillary tangles that he believed to be responsible for the neuronal cell death. He considered the senile plaques as being consequence of the disease but not the cause (Avila, 2006).

By placing Aβ as the primary incidence, the Aβ cascade hypothesis did put aside the potential role of both tau and the microglia in AD. Today, increased evidences are suggesting that both tau pathology and microglia activation affect the occurrence of the disease. In addition, these three pathophysiological hallmarks are closely linked and their crosstalk might be a key component to understand the disease development.

1.3.1 Tau

Tau physiological function

Tau is a microtubule-associated protein. The binding of tau to tubulin promotes microtubule assembly and stabilization (Weingarten et al., 1975). Regulation of tau binding to microtubules is mediated by its degree of phosphorylation. Low tau phosphorylation promotes binding to tubulin and microtubule stabilization, whereas high levels of phosphorylation prevents tau binding and destabilizes microtubules (Lindwall and Cole, 1984) (See Figure 6). Tau is encoded by the *MAPT (microtubule associate protein tau)* gene and can be alternatively spliced in 6 isoforms in humans. The isoforms either contain three or four microtubule binding repeats (3R or 4R tau) and zero, one or two amino-terminal inserts (0N, 1N or 2N) (Goedert et al., 1989). Tau isoforms, their function as well as their

entire phosphorylation sites are well described in the literature but it will not be covered here. We will focused on tau involvement in Alzheimer's disease and more precisely its interaction with Aβ and its influence on microglia activation.

Figure 1-6. Tau in Alzheimer's disease

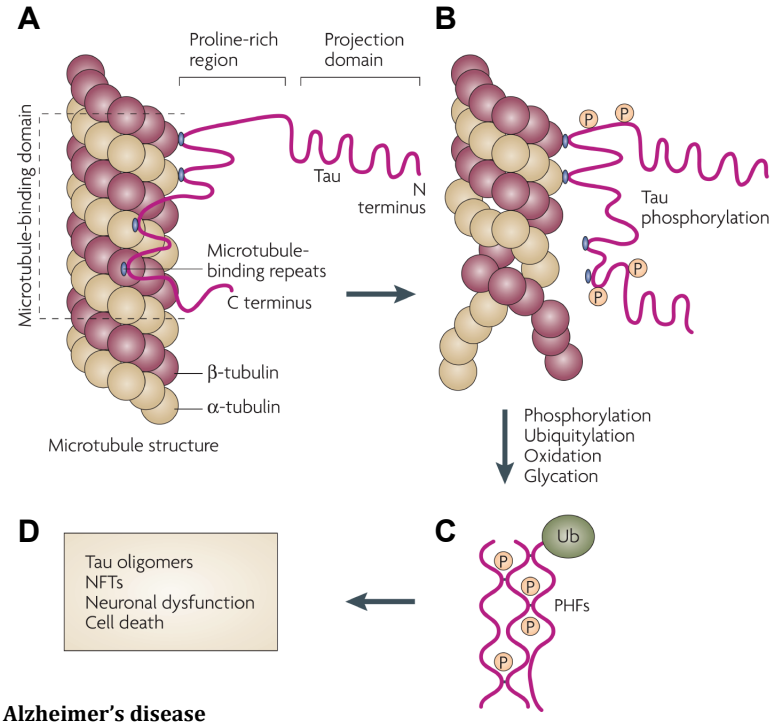

Figure 6: Tau in Alzheimer's disease

A | Tau protein is a microtubule-binding protein that stabilizes microtubule through its binding repeats on its C-terminal. **B |** In order to allow microtubules dynamic, tau affinity is regulated through phosphorylation. Phosphorylation of tau reduces tau binding and leads to destabilization of microtubules. **C |** In pathological condition such as AD, tau undergo hyperphosphorylation as well as conformational changes leading to the formation of paired helical filaments (PHFs) promoting the apparition of aggregated forms of tau. **D |** Aggregated forms of tau such as oligomers or neurofibrillary tangles (NFTs) causes neuronal dysfunction and can lead to cell death.
Illustration from *Nature Reviews Drug Discovery,* volume 6, pages 464–479 (2007)

Aβ effect on tau pathology

Interestingly, mutations of *MAPT* do not lead to development of familial Alzheimer's disease but trigger another set of neurodegenerative diseases called tauopathies. In AD, neurofibrillary tangles are composed of WT hyperphosphorylated tau. According to the amyloid beta hypothesis, Aβ accumulation, especially toxic Aβ oligomers, should trigger tau pathology and then lead to neurogeneration. Surprisingly, AD mouse models overexpressing mutant forms of *APP* or *PSEN* genes, such as 5XFAD or APP/PS1 mouse models, developed important Aβ pathology and exhibit synapse loss as well as cognitive

impairment but show no NFTs or severe brain atrophy (Oakley et al., 2006; Radde et al., 2006).

Therefore, the effect of Aβ on tau pathology has mainly been studied using mouse models overexpressing a mutant version of tau. P301L and P301S mutant forms of tau are involved in frontotemporal dementia and Parkinsonism linked to chromosome 17 (FTDP-17) and typically show pro-aggregant properties compared to WT tau. They also cause important tau pathology including NFT and neurodegeneration when overexpressed in mice (Lewis et al., 2000; Yoshiyama et al., 2007).

In these mouse models, Aβ increased insoluble and hyperphosphorylated forms of tau as well as the presence of NFTs in the brain (Bolmont et al., 2007; Götz et al., 2001; Lewis et al., 2001; Pérez et al., 2005; Pooler et al., 2015). Furthermore, mutant tau tended to spread faster and further in presence of Aβ (Lewis et al., 2001; Pooler et al., 2015). Gliosis, synapse loss and neurodegeneration were also enhanced in presence of the Aβ pathology. On the other hand, tau pathology in these animals did not impact Aβ pathology. These findings were corroborated using different approaches to induce the Aβ pathology. The facilitation of tau pathology by Aβ was observed in different genetic mouse models overexpressing *APP* mutations and *PS1* mutations (Bennett et al., 2017; Héraud et al., 2014; Lewis et al., 2001; Oddo et al., 2003; Pérez et al., 2005; Saul et al., 2013), but also in models were Aβ42 or AD brain extract were injected in the mouse brain (Bolmont et al., 2007; Götz et al., 2001). It was not required that Aβ forms neuritic plaques to facilitate tau pathology. Low concentration of Aβ from AD brain extract was not sufficient to trigger Aβ deposits but still induced tau neurofibrillary pathology (Bolmont et al., 2007).

These studies partially supported the Aβ cascade hypothesis: It demonstrated that Aβ pathology has a powerful impact on mutant tau pathology but that mutant tau pathology did not influence Aβ pathology. However, the relevance of these observations in the context of AD is questionable. WT tau ability to undergo pathological changes is very different than mutant tau. For example, overexpression of WT tau alone do not trigger neurofibrillary formation (Duff et al., 2000).

Aβ plaque environment and WT tau pathology

In a context more relevant to AD, recent studies showed that the deposition of Aβ and the formation of neuritic plaques is required but not sufficient for the pathological conversion of WT tau into NFTs (He et al., 2018; Li et al., 2016). In both studies, the induced deposition of Aβ alone triggered tau phosphorylation in neuritic plaques but failed to start NFTs formation and spreading. However, the low expression of human 4R truncated tau in an APP mouse model triggered brain atrophy, increased tau hyperphosphorylation and leaded to the formation of NFTs (Li et al., 2016). In absence of neuritic plaques, low expression of human 4R truncated tau (Tau4R mouse model) did not trigger WT tau hyperphosphorylation or NFTs formation. This study suggested that neuritic plaques allow tau hyperphosphorylation and tau propagation but only in presence of pathological tau.

This study was corroborated in another mouse model of Aβ accumulation (He et al., 2018). Single APP knock-in (APP-KI) mouse model developed moderate Aβ deposition in the cortex and hippocampus (Saito et al., 2014). These APP-KI mice did not develop tau pathology unless injected with sarkosyl insoluble human AD-tau extracted from sporadic AD brain (He et al., 2018). Compare with injected WT mouse, presence of Aβ plaques in APP-KI mice favored the formation of tau positive aggregate around neuritic plaques (NP-tau) followed by NFTs formation. Tau spreading progressed faster and further in presence of Aβ, suggesting an important role of neuritic plaque in the process. Interestingly, synthetic human tau preformed fibrils in presence of Aβ failed to cause pathological tau spreading (He et al., 2018).

Li et al. proposed a two steps mechanism for AD development: first Aβ accumulates with age but do not cause the disease and then a secondary event would cause tau conversion into pathological forms and trigger AD pathology. Once the initial tau conversion occurred, Aβ plaques allow spreading by conversion of endogenous tau into more pathological tau. According to He et al. the tau conversion into pathological tau occurs at the level of the neuritic plaques where the presence of Aβ already caused soluble tau accumulation and phosphorylation.

The secondary event that causes the initial tau conversion could be multifactorial and involves other risk factors for AD such as *APOE* ε4. The requirement of a secondary event might explain the late onset of sporadic AD as well as the diversity of pathological manifestations. In addition, according to this model, age-related Aβ plaques are harmless as long as WT tau is not converted into a pathological form able to spread throughout brain tissue. It might therefore provide reasonable explanations why Aβ deposits do not necessarily correlate with cognitive decline and why some people live cognitively healthy despite they harbor significant Aβ burden.

The mechanisms or possible factors involved in the pathogenic conversion of tau remain to be elucidated. Nevertheless, these findings may also provide clues for the recent failure of anti-Aβ therapies and guide future therapeutic approaches. Indeed, anti-Aβ interventions may not be effective when applied after initial tau conversion. But it appears that the neuritic plaques forming near Aβ deposits constitute a very specific environment that may play a critical role in AD development.

Interaction of Aβ and tau at the level of the neuritic plaques

In addition of playing an important role in tau spreading, the synergetic relationship of Aβ and tau at the level of the dystrophies in neuritic plaques could also be involved in synapse dysfunction. Synaptic dysfunctions and synaptic loss, which usually precede neuronal loss, are highly correlated with the emergence of cognitive deficits in patients (DeKosky and Scheff, 1990). As discussed earlier, synapse loss occurs around neuritic plaques and is another important hallmark of AD.

It was shown that toxic Aβo act as pathological ligands and target particular synapses, co-localizing with the postsynaptic density protein 95 (PSD95) (Lacor et al., 2004). It is well established that acute Aβ exposure impairs synaptic functions, induces long-term depression (LTD) and inhibits long-term potentiation (LTP) (Li et al., 2011, 2009; Shankar et al., 2008). Aβ effect on LTD required NMDA receptor activity (Shankar et al., 2007) and is thought to be mediated by NMDA receptor internalization (Snyder et al., 2005). However, several other receptors such as the prion protein (Laurén et al., 2009) and the

α7-nicotinergic receptors (Wang et al., 2000) have been involved in Aβo synaptotoxicity.

Consequently, it is likely that several receptors are involved in Aβo mediated synapse loss (Crimins et al., 2013; Ittner and Götz, 2011). The downstream molecular mechanisms behind the Aβo toxicity will not be reviewed here. Instead, we will focus on tau and Aβ interaction at the level of the dendrites as this interaction might be especially relevant in the context of AD.

It was first demonstrated *in vitro* that tau is essential for Aβ-induced neurotoxicity mediated by Aβ fibrils or dimers (Rapoport et al., 2002). Indeed, cultured hippocampal neurons from tau knock-out mice were resistant to Aβ-induced degeneration (Rapoport et al., 2002). In mouse, knocking-out tau also reduced neuritic disruption caused by the injection of toxic Aβ dimers derived from AD brain (Jin et al., 2011). In the same experiment, overexpression of human tau potentiated Aβ dimers toxicity, confirming the role of tau in Aβ-mediated toxicity.

In tau knock-out mice, the protection against Aβ toxicity was associated with a reduced localization of tyrosine protein kinase FYN at the level of the dendrites (Ittner et al., 2010). The study unveiled an additional function of the protein tau in the dendritic compartment (See Figure 7).

Besides its axonal role in microtubule stabilization, tau also acts as a postsynaptic scaffolding protein. Tau binds to FYN and controls its localization in the postsynaptic compartment. This localization has an important role as FYN can phosphorylate the NMDA receptor and mediate its association with PSD95. When soluble Aβ is present and binds to the NMDA receptor, the tau-induced NMDAR-PSD95 association is required for downstream excitotoxicity (Salter and Kalia, 2004). Consequently, the relocalization of tau in the dendrites increases Aβ toxicity. In tau knock-out neurons, the postsynaptic level of FYN is reduced, preventing NMDAR-mediated excitotoxicity in presence of Aβ (Ittner and Götz, 2011). In addition, it was demonstrated *in vitro* that phosphorylated tau has a stronger interaction with FYN, leading to an increase of FYN-tau localization in the synapse (Bhaskar et al., 2005).

Thereby, hyperphosphorylated tau in AD can further increase Aβ toxicity. It may contribute to the specific vulnerability of the neurons located around Aβ plaques, as the level of tau phosphorylation is likely to be increased in the vicinity of the Aβ plaques. This may trigger a vicious toxic circle.

Figure 1-7. Aβ and tau interaction at the level of the synapse

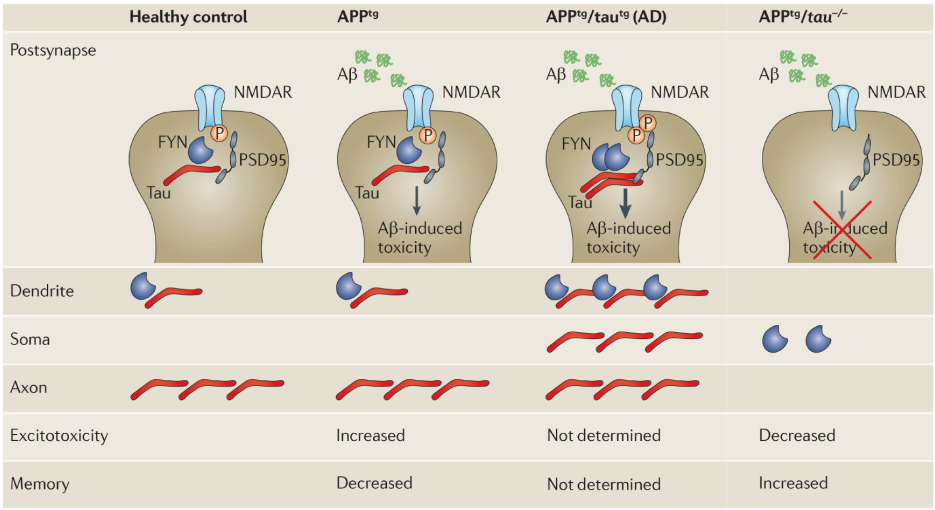

Figure 7: Aβ and tau interaction at the level of the synapse
Under physiological condition, tau is able to act as a scaffolding protein, recruiting FYN to the dendritic compartment. FYN can phosphorylated NMDAR and mediate its assembly with PSD95. In presence of Aβ peptide (APP^{tg} mice), this interaction allow NMDAR excitotoxicity. In the case of AD, especcially around neuritic plaque, tau is hyperphosphorylated (APP^{tg}/tau^{tg} mice). Hyperphosphorylated tau is able to recruit more FYN, increasing NMDAR phosphorylation and its association with PSD95, as well as Aβ-induced toxicity. In absence of tau ($APP^{tg}/tau^{-/-}$ mice) FYN localization in the dendrite is highly reduced, preventing the NMDAR-PSD95 complex formation Aβ neurotoxicity.
Illustration from *Nature Reviews Neuroscience,* volume 12, pages 67–72 (2011)

Evidence for the interaction between Aβo and the scaffolding role of tau was demonstrated *in vivo* using the ArcTau mouse model (Chabrier et al., 2012). ArcTau mice overexpress the Aβ Arctic mutation, which enhances the production of soluble Aβ oligomers and proto-fibrils and also overexpress WT human tau. In order to modulate the level of soluble Aβ, this ArcTau mouse model was crossed with the BACE heterozygous knock-out mouse model (BACE+/-). ArcTau BACE+/- mice exhibited reduced soluble Aβ compared to their ArcTau BACE+/+ littermates. Co-precipitation of PSD95 showed a reduction of the NMDA receptor complex formation when the level of soluble Aβ was reduced. In addition, a decrease of human tau and FYN associated with PSD95 was observed. These results illustrate the ability of soluble Aβ to modulate this pathway *in vivo*.

Again, these studies highlight the importance of the synergistic toxic effects of tau and Aβ, which may occur in the neuritic plaque environment. However, it is important to keep in mind that this is one of the many molecular pathways involved in Aβ and tau toxicity. In several instances, Aβ and tau toxicity tend to affect different component of the same system leading to an increased toxicity when combined. For example, both Aβ and hyperphophorylated tau impair mitochondrial respiration (Rhein et al., 2009). Whereas Aβ affects complex IV, pathological tau preferentially affects complex I. Consequently; mice combining Aβ and tau pathologies exhibit an amplified mitochondrial dysfunction, as compared to mice overexpressing Aβ or tau alone (Rhein et al., 2009).

The interplay of Aβ and tau pathologies is likely to play a key role in sporadic AD development. However, other factors are also involved in the disease. Among them, microglia were shown to play a crucial role. Modulation of microglia activity affects both Aβ and tau pathologies, and microglia dysfunction is tightly linked to aging. In the past few years, AD has been more and more perceived as a neuroinflammatory disease, with a strong implication of microglia dysfunction. Some of these findings will be reviewed in the next Chapter.

1.3.2 Microglia

Microglia function

Microglia are the primary innate immune cells of the central nervous system (CNS). They are distinct from the peripheral myeloid cells and have their own brain resident progenitors to self-renew their population (Askew et al., 2017). Microglia differs from peripheral myeloid cells as they express macrophage markers but have their unique homeostatic signature (Butovsky et al., 2014).

Microglia have two main roles in the CNS: homeostasis maintenance and response to neuronal injury (Butovsky and Weiner, 2018). In order to fulfill their role, microglial cells display phenotypes that are extremely heterogeneous, allowing them to respond to various triggering factors and adapt. During the adulthood under homeostatic conditions, microglia participate to neural circuitry shaping and neurogenesis (Sierra et al., 2010). They also prune axons and synapses that are not active (Schafer et al., 2012) and undergo routine non-

inflammatory clearance of dead brain cells (Mazaheri et al., 2014). In addition, they secrete neurotrophic factors to promote synaptic plasticity, participating in learning and memory (Parkhurst et al., 2013). In case of injury, activated microglia promote inflammation, phagocytosis and undergo cell proliferation (Heneka et al., 2015). In case of chronic activation however, microglia are able to produce multiple neurotoxic factors and can participate in neuronal damage and neurodegeneration (Lull and Block, 2010).

Basically, microglia can be found in two states: a surveillance state that is characterized by their homeostatic signature and an activated state, much more heterogeneous. In order to better understand the role microglia in disease and health, extended efforts have been made to categorize them according to their gene expression. It became quickly evident that such a task was extremely complex as microglia failed to be simply divided in the pro- and anti-inflammatory dichotomy (Holtman et al., 2015; Sarlus and Heneka, 2017). Instead microglia activation profiles can be highly diverse, depending on the type of injury or disease.

The regulation of these different states is extremely important to maintain a healthy environment in the brain but will not be discussed in details in this work. Instead, we will focus on microglia role in the AD pathology and more precisely their interaction with Aβ and tau.

Long neglected, microglia activation surrounding senile plaques in AD has already been described by Dr. Alois Alzheimer in its original publication (Stelzmann et al., 1995). However, it was considered as a secondary non-specific inflammatory event caused by Aβ (Heneka et al., 2014). A strong interest for microglia aroused with the first GWAS in AD (Hollingworth et al., 2011). It occurred that an important number of the genes associated with an increased risk of developing AD were either expressed by microglial cells or linked to microglia activation. These findings suggest that microglia dysfunction could actively contribute to the disease. Study of these genes has opened a new area for AD research.

Microglia as a protector against Aβ toxicity

As part of their ability to monitor their environment, microglia are able to sense Aβ (Zhao et al., 2018). Aβ deposits rapidly attract microglia and activate phagocytosis. In addition, microglia processes interact tightly with Aβ plaques and compact them. It was demonstrated that this microglial barrier reduces Aβ oligomer release from the plaques and prevents neurotoxicity around the amyloid plaques (Condello et al., 2015). According to the bioflocculant hypothesis, Aβ binds to toxins, such as metal ions, and precipitates them into local deposits (Robinson and Bishop, 2002). The anticipated role of microglia is to detect the presence of these Aβ deposits, in order to rapidly eliminate both the aggregated peptide and the co-precipitated toxic material (Robinson and Bishop, 2002). During that process, microglia also protect the surrounding brain parenchyma and act as a tight barrier to prevent toxic release from the plaques. As discussed earlier, it is now accepted that Aβ plaques alone are not able to trigger neurodegeneration and Alzheimer's disease (Li et al., 2016). Consequently, under normal conditions, it is likely that microglia activation surrounding plaques has a protective role in the brain.

GWAS studies linked genetic risk of AD and microglia

GWAS studies have brought clear evidence that the risk of developing late-onset AD is often associated with variations in genes which regulate microglial function (Bertram and Tanzi, 2009; Waring and Rosenberg, 2008). In particular, some of these genes including *APOE*, *TREM2* and *CD33*, are modulating microglial ability to remove Aβ deposits, suggesting that the interaction between microglial cells and Aβ plaques plays a critical role in the risk of developing AD.

APOE protein, which E4 variant is the major genetic risk factor for AD, is mostly expressed by astrocytes and microglia (Kim et al., 2009). In addition of driving APP transcription (Huang et al., 2017), APOE protein is strongly upregulated in microglia in presence of Aβ and is able to modulate microglia activation (Uchihara et al., 1995). APOE is thought to act together with TREM2. In conditions leading to AD, these two genes may contribute to microglial dysfunction (Krasemann et al., 2017).

The gene encoding the Triggering receptor expressed on myeloid cells 2 *(TREM2)* was first identified as a significant risk factor in a linkage-study for late-onset AD (Butler et al., 2009). Heterozygous *TREM2* variants, such as R47H, cause *TREM2* loss-of-function and are associated with almost a 3-fold increased risk of AD (Guerreiro et al., 2013; Jonsson et al., 2013). TREM2 protein is a receptor at the microglial surface able to detect damage-associated lipids as well as Aβ (Zhao et al., 2018). Its activation helps microglia to maintain their phagocytic ability, to degrade Aβ and to play their barrier role by clustering around the Aβ plaques (Yuan et al., 2016; Zhao et al., 2018). TREM2 deficiency, in the other hand, reduces microglia clustering around Aβ plaques (Jay et al., 2015; Wang et al., 2016; Yuan et al., 2016; Zhao et al., 2018).

Single-nucleotide polymorphism (SNP) in the *CD33* gene has also been found to be associated to the risk of AD by modulating Aβ phagocytosis. Indeed, it was observed that the minor allele (T instead of G) of the SNP rs3865444 situated in the *CD33* promoter region is protective against AD (Hollingworth et al., 2011). Individuals with this minor *CD33* SNP have reduced CD33 protein levels and reduced risk to develop the disease, suggesting a deleterious role for the CD33 protein (Bradshaw et al., 2013). Further studies showed that increased CD33 expression in AD impaired microglia Aβ42 uptake, slowing down Aβ clearance (Griciuc et al., 2013).

Therefore, APOE, TREM2 and CD33 protein functions highlight the importance of Aβ clearance in the context of AD. All together, these results suggest that efficient sensing by microglia and phagocytosis of Aβ throughout life is key in reducing the risk of developing the disease.

Disease-associated microglia

It was demonstrated that 5xFAD mouse brains exhibit two small populations of microglial cells that were not present in WT littermates (Keren-Shaul et al., 2017). This observation is compatible with the idea that a population of microglial cells is dedicated to Aβ clearance in AD. Using massive parallel single cell RNA sequencing, these two populations, which appear in response to Aβ accumulation, were categorized as disease-associated microglia and intermediate state microglia. Using sub-tissue single cell RNA sequencing, these

disease-associated microglia were then located around Aβ deposition. Microglia transitioned from the homeostatic to the disease-associated state through the intermediate state. This transformation allowed microglia to respond to Aβ accumulation by increasing their Aβ clearance ability. These microglia populations express microglial markers but also display a reduced homeostatic signature, coupled with patterns of gene expression corresponding to lipid metabolism and phagocytic activity. The different facets of disease-associated microglia in AD are illustrated in Figure 8.

Figure 1-8. Microglia functions in Alzheimer's disease

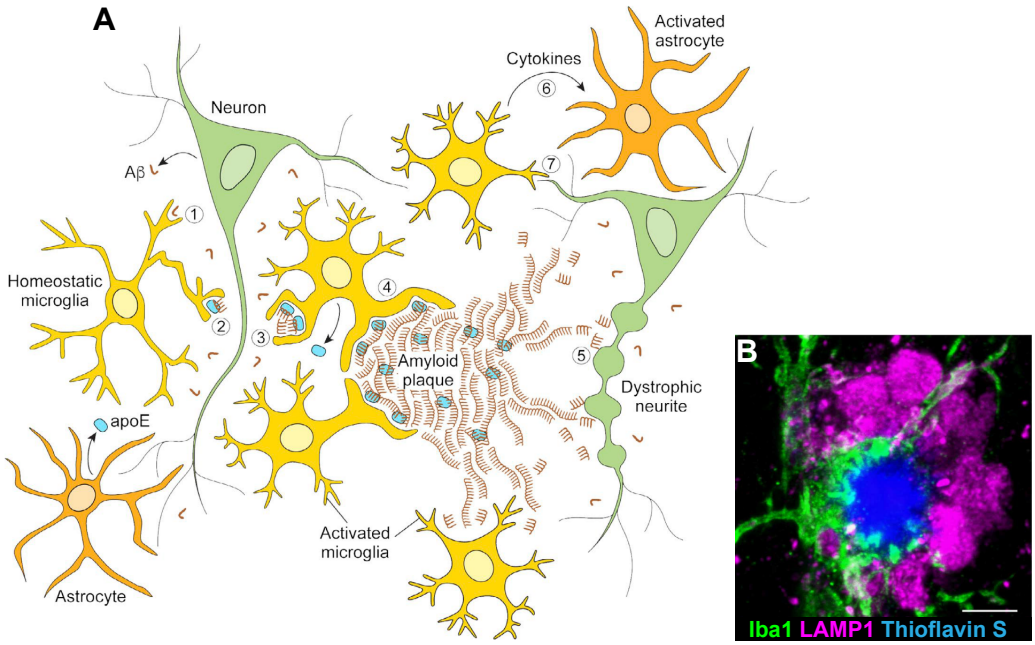

Figure 7: Microglia functions in Alzheimer's disease

A | (1-3) Microglia are able to phagocytose Aβ from monomers to fibrils. **(4)**Around large Aβ deposits, microglia can act as a protecting barrier reducing diffusion of Aβ toxic species. **(5)** Failur of microglia to act as a barrier leads to the formation of dystrophic neurites. **(6)** Microglia activation can become detrimental and maintain chronic inflammation through secretion of pro-inflammatory cytokines. **(7)** They can also cause synapse loss through synapse pruning. Illustration from *Journal of Cell Biology*, volume 217, number 2, pages 459 (2010)

B | Confocal image of microglia (in green) acting as a protecting barrier around an Aβ plaque (in blue), preventing the formation of dystrophic neurites (in magenta). Image from *Nature Communications*, volume 6, Article number: 6176 (2015).

TREM2 is required for efficient microglia activation against Aβ

The complete transformation of the microglia from the intermediate to disease-associated requires *TREM2* (Keren-Shaul et al., 2017). It is currently well documented that TREM2 is important for microglial activation, not only in the context of Aβ accumulation, but also in case of neuronal degeneration due to tau

aggregation (Bemiller et al., 2017; Keren-Shaul et al., 2017; Leyns et al., 2017; Wang et al., 2016; Zhao et al., 2018). In WT mice, *TREM2* is required for microglia response against neuronal injury (Mazaheri et al., 2017). A plausible hypothesis is that *TREM2*-deficient microglial cells are locked in resting state and remain unable to respond to threats such as Aβ accumulation. Consequently, both the activity of the TREM2 protein as well as disease-associated microglia would be necessary to fight against AD.

Activated microglia, friend or foe?

Further studies on the effect of microglia depletion and *TREM2* deficiency show that the situation is likely to be more complex. The stage of the disease seems to play a very important role. Indeed, microglia depletion or impairment of microglia activation through *TREM2* deficiency can be either beneficial or detrimental. *TREM2* deficiency in Aβ mouse models always reduced microglia clustering around Aβ plaques. However, it also reduced Aβ deposition at early stages of the disease (Jay et al., 2015) and was found to exacerbate Aβ pathology only at later stages (Jay et al., 2017). The same phenomenon happens with tau pathology. In hTau mouse model, a mouse model expressing human WT tau but not the endogenous mouse tau (Andorfer et al., 2003), *TREM2* deficiency increases tau pathology (Bemiller et al., 2017). Whereas in the P301S tau mouse model, *TREM2* deficiency reduced tau pathology (Leyns et al., 2017). In both models however, *TREM2* deficiency did reduce microglia activation as expected. Therefore, these results suggest an important difference in the role of microglia when interacting with mutant or WT human tau, or a possible role of endogenous mouse tau.

Whether microglia are beneficial or detrimental in AD is therefore a complex question that may have multiple answers and which will require further analysis. It was shown that microglia can both alleviate or contribute to various facets of AD pathology, such as Aβ burden, tau aggregation, synaptic loss and cognitive impairment. The heterogeneity of microglia and their versatile ability to rapidly change their phenotype depending on the local environment is thought to underlie these apparently contradictory results. Consequently, activation or inhibition of the same genes could shift microglia activation towards protective

or rather detrimental activity, depending on the mouse model, the time of the intervention or the severity of the disease.

Chronic activation of microglia

It is thought, however, that as the disease progresses, microglia tend to lose their initial beneficial role and become neurotoxic in AD (Jimenez et al., 2008). Indeed, similar to all innate immune reactions, microglia activation should be transient and carefully controlled in order to be beneficial. In the case of acute injury, exposure to pathogens or transient Aβ deposition, microglia become activated and quickly resolve the situation, to restore homeostatic conditions. In the context of AD however, the situation is different as chronic exposure of microglia to Aβ deposition leads to continuous inflammation (Heneka et al., 2015). Therefore, the noxious neuroinflammatory environment induced by exposure to Aβ might cause microglia dysfunction (Krabbe et al., 2013; Streit et al., 2009). Microglia dysfunction may induce aberrant synapse pruning (Hong et al., 2016) and Aβ spreading through apoptosis associated speck-like protein (Venegas et al., 2017). Other factors such as age and tau accumulation may also contribute to these detrimental processes.

The influence of aging on microglia

Aging is the most important risk factor for AD and, in microglia, aging is known to dysregulate the expression of homeostatic genes and affect the ability of these cells to sense homeostatic signaling (Butovsky and Weiner, 2018). The downregulation of homeostatic genes leads to a “primed microglia” state, with an lower threshold for activation (Perry and Teeling, 2013). This activity profile is thought to be triggered by low chronic activation (Holtman et al., 2015). In addition, due to this chronic activity, aged microglia also lose their ability for effective phagocytosis. Chronically activated microglia found around plaques in AD display very similar profiles (Yin et al., 2017), suggesting that common mechanisms may be involved in both aging and AD in terms of microglia impairment (Hickman et al., 2013; Holtman et al., 2015). In conclusion, age is very likely to increase the risk that microglial cells engage detrimental patterns of activity, in particular in the challenging conditions typically associated with neurodegenerative diseases.

Influence of tau on microglia

Exposition to tau might also be involved in abnormal and neurotoxic behavior of microglia in AD. In humans, Streit et al. showed the presence of dystrophic fragmented microglia in old age subjects or in the presence of tau pathology, but not in the case of Aβ plaque accumulation only (Streit et al., 2009, 2004). This finding was confirmed in the marmoset (Rodriguez-Callejas et al., 2016). Dystrophic microglia, but not active microglia, were found to be immunoreactive for phosphorylated (AT100) or early aggregated (Alz50) forms of tau. It was suggested that long-term phagocytosis of tau might cause premature senescence of microglia (Navarro et al., 2018). A recent Nature publication by Bussian et al. also revealed increased senescent glia bearing the cell cycle inhibitory protein $p16^{INK4A}$ in a mutant tau mouse model. More interestingly, the selective elimination of these dysfunctional glial cells can prevent dentate gyrus degeneration and improve the cognitive function of these animals (Bussian et al., 2018). Further corroborating the role of tau in microglia dysfunction in AD.

Microglia as an amplifier of tau pathology

Once aberrantly activated, microglia might be able to amplify the pathological effects of tau, including neuronal loss, leading to a catastrophic vicious circle.

It was demonstrated in different mouse models overexpressing mutant tau, with or without Aβ, that increased microglia activation exacerbated mutant tau phosphorylation and aggregation (Chen et al., 2016; Kitazawa et al., 2005; Yoshiyama et al., 2007). This effect on mutant tau was triggered by acute microglia activation using lipopolysaccharide (Kitazawa et al., 2005) as well as chronic microglia activation due to Aβ (Chen et al., 2016) and tau accumulation (Yoshiyama et al., 2007). Immunosuppression using FK506 had the opposite effect and reduced P301S tau pathology (Yoshiyama et al., 2007). In the hTau mouse model, a mouse model expressing human WT tau but not the endogenous mouse tau, acute microglial activation using lipopolysaccharide also induced hyperphosphorylation and aggregation of tau (Bhaskar et al., 2010).

This increased aggregation of tau, due to microglia activation, has then the ability to aggravate neuronal loss. Indeed, live neurons with tau aggregates appear to

expose “eat me” phosphatidylserine signals. These neurons are then opsonized and phagocytosed by microglia (Brelstaff et al., 2018). Uptake of tau inclusion present in these neurons by microglia, in turn, further increases microglia dysfunction and tau pathology.

In addition, it has also been proposed that microglia can propagate tau pathology (Asai et al., 2015). When ubiquitinated, tau aggregates internalized by microglia, can be incorporated in the microglia exocytotic pathway and released by microglia via exosomes. These exosomes can then transduce tau to neurons, further seeding tau pathology (Asai et al., 2015).

In conclusion, there is a lot of evidence that once the disease is established and tau pathology initiated, microglia play an important role which may contribute to disease worsening.

1.4 Perspectives in passive anti-Aβ immunization

Based on the Aβ hypothesis, most preclinical studies for passive anti-Aβ were performed in mouse models exhibiting Aβ pathology only. At the time, the importance of Aβ and tau interaction, especially at the level of the neuritic plaque, was unknown. Consequently, it exists only few studies investigating the effect of passive Aβ immunization on tau pathology, or on the effect that tau could have on the efficacy of passive Aβ immunization, by modulating the microglial response for example.

1.4.1 Interaction of passive anti-Aβ immunization and tau

A study published in 2004 demonstrated that intra-hippocampal injection of anti-Aβ antibodies in 3xTg mice reduced mutant tau accumulation in the somatodendritic compartement (Oddo et al., 2004). The 3xTg mouse model is based on the overexpression of mutated forms of human APP and PS1, as well as human tau carrying the P301L mutation. In this study, the somatodendritic hyperphosphorylated tau reduction was following Aβ removal and was more efficient if the anti-Aβ antibody was administrated early during the course of the disease. However, passive immunization did not reduce NFTs, suggesting that well-established tau pathology was resistant to passive immunization against Aβ. This is an important point as the development of tau pathology is considered to more closely correlate with cognitive decline in AD patients than Aβ burden.

In 2011, Wilcock and al. pointed out that microglia activation was different in presence or absence of tau pathology and neurodegeneration (Wilcock et al., 2011). Wilcock et al. crossed an APP mouse model developing Aβ plaques with a nitric oxide synthase (NOS) knock-out mouse model that develop tau pathology and neurodegeneration (Huang, 2000). The resulting mouse model (APP/NOS$^{-/-}$) developed Aβ deposits followed by tau pathology and neuronal loss (Wilcock et al., 2011). In the APP/NOS$^{-/-}$ mouse model, the microglial activation pattern was different than in APP mice. In both animal models, the administration of passive immunization shifted the immune response towards activation of pro-inflammatory genes and triggered microglia-mediated clearance of Aβ. However,

further studies are needed to understand the effects of passive immunization against Aβ in the context of the tau pathology.

In the following studies, we aimed to address this question by investigating how passive anti-Aβ immunization affect tau pathology and if tau pathology can, in return, have an effect on passive immunization.

In addition, we also aimed on improving the available technologies for passive immunization and more precisely, improve antibody delivery for chronic application.

1.4.2 The need for alternative techniques to continuously deliver antibodies in applications that require chronic exposure

As discussed previously, there are still several ongoing phase-III clinical trials testing the efficiency of passive anti-Aβ immunization. The prevention trials on patients with autosomal familial AD, DIAN-TU and API, will determine if administration of anti-Aβ antibodies before the onset of the disease could be efficient. In case these trials show some effects on disease progression, the prevention study will raise important issues for which the scientific community needs to develop dedicated technologies. The chronic administration of anti-Aβ antibodies over years or even decades for AD prevention is going to be a challenge for the industry, for the society and for the patient himself. Antibody production and delivery are two mains questions that would need to be addressed.

The industry will have to develop cost-efficient and fast ways to produce high amounts of recombinant antibodies. In addition, administration of the antibody will require monthly visits to the hospital and medical staff intervention. Both will have an impact on health costs and limit the applicability of these treatments. Even though costs linked to AD might decrease if the rate of cognitive decline is slowed down in the treated patients, the benefits of the treatment for the society at large could be overshadowed by its actual cost. Other questions will need to be taken into account, such as patient compliance, or the development of effective biomarkers to identify patients at risk during the early phase of the disease.

In this context, we believe that alternative methods for antibody delivery and production need to be developed.

Encapsulated Cell Technology for continuous antibody delivery

Among the possible approaches, Encapsulated Cell Technology (ECT) can be used to implant human cells genetically engineered to continuously secrete a recombinant antibody. In this chapter, we will only discuss the use of macroencapsulation devices that can be safely retrieved from the body. The principle of ECT is to isolate the producing cells from the surrounding host tissue using a porous membrane. The main purpose of encapsulating the cells within a permeable polymer membrane is to protect them from host immune rejection by preventing any cell-to-cell contact with host immune system. This approach has been shown to allow for long-term survival of cells in allogeneic conditions.

For some applications, ECT implants contain cells that are engineered for recombinant protein production (Uludag et al., 2000). As ECT allows for allogeneic transplantation, it is possible to use a single renewable source of engineered cells for all recipients (Duvivier-Kali et al., 2001). The porous membrane is permeable to macromolecules and allows the cells to be supplied with nutriments and oxygen by diffusion. Once successfully engrafted, the cells continuously produce the protein of interest, which diffuses outward of the implant, to be systemically distributed in the recipient organism via the blood flow. ECT can also be used for *in situ* protein production after a surgery, in the case of cancer for example (Orive et al., 2015).

Flat-sheet implant for subcutaneous release of anti-Aβ antibodies

Although the potential use of ECT is broad, one of the main challenges is to engineer an implant able to produce the protein of interest in sufficient quantities to achieve therapeutic efficacy. Because antibodies are highly specific and can be efficient even at low dose, ECT is particularly adapted to antibody production and delivery for applications, which require chronic exposure.

In the context of AD, we engineered an implant based on ECT to continuously deliver anti-Aβ antibodies (Lathuilière et al., 2015). The progressive increase in antibody secretion during the initial phase of implantation might be able to

mitigate ARIA incidence at the beginning of the treatment, whereas continuous antibody delivery following engraftment is expected to maintain antibody plasma concentration at a steady level during the long-term implantation phase.

The concept of the "flat-sheet" device developed by Lathuilière et al. is to maximize antibody delivery following subcutaneous implantation (Lathuilière et al., 2014b). The device is a flat implant with only 1.2 mm thickness. The shape was chosen in order to obtain a large inner volume, while maintaining a small distance between the grafted cells and the host blood vessels, a critical factor for oxygen supply within the capsule. In addition, the device was optimized to facilitate implantation in the subcutaneous tissue. The system was tested in mice for implantation of the murine C2C12 myoblast cell line. The proof-of-concept *in vivo* studies demonstrated that through optimization, cells were able to grow and survive at high cell density for months within the implant. Optimal cell seeding conditions were determined in order to maximize cell survival inside the device.

Cells were then genetically modified using lentiviral vectors to express mAb11, a murinized recombinant anti-Aβ IgG2a antibody. By selection of single cell clones, a cell line with high mAb11 antibody expression level was isolated, which was demonstrated to long-term survive inside the device (Lathuilière et al., 2014a). The implant progressively secreted recombinant antibodies. Plasma antibody levels reached a plateau after 4 months of device implantation and remained stable up to month 10 (Lathuilière et al., 2016).

These studies showed that ECT is a potential alternative technology for the continuous delivery of recombinant antibodies. Proof-of-concept that ECT is able to secrete enough anti-Aβ in AD mouse models to reduced Aβ burden will be discussed later in the result section.

1.5 Aims of the thesis

The topic of this thesis is focused on the development and efficacy testing of continuously delivery of anti-Aβ antibodies in the subcutaneous tissue using encapsulated cell technology (ECT), as an approach for passive immunization against Alzheimer's disease.

In the first part of the thesis, we use ECT for anti-Aβ antibody administration in the TauPS2APP triple transgenic mouse model. We determine the effects of anti-Aβ passive immunization on amyloid beta and tau pathologies when applied *before the onset of plaque deposition* in this mouse model of Alzheimer's disease.

In the second part, our aim is to assess the effects of Aβ passive immunization when applied *in the context of established Aβ and tau pathologies*. Towards this goal, we developed a mouse model of the Alzheimer's pathology based on 5xFAD mice, which show an aggressive Aβ pathology. In order to explore possible interactions between Aβ and tau pathologies, the mice are injected in the hippocampus with an AAV-tau vector to induce local overexpression of the wild-type 4R0N human tau protein. We investigate how Aβ and tau, respectively, contribute to Alzheimer's pathological hallmarks, and how they affect microglia activation. Finally, we determine the effects of ECT-mediated anti-Aβ immunization in this mouse model of combined Aβ and tau pathologies.

In the last chapter, our aim was to further develop the ECT for translation into human applications. The goal was to adapt the system using a *renewable cell source of human origin*, in order to avoid the need for implantation of mouse myoblasts, which are likely to elicit a strong immune response in xenogeneic conditions. Here, we consider that continuous delivery of recombinant antibodies using ECT is not limited to anti-Aβ immunization and may find application for a broad range of applications, both inside the central nervous system and in the periphery.

2

Chapter 2 : Effect of early administration of passive anti-Aβ immunization using encapsulated cell technology

Vanessa Laversenne[1], Aurélien Lathuilière[1], Alberto Astolfo[2], Erhard Kopetzi[3], Helmut Jacobsen[4], Marco Stampanoni[2], Bernd Bohrmann[4], Bernard L. Schneider[1,*] and Patrick Aebischer[1,*]

* These authors contributed equally to this work.

1 Neurodegenerative Studies Laboratory, Brain Mind Institute, Ecole polytechnique Fédérale de Lausanne (EPFL), CH-1015 Lausanne, Switzerland

2 Swiss Light Source, Paul Scherrer Institute (PSI), 5232, Villigen-PSI, Switzerland

3 Pharma Research and Early Development, DTA Neuroscience, Roche Innovation Center Penzberf, F. Hoffman-La Roche, Switzerland

4 Pharma Research and Early Development, DTA Neuroscience, Roche Innovation Center Basel, F. Hoffman-La Roche, Switzerland

(Published work)

2.1 Abstract

Passive anti-Aβ immunization in the context of Alzheimer's disease (AD) has been extensively studied in the past 15 years. Antibodies targeting different forms of Aβ from soluble monomers to Aβ plaques have been tested in phase III clinical trials. Besides evidences of target engagement, and in some case reduction of Aβ burden, none of these antibodies showed clinical benefits for the patients. One of the current hypotheses in the field is that the antibodies have been administered too late. According to this point of view, once the disease is already established, passive anti-Aβ immunization is not able to affect cognitive decline.

In this context, we investigated the administration of passive anti-Aβ immunization before the onset of the disease (primary prevention) in the TauPS2APP mouse model. TauPS2APP mouse model exhibits both progressive Aβ pathology and tau (P301L) pathology starting at 4 months. We used encapsulated cell technology (ECT) in order to achieve continuous administration of the antibody subcutaneously. For primary prevention, animals were implanted at 2 months.

ECT-mediated administration of the antibody before the onset of the disease significantly prevented Aβ deposition in the cortex, the hippocampus and the thalamus of treated animals. Interestingly, it also significantly reduced pathological tau phosphorylation and tau misfolding in the somatodendritic compartment of hippocampal neurons.

For further applications, we also evaluated early implantation (5-6 weeks) in the 5xFAD mouse model (B6SJL background). In this model, soluble Aβ appeared at 6 weeks of age and Aβ deposition at 8 weeks. Consequently, these animals were implanted at the onset of the disease. In this second, more aggressive AD mouse model, ECT continuous administration modulated Aβ pathology and reduced the number of Aβ plaques in the hippocampus but did not reduce Aβ burden in any of the assessed brain regions.

2.2 Effect of passive anti-Aβ immunization before the onset of the disease in an AD mouse model with Aβ and P301L tau.

2.2.1 Introduction

Passive immunization against aggregated toxic proteins is a promising approach to treat neurodegenerative disorders. Unfortunately, in the field of Alzheimer's disease (AD), the pharmaceutical industry repeatedly failed to improve cognitive decline using passive immunization against amyloid beta (Aβ). In January 2019, Roche reported the failure of phase III clinical trials CREAD 1 and 2 with the antibody Crenezumab initially developed by the company AC Immune, and two months later, Biogen halted the Aducanumab phase III trial for futility. After these recent events, it appears even more crucial to further explore the mechanisms of action of the anti-Aβ antibodies tested in clinical trials.

In this study, we focused on the anti-Aβ antibody mAb11 developed by Roche during their pre-clinical studies on Gantenerumab. MAb11 shares similar important features with Gantenerumab (Bohrmann et al., 2012): it binds to a conformational epitope of the Aβ peptide in order to target the aggregated form of the protein. In addition, its constant chain is designed to activate cell-mediated Aβ plaque removal (Bohrmann et al., 2012; Xiang et al., 2016). Gantenerumab is still currently tested in the new GRADUATE phase III trial. Compared to previous clinical trials of Gantenerumab, the novelty of the present trial resides in the antibody dosing: it is gradually increased over time to reach a monthly subcutaneous dose of 1200mg. In addition, Gantenerumab is being tested in the Dominantly Inherited Alzheimer Network Trials Unit (DIAN-TU) in order to assess if it could slow or prevent disease progression in autosomal dominant familial AD (Bateman et al., 2017). In DIAN-TU, the treatment is administrated long before the onset of the disease as a primary preventive approach. In this context, it is relevant to study the mechanisms of action of a similar antibody such as mAb11. In addition, for both applications, the use of encapsulated cell technology (ECT) for gradual and continuous subcutaneous antibody delivery is of potential relevance.

Lathuilière et al. performed the first studies using the subcutaneous delivery of the mAb11 antibody by ECT (Lathuilière et al., 2014b, 2014a). The results showed that the antibodies can be successfully secreted using ECT, reaching concentrations in the plasma up to 60 μg/ml (Lathuilière et al., 2016). It was demonstrated that the antibody could cross the blood brain barrier and reached its target. In 5xFAD mice, the treatment significantly reduced the Aβ load by 30% in the cortex, the hippocampus and the thalamus when implanted at 5 to 11 weeks of age (Lathuilière et al., 2016).

However, due to the very aggressive Aβ pathology in 5XFAD mice, it is really difficult to perform a primary preventive treatment in this model. Indeed, the first signs of Aβ pathology appear at 6 weeks in 5xFAD mice (Oakley et al., 2006). But it is not possible to implant the mice earlier than week 5 because of their limited size. In addition, the ECT requires several weeks to secrete therapeutic amounts of antibodies. Thus, delivery of the antibody using ECT before the onset of the disease in 5xFAD model is not possible.

Consequently, in order to assess the effect of the antibody using a primary preventive approach, we used the TauPS2APP mouse model. This model exhibits much slower Aβ pathology, with few Aβ deposits at 4 months but important Aβ load around 8 months (Grueninger et al., 2010). In addition, the model also expresses mutated P301L tau and develops tau pathology. This pathology spread in the hippocampus and the amygdala starting at 4 months. Consequently, TauPS2APP is a better model to investigate the effect of a preventive approach with a continuous antibody delivery using the ECT. In addition, it is more relevant for the study AD as it combines tau and Aβ pathologies.

Note

The following chapter as well as the corresponding figures are directly extracted from the original publication in Brain (Lathuilière et al., 2016), see annex. The *in vivo* experiment on TauPS2APP mice were designed and initiated by Aurélien Lathuilière, and fully analyzed by the author of this thesis, Vanessa Laversenne.

Figure 2-1. Preventive mAb-11 delivery using ECT affects the local recruitment of microglial cells in TauPS2APP mice.

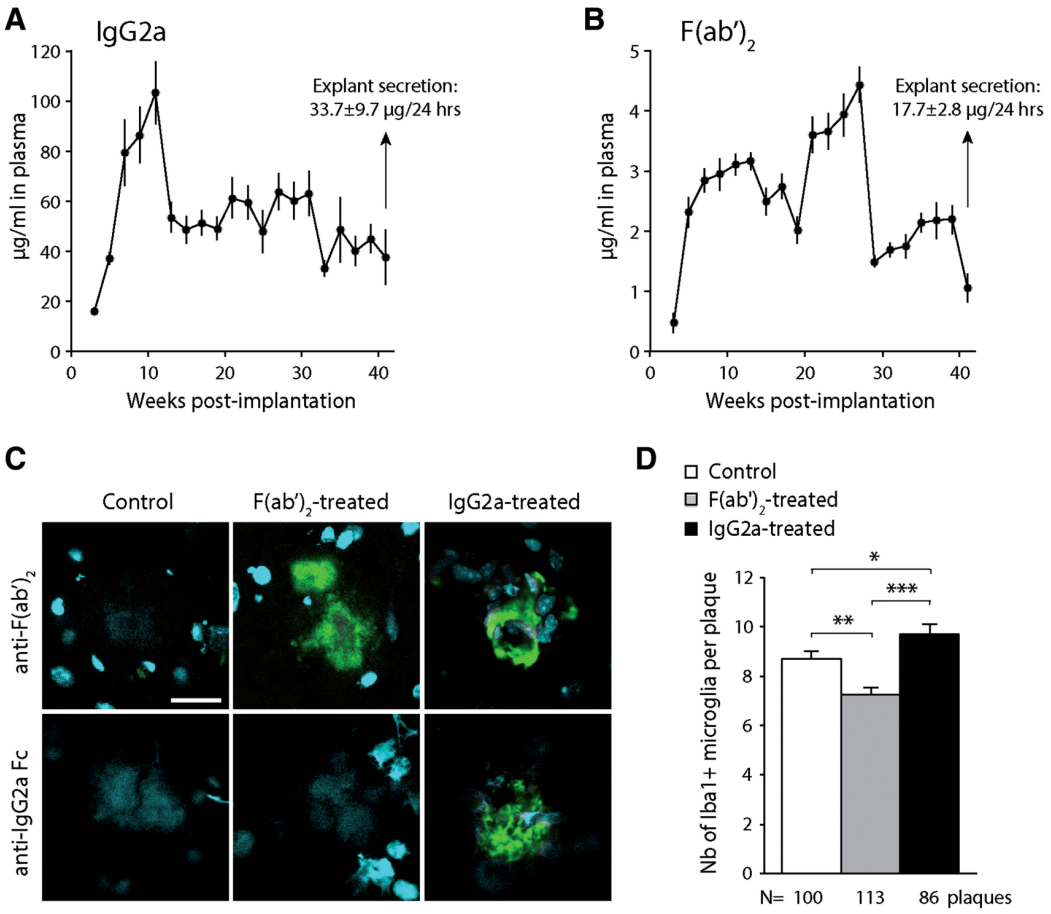

Figure 1: Preventive mAb-11 delivery using ECT affects the local recruitment of microglial cells in TauPS2APP mice.

A - B | Plasma levels of mAb-11 in TauPS2APP mice implanted for 41 weeks with devices containing either IgG2a-secreting C2C12 myoblasts (A), or F(ab') 2 fragment-secreting C2C12 myoblasts (B). The bar graph shows the mAb-11 secretion rate of the ECT devices after explantation. Data are expressed as the mean ± SEM; n = 10. **C |** Representative photomicrographs showing mAb-11 immunodecoration (green pseudocoloured immunostaining) on amyloid-β plaques in the frontal cortex of a TauPS2APP mice implanted with either control, IgG2a-secreting or F(ab') 2 -secreting devices. Note that the anti-IgG2a Fc antibody detects only the presence of the full IgG2a antibody, confirming staining specificity. Nuclei are stained with DAPI. **D |** Quantification of Iba1-positive microglial cells present around amyloid plaques in each group of mice. Note the significant decrease in microglial cell density around plaques in F(ab') 2 -treated TauPS2APP mice and the increase in IgG2a-treated mice. The number of plaques analysed in each group is indicated. Data are expressed as the mean ± SEM; F(ab') 2 - and IgG2a-treated groups: n = 10. One-way ANOVA with Newman-Keuls post hoc test: * P < 0.05, **P < 0.01, ***P < 0.001. Scale bar = 20 µm

2.2.2 Results

Preventive mAb-11 immunization by ECT reduces amyloid pathology in the brain of TauPS2APP mice

Immunization against Aβ has been shown to be most effective when initiated before the onset of plaque deposition in mouse models of AD (Das et al., 2001; Levites et al., 2006). To further assess the effect of passive immunization, we used TauPS2APP mice, a slowly progressing model, which develops both amyloid and tau pathologies, and therefore more closely mimics sporadic AD.

ECT devices were subcutaneously implanted in 2-months old TauPS2APP mice to deliver mAb-11 antibodies 6 months before the onset of amyloid deposition outside the hippocampus. The mice were transiently injected with anti-CD4 antibodies to block the anti-drug antibody (ADA) response against mAb11. Three groups of mice received either control GFP-expressing myoblasts, myoblasts secreting the mAb11 IgG2a antibody (clone #29), or myoblasts producing a mAb11-derived $F(ab')_2$ fragment. Already 3 weeks after implantation of the antibody-releasing device, both the full mAb11 IgG2a (16.2 µg/ml, Fig. 1A) and the mAb11 $F(ab')_2$ fragment (0.5 µg/ml, Fig. 1B) were detectable in the plasma of the respective groups of mice. Plasma levels then stabilized at approximately 50 µg/ml (mAb11 IgG2a) and 2 µg/ml (mAb11 $F(ab')_2$) until the experimental end-point, 41 weeks after implantation. Explanted devices showed secretion rates reaching on average 33.7±9.7 µg/24 hrs for the mAb11 IgG2a (ca. 150 kDa) and 17.7±2.8 µg/24 hrs for the mAb11 $F(ab')_2$ fragment (ca. 110 kDa). Higher secretion rate, higher stability and longer half-life of the full IgG, compared to the $F(ab')_2$ fragment, all contribute to the 25-fold difference seen in the plasma concentration. Total plasma exposure to mAb11 IgG2a during the 41-week implantation period (14.8 mg*day/ml) was estimated to be equivalent to a regimen of weekly intravenous injections at a dose of 29.5 mg/kg.

The amyloid pathology was analysed in one-year old TauPS2APP mice, 41 weeks after device implantation. The recombinant antibodies produced by ECT were found to immunodecorate Aβ plaques in the cortex of the treated mice (Fig. 1C). As expected, detection of mouse IgG $F(ab')_2$ fragments revealed the presence of both the full IgG2a and the $F(ab')_2$ fragment on amyloid plaques in the two

groups of treated mice, whereas an Fc region-specific antibody was able to detect plaque immunodecoration only in the IgG2a-treated mice. Next, we assessed if the mAb-11 treatment had any effect on the recruitment of Iba1-positive microglial cells near amyloid deposits (Congo red staining) (Fig. S1 and Fig. 1D). In the cortex of control TauPS2APP mice, there were on average 8.7±0.3 Iba1-positive microglial cells neighbouring Congo-red-stained individual plaques. The number of microglial cells around plaques was significantly decreased to 7.3±0.3 in the $F(ab')_2$ treated mice, whereas it was increased to 9.7±0.4 in the IgG2a treated mice. Therefore, the recruitment of microglial cells depends on the presence of the Fc region of the mAb-11 antibody bound to the amyloid plaques.

When initiated before plaque deposition occurred in TauPS2APP mice, the chronic subcutaneous delivery of mAb-11 IgG2a led to a dramatic reduction in amyloid burden detected by anti-Aβ immunohistochemistry, compared with the mice implanted with control devices (Fig. 2A). Plaque load was clearly reduced throughout the cortex (-79.9%, P=0.004) and hippocampus (-78.5%, p=0.017) (Fig. 2B). Similarly, the number of plaques was dramatically decreased in both regions (-94.5% and -92.7%, respectively; Fig. 2C). There was minimal deposition of amyloid plaques in the thalamus of 12-months old TauPS2APP mice. In contrast, the amyloid burden was reduced by only 15-20% with $F(ab')_2$-secreting devices, an effect which was not significant (P>0.2). Compared to the control group, Aβ levels were also dramatically reduced in the cortex of IgG2a-treated mice, for both Aβ42 (−87.4%, P=0.0002) and Aβ40 (−82.5%, P=0.024), whereas the effect of the $F(ab')_2$ fragment remained minimal (Fig. 2D). Of note, the level of Aβ42 in the cortex of 12-months old TauPS2APP mice was more than five-fold lower compared to 7-months old 5XFAD mice. Altogether, these results indicate that when delivered by ECT, full IgG2a antibodies are more effective than $F(ab')_2$ fragments for the clearing of amyloid pathology, most likely because ECT leads to higher levels of circulating mAb11 IgG2a in the plasma (Fig. 1A,B).

Figure 2-2. Preventive mAb-11 immunization using ECT delivery strongly reduces amyloid load in the brain of TauPS2APP mice.

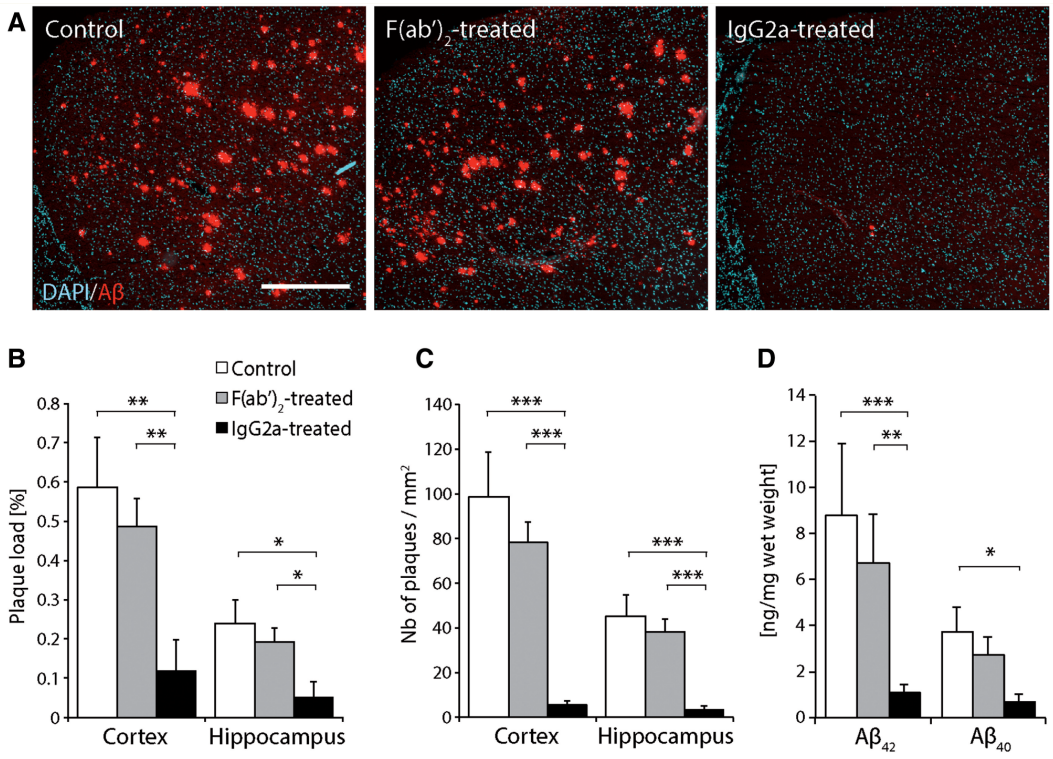

Figure 2: Preventive mAb-11 immunization using ECT delivery strongly reduces amyloid load in the brain of TauPS2APP mice.

A | Amyloid burden revealed by anti-amyloid-β immunostaining (6E10) in the frontal cortices of 12-month-old TauPS2APP mice. Note the decreased amyloid pathology in the cortex of the TauPS2APP mouse continuously treated with mAb-11 IgG2a. **B |** Plaque load, expressed as the percentage of the brain area occupied by amyloid-β-positive plaques, is significantly reduced in the cortex and hippocampus of mice treated with mAb-11 IgG2a. **C |** The density of amyloid plaques is significantly decreased in these brain regions. **D |** The amount of amyloid-β 42 and amyloid-β 40 is significantly decreased in the cortex of mice treated with mAb-11 IgG2a. Data are expressed as the mean ± SEM; Control group: n = 8, F(ab') 2 - and IgG2a-treated groups: n = 10. One-way ANOVA with Newman-Keuls post hoc test: * P < 0.05, ** P < 0.01, *** P < 0.001. Scale bar = 500 µm (A).

Strong reduction of plaque density throughout the whole cortex of ECT-mAb11 treated mice

To further quantify the number of amyloid plaques in ECT-treated mice, the entire contralateral hemicortex of the treated mice was analysed by gratings-based X-ray phase contrast tomographic microscopy (Pinzer et al., 2012; Weitkamp et al., 2005). This technique allows full brain visualization and does not rely on immunodetection methods, which may be subject to interference with the therapeutic antibody bound to Aβ. X-ray phase contrast revealed the presence of discrete hyper-intense dots throughout the entire cortex of 12-months old TauPS2APP mice implanted with control devices. These dots were previously shown to correspond to amyloid deposits (Pinzer et al., 2012). The density of plaques in the cortex (plaques/mm^3) was determined following threshold segmentation (Fig. 3A,B). Coronal maximum-intensity maps show that plaque density was clearly reduced in the entire hemicortex of the mAb11 IgG2a-treated mice (Fig. 3C). In contrast, the density and distribution of amyloid plaques were similar in control and $F(ab')_2$-treated mice. Volumetric information from the phase contrast CT datasets was used to determine the total number of plaques in the hemicortex of the mice in each group (Fig. 3D). The mAb-11 IgG2a treatment dramatically reduced the number of detectable plaques (-83%, P=0.00013), whereas the effect of the $F(ab')_2$ treatment was not significant (-25%, P=0.0697).

Figure 2-3. ECT delivery of mAb-11 IgG2a prevents amyloid plaque deposition throughout the entire cortex of TauPS2APP mice.

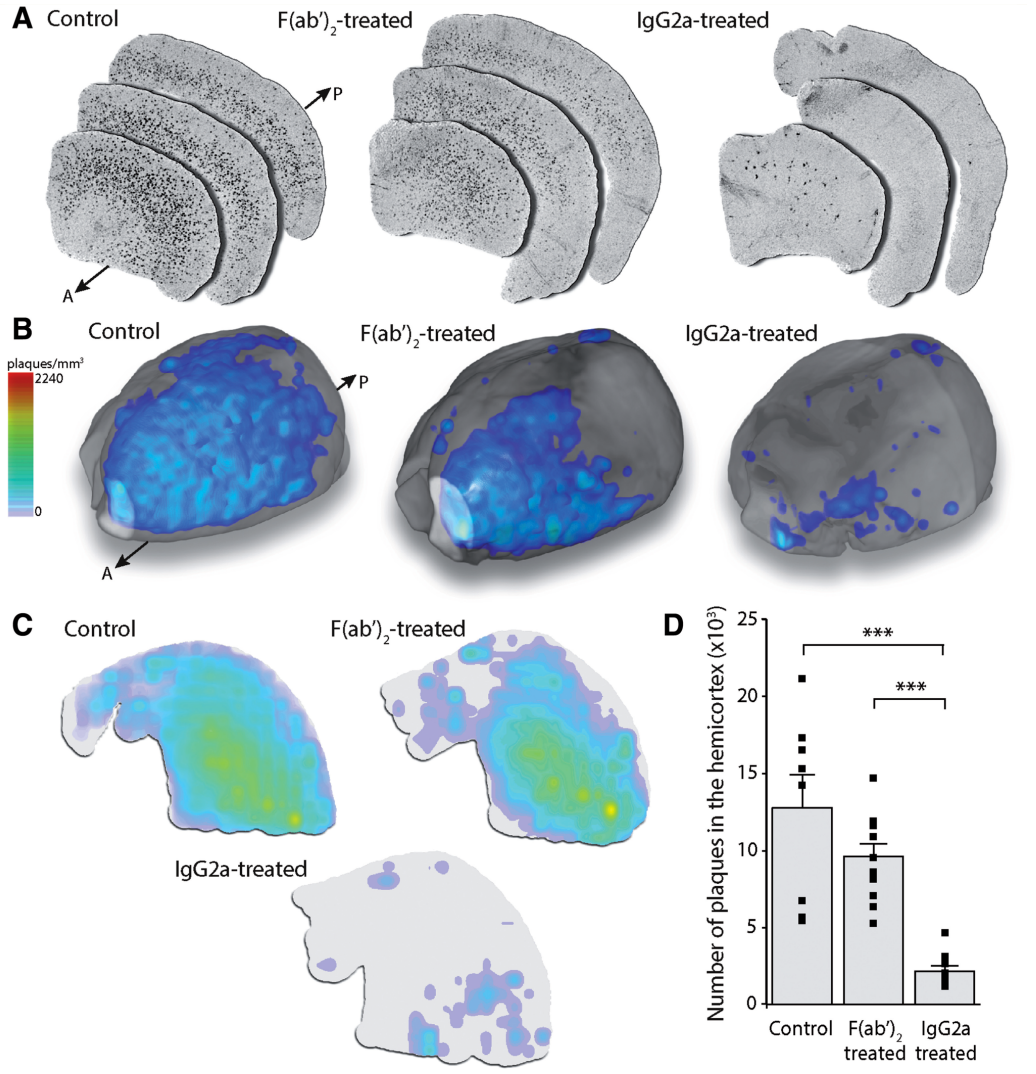

Figure 3: ECT delivery of mAb-11 IgG2a prevents amyloid plaque deposition throughout the entire cortex of TauPS2APP mice.

A | Phase-contrast tomographic microscopy of the whole hemicortex reveals hyperintense signals in 12-month-old TauPS2APP mice. The signals are shown on three cortex sections for three representative mice, one from each group, along the anterior (A)–posterior (P) axis. Note the reduction in hyperintense signals in the mAb-11 IgG2a-treated mice. **B |** Representative hemicortex with superimposed colour-coded density of the hyperintense dots (plaques/mm 3). Note that IgG2a-treated mice have detectable plaques only in the most frontal part of the cortex.**C |** Coronal maximum-intensity maps of the representative hemicortex. Note the overall reduction in plaque density in the IgG2a-treated mouse. **D |** Quantification of the total number of plaques in the hemicortex of mice implanted either with control, mAb-11 F(ab') 2 - and mAb-11 IgG2a-secreting ECT devices. Data are expressed as the mean ± SEM; Control group: n = 8, F(ab') 2 -treated: n = 11, IgG2a-treated: n = 10. One-way ANOVA with Newman-Keuls post hoc test: ***P < 0.001.

Reduced Aβ deposition correlates with decreased tau pathology in the CA1 hippocampus

Next, we analysed the presence of hyperphosphorylated forms of human tau in the CA1 region of the hippocampus of TauPS2APP mice, which overexpress P301L-mutated human tau (Fig. 4A). We assessed the number of neurons located in the CA1 pyramidal layer with an accumulation of AT8-positive phospho-tau (S202/T205) in the somatodendritic compartment (Fig. 4B). In mAb11 IgG2a-treated mice, the number of AT8-positive neurons was significantly decreased with respect to both control (P=0.005) and F(ab')$_2$-treated mice (P=0.035). However, there was no significant difference between the control and F(ab')$_2$-treated groups (P=0.2). Furthermore, the number of AT8-positive neurons in the CA1 was strongly correlated with amyloid burden in the cortex across all three groups (Fig. 4C), confirming that pathological hyperphosphorylation of tau is linked to Aβ deposition in this mouse model (Grueninger et al., 2010).

To confirm the effect of immunotherapy on another tau phosphorylation site, phospho-S422 tau was stained on adjacent sections of the hippocampus. Again, the number of CA1 neurons with a somatodendritic accumulation of phospho-S422 tau was significantly reduced in the mAb-11 IgG2a-treated mice compared to control animals (P=0.006) (Fig. 4D,E). Next, in order to assess the effect on tau misfolding, we performed a staining with the conformation-dependent MC1 antibody. The number of MC1-positive neuronal cell bodies in CA1 hippocampus was significantly decreased in mAb11 IgG2a-treated mice (P=0.0098).

Altogether, these results indicate that preventive passive immunization using ECT delivery of recombinant mAb11 IgG2a antibodies in the periphery is an effective approach to chronically deliver therapeutic antibodies, reduce amyloid deposition throughout the brain and mitigate downstream effects on the tau pathology.

Figure 2-4. ECT delivery of mAb-11 IgG2a decreases tau pathology in the CA1 region of the hippocampus of TauPS2APP mice.

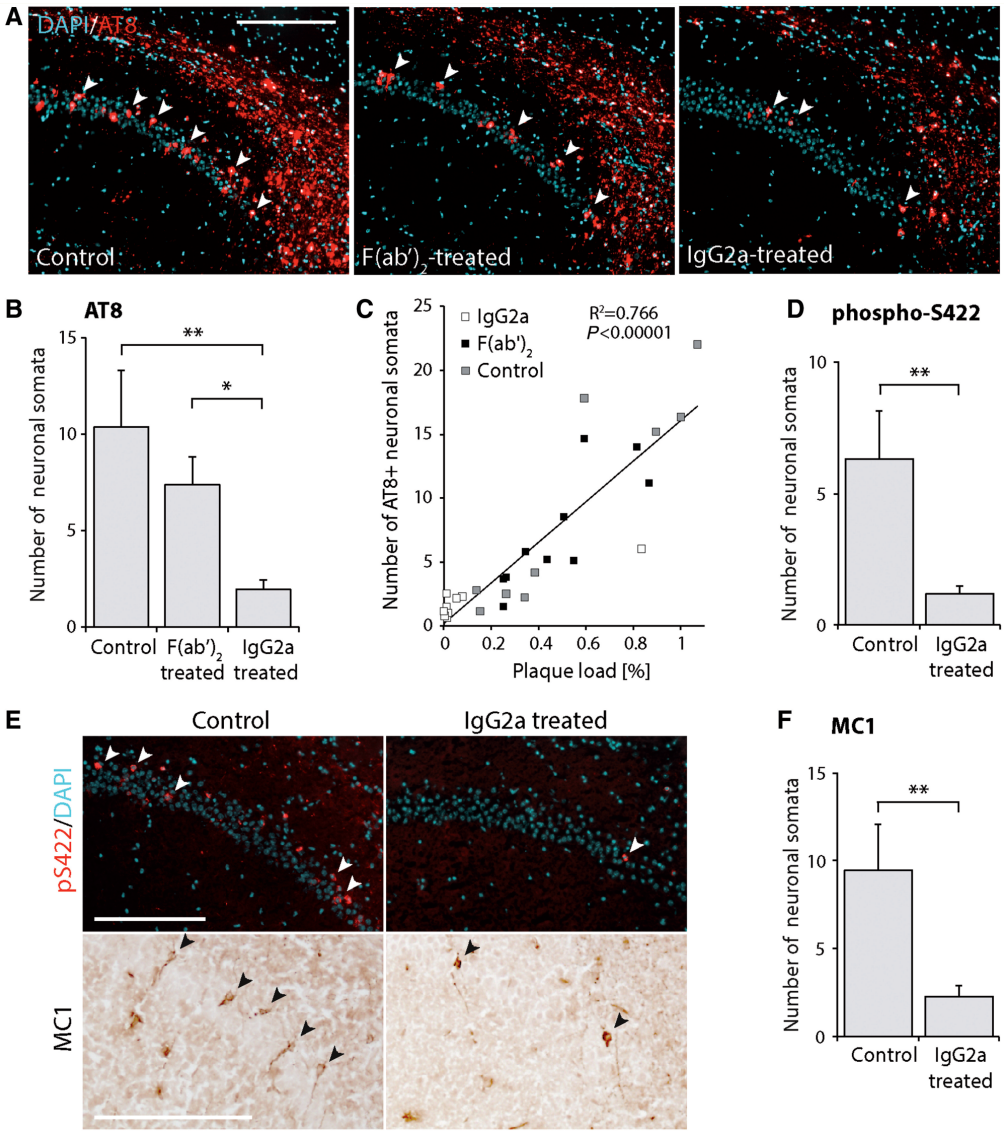

Figure 4: ECT delivery of mAb-11 IgG2a decreases tau pathology in the CA1 region of the hippocampus of TauPS2APP mice.

A | Representative photomicrographs of the CA1 region of the hippocampus. Neurons are stained for tau phosphorylated at serine 202 and threonine 205 residues (AT8), and nuclei are stained with DAPI. AT8-positive neuronal somata in the pyramidal layer are indicated with arrowheads. **B |** Quantification of the number of AT8-positive neurons in the CA1 pyramidal layer of the hippocampus. Note the significant reduction in mAb-11 IgG2a treated mice. **C |** Correlation between amyloid-β burden and the number of AT8-positive neurons in the CA1 hippocampal region. Individual values from control, mAb-11 F(ab') 2 -treated and IgG2a-treated mice are shown in the same graph for correlation. **D |** Quantification of the number of neurons with somatodendritic localization of phospho-S422 tau in the CA1 pyramidal layer of the hippocampus. **E |**Representative images of phospho-S422 tau and MC1 stainings in the hippocampal CA1 region. Arrowheads indicate neurons with somatodendritic staining. **F |** Quantification of the number of MC1-positive neuronal somata in the CA1 pyramidal layer. Data are expressed as the mean ± SEM; Control group: n = 8, F(ab') 2 - and IgG2a-treated groups: n = 10. One-way ANOVA with Newman-Keuls post hoc test (B) and two-tailed heteroscedastic t -tests (D and F): * P < 0.05, **P < 0.01. Correlation in (C) is analysed with the Pearson's test. Scale bar = 200 µm (A and E).

2.2.3 Discussion

The implantation of genetically engineered cells within a retrievable subcutaneous device leads to the continuous production of mAbs *in vivo*. This technology achieves steady therapeutic mAb levels in the plasma, offering an effective alternative to bolus injections for passive immunization against chronic diseases. Compare with previous experiments performed by Auélien Lathuilière on 5xFAD mice, the effect of the ECT treatment is more pronounced when passive immunization is preventively administered in TauPS2APP mice, most notably decreasing the phospho-tau pathology.

With the recent development of biomarkers to monitor Alzheimer's pathology, it is recognized that a steady increase in cerebral amyloid over the course of decades precedes the appearance of the first cognitive symptoms (reviewed in (Sperling et al., 2011)). The current consensus therefore suggests applying anti-Aβ immunotherapy during this long asymptomatic phase to avoid the downstream consequences of amyloid deposition and to leverage neuroprotective effects. Several preventive clinical trials have been recently initiated for Alzheimer's disease. The Alzheimer's Prevention Initiative (API) and the Dominantly Inherited Alzheimer Network (DIAN) will test antibody candidates in presymptomatic dominant mutation carriers, while the Anti-Amyloid treatment in the Asymptomatic Alzheimer's disease (A4) trial enrols asymptomatic subjects after risk stratification. If individuals with a high risk of developing Alzheimer's disease can be identified using current biomarker candidates, these patients are the most likely to benefit from chronic long-term anti-Aβ immunotherapy. However, such a treatment may pose a challenge to healthcare systems, as the production capacity of the antibody and its related cost would become a challenging issue (Sköldunger et al., 2012). Therefore, the development of alternative technologies to chronically administer anti-Aβ antibody is an important aspect for therapeutic interventions at preclinical disease stages.

Remarkably, continuous administration of mAb11 initiated before plaque deposition had a dramatic effect on the amyloid pathology in TauPS2APP mice, underlining the efficacy of preventive anti-Aβ treatments. In this mouse model,

where tau hyperphosphorylation is enhanced by Aβ (Grueninger et al., 2010), the treatment decreases the number of AT8- and phospho-S422-positive neurons in the hippocampus. Furthermore, the number of MC1-positive hippocampal neurons is significantly reduced, which also indicates an effect of anti-Aβ immunotherapy on the accumulation of misfolded tau. These results highlight the effect of Aβ clearance on other manifestations of the Alzheimer's pathology. In line with these findings, previous studies have shown evidence for a decrease in tau hyperphosphorylation following immunization against Aβ, both in animal models and in Alzheimer's patients (Boche et al., 2010; Oddo et al., 2004; Salloway et al., 2014; Serrano-Pozo et al., 2010; Wilcock et al., 2009).

Further developments will be needed to scale up this delivery system to humans. The possibility of using a single allogeneic cell source for all intended recipients is a crucial advantage of the ECT technology to standardize mAb delivery. However, the development of renewable cell sources of human origin will be essential to ECT application in the clinic. Although the ARPE-19 cell line has been successfully adapted to ECT and used in clinical trials (Dunn et al., 1996; Zhang et al., 2011), the development of human myogenic cells (Negroni et al., 2009) is an attractive alternative that is worth exploring. Based on the PK analysis of recombinant mAb11 antibody subcutaneously injected in mice (see Supplementary Note 1), we estimate that the flat sheet devices chronically release mAb-11 at a rate of 6.8 and 11.8 µg/hr, to reach a plasma level of 50 µg/ml in the implanted animals. In humans, injected IgG1 has a longer half-life (21-25 days), with a volume of distribution of approximately 100 ml/kg and an estimated clearance of 0.2 ml/hr/kg. These values indicate that the predicted antibody exposure in humans, based on the rate of mAb11 secretion achieved by ECT in mice, would be only 10 to 20-fold lower than the typical regimens based on monthly bolus injection of 1 mg/kg anti-Aβ mAb. Hence, it is realistic to consider ECT for therapeutic mAb delivery in humans, as the flat sheet device could be scaled up to contain higher amounts of cells. Furthermore, recent progress to engineer antibodies for increased penetration into the brain will enable lowering dosing of biotherapeutics to achieve therapeutic efficacy (Bien-Ly et al., 2014; Niewoehner et al., 2014). For some applications, intrathecal

implantation could be preferred to chronically deliver mAbs directly inside the CNS (Aebischer et al., 1996; Belaunzaran et al., 2011).

Overall, ECT provides a novel approach for the local and systemic delivery of recombinant mAbs in the CNS. It will expand the possible therapeutic options for immunotherapy against neurodegenerative disorders associated with the accumulation of misfolded proteins, including Alzheimer's and Parkinson's diseases, dementia with Lewy bodies, frontotemporal lobar dementia and amyotrophic lateral sclerosis (Bae et al., 2012; Gros-Louis et al., 2010; Rosenmann, 2013).

2.2.4 Conclusion

This study of the preventive approach on TauPS2APP mouse model allowed us to draw two very important conclusions about mAb11 effects. First, the primary preventive approach with a continuous delivery using the ECT is efficient at reducing the Aβ load. Therefore, preventing the Aβ deposition is a better approach than clearing existing Aβ plaques. It confirms the current paradigm in the pharmaceutical industry that "earlier is better" for passive anti-Aβ immunization. And it reinforces the hypothesis that previous phase III clinical trial using Gantenerumab on mild AD, such as Marguerite RoAD, failed because they acted too late on the disease. Second, we shown that by preventing Aβ deposition, it is possible to reduce tau pathology in the TauPS2APP mouse model. It suggests that the effects of anti-Aβ passive immunization go beyond Aβ pathology and can impact other hallmarks of the disease.

Supplementary Figure S1. Microglial cells accumulate around amyloid plaques in the TauPS2APP mouse model

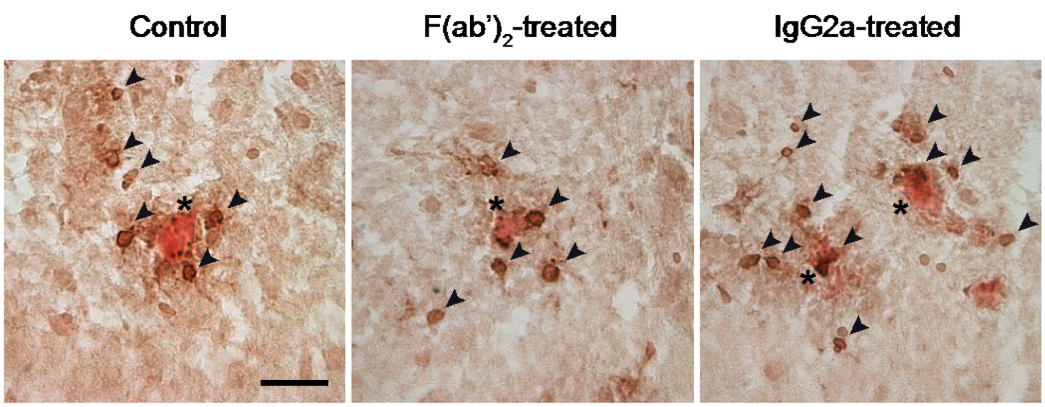

Microglial cells accumulate around amyloid plaques in the TauPS2APP mouse model.
Sections of the cortex of 12-months old mice accumulating amyloid plaques were immunostained for Iba1. Discrete Iba1-positive cells (arrowheads) with a microglial morphology are frequently observed near amyloid plaques stained with Congo Red (*). Representative images are shown for each treatment group. Scale bar: 50 µm.

2.3 Effect of passive anti-Aβ immunization at the onset of the disease in the 5xFAD B6SJL mouse model.

2.3.1 Introduction

We confirmed that the preventive approach is key in the treatment of AD in our proof of concept in the TauPS2APP mouse model where we administered the antibody before the onset of the disease. Unfortunately, most AD cases are sporadic and primary preventive treatment is not relevant in this case. In addition, the TauPS2APP mouse model is overexpressing the mutated P301L form of human tau (Grueninger et al., 2010). This mutation causes frontotemporal dementia and parkinsonism linked to chromosome 17 (FTDP-17) in humans and is known to trigger neurofibrillary pathology and neurodegeneration in mice (Götz and Ittner, 2008; Lewis et al., 2000). However, there is no evidence of tau mutations in AD.

Based on this evidence, we aimed to develop a more realistic mouse model of AD with tau and Aβ pathologies in which we could study the effect of passive anti-Aβ immunization using a secondary or tertiary preventive approach. In order to be closer from the context of sporadic AD, we first established the effect of passive anti-Aβ immunization in 5xFAD mice at different stages of the disease. Previous results on passive anti-Aβ immunization using ECT were performed in 5xFAD mice with the C57BL/6J genetic background (Lathuilière et al., 2016) and the animals were implanted at a large range of age (from 5 weeks old to 11 weeks old). According to the mutant mouse resource and research center (MMRRC), the B6SJL genetic background of 5xFAD is more robust than the C57BL/6J background.

The aim of the following study was to evaluate the effect of passive anti-Aβ immunization on the 5xFAD mouse model with the B6SJL genetic background. In addition, we evaluate the effect of passive immunization on the Aβ pathology when the treatment is administered at the onset of soluble Aβ accumulation (secondary prevention) and at the onset of Aβ plaque deposition (tertiary prevention).

Figure 2-5. Early antibody delivery in 5xFAD B6SJL mice

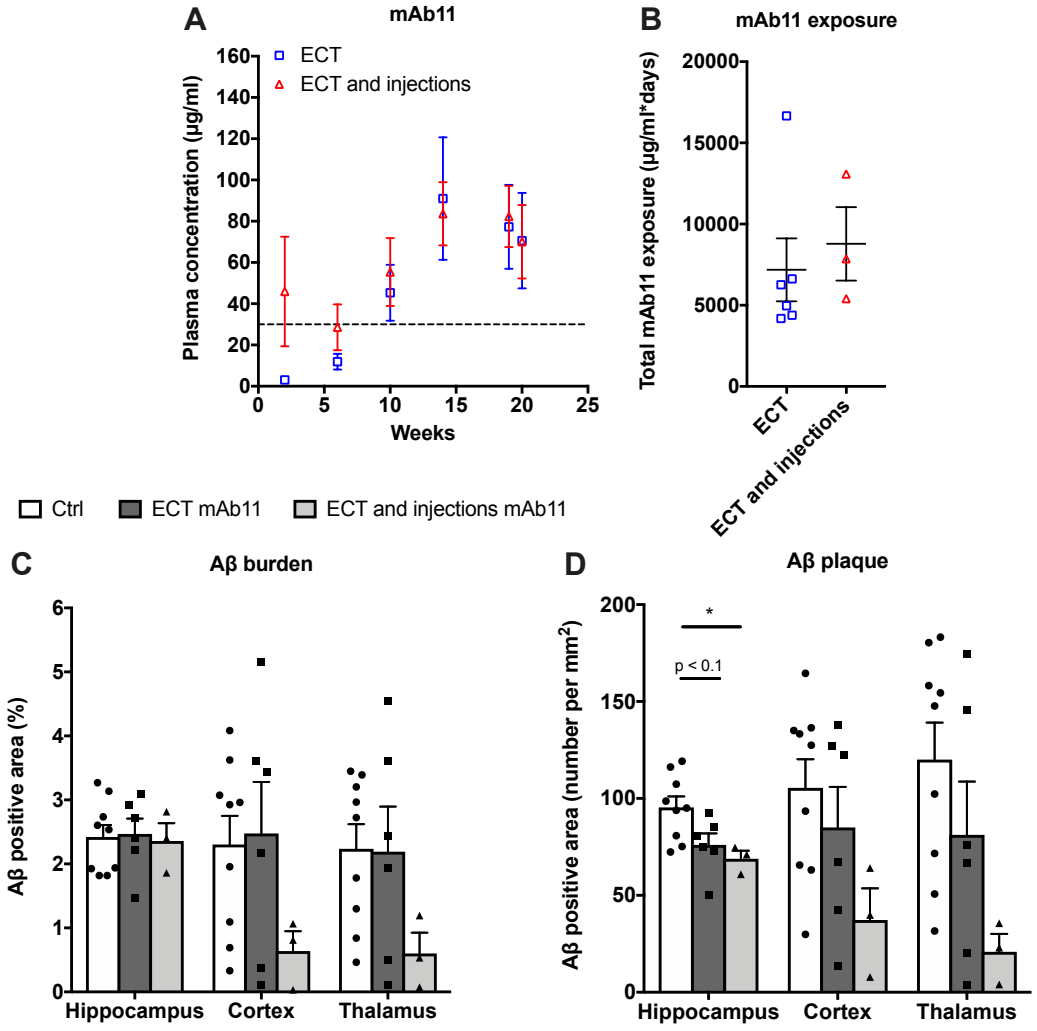

Figure 5: Early antibody delivery in 5xFAD B6SJL mice

A | Average anti-Aβ mAb11 concentration detected in the plasma of 5xFAD B6SJL mice implanted with the encapsulation device containing C2C12 cells secreting mAb11 antibody. The animals with the injections were injected mAb11 antibodies every week during the first 4 weeks in order to obtain a plasma concentration above 30 µm/ml during the first weeks post-implantation. **B |** Accumulated exposure of these animals to mAb11 anti-Aβ antibody during the 5 months of the experiment (144 days exactly). **C |**Percentage of each brain region covered by Aβ staining in controls and mAb11-treated animals with and without mAb11 injections. **D |** Number of Aβ positive area per mm² detected in each brain region of the controls *versus* mAb11-treated animals. **E |** Average area of the detected Aβ plaques in each brain region. Each brain region were analysed independantly using a one-way ANOVA. * $p < 0.05$, ** $p < 0.01$, *** $p < 0.001$.

2.3.2 Results

Early administration of passive immunization decreases the number of Aβ plaques but not the Aβ plaque load in 5xFAD B6SJL mice

We evaluated the effect of passive anti-Aβ immunization, at the time of soluble Aβ apparition but before the onset of Aβ plaque deposition. We implanted mice at 5 to 6 weeks of age. Lathuilière et al. observed that the ECT took more than 8 weeks to reach the therapeutic dosage of 40-50 µg/ml of mAbs in the plasma (Lathuilière et al., 2016). Consequently, these mice were exposed to small dose before the onset of the disease and therapeutic mAbs dose only after the onset of Aβ plaque deposition. The mice could not be implanted earlier due to their small size.

In order to compensate for the low antibody secretion during the early phase of ECT implantation, we injected a group of mice with 350 µg of mAb11 per week during the first 4 weeks post implantation (5 to 9 weeks of age). Overall, these animals received a therapeutic dose of mAb11 already during the early stages of soluble Aβ accumulation (6 weeks) and Aβ plaque deposition (8 weeks). The injections resulted in plasma concentration averaging 50 µg/ml during the first weeks (Fig. 5A). Then the ECT took over and secreted mAb11 at a level similar to the group of mice without injections. All animals were treated during 5 months in order to maximize exposure to mAb11. Total exposure reached an average of 7180 µg/ml of plasma in the group treated with ECT only, and 8780 µg /ml of plasma in the group initially treated with mAb11 injections plus ECT (Fig. 5B).

After 5 months of treatment, we evaluated the Aβ plaque burden by immunohistochemistry using the anti-Aβ antibody 6e10. We compared the control group with the mAb11-treated animals using the ECT only and with the ECT and the mAb11 injections. We did not measure any changes in the Aβ positive area between these groups (Fig. 5C). The Aβ plaque burden was evaluated in the hippocampus, the cortex and the thalamus with similar results. However, we observed a significant decrease of the Aβ plaque number in the hippocampus of the animals treated with the ECT and the mAb11 injections as compared to the control non-treated animals (Fig. 5D). In the 5xFAD mice treated with ECT only, we observed the same trend, but the effect did not reach

statistical significance. In the cortex and in the thalamus, we could not measure such effect due do the high variability in between the animals. The significant decrease of the number of plaques in the hippocampus was compensated by a highly significant increase in plaque size area in both groups treated with mAb11.

2.3.3 Discussion

Compared to the results previously obtained by our group in the 5xFAD C57BL/6J mice (Lathuilière et al., 2016), we observed a lower efficacy of the treatment at clearing Aβ pathology in the 5xFAD B6SJL mice using the same ECT technology. Integrated exposure to mAb11, as well as measured plasma concentrations, were similar in both experiments. The MMRRC described the 5xFAD B6SJL model as being more robust than the 5xFAD C57BL/6J. The fact that the Aβ pathology develops more aggressively in the B6SJL genetic background could explain why there is such a difference in the efficacy of passive immunization in these two strains of 5xFAD mice.

Nevertheless, we measured a decrease in the Aβ plaque number, this effect was restricted to the hippocampus of the animals treated at 5 weeks with mAb11 injection in addition of the ECT. However, animals treated with the ECT (without injections) also showed a trend toward a reduced number of Aβ depositions. We did not measure any decrease of the Aβ plaque load in any condition in the 5xFAD B6SJL mice. The decrease of Aβ plaque number was compensated by a highly significant increase of the plaque size area in the hippocampus. This effect has also been previously observed in the 5xFAD C57BL/6J mice. We conclude that instead of decreasing the Aβ burden, passive anti-Aβ immunization modulates the Aβ depositions when administered during the onset of the Aβ pathology.

We next sought to study this modulation effect in presence of tau pathology and extended our analysis to not only the Aβ deposition but also the neuritic plaques. Indeed, by binding to the Aβ plaques, anti-Aβ antibodies have the opportunity to affect the microenvironment at the vicinity of the Aβ depositions, which involved surrounding phosphorylated tau, dystrophic neurites as well as microglial cells.

2.3.4 Conclusion

The evaluation of the different implantation age as well as the different exposure to mAb11 does confirmed that earlier administration of the treatment is slightly more effective as well as increased dosage. This conclusion corroborates the current view in the pharmaceutical industry that passive immunization should be used earlier and at higher dosage to have a significant impact on Alzheimer's disease. In this experiment we are administering passive anti-Aβ immunization at the time of the Aβ pathology onset mimicking the current situation with Alzheimer's disease patients that are treated only when Aβ pathology is diagnosed (secondary and tertiary prevention). Consequently, we decided to base our combined Aβ/tau mouse model on the 5xFAD B6SJL background to study the effect of passive anti-Aβ immunization at the time of established Aβ pathology.

3

Chapter 3 : Effect of passive anti-Aβ immunization in a combined Alzheimer's disease mouse model with established WT tau and Aβ pathologies

Vanessa Laversenne[1], Sameer Nazeeruddin[1], Patrick Aebischer[1] and Bernard L. Schneider[1]

1 Neurodegenerative Studies Laboratory, Brain Mind Institute, Ecole polytechnique Fédérale de Lausanne (EPFL), CH-1015 Lausanne, Switzerland

(Manuscript in final preparation)

3.1 Abstract

The brain pathology of Alzheimer's disease (AD) is characterized by the misfolding and aggregation of both the amyloid beta (Aβ) peptide and hyperphosphorylated forms of the tau protein. Initial Aβ deposition is considered to trigger a sequence of deleterious events contributing to tau pathology, neuroinflammation and ultimately causing the loss of synapses and neurons. To address the interaction between the Aβ and tau pathologies and assess the effect of passive anti-Aβ immunization in this context, we generated a mouse model of Alzheimer's disease by locally overexpressing the human tau protein in the hippocampal CA3 region of 5xFAD mice. We find that Aβ plaque deposition combined with human tau overexpression leads to an array of pathological manifestations including the formation of tau-positive dystrophic neurites and accumulation of hyperphosphorylated tau at the level of neuritic plaques. Furthermore, the presence of human tau reduces the clustering of microglia typically observed in close proximity to the Aβ plaques.

Anti-Aβ antibodies chronically delivered using the encapsulated cell technology target Aβ deposits in the brain, where they recruit microglial cells even in the presence of tau, and induce phagocytic activity. Anti-Aβ immunization increases plaque compaction, reduces the spread of human tau in the hippocampal formation and prevents the formation of tau-positive dystrophic neurites at the level of the neuritic plaques. However, the treatment is not sufficient to reverse hyperphosphorylated tau accumulation as well as tau-induced neurodegeneration in the dentate gyrus.

This study highlights that passive immunization against Aβ might not be sufficient to halt the ongoing progression of AD as it does not revert all the pathological effects of tau accumulation.

3.2 Introduction

In the absence of any disease-modifying treatment, Alzheimer's disease (AD) leads to the progressive loss of memory and other cognitive functions. Brain pathology is characterized by the accumulation of senile plaques mainly composed of amyloid beta (Aβ) fibrils (Glenner and Wong, 1984b; Masters et al., 1985), and neurofibrillary tangles (NFTs) which contain hyperphosphorylated tau protein (Brion et al., 1985). The Aβ cascade hypothesis has proposed that Aβ accumulation and deposition are primary pathogenic events leading to the major disease hallmarks including tau hyperphosphorylation, microglia activation, as well as the loss of synaptic connections and neuronal cells (Hardy and Higgins, 1992; Selkoe, 1991). Based on this assumption, treatments targeting the production and deposition of Aβ have dominated the therapeutic landscape. Among these, passive immunization using monoclonal antibodies against Aβ have shown some efficacy at clearing senile plaques in AD patients, but so far failed to slow down the cognitive decline (Mehta et al., 2017). In the light of the failed clinical trials, it is important to revisit the Aβ cascade hypothesis (Makin, 2018), also considering that Aβ accumulation does not correlate with cognitive decline (Edison et al., 2007; Snowdon, 1997) and that the mechanistic links between Aβ and tau pathologies are not yet elucidated.

In particular, there is a need for a better understanding of the interaction between Aβ deposition and the conditions leading to pathological changes at the level of the normal tau protein. Indeed, most studies have addressed this question using pro-aggregant tau mutations associated with frontotemporal dementia (Bolmont et al., 2007; Götz et al., 2001; Héraud et al., 2014; Lewis et al., 2001; Oddo et al., 2003; Pérez et al., 2005; Saul et al., 2013).

Indeed the overexpression of human WT alone in mouse models seemed to not be sufficient to trigger pathological tau propagation (Duff et al., 2000). Recent studies, however, showed that the presence of neuritic plaques could promote WT tau conversion into pathological tau forms and allow its propagation as NFTs (He et al., 2018; Li et al., 2016). In one study, a mouse model overexpressing WT truncated 4R tau was used, in the other the mice were injected with human AD-

brain derived pathological tau. In both studies, tau alone, in the absence of neuritic plaque, did not trigger the formation of NFTs. These studies highlighted the importance of neuritic plaques and the interaction of Aβ and WT tau in the development of tau pathology.

In the present study, we locally overexpress the WT form of 4R0N human tau using an AAV8 vector injected in the hippocampal CA3 region of 5xFAD mice, which express mutated forms of APP and presenilin 1 leading to the production of Aβ peptides and rapid deposition of plaques in the brain (Oakley et al., 2006). The model recapitulates some hallmarks of the disease, including neuronal loss, tau spreading throughout the hippocampal formation as well as the formation of tau-positive neuritic plaques, characterized by tau accumulation and hyperphorphorylation, the formation of dystrophic neurites and microglial activation. Here, we used this model to assess the respective contribute of Aβ and tau in these various pathological indicators of AD. Furthermore, we assessed the effects of passive anti-Aβ immunization delivered by peripheral implantation of encapsulated myoblasts genetically modified to continuously secrete the recombinant mAb11 antibody. We found that binding of the anti-Aβ antibody to amyloid plaques is a potent modulator of the local microglial activity. At the level of neuritic plaques, passive immunization promoted microglial clustering around plaques, increased plaque compaction and reduced the formation of tau-positive dystrophic neurites. Although anti-Aβ immunization reduced the spread of tau immunoreactivity in the hippocampal formation, we found only limited effects on the treatment on tau-induced neuronal loss.

Figure 3-1. Hallmarks of the 5xFAD/AAV-tau mouse model.

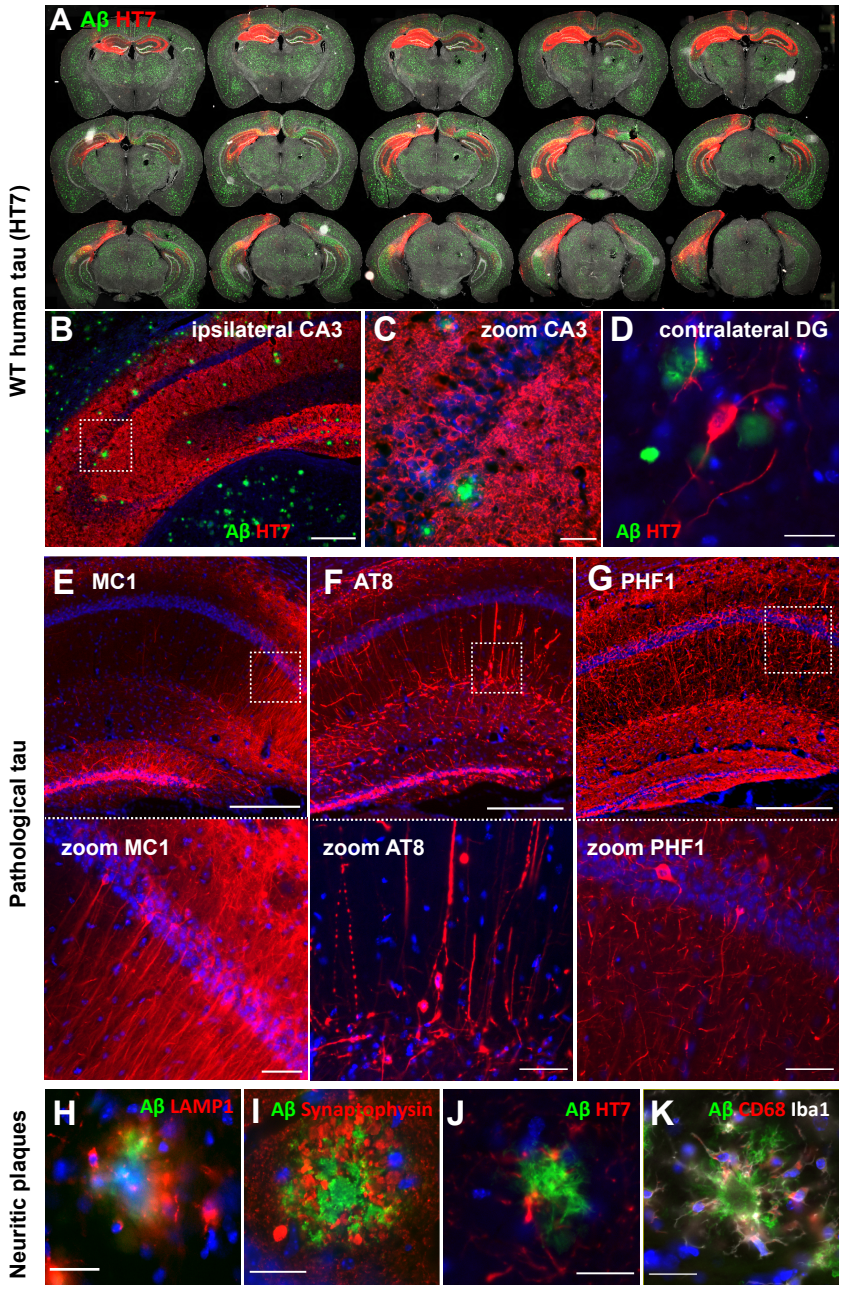

Figure 1: Hallmarks of the 5xFAD/AAV-tau mouse model.

A-D | Representative images of WT human tau distribution (HT7 in red) in the 5xFAD/AAV-tau mouse model (Aβ in green, 4G8 antibody). Nuclei are labelled with DAPI. (A) HT7 distribution throughout the entire ipsi - and contralateral hippocampus. (B) Ipsilateral HT7 immunoreactivity in the hippocampus. Scale bar: 250 µm (C) Zoom into the ipsilateral CA3. Scale bar: 25 µm. (D) HT7-positive cell body in the contralateral dentate gyrus. Scale bar: 25 µm.

E-G | Stainings for pathological forms of tau (in red) in the same representative 5xFAD/AAV-tau animal. (E) Misfolded MC1-positive tau (F) AT8-phosphorylated tau and (G) PHF1 phosphorylated tau . Note the different distribution depending on the tau species, and their somatodendritic localization. Scale bars: 250 µm; zoom panels: 25 µm.

H-K | Representative images of neuritic plaques with an Aβ-positive core (4G8 or 6e10 in green) surrounded by (H) LAMP1 immunoreactivity (red); (I) dystrophic presynaptic neurites (synaptophysin in red); (J) HT7 positive dystrophic neurites (in red); and (K) microglia (Iba in white) and lysosome marker (CD68 in red). Scale bar: 25 µm. Nuclei are stained with DAPI (in blue for all images, except (A) in grey).

3.3 Results

Unilateral injection of AAV-tau in the CA3 hippocampus of 5xFAD mice to generate a model of Aβ/tau pathology

In order to assess the interaction between the Aβ and tau pathologies *in vivo*, we developed a mouse model based on the unilateral intrahippocampal injection of a serotype 8 adeno-associated viral (AAV8) vector encoding the wild-type 4R0N form of human tau under the control of the mouse Pgk1 promoter (AAV-tau). The vector was injected in the hippocampal CA3 region of 2-months old 5xFAD mice, to overexpress the human tau protein in the context of the Aβ pathology rapidly developing in this AD mouse model.

HT7 immunostaining for human tau revealed a progressive spreading of the human tau protein overexpressed in the hippocampal formation over the course of several months (Fig. 1A). The human tau protein is highly expressed near the injection site, in the CA3 and dentate gyrus (DG) (Fig. 1B-C), and then progressed towards the CA1 and CA2 areas.

Human tau immunoreactivity was found to spread via the axonal projections to the contralateral hippocampus, and was also detected in neuronal cell bodies located in the contralateral DG and CA3, distal to the site of vector injection (Fig. 1D). Concomitant with the accumulation of human tau, immunohistology revealed the presence of misfolded tau (detected by the MC1 antibody, Fig. 1E), tau phosphorylated at Ser202/Thr205 residues (AT8 antibody, Fig. 1F) as well as tau phosphorylated at Ser396/Ser404 residues (PHF1 antibody, Fig. 1G). These findings confirmed the propensity of human tau to form pathological species when overexpressed in the hippocampal formation.

As previously reported, the local deposition of Aβ was coinciding with the formation of neuritic plaques. They were characterized by the abundant presence of the pathological autophagic marker Lysosomal-associated membrane protein 1 (LAMP1, Fig. 1H), which was found to surround the plaques, and by the local accumulation of the presynaptic protein synaptophysin (Fig. 1I). Furthermore, we observed in 5xFAD mice the formation of dystrophic neurites adjacent to Aβ plaques, with local accumulations of the human tau

protein (HT7 immunostaining, Fig. 1J), mainly visible in the hippocampus contralateral to AAV-tau injection. In addition, the neuritic plaques were surrounded by phagocytic microglia (Fig. 1K)

Aβ promotes hyperphosphorylation of the WT human tau protein

It has been extensively reported that different forms of Aβ accelerate human mutant tau aggregation and propagation (Bolmont et al., 2007; Götz et al., 2001; Lewis et al., 2001; Oddo et al., 2003; Pooler et al., 2015). However, little is known about the effect of Aβ on WT tau spreading.

Using HT7 immunohistochemistry, we quantified the distribution of human tau throughout the hippocampal formation. In the ipsilateral hippocampus, the protein was broadly distributed in the somatodendritic and axonal compartments (Fig. 2A), and the HT7-positive area reached nearly 40% of the total hippocampus. In the contralateral hippocampus, human tau was mainly observed within the projecting axons (Fig. 2B). On both sides, the fraction of the hippocampal surface covered by the HT7 staining remained similar when comparing WT/AAV-tau and 5xFAD/AAV-tau mice (Fig. 2C).

To further assess the effects of the Aβ pathology on tau, brain tissue was stained for markers of tau hyperphosphorylation (AT8) and misfolding (MC1). In the ipsilateral hippocampus, there was a trend towards an increase in the AT8-immunoreactive area when comparing the 5xFAD/AAV-tau and WT/AAV-tau mice (Fig. 2D). However, the effect of the Aβ pathology was most prominent in the contralateral side of the hippocampus, where we observed a 5-fold increase of AT8 immunoreactivity (Fig. 2E). AT8-positive structures appeared as *puncta* located around Aβ plaques (Fig. 2F). As these puncta did not necessarily colocalize with HT7-positive structures, they likely also contained phosphorylated forms of the endogenous mouse tau.

The presence of the Aβ pathology did not change the surface positive for misfolded tau detected with the MC1 antibody (Supplementary figures S1), suggesting that Aβ induces human WT tau hyperphosphorylation, but does not necessarily enhance tau misfolding.

Figure 3-2. Effects of Aβ accumulation on overexpressed WT human tau protein.

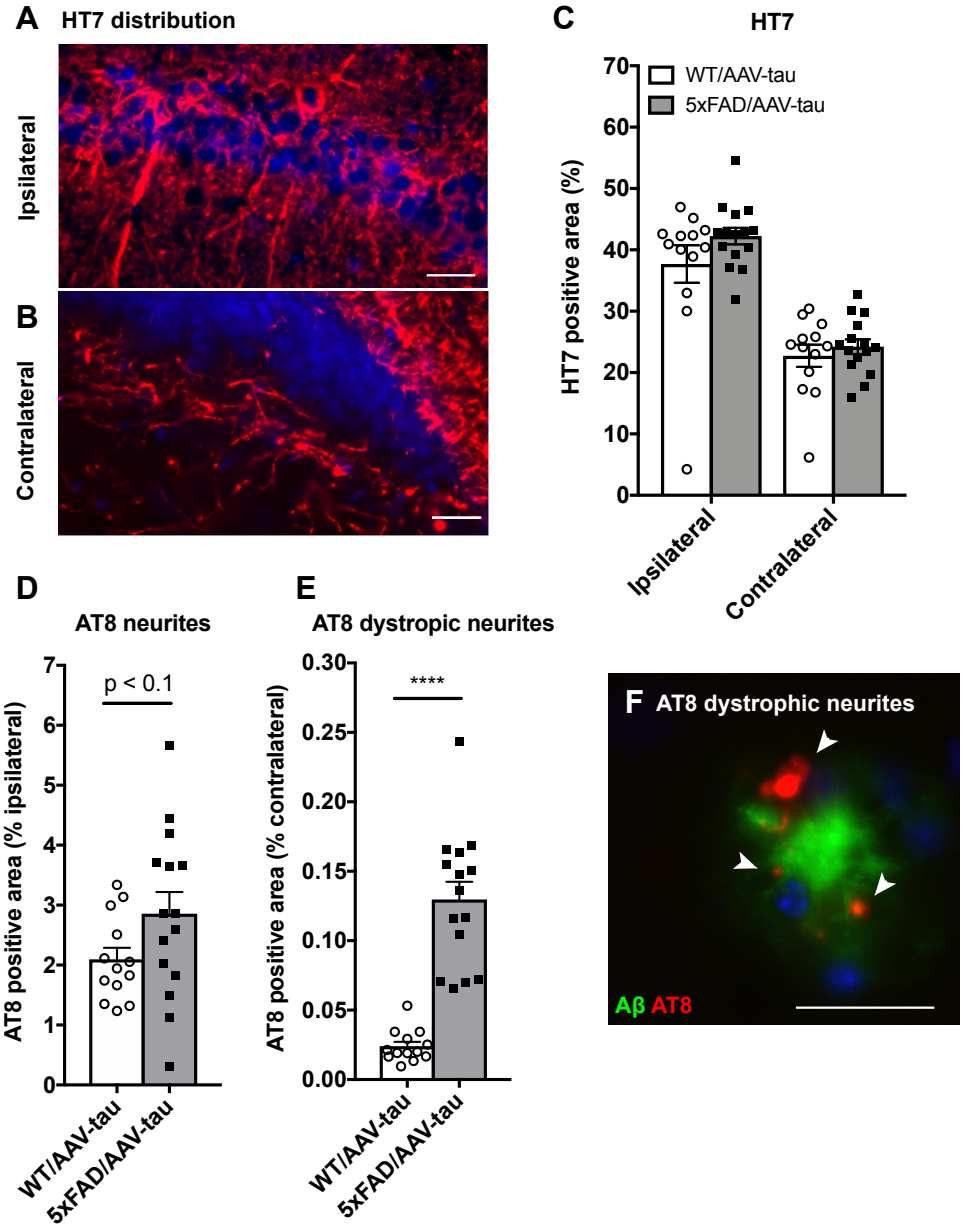

Figure 2: Effects of Aβ accumulation on overexpressed WT human tau protein.

A-B | Representative images of total human tau expression (HT7, red) in the ipsilateral (A) and contralateral (B) hippocampus of AAV-tau injected animals. DAPI stains nuclei in blue. Scale bars: 25 µm. **C |** Percentage surface covered by the HT7 positive staining in the ipsi- and contralateral hippocampus in WT/AAV-tau and 5xFAD/AAV-tau. **D-E |** Percentage of the hippocampal surface covered by the AT8 staining for phospho-tau in the ipsi- (D) and contralateral (E) hippocampus of WT/AAV-tau mice compared with 5xFAD/AAV-tau mice. **F |** Representative image of the AT8-positive puncta located near amyloid plaques (4G8, in green) in the contralateral hippocampus of a 5xFAD/AAV-tau mouse. DAPI stains nuclei in blue. Scale bar: 25 µm. **** $p < 0.0001$

Overexpression of human WT tau leads to degeneration of the dentate gyrus, an effect which is not enhanced by Aβ pathology

In the hemisphere injected with AAV-tau, we noticed a significant hippocampal atrophy, which was most evident in the dentate gyrus (DG), and was not observed in the contralateral hippocampus (Fig. 3A). To determine if the Aβ pathology further enhanced tau-induced neurodegeneration, we compared the ipsilateral DG area between cohorts of 5xFAD/AAV-tau and WT/AAV-tau mice (Fig. 3B). There was no difference between these groups, suggesting that the Aβ pathology did not affect tau-induced hippocampal neurodegeneration in this model.

Next, we sought to further assess the contribution of the tau pathology in this combined Aβ/tau model of AD. Two-months old 5xFAD mice were injected into the CA3 hippocampal region with the AAV-tau vector (5xFAD/AAV-tau) and compared to 5xFAD littermates injected with a similar GFP-expressing AAV8 vector as control (5xFAD/AAV-GFP). At 3 months post-injection (5 months old mice), the induced neurodegeneration was assessed by determining the surface of the injected hippocampus, which was again reduced in the 5xFAD/AAV-tau mice as compared to the contralateral non-injected hippocampus (Fig. 3C). In the DG, the area normally covered by the polymorphic layer was dramatically reduced and the thickness of the granular layer was also decreased (Fig. 3D). This effect was not observed in the mouse littermates injected with AAV-GFP (Fig. 3E), which indicates that hippocampal degeneration was mainly caused by tau overexpression.

Figure 3-3. Overexpression of human WT tau leads to degeneration of the dentate gyrus.

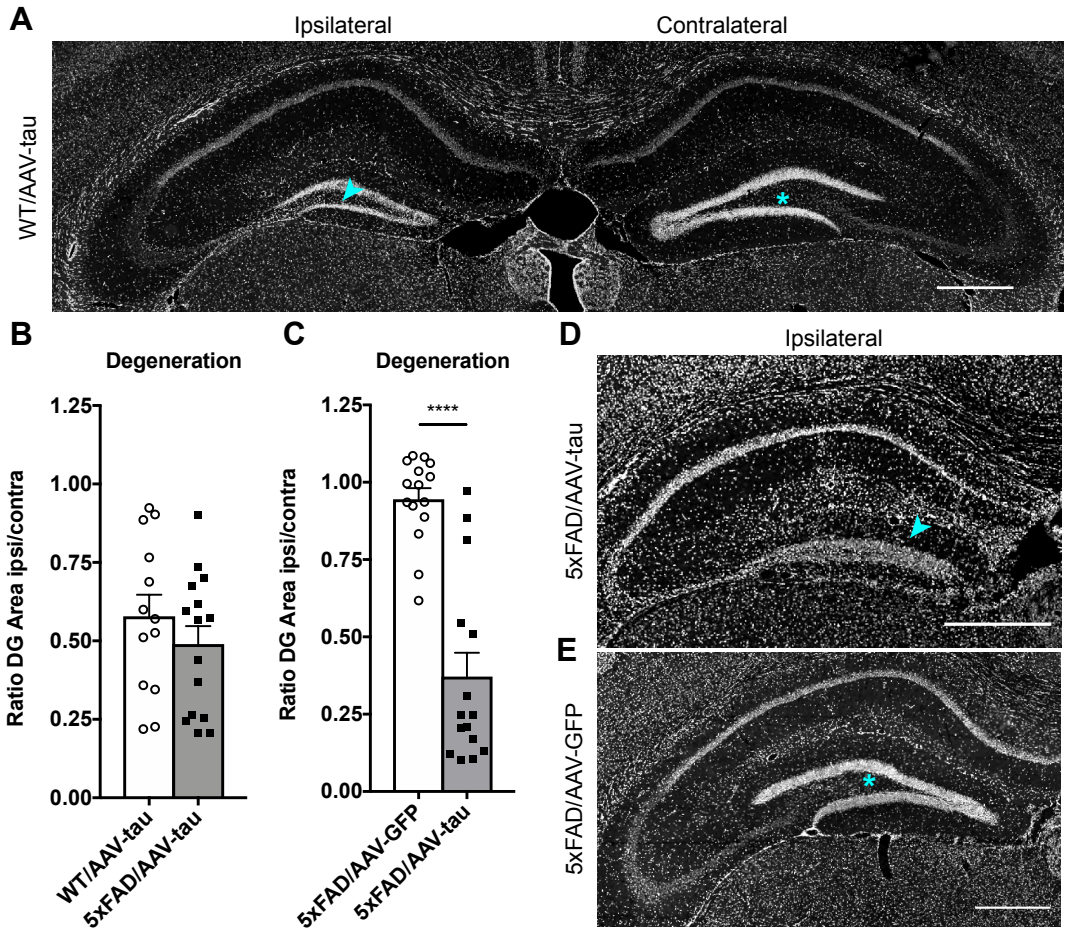

Figure 3. Overexpression of human WT tau leads to degeneration of the dentate gyrus.

A| Representative images of the nuclei (DAPI staining in grey) in the ipsilateral and contralateral hippocampus of a WT mouse injected in the left hemisphere with AAV-tau. **B-C|** Measured ratio of the ipsi/contralateral area of the dentate gyrus (DG) area comparing in (B) WT/AAV-tau and 5xFAD/AAV-tau mice and in (C) 5xFAD/AAV-GFP and 5xFAD/AAV-tau mice. Note the significant degeneration of the DG induced by AAV-tau injection. **D-E|** Representative images of the ipsilateral hippocampus of (D) a 5xFAD/AAV-tau mouse and (E) a 5xFAD/AAV-GFP mouse. DAPI staining in grey. Scale bars: 500 μm. Note the degeneration of the DG polymorphic layer and the thining of the granular layer (cyan arrowhead) in the hippocampus injected with AAV-tau, in contrast to the hippocampus injected with AAV-GFP (cyan *) . Unpaired two-tailed Student's *t*-test, **** $p < 0.0001$

Human tau overexpression does not significantly affect Aβ pathology

In 5xFAD mice, it has been reported in several studies that human mutant tau overexpression can decrease the Aβ pathology (Chen et al., 2016; Héraud et al., 2014; Saul et al., 2013). However, the effects of human WT tau, which has a lower propensity for pathological aggregation, have been less explored. To determine whether the overexpression of human WT tau could affect Aβ deposition, we compared the number of amyloid plaques and the hippocampal area covered by these plaques in 5xFAD/AAV-tau and 5xFAD/AAV-GFP mice. There were no differences in Aβ pathology between groups, as these parameters showed similar values, both in the ipsi- or contralateral hippocampus (Fig. 4A-B). In addition, overexpression of WT human tau did not affect the size of the Aβ plaques (Fig. 4C). However, we observed a gender effect. In females but not males, the Aβ positive area (Fig. 4D), as well as the number of Aβ deposits (Fig. 4E), tended to be increased in the 5xFAD/AAV-tau model compared to the 5xFAD/AAV-GFP mouse model.

Figure 3-4. Human tau overexpression marginally affects Aβ pathology in female 5xFAD mice.

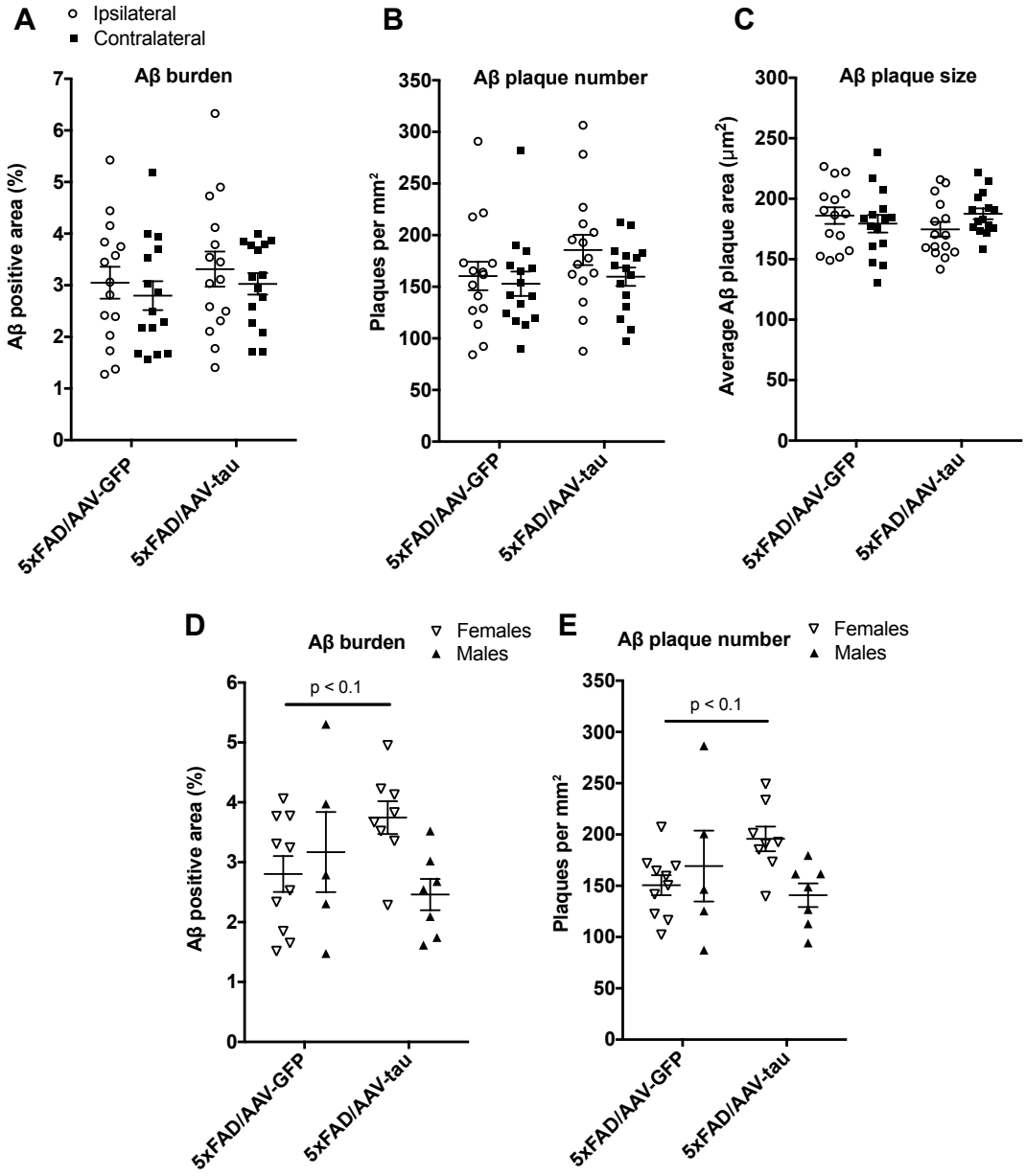

Figure 4. Human tau overexpression marginally enhances Aβ pathology in female 5xFAD mice.
A | Percentage of the ipsi- and contralateral hippocampus covered by Aβ deposits (4G8 staining) in 5xFAD/AAV-GFP and 5xFAD/AAV-tau mice. **B |** Number of Aβ plaques per mm^2. **C |** Average Aβ plaque area. **D-E |** Analysis of the effect of mouse gender on (D) the Aβ burden (in both ipsi- and contralateral hippocampus) and (E) the number of Aβ plaques per mm^2. Note the marginal effect of tau overexpression on the Aβ pathology in the female 5xFAD mice. Two-way ANOVA with Sidak post-hoc analysis.

Aβ pathology increases microglia phagocytic activation and clustering around Aβ plaques

Next, we sought to determine the effects of Aβ and tau accumulation on the activity and distribution of microglial cells. Distribution and activation of microglia (Iba1 marker), as well as their phagocytic activity (CD68 phagolysosome marker) were measured by immunohistochemistry in the hippocampus (Fig. 5A-D). First, we compared 5xFAD/AAV-tau and WT/AAV-tau littermates to assess the effects of the Aβ pathology on microglial activity. As expected, the fraction of the hippocampal tissue covered by Iba1 immunoreactivity was increased by 1.95-fold in 5xFAD/AAV-tau mice as compared to WT/AAV-tau littermates (Fig. 5E). Furthermore, the presence of phagocytic microglia was increased by nearly 3.2-fold (Fig. 5F). Both parameters were highly correlated with Aβ burden in the brain tissue, as determined by staining with the 4G8 antibody (Fig. 5G). This result reflected the accumulation and clustering of microglial cells around Aβ plaques. To quantify the grouping of microglia in 5xFAD/AAV-tau versus WT/AAV-tau mice, the number of microglial clusters was determined according to the surface covered by the Iba1 staining (Fig. 5H-I). We considered that areas <150 μm^2 were mostly representing individual microglial cells, whereas clusters covering >300 μm^2 showed the presence of groups of at least three microglial cells. In WT/AAV-tau mice, more than 90% of the Iba1-positive structures were identified as single microglial cells, whereas in 5xFAD/AAV-tau mice, more than 30% of the Iba1-positive areas corresponded to >300 μm^2 clusters, indicating extensive grouping of the microglial cells near the sites of Aβ deposition (Fig. 5J).

Figure 3-5. Aβ pathology increases microglia activation and clustering around Aβ plaques.

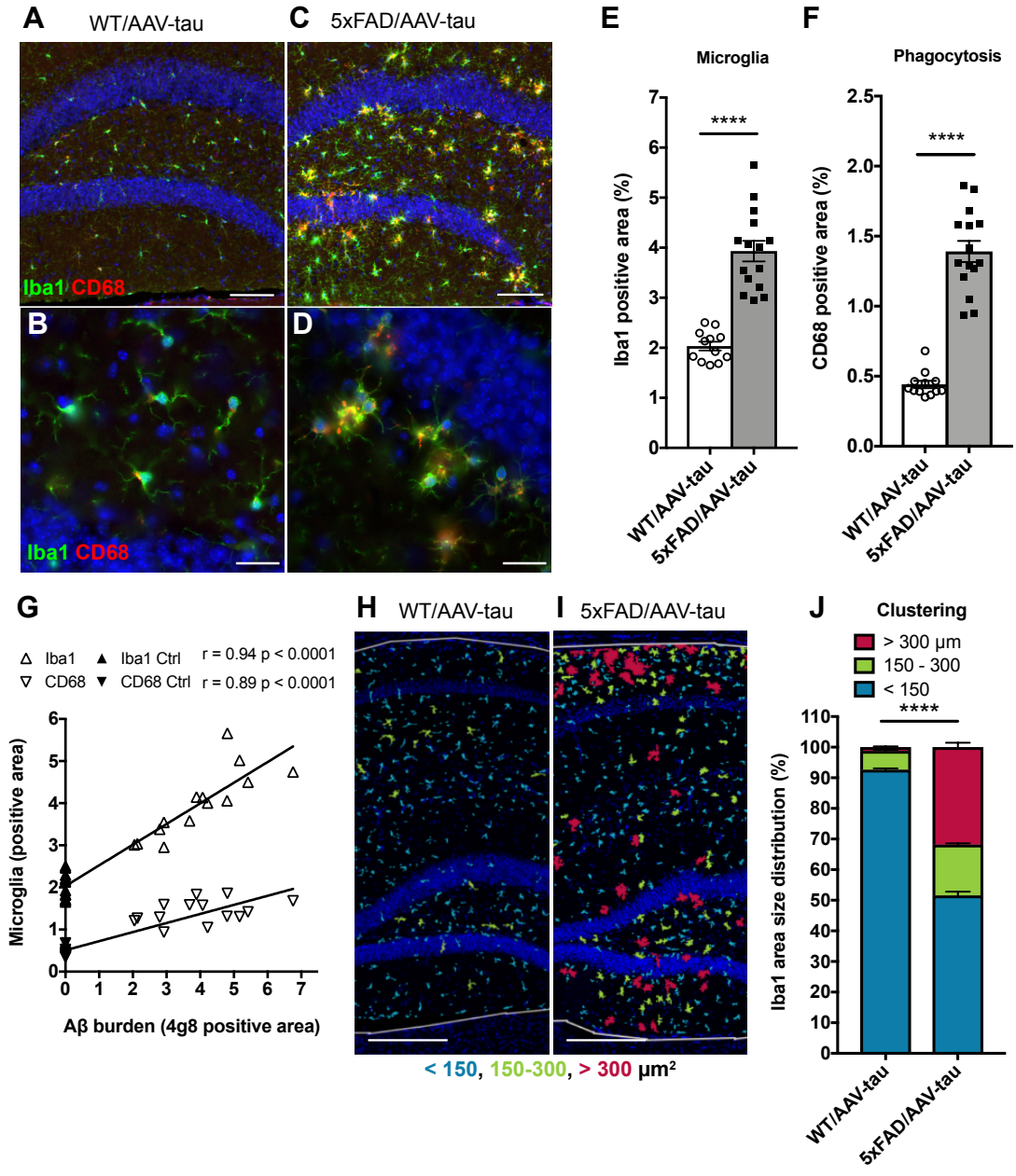

Figure 5: Aβ pathology increases microglia activation and clustering around Aβ plaques.

A-D | Representative images of the Iba1 (in green) and CD68 (in red) staining of microglia in the hippocampus. (A-B) WT/AAV-tau mice and (B-C) 5xFAD/AAV-tau mice. DAPI in blue. Scale bars: (A, C) 100 µm; (B, D) 25 µm. **E-F |**Percentage of the hippocampal area covered by (E) Iba1 staining and (F) CD68 staining. **G |** Correlation analysis between the Aβ burden and the Iba1 or CD68 positive area coverage in the hippocampus. **H-J |** As a measurement of microglia clustering, Iba1 positive areas are sorted depending on their size. In blue: single microglial cells (areas <150 µm²); in green: groups of 2 to 3 microglial cells (150 µm²≤area≤300 µm²); in red: clusters of microglial cells (areas >300 µm²). (H-I) Representative images showing the mask of the Iba1-positive areas detected using the thresholding algorithm for (H) a WT/AAV-tau mouse and (I) a 5xFAD/AAV-tau mouse. (J) Quantification of the Iba1 area size distribution. Note the effect of Aβ on microglia clustering around plaques. Scale bars: (I-J) 250 µm. Unpaired two-tailed Student's *t*-test and Pearson's correlation coefficient r, **** p < 0.0001.

Figure 3-6. Human tau overexpression affects the clustering of microglia around Aβ plaques.

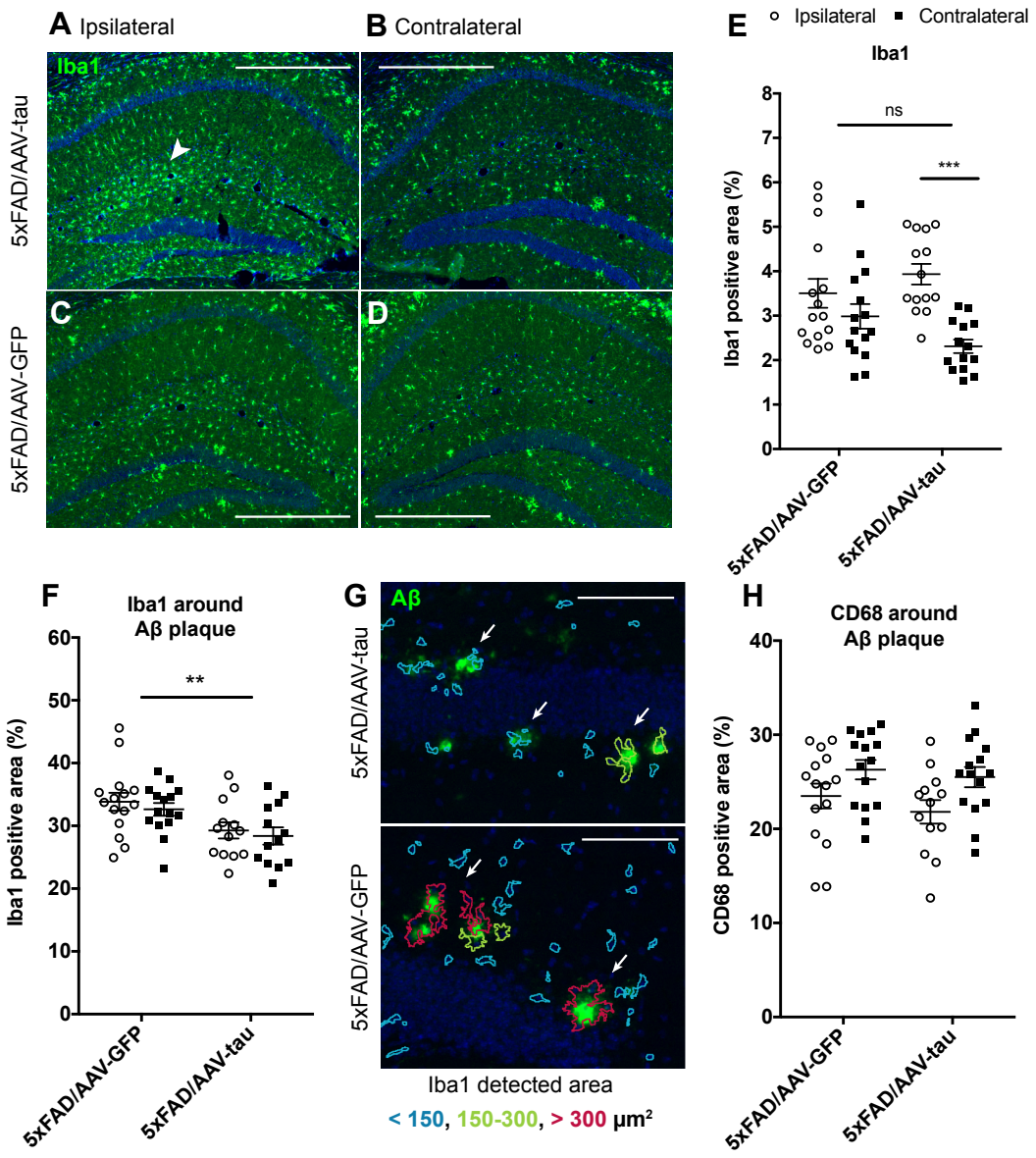

Figure 6: Human tau overexpression affects the clustering of microglia around Aβ plaques.

A-D | Representative images of the Iba1 staining (green) in the (A) ipsi- and (B) contralateral hippocampus of a 5xFAD/AAV-tau mouse, and in the (C) ipsi- and (D) contralateral hippocampus of a 5xFAD/AAV-GFP mouse. (A) Note the recruitment of activated microglia in the hippocampus injected with AAV-tau (white arrow head). Scale bars: 500 µm. DAPI in blue. **E |** Percentage of the ipsi - and contralateral hippocampus covered by Iba1 positive staining. **F |** Percentage of the extended plaque area (5 µm broad band in the periphery of the Aβ plaque) covered by Iba1 positive staining in both ipsi - and contralateral hippocampus. **G |** Representative images of the detected masks for Iba1 positive areas. In blue: single microglial cells (areas <150 µm²); in green: groups of 2 to 3 microglial cells (150 µm²≤area≤300 µm²); in red: clusters of microglial cells (areas >300 µm²). Note the decreased clustering of microglia (shown by white arrows) around Aβ deposits (6e10, in green) in presence of tau overexpression as compared to 5xFAD/AAV-GFP condition. DAPI in blue. Scale bars: 100 µm. **H |** Percentage of the extended plaque area (5 µm broad band in the periphery of the Aβ plaque) covered by CD68 positive staining. Two-way ANOVA with post-hoc Sidak's multiple comparison test; ns non-significant, ** p< 0.01, *** p < 0.001.

Human tau overexpression reduces the number of microglia located near Aβ plaques

It has been suggested that microglia degeneration in Alzheimer's disease patient could be mediated by accumulation of toxic phospho-tau species (Bussian et al., 2018; Jimenez et al., 2008; Streit et al., 2009). Therefore, we analyzed the effects of WT tau overexpression on microglia in the 5xFAD/AAV-tau mouse model.

In our model, we observed an important accumulation of Iba1 positive microglia in the injected side of the hippocampus in the 5xFAD/AAV-tau animals (Fig. 6A-B). But GFP expression in the DG seemed to also activate microglia (Fig. 6C-D). When we compared Iba1 positive microglia coverage of the hippocampus in the 5xFAD/AAv-tau with the 5xFAD/AAV-GFP animals, the effect was not significant (Fig. 6E). Of note, the effect of AAV-tau on the accumulation of Iba1 positive cells was more prominent in the ipsi- than in the contralateral hippocampus (Fig. 6E), consistent with the observed neurodegeneration. As there was no difference in the area covered by Aβ plaques neither when comparing 5xFAD/AAV-GFP and the 5xFAD/AAV-tau mice, nor between the ipsilateral and contralateral hippocampus, this increase is unlikely to be due to any effect of tau on the Aβ pathology (see Fig. 4). It is therefore likely that the injection itself or the expression of a foreign protein was sufficient to trigger microglia activation.

However, when assessing the presence of microglia in close vicinity of Aβ plaques (5 μm around), there was a significant decrease in the local coverage by Iba1-positive microglia in the group of 5xFAD/AAV-tau mice as compared to the 5xFAD/AAV-GFP group (Fig. 6F). This effect was apparent both in the ipsilateral and contralateral hippocampus. Tau was found to reduce the tight interaction between the microglia and the Aβ plaques and "distract" the microglia away from the sites of Aβ deposition compared to GFP (Fig. 6G). This effect might disrupt the ability of microglial cells to act as a protective barrier around plaques and thereby increase Aβ toxicity. The phagocytic ability of the microglia did not appear to be affected, as CD68 coverage at the vicinity of Aβ plaques remained similar in both groups (Fig. 6H). These data confirmed tau ability to locally modulate the distribution of active microglial cells in presence of the Aβ pathology.

Next, we sought to determine the effects of passive anti-Aβ immunization in this model combining amyloid and tau pathologies.

Passive anti-Aβ immunization via ECT technology delivers mAb11 antibodies in the plasma and brain of 5xFAD mice

To determine the effects of anti-Aβ immunization, we administrated mAb11 antibody subcutaneously using encapsulated cell technology (ECT), both in 5xFAD and WT mice. The treatment was initiated at the age of 12 weeks, one week after the injection of the AAV-tau vector in the CA3 hippocampus. The ECT technology has been previously described (Lathuilière et al., 2015). Briefly, it consists of an implant made of a porous polymer membrane, which is used to encapsulate C2C12 myoblasts genetically engineered to secrete recombinant mAb11 anti-Aβ antibodies. In the control group, mice were implanted with a capsule loaded with non-modified myoblasts. The implant is surgically inserted in the subcutaneous tissue. Following engraftment, the encapsulating membrane is in close contact with the host blood vessels, which allows for the continuous delivery of anti-Aβ antibodies, the plasma concentration of which can be measured using an ELISA for the detection of mAb-11. With cell growth inside the implant, the antibody concentration was found to progressively rise in the plasma of the treated 5xFAD/AAV-tau mice, reaching on average 58 µg/ml at week 20 after implantation (Fig 7A). Based on plasma mAb-11 concentration measured every week, a total exposure was calculated over 20 weeks of implantation, reaching on average 4800 µg of mAb11 per ml of plasma (Fig. 7B).

It was previously shown that following peripheral administration, a fraction of the antibodies can cross the blood brain barrier and bind Aβ plaques in the brain parenchyma (Bard et al., 2000; Lathuilière et al., 2016). In order to show target engagement of mAb11, we assessed IgG2a immunoreactivity at the level of Aβ plaques using an isotype-specific antibody. In the 5xFAD/AAV-tau mice treated with mAb11-secreting ECT, IgG2a signal could be detected in the core of Aβ plaques revealed by DAPI staining (Fig. 7C). In contrast, no IgG2a immunoreactivity could be detected in the untreated 5xFAD/AAV-tau mice (Fig. 7D).

Next, we investigated the effects of passive anti-Aβ immunization on Aβ pathology in the hippocampus of 5xFAD mice.

Figure 3-7. mAb11 anti-Aβ antibody delivery.

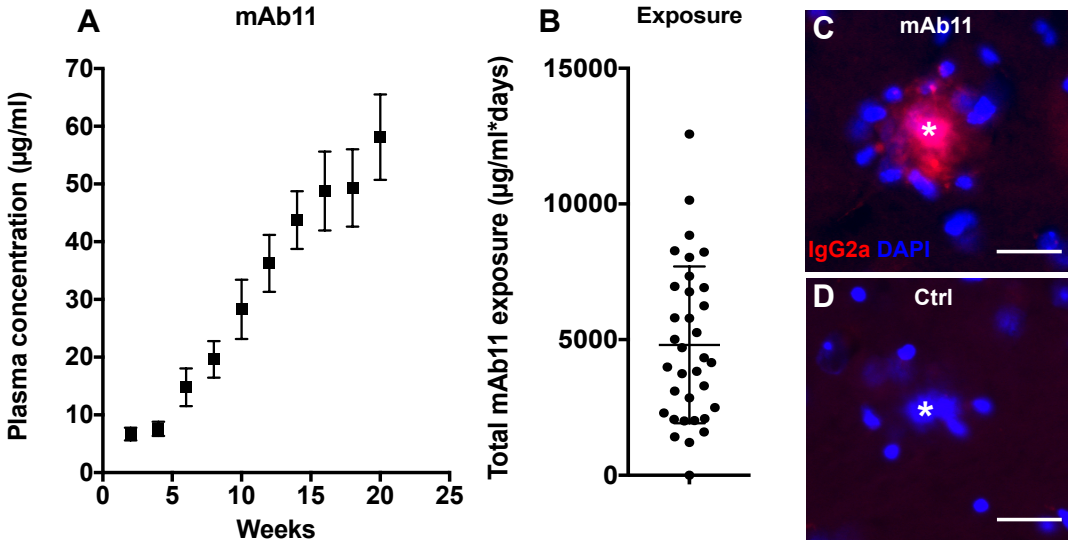

Figure 7: mAb11 anti-Aβ antibody delivery.

A | Average anti-Aβ mAb11 concentration detected in the plasma of 5xFAD/AAV-tau and WT/AAV-tau animals implanted with encapsulation devices containing C2C12 cells secreting the mAb11 antibody. **B |** Integrated exposure of these animals to the mAb11 anti-Aβ IgG2a antibody during the entire duration of the treatment (144 days). **C-D |** Representative images of the immunodecoration of the Aβ plaques by the mAb11 antibody revealed using a specific anti-IgG2a antibody (red) in (C) treated animals. (D) There are no detectable IgG2a antibodies on Aβ plaques in control animals. DAPI in blue marks both the cell nuclei and the Aβ plaque core (white asterix). Scale bars: 25 µm.

Passive immunization against Aβ reduces the number of amyloid plaques in the hippocampus and enhances their size and compaction

Passive anti-Aβ immunization delivered by ECT has previously been found to decrease Aβ burden in different Alzheimer's mouse models (Lathuilière et al., 2016). However, this effect was highly dependent of the extent of the Aβ pathology at the onset of passive anti-Aβ immunization administration. Here, as the 5xFAD mice used in the present study develop an aggressive amyloid pathology already after two months (Oakley et al., 2006), the implantation of the ECT device at the age of 3 months delivers anti-Aβ when the pathology is already established.

To assess passive anti-Aβ immunization effect in the 5xFAD/AAV-tau mouse model, brain tissue was collected 5 months after device implantation and stained using the 4G8 anti-Aβ antibody (Fig. 8A-B). We measured a significant decrease in the number of 4G8-positive Aβ plaques per mm^2 in the hippocampus of the treated 5xFAD/AAV-tau mice compared with the control group (Fig. 8C). However, the 4G8-positive area in the hippocampus remained similar in both groups (Fig. 8D). Indeed, in the mAb11-treated 5xFAD/AAV-tau mice, the decreased number of Aβ plaques was compensated by a significant increase of the average plaque size, from 303 μm^2 in control mice to an average of 495 μm^2 in mAb11-treated 5xFAD/AAV-tau mice (Fig. 8E). In addition, these larger 4G8-positive Aβ plaques appeared more compact and lacked the fibrillary halo typically observed in non-treated 5xFAD mice (Fig. 8F-G). To further assess the effect of passive anti-Aβ immunization on amyloid plaques, we analyzed the plaque size distribution (Fig. 8H-J). Whereas the proportion of large 4G8-positive Aβ plaques (area > 500 μm^2) nearly doubled in response to mAb11 treatment, the proportion of smaller 4G8-positive Aβ plaques (30 to 500 μm^2) was significantly decreased.

Although the late administration of anti-Aβ antibodies in the 5xFAD/AAV-tau mouse model did not significantly reduce the Aβ plaque burden, it was found to modulate Aβ pathology by reducing the number of Aβ deposits, as well as enhancing their size and compaction.

Figure 3-8. Effects of passive anti-Aβ immunization on Aβ pathology.

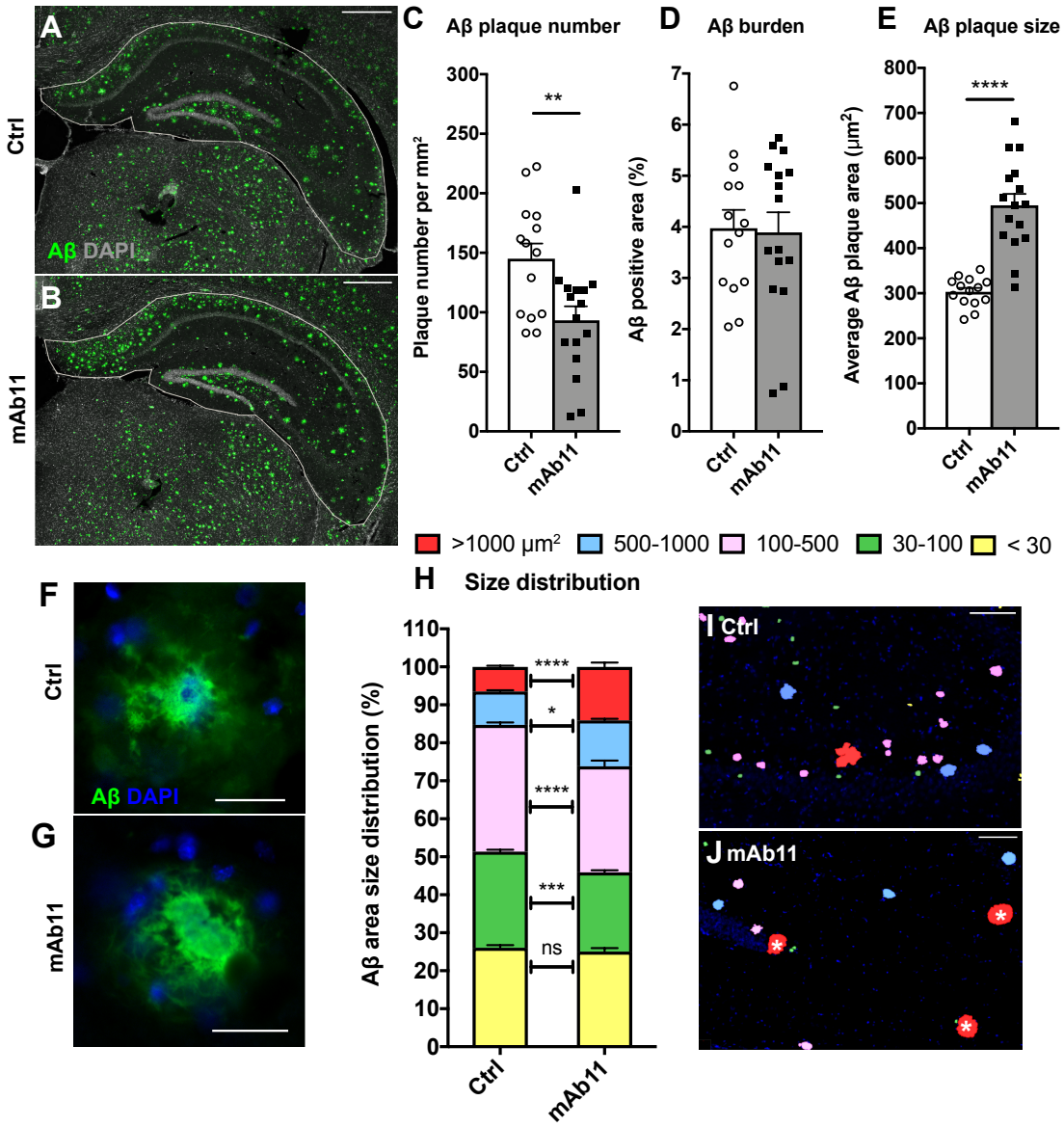

Figure 8: Effects of passive anti-Aβ immunization on Aβ pathology.

A-B | Representative images of the Aβ staining 4G8 (green) in the contralateral hippocampus of (A) control and (B) mAb11-treated 5xFAD/AAV-tau mice. The white line delineates the region of interest (ROI) used for analysis of Aβ pathology. DAPI in grey. Scale bars: 500 µm **C |** Number of Aβ positive areas per mm² detected in the hippocampal ROI. **D |** Percentage of the hippocampal ROI covered by Aβ staining. **E |**Average area of individual Aβ plaques. **F-G |** Representative images of 4G8 positive plaques in (F) a non-treated mouse and (G) a mAb11-treated mouse. DAPI in blue. Scale bars: 50 µm. **H-J |** Distribution of Aβ plaques according to their size: yellow for plaques <30 µm²; green for 30-100 µm² large plaques, pink for 100-500 µm², blue for 500-1000 µm² and red for Aβ deposits >1000 µm². Areas below 10 µm² were not considered as Aβ plaques. (H) Plaque size distribution in percentage of the total Aβ-positive area detected with the 4G8 antibody. Note the significant increase in the fraction of plaques with a size >500 µm² following mAb11 treatment. (I-J) Representative images of the masks of the thresholded Aβ signal used for the analysis. Note the presence of large size Aβ deposits with a compact shape (white *) in the mAb11-treated condition. DAPI in blue. Scale bars: 100 µm. Unpaired two-tailed Student's *t*-test, * $p < 0.05$, ** $p < 0.01$, *** $p < 0.001$, **** $p < 0.0001$.

Passive immunization enhances microglia activation around Aβ plaques in the 5xFAD/AAV-tau model

The anti-Aβ antibody mAb11 was initially designed to bind Aβ plaques and trigger cell-mediated Aβ clearance (Bohrmann et al., 2012; Xiang et al., 2016). In the TAUPS2APP mouse model, we previously demonstrated that passive immunization with mAb11 indeed increased the number of Iba1-positive microglia around Aβ plaques (Lathuilière et al., 2016).

Next, we sought to further explore the effects of passive anti-Aβ immunization on microglia in the 5xFAD/AAV-tau mouse model. We quantified the Iba1 microglial marker and the CD68 phagolysosome marker using immunohistochemistry in the hippocampus of mAb11-treated and control 5xFAD/AAV-tau mice (Fig. 9A-B). When measured over the whole hippocampal area, passive anti-Aβ immunization did not affect neither the Iba1-positive area (Fig. 9C) nor the CD68-positive area (Fig. 9D). Next, the analysis was focused on the area in close proximity to Aβ plaques in the hippocampus identified using the 4G8 immunostaining. We measured a significant increase in the Iba1-positive area in the mAb-11 treated 5xFAD/AAV-tau mice (Fig. 9E). Furthermore, the CD68-positive area was also increased around Aβ plaques in the mAb11-treated group (Fig. 9F). These results confirmed that even in presence of overexpressed human tau previously found to reduce the presence of microglia near the amyloid plaques, the anti-Aβ treatment is able to recruit and cluster microglia near the Aβ deposits and increase their phagocytic activity.

Next, we sought to determine the effects of passive anti-Aβ immunization on local tau pathology in 5xFAD/AAV-tau mouse model.

Figure 3-9. Passive anti-Aβ immunization enhances the presence of activated microglia near Aβ plaques.

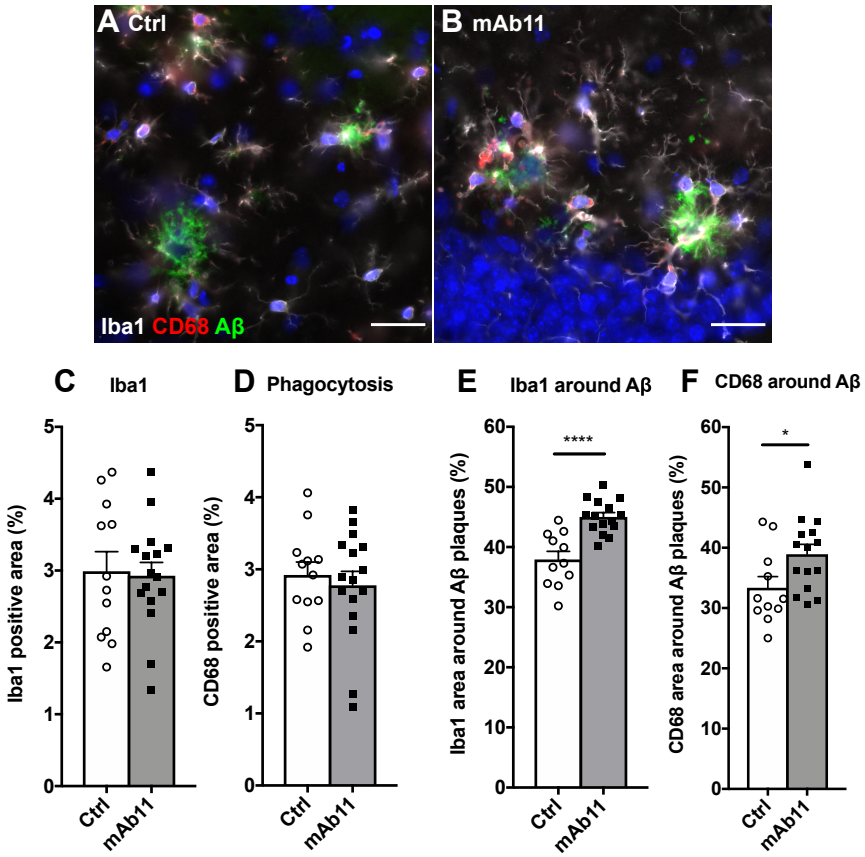

Figure 9: Passive anti-Aβ immunization enhances the presence of activated microglia near Aβ plaques.
A-B | Representative images of Aβ deposits (6e10 in green) surrounded by activated microglia (Iba1 staining in white) in a non-treated (D) and a mAb11-treated (E) 5xFAD/AAV-tau mouse. Shown in red, note the presence of microglia positive for the CD68 phagolysosome marker. DAPI in blue. Scale bars: 25 µm. **C-D |** Percentage of the hippocampal region covered by (C) the Iba1 staining and (D) the CD68 positive staining in control and mAb11-treated 5xFAD/AAV-tau mice. **E-F |** Percentage of the extended plaque area (5 µm broad band in the periphery of the Aβ plaque) covered by (D) the Iba1 staining and (E) the CD68 staining in the hippocampal region of control non-treated and mAb11-treated 5xFAD/AAV-tau mice. Note the significant effects of the mAb11 treatment on the recruitment of Iba1- and CD68-positive microglia near the Aβ plaques. Unpaired two-tailed Student's *t*-test, * $p < 0.05$, **** $p < 0.0001$

Figure 3-10. Passive anti-Aβ immunization reduces human tau spreading and prevents the formation of tau-positive dystrophic neurites

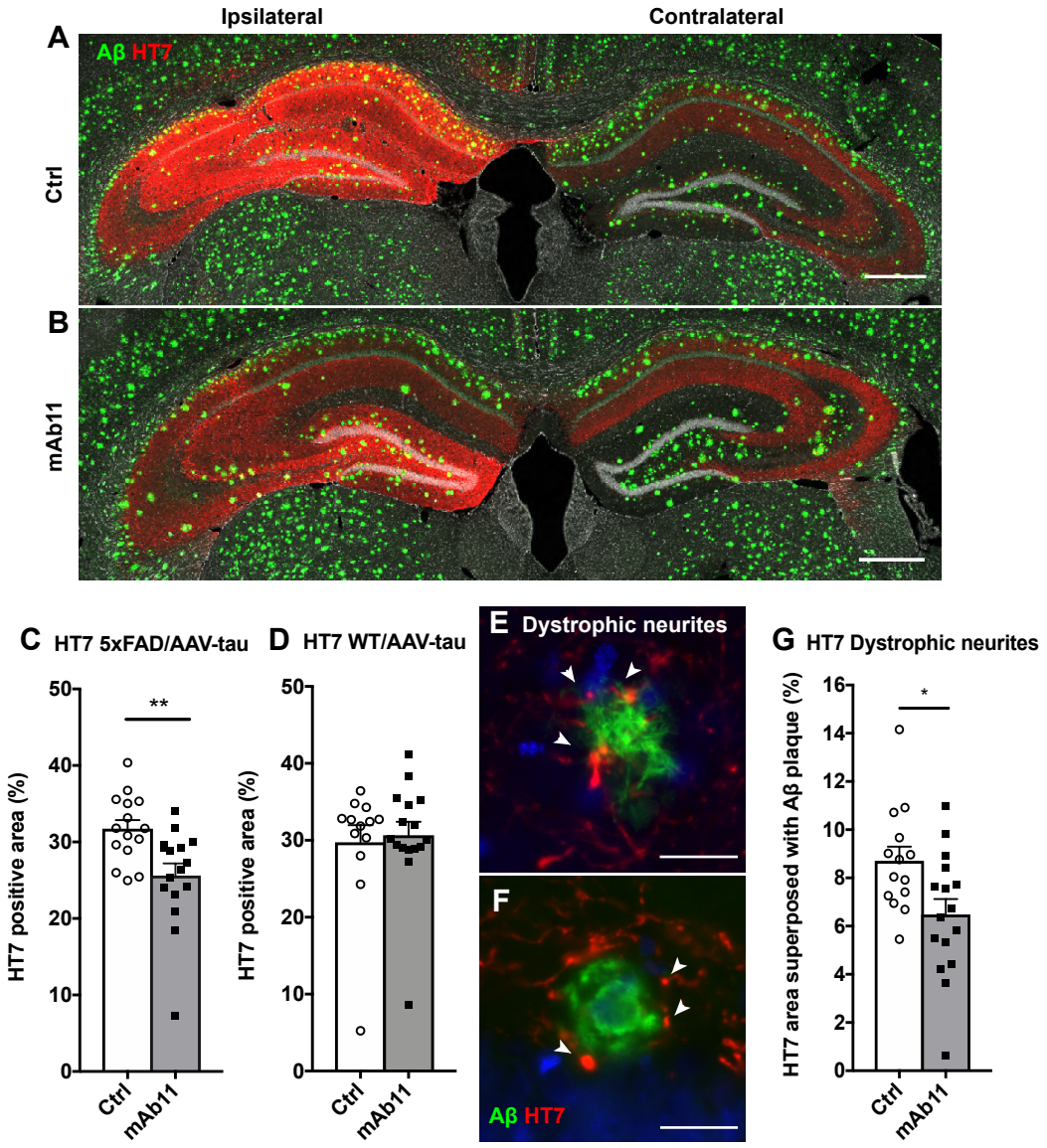

Figure 10: Passive anti-Aβ immunization reduces human tau spreading and prevents the formation of tau-positive dystrophic neurites near Aβ plaques.

A-B | Representative images of the human WT tau protein distribution (HT7 staining in red) in the ipsi- and contra-lateral side of the hippocampus in (A) a non-treated and (B) a mAb11-treated 5xFAD/AAV-tau mouse. DAPI in grey. Scale bars: 500 µm **C-D|** Percentage of the entire hippocampal region (both ipsi- and contralateral hippocampus) covered by the HT7 staining in control non-treated and mAb11-treated mice. (C) Note the significant effect of the mAb11 treatment in the 5xFAD/AAV-tau mice. (D) In contrast, the mAb11 treatment has no effect in WT/AAV-tau mice. **E-F|** Representative images of the HT7-positive dystrophic neurites (red puncta indicated by arrowheads) surrouding the Aβ deposits (4G8 staining in green) in the contralateral hippocampus of (E) a control non-treated and (F) a mAb11-treated 5xFAD/AAV-tau mouse. DAPI in blue. Scale bars: 25 µm. **G |** Percentage of the Aβ-positive area (plaque with halo) covered by the HT7 signal which typically labels dystrophic neurites in the contralateral hippocampus of 5xFAD/AAV-tau mice. Note the significant decrease of the surface covered by human tau positive dystrophic neurites in the mAb11-treated mice. Unpaired two-tailed Student's *t*-test, * $p < 0.05$, ** $p < 0.01$.

Passive immunization in 5xFAD/tau model reduces human tau spreading in the hippocampal formation

Using immunohistochemistry, we quantified the distribution of HT7 human tau immunoreactivity to determine the effects of anti-Aβ immunization on tau spreading throughout the hippocampal formation (Fig. 10A-B). In both ipsi- and contralateral hippocampus of the mAb11-treated 5xFAD/AAV-tau animals, we observed a decreased of the HT7-positive area (Fig. 10C). Importantly, there was no difference in the HT7-positive area in WT/AAV-tau mice treated with mAb11, showing that the presence of amyloid plaques is required to reveal this effect of anti-Aβ immunization (Fig. 10D). To further assess the effects of passive anti-Aβ immunization on tau distribution, we quantified the abundance of HT7-positive dystrophic neurites associated to Aβ plaques in the hippocampus contralateral to AAV-tau injection (Fig. 10E-F). Again, we observed a significant reduction of the HT7-positive dystrophic neurites in the mAb11-treated 5xFAD/AAV-tau mice (Fig. 10G), demonstrating a positive effect of the treatment on tau-related pathological manifestations at the level of the neuritic plaques.

Passive immunization does not rescue tau hyperphosphorylation or hippocampal degeneration in 5xFAD/AAV-tau model

Next, we sought to evaluate the effects of passive anti-Aβ immunization on the abundance of phosphorylated tau and tau-induced degeneration of the DG. We compared the area covered by AT8 immunoreactivity in mAb11-treated and control 5xFAD/AAV-tau mice. In the ipsilateral hippocampus, where AT8 immunoreactivity is most abundant, there was no difference between these groups (Fig. 11A). In the contralateral hippocampus, where AT8-positive puncta were mainly associated to the neuritic plaques, there was also no significant effect of the treatment, despite the previously observed reduction of HT7 immunoreactivity (Fig. 11B). Altogether, these results suggest that late administration of passive anti-Aβ immunization does not affect AT8 immunoreactivity (Fig. 11A-B). Similar results were obtained when assessing the level of misfolded tau (MC1 staining, Supplementary S1).

In order to determine the effects of anti-Aβ immunization on hippocampal degeneration, we measured the ipsilateral/contralateral ratio of the DG area. The

measured ratio was similar in the mAb11-treated and control groups of 5xFAD/AAV-tau mice, which suggests that passive anti-Aβ immunization did not alleviate the degeneration of the hippocampus observed on the side ipsilateral (Fig. 11C).

Overall, we found that passive immunization with ECT-mediated delivery of the mAb11 anti-Aβ antibodies effectively clusters phagocytic microglia around Aβ deposits in 5xFAD/AAV-tau mice. The treatment leads to the compaction of Aβ plaques and prevents the spreading and accumulation in the neuritic plaques of the human tau protein overexpressed in the hippocampal formation.

Figure 3-11. Passive anti-Aβ immunization does neither reduce phosphorylated tau nor rescue hippocampal degeneration.

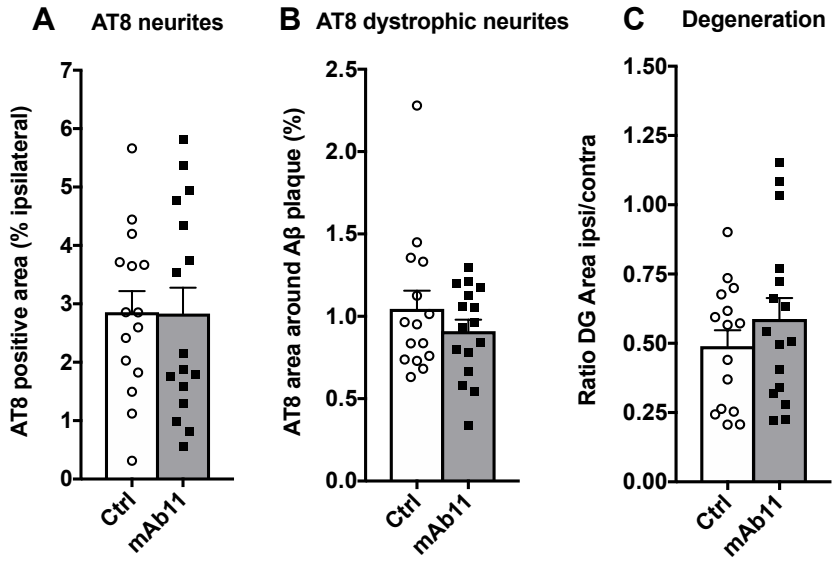

Figure 11: Passive anti-Aβ immunization does neither reduce phosphorylated tau nor rescue hippocampal degeneration.

A | Percentage of the ipsilateral hippocampus covered with AT8 positive signal in the control 5xFAD/AAV-tau mice compared to mAb11-treated mice. **B |** Percentage of the extended plaque area (5 μm broad band in the periphery of the Aβ plaque) covered by AT8 positive puncta in the contralateral hippocampus of control non-treated and mAb11-treated 5xFAD/AAV-tau mice. **C |** Hippocampal degeneration assessed by the ratio of the ipsi/contralateral dentate gyrus area in the control non-treated and mAb11-treated 5xFAD/AAV-tau mice. Unpaired two-tailed Student's *t*-test.

3.4 Discussion

Here we assess the effect of passive immunization in a mouse model of AD with combined ongoing Aβ and tau pathologies. Whereas the onset of Aβ plaque deposition is usually observed at the age of 8 weeks in 5xFAD mice, human tau accumulation will be induced after AAV-tau injection at week 11. The condition at the time anti-Aβ immunization is initiated might be representative of the stage of prodromal to mild AD, at which patients are usually enrolled in clinical trials (Ostrowitzki et al., 2017). At this stage, the development of the tau pathology is a prominent feature of the disease, which correlates with cognitive decline (Buerger et al., 2002).

The combined Aβ and tau mouse model used in the present study has the advantage of modularity, which allows to separately assess the contribution of Aβ and tau pathologies. Aβ accumulation creates a neurotoxic microenvironment around deposits contributing to the formation of the neuritic plaque, but does not cause any major neuronal degeneration. On the other hand, tau overexpression triggers clear hippocampal neurodegeneration near the site of AAV-tau vector injection in the CA3 hippocampus. We observed evident interaction between the Aβ and tau pathologies at the level of the neuritic plaques with the apparition of phospho tau (AT8) positive punctae as well as total tau positive dystrophic neurites. Aβ deposition has recently been shown to promote tau pathological conversion around plaques by potentially creating an environment favorable to seeding and spreading of tau aggregates (He et al., 2018; Li et al., 2016). In these studies, human WT tau, overexpressed as truncated 4R WT tau in one study or injected as human AD-brain derived pathological tau in the other, only formed NFTs in presence of neuritic plaques. It suggested that both tau and Aβ pathology might be required for pathological spreading of WT human tau.

Aβ and tau have seemingly different effects on the distribution and activity of microglial cells. Although it is well known that Aβ deposition triggers microglia clustering around amyloid plaques, the effect of tau on microglia activation has been less explored. There is evidence that long-term phagocytosis of tau could

induced microglia premature senescence (Bussian et al., 2018; Streit et al., 2009), impairing microglia functions. In our study, we observed a reduction of microglia clustering behavior around Aβ deposition in presence of human tau, suggesting that tau overexpression may affect the normal interaction of microglia with the Aβ plaques.

In this context, animals were treated using passive anti-Aβ immunization. We considered the treatment as late administration of anti-Aβ antibody as both Aβ and tau pathologies are already present at the time. The mAb11 antibody was designed to target Aβ plaques and fibrils and activate cell-mediated removal of Aβ (Bohrmann et al., 2012; Lathuilière et al., 2016). In the present study, passive immunization with mAb11 did not decrease Aβ burden in 5xFAD/AAV-tau mice, but instead modulated the Aβ deposition, as shown by the lower number of plaques with a larger size. The resulting Aβ plaques appear more compact, suggesting that the binding of anti-Aβ antibodies can remove or prevent the Aβ fibrillary halo surrounding the plaques. Furthermore, passive anti-Aβ immunization increases microglia area coverage around the plaques and enhances the phagocytic activity of microglia. Remarkably, passive anti-Aβ immunization is able to counteract the effect of tau overexpression, by recruiting microglia towards the Aβ plaques. Microglia processes which tightly surround the Aβ deposits are likely to be responsible for the observed amyloid plaque compaction.

It has been reported that plaques may act as a reservoir of Aβ oligomers and slowly release toxic Aβ species in the brain parenchyma (Condello et al., 2015). Protective microglia are able to form a barrier around the Aβ plaques to reduce this toxic release and mitigate local pathological manifestations, such as the formation of dystrophic neurites around the plaques (Ulland et al., 2017). In mice treated with passive immunization, we indeed observed a reduction of human tau positive dystrophies at the level of the neuritic plaques, as well as a decrease of human tau spreading throughout the hippocampal formation. It is conceivable that these effects are indirectly related to the clustering and activity of microglia around plaques.

3.4 Discussion

In AD, the chronic stimulation of microglia and their exposure to pathological tau might impair their activity. We show in this study that overexpression of human tau can also 'distract' the microglia, redirecting these cells away from the sites of Aβ deposition in the hippocampal tissue. Other factors, such as genetic determinants, might also be involved. *TREM2* gene variation, for example, is an important risk factor in sporadic Alzheimer's disease. *TREM2* variants impair microglia activation (Keren-Shaul et al., 2017; Zhao et al., 2018). Microglia with TREM2 dysfunction lose their ability to cluster and fail to act as a barrier, which results in increased neuritic damage in close proximity to the Aβ plaque (Wang et al., 2016; Yuan et al., 2016).

Following passive immunization, microglia clustering around plaques may decrease the local release of toxic Aβ species and thereby prevent downstream pathogenic effects mediated by tau. Here, we observe a reduced accumulation of human tau in the neuritic plaques. This effect may prevent the recently proposed pathogenic role of tau deposition at the level of neuritic plaques, further spreading and seeding tau aggregation (Li et al., 2016). Along these lines, another recent report has shown that TREM2 impairment in mice increases the level of phosphorylated tau in neuritic plaques (Leyns et al., 2019). This result is reinforcing the evidence that microglia clustering around Aβ deposits may affect nearby tau pathology. However, even though we observed a reduction of total human tau around neuritic plaque with passive anti-Aβ immunization, we did not see any reduction of AT8 phosphorylated tau. Although other phosphorylation sites should be analyzed, this result suggests that the treatment might not be sufficient to alleviate all aspects of the tau pathology (Oddo et al., 2004). Indeed, passive anti-Aβ immunization does not show any significant effects on the tau-induced hippocampal degeneration in our combined Aβ/tau mouse model. Hence, late administration of anti-Aβ antibodies may not be sufficient to fully rescue the pathogenic effects of tau, suggesting that complementary therapeutic therapies are likely to be needed to alter the course of AD.

3.5 Conclusion

The combined Aβ/WT tau mouse model we developed is recapitulating important hallmarks of Alzheimer's diseases. It is particularly relevant because we were able to mimic the sequence of Alzheimer's disease development observed in patient and because we are expressing WT tau. In addition of both Aβ and tau pathologies, it also show synaptic abnormalities, neurodegeneration and microglial activation. Our modular approach using the injection of a viral vector allowed us to better delineate the respective contributions of Aβ and WT tau in the induced pathology as well as investigate their interaction. We were able to study the impact of passive anti-Aβ immunization on both pathologies.

Supplementary Figure S2. The Aβ pathology and the passive immunization against Aβ have no effects on MC1 tau immunoreactivity.

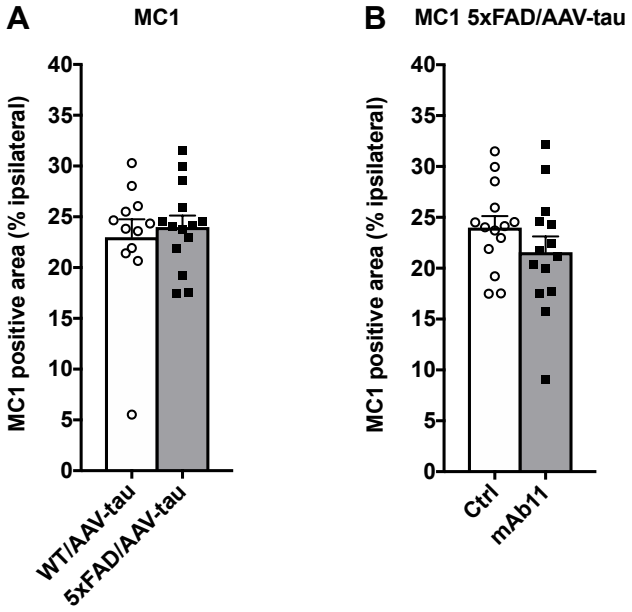

Supplementary figure S2: The Aβ pathology and the passive immunization against Aβ have no effects on MC1 tau immunoreactivity.

A | Percentage of the ipsilateral hippocampus covered by MC1 positive area in WT/AAV-tau *versus* 5xFAD/AAV-tau mice. **B |** Percentage of MC1 positive area coverage in the ipsilateral hippocampus in the 5xFAD/AAV-tau mouse model. Comparison between the control non-treated group and the mAb11-treated group of 5xFAD/AAV-tau mice. Unpaired two-tailed Student's *t*-test.

4

Chapter 4 : Developing a human cell line secreting antibodies for encapsulated cell technology

Vanessa Laversenne[1], Kamel Mamchaoui[2], Bernd Bohrmann[3], Patrick Aebischer[1] and Bernard L. Schneider[1]

1 Neurodegenerative Studies Laboratory, Brain Mind Institute, Ecole polytechnique Fédérale de Lausanne (EPFL), CH-1015 Lausanne, Switzerland

2 Thérapie des maladies du muscle strié, Institut de Myologie, UM76, UPMC Université de Paris 6, Paris, France

3 Pharma Research and Early Development, DTA Neuroscience, Roche Innovation Center Basel, F. Hoffman-La Roche, Switzerland

4.1 Abstract

The administration of monoclonal antibodies (mAbs) against a precise target, such as cancerous cells or aggregated proteins, holds promise for the treatment of various diseases. For Alzheimer's disease (AD), this approach is tested in prevention trials such as Dominantly Inherited Alzheimer Network Trial Unit (DIAN-TU). Such preventive trials, if successful, might raise difficulties in terms of antibody production as well as chronic administration. Indeed, passive anti-amyloid beta (Aβ) immunization will likely require monthly injections of mAbs, and the treatment may need to be administered for years, possibly decades.

As an alternative system for the chronic delivery of mAbs, we developed a subcutaneous implant based on encapsulated cell technology (ECT). The encapsulating polymer membrane is able to prevent the immune rejection of cells implanted in allogeneic conditions. The implant is able to continuously produce and deliver mAbs subcutaneously. Antibodies are then able to diffuse via the blood stream, reaching distant organs such as the brain. In AD mouse models, antibodies delivered using the implant were able to cross the blood brain barrier and reach the Aβ plaques, reducing Aβ burden. This proof-of-concept study in mice was based on a murine myoblast cell line. For translation into human, we aimed at finding a renewable source of human myoblasts, and at defining optimal conditions for implantation using ECT.

We tested the C25 immortalized human myoblast cell line to assess their ability to be encapsulated and to secrete sufficient amounts of mAbs. Encapsulated C25 cells were engineered to secrete the therapeutic amount of mAbs *in vitro*. *In vivo*, encapsulated C25 cells were able to engraft and form a viable tissue inside the device. C25 survival remained stable up to 4 months after implantation, but remained limited to a few cell layers. Unfortunately, the density of surviving cells did not reach the level needed for the systemic delivery of mAbs, as demonstrated by the rapid decline of mAb plasma concentration.

4.2 Introduction

Immunotherapy is currently one of the most promising approaches to treat diseases such as cancer or neurodegenerative diseases (Buss et al., 2012). Among the possible immunotherapy approaches, the administration of recombinant antibodies directed against a precise target, also called passive immunization, is widely developed. Early 2019, there were over 80 monoclonal antibodies that have been granted market approval. This number is expected to grow as there are currently 975 clinical trials recruiting on clinicaltrial.gov that involve monoclonal antibodies. These antibodies are directed against a wide range of targets in order to treat or stop multiple diseases such as cancers, autoimmune or neurodegenerative diseases.

Whereas developing efficient antibodies will continue provide therapeutic benefits to society, the delivery of these antibodies to the human body has limitations. Indeed, for applications such as Alzheimer's disease (AD) or multiple sclerosis, the treatment is very likely to be chronic and to necessitate repeated injections every month.

The treatment might be costly due to the necessity to produce large amounts of antibodies to cover the needs of treating chronic diseases. In addition, it might impact the patient's quality of life, as antibody administration would require regular interventions by trained medical staff. Side effects due to high dose injections at elevated concentrations may also limit the therapeutic applications of recombinant antibodies.

To address these questions, we developed an alternative antibody delivery system based on the encapsulated cell technology (ECT). The implant was designed as a "flat-sheet" device with 1.2 mm thickness in order to maximize the available inner space for cell load, and optimize the exchange of oxygen and nutrients when implanted into the host tissue (Lathuilière et al., 2014b). Cells are loaded inside the device with a polyethylene glycol (PEG) hydrogel matrix, which supports 3D growth. Following subcutaneous implantation using a minimal surgical procedure, this "flat-sheet" device allowed for continuous cell-mediated antibody delivery for up to 10 months in mice (Lathuilière et al., 2016).

In the context of AD, the implant was used to secrete mAb11, a murinized recombinant IgG2a antibody targeting Aβ plaques. The systemic and continuous delivery of mAb11 using ECT was able to decrease Aβ burden in AD mouse models (Lathuilière et al., 2016). This proof-of-concept study was performed using encapsulated mAb11 secreting C2C12 murine cells (Yaffe and Saxel, 1977).

Unfortunately, it is not possible to use C2C12 myoblasts to translate the ECT towards human applications. Indeed, ECT efficiently protects cells of allogeneic origin from immune rejection by preventing cell-to-cell contacts with host immune system. In xenogeneic conditions however, the immunoprotection provided by ECT is limited and typically requires immunosuppression (Song and Roy, 2016). Therefore, the development of a human cell line adapted to ECT and able to secrete recombinant antibodies at high levels would benefit the application of this technology.

To adapt our system using human cells, we decide to use a human cell that shares as many characteristics with C2C12 myoblasts as possible. C25cl48 is a clonal immortalized myoblast cell line developed at the Myology Institute in Paris. Mamchaoui et al. modified myoblasts coming from human donors using lentiviral vectors to express human telomerase reverse transcriptase (hTERT) and cyclin-dependent kinase (CDK)-4 (Mamchaoui et al., 2011). hTERT allows elongation of the telomere whereas CDK-4 blocks activation of p16-mediated cellular stress pathway. When combined, these two factors prevent senescence of the human myoblasts and allow their long-term culture *in vitro*. “C25” cells are derived from a healthy 25 year-old donor.

In order to evaluate if C25 were suitable for encapsulation, we first characterized their survival and differentiation in PEG hydrogel and tested their ability to survive inside the flat sheet device *in vitro*. Next, the C25 cell line was genetically engineered using lentiviral vectors to produce the recombinant mAb11 antibody. Finally, we tested the survival of encapsulated C25 myoblasts and their antibody secretion *in vivo*, following implantation in immunocompromised Rag2/Ilr2g double knock-out mice.

4.3 Results

C25 cells survive for weeks when grown in the PEG gel

In order to evaluate the ability of the C25 cells to colonize the implant, cells were grown in biodegradable PEG hydrogel with different stiffness conditions (3 kPa and 300 Pa) and seeded in the gel at different densities (320 cells/µl, 1200 cells/µl and 10'000 cells/µl). The stiffness of the gel depends on PEG content in the hydrogel mix and is measured in Pascal (Nicodemus and Bryant, 2008). The morphology of the cells as well as their survival was evaluated by bright-field microscopy every week.

In stiff PEG gels over 3 kPa (3% PEG hydrogel), C25 cells extended and changed their morphology during the first week (Fig. 1A). After 4 weeks, the C25 cells formed a three-dimensional (3D) tissue made of myotubes (Fig. 1B). This 3D cell network grew and became denser over time (Fig. 1C). In soft PEG gel, with a stiffness around 300 Pa (1.5% PEG hydrogel), C25 appeared to lack mechanical support and displayed a round shape morphology during the first week (Fig. 1D). At month 1, myoblasts showed a tendency to migrate towards the surface of the PEG gel, and fused to form aligned cell clusters (Fig. 1E). At month 2, cells formed a 2D network at the surface of the PEG gel only (Fig. 1F).

C25 cells did not occupy the entire space available inside the hydrogel, regardless of the initial seeding density (Fig. 1G-I). At high density seeding, the fibers network was slightly denser with thinner fibers (Fig. 1I). After 2 months, the cells stabilized and the network did not grow significantly.

In conclusion, C25 cells were able to grow in the PEG hydrogel and seemed to be better under stiff conditions. The seeding density, on the other hand, did not appear to be an important parameter for cell growth.

Figure 4-1. 3D growth of C25 cells in PEG hydrogel

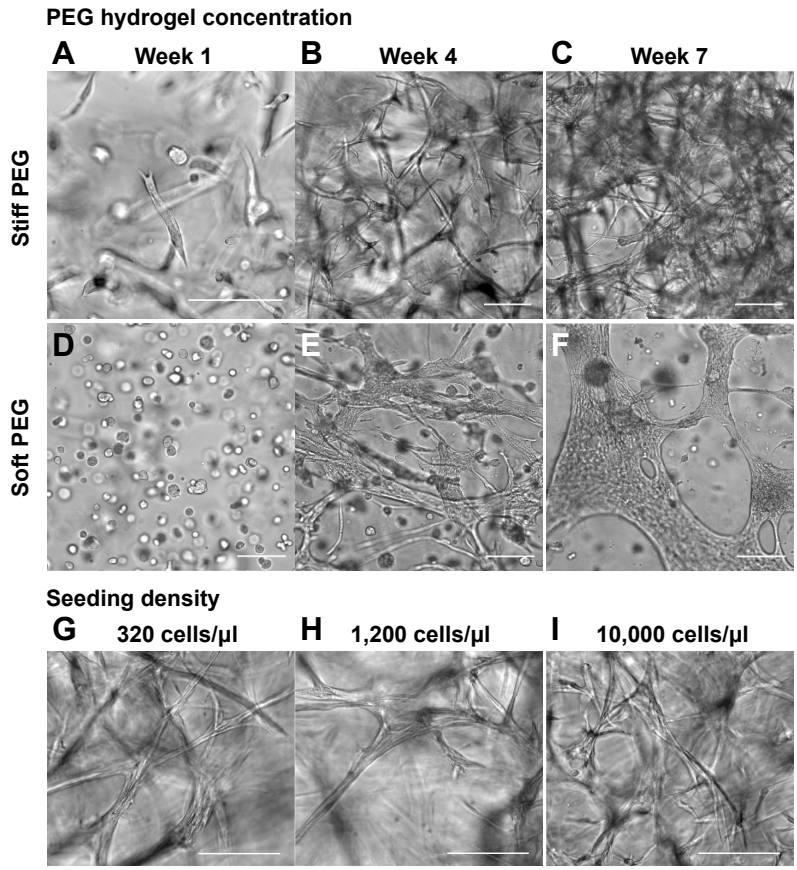

Figure 1: 3D growth of C25 cells in PEG hydrogel

A-F | Representative bright-field images of C25 cell growth over time in PEG hydrogel (A-C) >3kPa (stiff , 3% w/v PEG) and (D-F) at 300Pa (soft, 1.5% w/v PEG). (A) Note the exploratory behavior of the cells as soon as week 1 in stiff gel compared to (D) soft gel. Cells were seeded at 1'200 cells per µl PEG hydrogel. **G-I |** Representative images of C25 cell density after 4 weeks growth in stiff hydrogel (>3kPa, 3% w/v PEG). Cells were initially seeded at (G) 320 cells/µl, (H) 1'200 cells/µl and (I) 10'000 cells/µl. Scale bars: 100 µm.

C25 spontaneously differentiated in PEG gel

To evaluate the differentiation of C25 cells into myotubes in two-dimension (2D) and three-dimension (3D) cell cultures, we performed immunohistochemistry using anti-myosin heavy chain (MHC) antibody. In 2D culture, C25 cells did not spontaneously express MHC (Fig. 2A). However, there were able to differentiate when exposed to differentiation medium (Fig. 2B). After 5 days, C25 cells exposed to differentiation medium exhibit uniform MHC positive staining and fused to form multinucleated myofibers. Interestingly, C25 cells grown in 3D using the PEG hydrogel spontaneously expressed MHC after 5 weeks of culture (Fig. 2C-D). They also formed 3D multinucleated myofibers. This result suggests that 3D culture in PEG hydrogel stimulates differentiation of C25 cells.

Next we sought to evaluate C25 ability to be genetically modified for antibody secretion.

Figure 4-2. C25 myoblasts spontaneously differentiate when cultured in 3D in PEG hydrogel

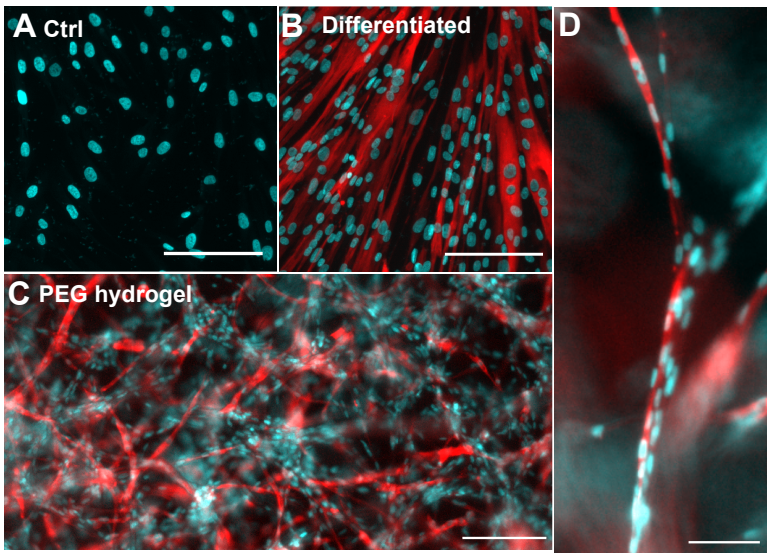

Figure 2: C25 myoblasts spontaneously differentiate when cultured in 3D in PEG hydrogel
Representative images of C25 myoblasts after immunocytochemistry using the anti-myosin heavy chain (MHC) MF20 antibody (red) and DAPI (cyan). **A-B |** C25 myoblasts cultured on glass coverslips (2D-culture) in (A) myoblast growth medium and (B) muscle differentiation medium. **C-D |** C25 myoblasts cultured in 3D in PEG hydrogel with myoblast growth medium. No differentiation medium was used in PEG hydrogel culture. (D) High magnification image showing multinucleated myofibers. Scale bars: (A-C) 100 µm; (D) 25 µm.

C25 cells can be genetically modified using lentiviral vectors

In order to assess the efficacy of lentiviral transduction in each of these different cell types, C25, HeLa and C2C12 cells were exposed to a lentiviral vector encoding GFP under the control of the pgk promoter at different multiplicity of infection from 0.5 to 2 (MOI). The number of GFP-expressing transgenes per cell was estimated using the Poisson formula (Balbás and Lorence, 2004). Number of GFP-expressing copies per cell was higher in C25 cells than in the two other cell types at equivalent MOI (Fig. 3A). At a MOI of 1, C25 cells had an estimated of 0.33 transgene per cell when HeLa had 0.12 and C2C12 0.07. In addition, C25 cells were significantly more fluorescent than HeLa and C2C12 cells (Fig. 3B), suggesting that the GFP transgene was highly expressed in these cells. Using this transduction protocol, we generated two different C25 cell lines for *in vivo* testing: a luciferase-expressing cell line and an antibody-secreting cell line.

For the luciferase expressing cell line, the cells were infected at different MOI with a pgk-luciferase lentiviral vector. As expected, higher MOI resulted in higher bioluminescence emission per cell (Fig. 3C). As the emission of bioluminescence was also directly proportional to the cell number (Fig. 3D), we considered the C25 luciferase cell line as a useful tool to visualize in real time the number of cells and monitor cell growth in the implant, both *in vitro* and *in vivo* (Lathuilière et al., 2014b; Zinn et al., 2008).

To genetically engineer the C25 cells for the secretion of a recombinant IgG2a antibody, the cells were infected at different MOI with two different constructs: a construct for the IgG light chain (LC) and a construct for the IgG heavy chain (HC) both under the control of the pgk promoter. In particular, we used different MOI ratio between the HC and LC encoding constructs, as this ratio needs to be optimized in order to properly assemble the antibody in the endoplasmic reticulum and maximize its secretion (Feige et al., 2010). Based on the measured antibody secretion in the C25 culture medium, we determined that the most effective ratio was 3 HC for 1 LC (Fig. 3E). Increasing the MOI further than a MOI of 75 for the HC construct and 25 for the LC construct did not result in any significant increase of antibody secretion (Fig. 3F). With higher MOI, the morphology of the transduced C25 myoblasts changed and the cell culture displayed apoptotic bodies. At an optimal injection ratio of MOI 75 (HC)/ MOI 25 (LC), we obtained a population of C25 myoblasts secreting 13 pg/cell/day of the mAb11 IgG2a antibody. We next sought to determine if C25 myoblasts could survive inside the device and continue to secrete the recombinant antibody once encapsulated.

Figure 4-3. C25 myoblasts can be efficiently transduced with lentiviral vectors for mAb11 expression.

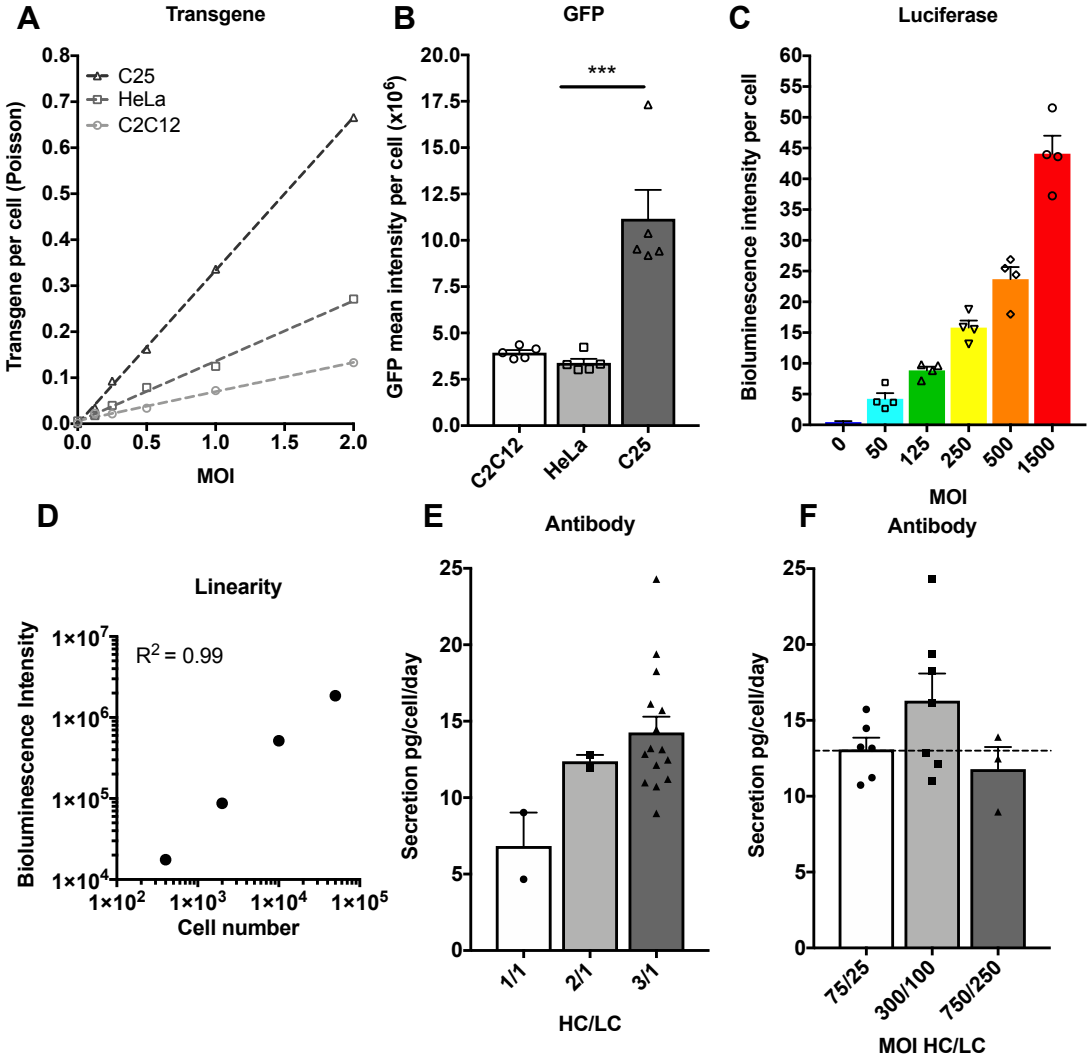

Figure 3: C25 myoblasts can be efficiently transduced with lentiviral vectors for mAb11 expression.
A-B | C25, C2C12 and HeLa cells were infected under the same conditions with a lentiviral vector for expression of GFP. (A) For each cell line, the estimated number of GFP transgene copies per cell was determined according to multiplicity of infection (MOI). (B) Mean GFP fluorescence intensity measured for each cell line 10 days after infection at an MOI of 1. One-way ANOVA. *** p< 0.001. **C-D |** C25 myoblasts transduced with a lentivirus for expression of the firefly luciferase. (C) Bioluminescence intensity per C25 cell measured at different MOI. (D) Bioluminescence intensity measured on increasing cell numbers. Note the linearity of the signal. **E-F |** C25 myoblasts are transduced with two lentiviral vectors encoding the heavy chain (HC) and light chain (LC) of the mAb11 IgG2a antibody: the bar graphs show the mAb11 antibody secretion levels of different cell pools. (E) Antibody secretion rate of C25 myoblasts according to the HL/LC ratio. (F) Antibody secretion rate of pools of C25 myoblasts infected with a ratio of 3:1 HC:LC at different MOI.

C25 cells grew and stabilized in ECT regardless of the seeding condition.

In order to assess cell survival after capsule loading, we first used the C25 luciferase line to monitor growth *in vitro* inside the device. The cells were seeded using different conditions of PEG gel stiffness (1.5% = 300 Pa and 3% = 3000 Pa) and at different densities (1 million, 400'000 or 100'000 cells per device). The capsules were then sealed and kept in cell culture conditions for 2 months. Every week, after adding luciferin in the medium, bioluminescence emission was recorded using an IVIS system (Zinn et al., 2008) (Fig. 4A). Average radiance (photons per second per cm^2 per steradian) was measured by integration of the bioluminescence signal over the surface of the implant and plotted over time (Fig. 4B). During the first two weeks, the increase in bioluminescence showed regular growth of the C25 cells within the implants. As expected, the emitted bioluminescence was related to the initial cell seeding density. However, at around weeks 3, the cells in the devices loaded at high density stopped growing whereas cell growth continued in the low density condition. After one month, bioluminescence intensity stabilized in all conditions and remained stable until endpoint.

C25 cells were able to grow in the encapsulation device indifferently of the PEG hydrogel stiffness or the initial seeding density. For all seeding conditions, the average variance converged and stabilized in between a range of 5 to 12.5 $x10^8$ photons/s/cm^2/sr after 3-4 weeks. We estimated the device to contain 2 to 4 millions cells total.

Figure 4-4. C25 cells growth in implant in vitro

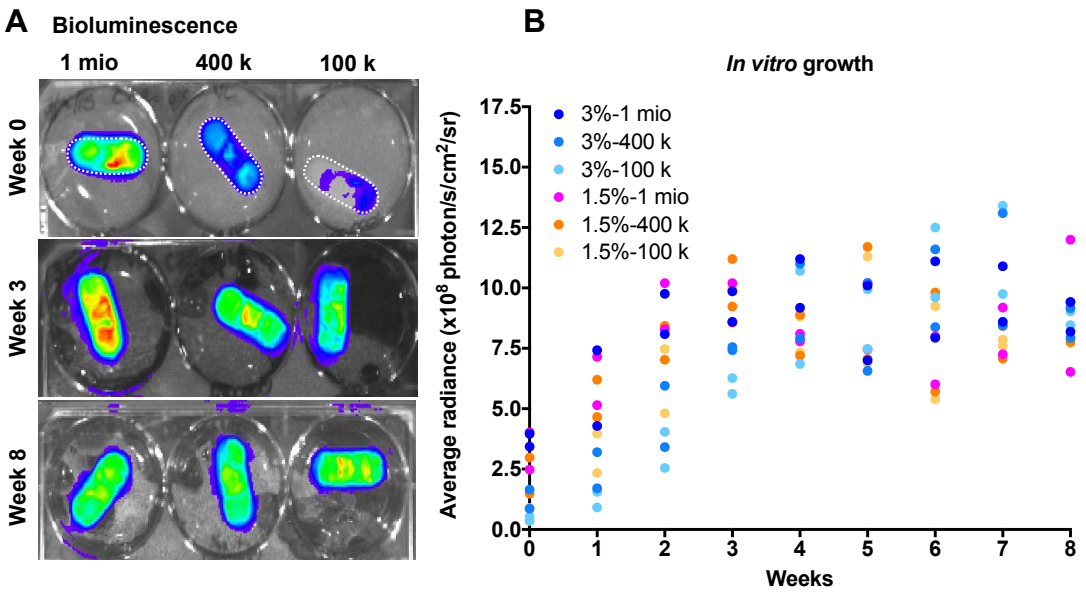

Figure 4: C25 cells growth in implant *in vitro*

Bioluminescence measurements over time of luciferase-expressing C25 myoblasts encapsulated in flat-sheet devices with different seeding conditions (initial cell density and PEG hydrogel stiffness). **A |** Representative images of devices seeded with 1 million, 400'000 and 100'000 cells per implant at different time points. Images were taken with the IVIS system. The bioluminescence signal is color coded (blue for the lowest signal, red for highest signal) and superposed with a black and white image of the 6-well plate. The average radiance is calculated by integrating the signal over the area of the device (white dashed lines) for each implant. **B |** Average radiance measured for each implant in million photons/sec/cm^2/sr over weeks of culture, following device seeding in different conditions.

C25 cell are able to secrete therapeutic dose of antibodies when encapsulated in vitro.

In order to determine the antibody secretion rate of encapsulated C25 cells, we used the C25 75HC/25LC cell line described above. Cells were encapsulated using 3% and 1.5% PEG hydrogel with 1 millions and 3 millions seeding densities. The devices were kept in culture for 12 weeks. Every week, fresh medium was conditioned over of a 4-hrs period and the concentration of mAb11 was measured by ELISA (Fig. 5A). At the time of encapsulation, implants secreted 25 to 75 µg of antibodies per day. The antibody secretion rate increased, and already after one week in culture, all capsules were secreting more than 30 µg per implant per day, the dose considered to be effective at preventing Aβ plaque deposition in the TauPS2APP mouse model (Lathuilière et al., 2016). Some capsules reached antibody secretion rates >200 µg per day. In this experiment, initial loading density appeared to have a long-lasting effect on antibody secretion, with the 1 million density showing higher secretion rates than the 3 million density. At the end of the experiment, the devices were analyzed with hematoxylin and eosin (HE) staining (Fig. 5B-C).

After three months in culture inside the flat sheet device, C25 myoblasts formed a highly viable and regular layer of cells. Although the thickness of the cell layer was found to vary between conditions, cell viability appeared to be very similar.

Based on these encouraging *in vitro* results, we sought to evaluate the efficiency of C25 encapsulated cells to survive and secrete mAb11 antibody *in vivo*.

Figure 4-5. mAb11 secretion by encapsulated C25 myoblasts

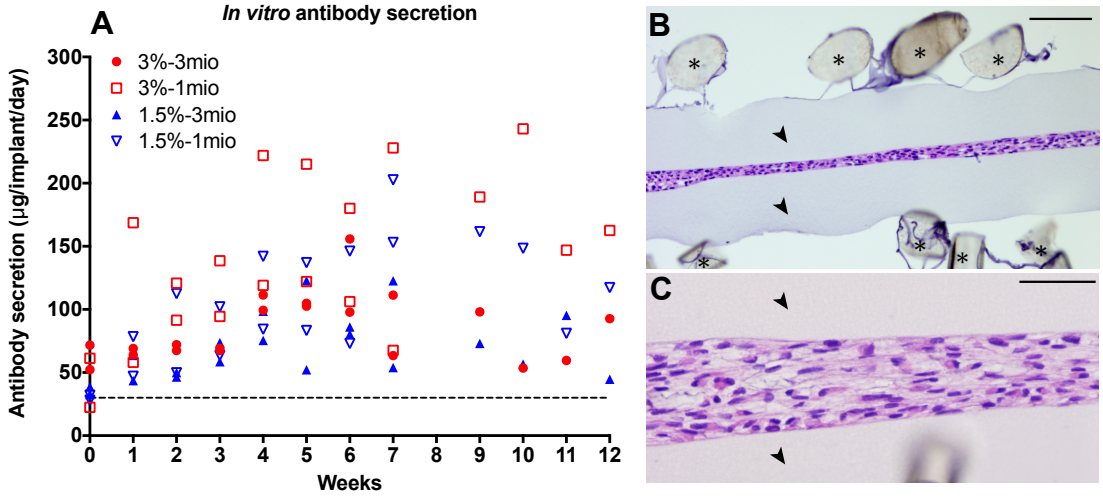

Figure 5: mAb11 secretion by encapsulated C25 myoblasts

A | mAb11 antibody secretion rate measured over time from individual devices seeded in different conditions (PEG % and cell density). Dashed black line at 30 µg/implant/day represents the threshold for the therapeutical mAb11 secretion rate *in vivo.* **B-C |** Representative images of implants cross-sections stained with HE. Legend for (B) and (C): *, polyester mesh; arrowhead, polypropylene membrane. Note the encapsulated multilayer of highly viable myoblasts. Scale bars: (B) 100 µm and (C) 25 µm.

C25 encapsulated cells were rejected in Rag2KO mice

Implantation of ECT in xenogeneic conditions requires immunosuppression (Song and Roy, 2016). We first used Rag2KO mouse model to implant the encapsulated C25 cells. Rag2KO mice harbor a deletion of the entire Rag-2 protein coding sequence in both alleles. This deletion prevents B-cell and T-cell maturation from the pro-B and the pro-T cell stage. Consequently these animals develop a limited adaptive immune system with only natural killer cells (NK cells) but no T-cell mediated antibody response (Shinkai et al., 1992).

C25 luciferase cells were encapsulated using the same seeding conditions used to evaluate their ability to secrete mAb11 *in vitro* (See Fig.5): 3 millions cells in 3% PEG ("3%-3mio") hydrogel, 1 million in 3% PEG ("3%-1mio"), 3 millions in 1.5% PEG ("1.5%-3mio") and 1 million in 1.5% PEG ("1.5%-1mio"). C25 cell survival inside the implanted device was monitored using bioluminescence (Fig. 6A).

Cell growth was monitored twice a week the first two weeks and then once a week during 2 months (Fig. 6B). During the three first weeks, luminescence quickly dropped regardless of the seeding conditions. During the following weeks, values stabilized at an average radiance of $2x10^6$ photon/cm^2/s/sr. After 2 months however, bioluminescence fell under the detection limit for all conditions except the 1.5%-1mio that was very low.

During the necropsy, we observed that 5 implants over the 13 were embedded in a thick layer of tissue (Fig. 6C). Histological analysis was performed using HE and Masson's Trichrom (MT) stains. Implants embedded in a thick layer of tissue exhibit high inflammation (Fig. 6D). The polyester mesh (asterix) of these capsules was embedded by collagen in blue and infiltrated by a thick layer of activate immune cells. The cell layer inside the capsules was present but either dead or undergoing apoptosis. All together this analysis suggested important graft rejection of at least 5 over 13 implants. The other implants did not exhibit such spectacular immune cell activation but the encapsulated cells did not survive better (data not shown).

Figure 4-6. Encapsulated C25 myoblasts implantation in Rag2KO induces immune rejection

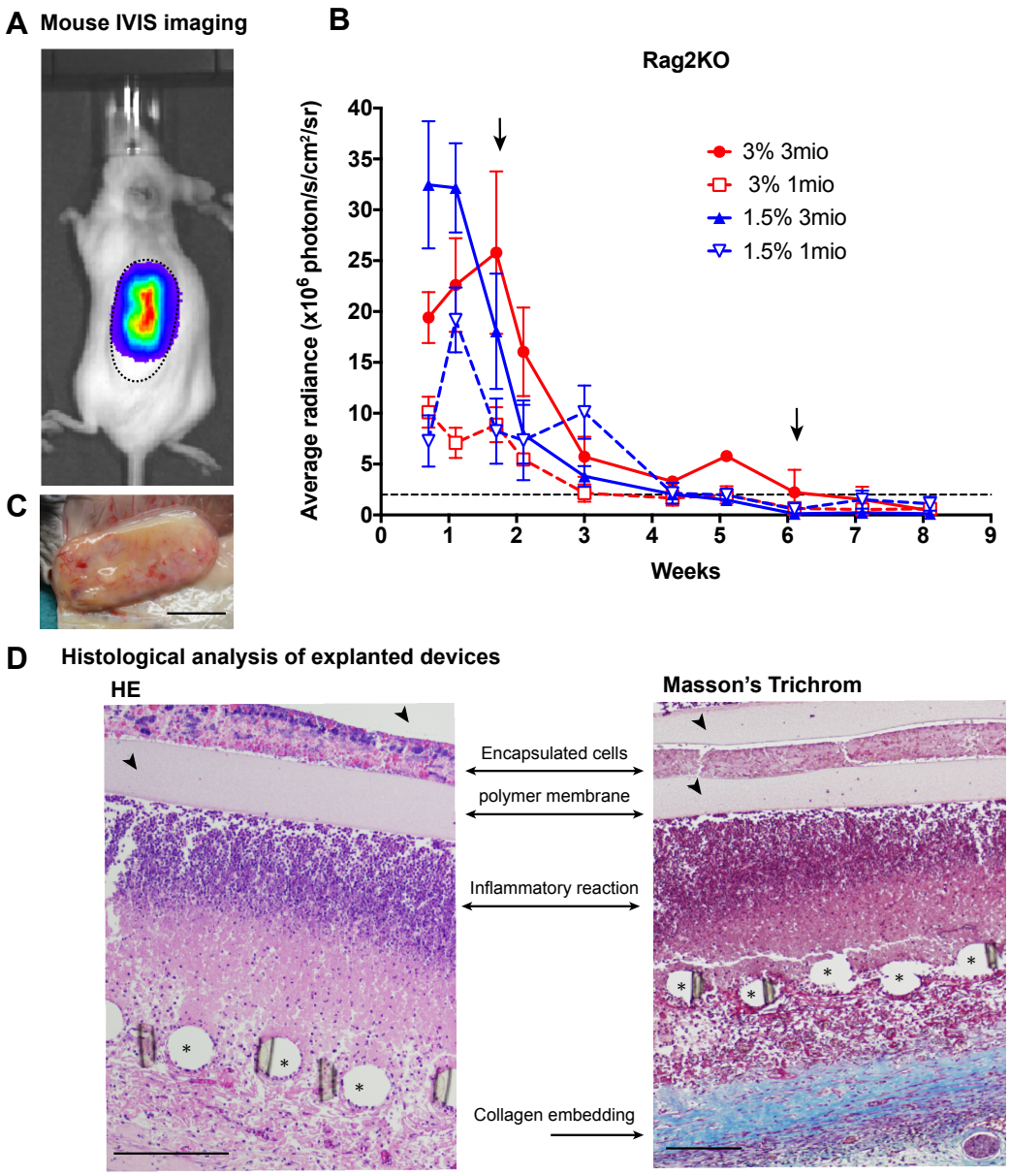

Figure 5: Encapsulated C25 myoblasts implantation in Rag2KO induces immune rejection

A | IVIS imaging of a mouse implanted with a bioluminescent flat sheet device in the subcutaneous tissue. The bioluminescence signal is color-coded (blue: low signal; red: high signal). The average radiance is calculated by integrating the signal over the area of the device. This area of the device is determined on the black and white image (black dotted line). **B |** Average radiance measured over time after implantation for the flat-sheet devices loaded with different cell seeding conditions. For the most efficient condition (3% - 3 mio), the arrows indicate the two critical time points (week 2 and week 6) at which a significant drop in the bioluminescence signal is observed. n=13 implanted mice in total. **C |** Representative image of an explanted flat-sheet device embedded in a highly reactive tissue indicating ongoing immune rejection of the implant. Scale bar: 10 mm. **G |** Representative images of HE and Masson's trichrom histological stainings showing ongoing immune rejection directed against the implant. Note the intense inflammatory reaction and the thick collagen layer. Legend: * polyester mesh; arrowheads: polypropylene membrane. Scale bars: 200 µm.

C25 encapsulated cell were able to engraft in Rag2KO Ilr2gKO mice but at very low density

In order to avoid activation of the immune system against the ECT, we decide to use the Rag2KO-Ilr2gKO mouse model. Compared to the Rag2KO mouse model, the Rag2KO-Ilr2gKO mice also lack the *Ilr2g* gene. Consequently, this immunodeficient mice are deprived of NK cells, in addition to the lack of T and B cells (Rijn et al., 2003).

To assess implant engraftment, we first used the best seeding condition for long-term implantation observed in the previous *in vivo* experiment (1.5%-1mio, see Fig. 6B) as well as a lower seeding density of half a million cells per capsule in 1.5% PEG ("1.5%-500k").

The bioluminescence was measured once a week (Fig. 7A). In Rag2KO-Ilr2gKO mouse model, the bioluminescence reading was lower than in the Rag2KO mouse model at week 1 (See Fig. 6B). Both experiments were performed under the same condition in the same IVIS device. Within the first week in Rag2KO-Ilr2gKO mouse model, the signal was $3x10^6$ instead of $6x10^6$ photons/cm^2/s/sr in Rag2KO mouse model for the 1.5%-1mio condition. However, the evolution of the signal from week 1 to 3 was the same for both experiments. In the Rag2KO-Ilr2gKO mouse model, the signal also rapidly declined during the first three weeks, and remained stable after week 7, at a radiance of $5x10^5$ and $7.5x10^5$ photon/cm^2/s/sr for the 1.5%-500k and 1.5%-1mio conditions, respectively. We estimated that these values corresponded to a range of 125'000 to 250'000 living cells.

During the necropsy, there were no sign of rejection and the implants were vascularized (Fig. 7B). Histology with the HE staining confirmed the absence of immune reaction (Fig. 7C). Loose conjunctive tissues surrounded the polyester mesh and vascularization was present near the membrane and the mesh. However, the layer of cells inside the device was really thin with scarce nuclei (Fig. 7D), confirming cell survival at very low density.

Figure 4-7. Implantation of encapsulated C25 myoblasts in Rag2KO-Ilr2gKO mice leads to long-term implant survival at low cell density.

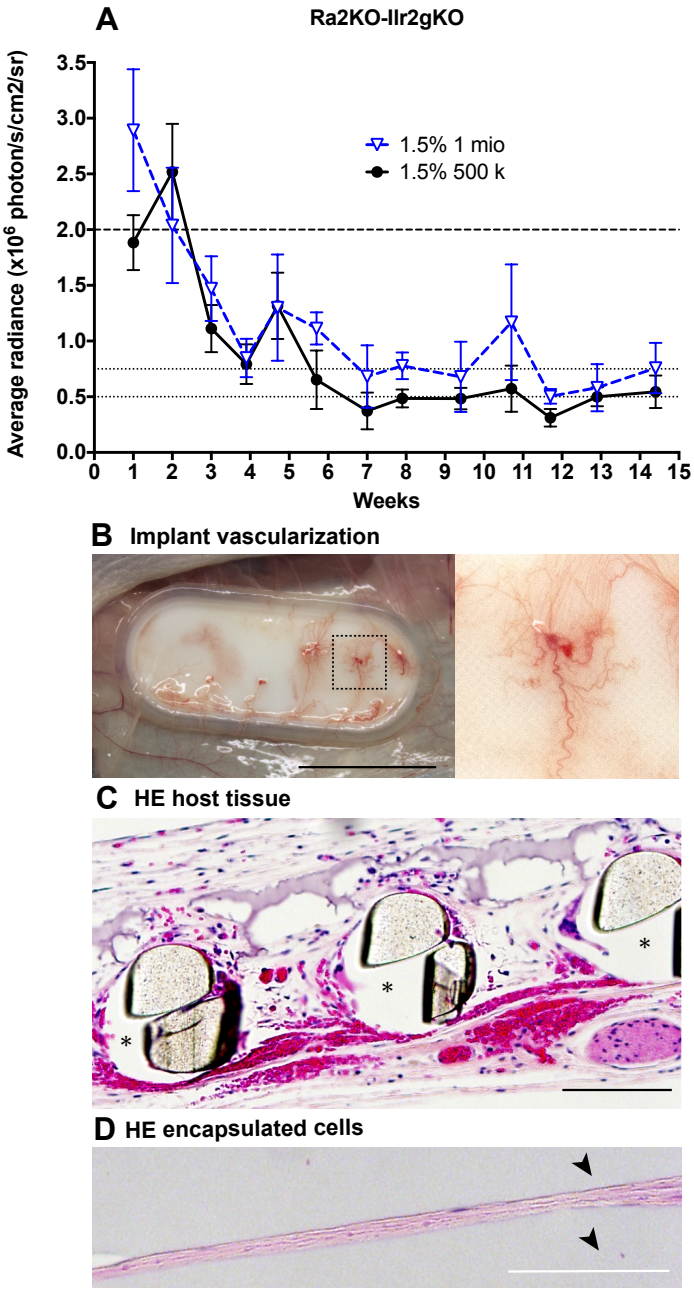

Figure 7: Implantation of encapsulated C25 myoblasts in Rag2KO-Ilr2gKO mice leads to long-term implant survival at low cell density.

A | Average radiance values of the bioluminescence signal over time for flat-sheet devices loaded with two different cell density conditions. The signal drops rapidly under $2x10^6$ photon/s/cm^2/sr radiance (dashed black line) and stabilizes at 0.5 and $0.75x10^6$ photon/s/cm^2/sr (dotted black lines) for the 0.5 and 1 mio cell seeding conditions, respectively. n = 5 animals per condition. **B |** Representative images of the explanted devices. Note the apparent vascularization (dotted back square). Scale bar: 10 mm. **C |** HE staining of the host tissue shows vascularization surrounding the implant at the level of the polyester mesh (*). Scale bar: 100 µm. **D |** Representative image of the inner layer formed by encapsulated C25 myoblasts, 14 weeks post-implantation. Black arrowhead: porous polypropylene membrane. Scale bar: 100 µm.

Tissue formation in vitro before implantation improved C25 encapsulated cell survival

To maximize cell survival in the device, C25 myoblasts were first grown *in vitro* inside the device and later implanted in Rag2KO-Ilr2gKO mice. The C25 cells were seeded in the implant using the same PEG stiffness and cell seeding density conditions as in the *in vitro* experiment (See Fig. 5A). Implants were kept 3 weeks in culture in myoblast medium to form a cell layer within the device as shown in Fig. 5B-C. The capsules were implanted at week 3 in Rag2KO-Ilr2gKO mice and bioluminescence was monitored (Fig. 8A). Two days after implantation, we noted an average radiance twice higher than in the previous experiment (see Fig. 7A). However, the radiance again quickly declined during the first 3 weeks of implantation and stabilized at week 4. Signal remained stable from week 4 to week 12. C25 cells encapsulated in 1.5% PEG stabilized at $2x10^6$ photon/cm^2/s/sr regardless of the initial seeding condition. C25 cells encapsulated in 3% PEG stabilized at 4 times lower bioluminescence values ($5x10^5$ photon/cm^2/s/sr).

The implanted flat sheet devices showed clear vascularization, with no signs of immune rejection (Fig. 8B). HE staining revealed a thin layer of C25 cells (Fig. 8C) in the best conditions (1.5%-1mio and 1.5%-3mio). We estimated these implants to contain half a million cells according to the average radiance measured using bioluminescence. Our next step was to determine using mAb11-secreting cells if this was sufficient to secrete antibodies in sufficient amount to be detected in the plasma of Rag2KO-Ilr2gKO mice.

Figure 4-8. Optimization of the conditions for implantation of encapsulated C25 myoblasts in Rag2KO-Ilr2gKO mice.

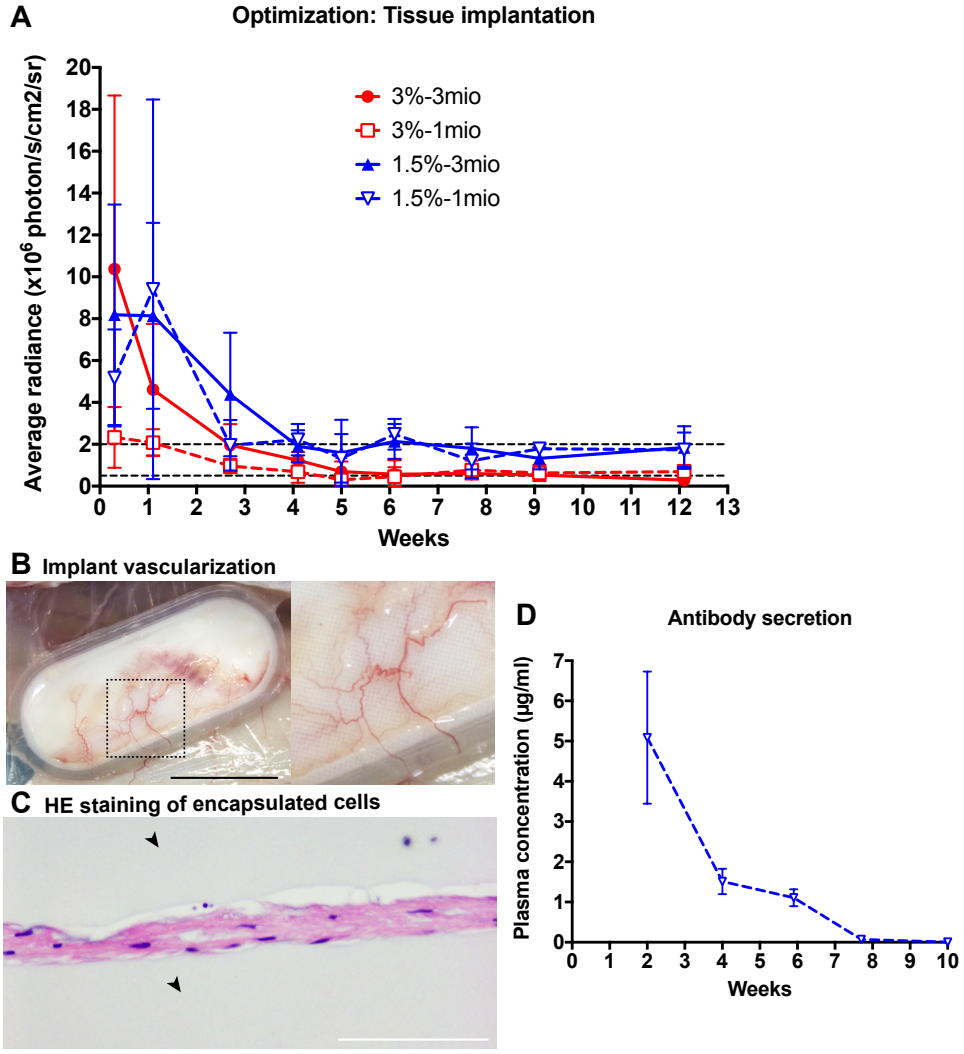

Figure 8: Optimization of the conditions for implantation of encapsulated C25 myoblasts in Rag2KO-Ilr2gKO mice.

A | Average radiance for devices loaded with different seeding conditions, measured after subcutaneous implantion of encapsulated luciferase-expressing C25 myoblasts in Rag2KO-Ilr2gKO mice. Devices are implanted after 3 weeks of culture in growth medium to let the C25 myoblasts form an organized cell layer prior to implantation. The signal stabilizes at 0.5 and $2x10^6$ photon/s/cm^2/sr (dashed black lines) for the C25 encapsulated in 3% PEG and 1.5% PEG, respectively. n = 4 mice per condition. **B |** Representative image of an explanted device showing host tissue vascularization (dotted back square). Scale bar: 10 mm. **C |** Histological analysis shows the C25 cell layer (1.5% PEG hydrogel) after 12 weeks of implantation (1.5% PEG hydrogel) . Black arrowhead: porous polypropylene membrane. Scale bar: 100 µm. **D |** mAb11 plasma concentration (µg per ml) in mice implanted with encapsulated mAb11-secreting C25 cells in the same cell seeding condition (1 mio cells in 1.5% PEG hydrogel). Note that the mAb11 antibody concentration is no more detectable after week 6 of implantation. n=4.

Implantation of encapsulated mAb11-secreting C25 myoblasts in optimal conditions does not allow for antibody detection in the plasma

We used the optimal seeding conditions determined using the C25 luciferase cell line (1.5%-1mio) to encapsulate mAb11-secreting C25 myoblasts before implantation in Rag2KO-Ilr2gKO mice. We used the C25 75HC/25LC cell line with the highest antibody secretion rate *in vitro* (See Fig. 5A). The implants were kept 3 weeks *in vitro* before subcutaneous implantation in Rag2KO-Ilr2gKO mice. Every 2 weeks, the mAb11 plasma concentration was measured by ELISA (Fig. 8D). Antibody plasma concentration showed a similar progression than the bioluminescence signal measured in the previous experiment, but shifted in time due to the half-life of the antibodies. The mAb11 antibody remained detectable in the mouse plasma until week 6, but its concentration dropped below the ELISA detection range at week 8. Consequently, we concluded that the amount of antibody secreted by the surviving C25 cells was too low to be detected.

C25 encapsulated cells engrafted better in temporary immunosuppressed mice compare with immunodeficient mice

We noticed in the first experiment in Rag2KO that C25 cells number started much higher and even grew under certain conditions before dropping within the 3 weeks (see Fig. 6B). We hypothesized that the immune system might facilitate the implant engraftment. In order to beneficiate from this positive effect, we submitted immunocompetent mice through different tolerization protocol. It was demonstrated in several studies that anti-CD4 antibodies transient treatments could induce immune tolerance or dampen graft rejection in mice and rats (Lehmann et al., 1997; Sun et al., 2014). We used two anti-CD4 antibodies: a depleting anti-CD4 (clone Gk1.5) and a non-depleting anti-CD4 (clone YTS177).

In order to test the protocols, we first used C25 luciferase cells. We injected B6SJL mice with anti-CD4 antibodies one day before the implantation and at day 7 and 14 after the implantation. Both protocols aimed to impair CD4+ T-cell activity at the time of the engraftment and prevent the immune rejection of the implant.

We compared C25 luciferase survival in the same seeding condition in Rag2KO-Ilr2gKO, in tolerized B6SJL and in control B6SJL injected with saline solution (Fig. 9A-B). Using both CD4 depleting and non-depleting antibody, C25 cells engrafted better in tolerized B6SJL mice than in Rag2KO-Ilr2gKO mice. During the first two weeks, C25 cells engrafted even better in immunocompetent control mice compared with the CD4-depleted mouse (Fig. 9A), suggesting an important role of the immune system in the first weeks post-implantation. Both CD4 depleting and non-depleting protocols seemed to delayed the cell survival drop. Unfortunately, after the last anti-CD4 injection, bioluminescence signal rapidly decreased to reach the radiance of $2x10^6$ photons/cm^2/s/sr corresponding to half a million cells.

We confirmed these results using antibody secreting C25 cells. For both experiment, antibody secreting C25 cell were seeded at 1.5%-1mio condition. The CD4 depleting or non-depleting antibodies were injected throughout the entire experiment (instead of only 3 injections) to maximize the chance of cell survival. Antibody plasma concentration was measured every 2 weeks using an ELISA (Fig. 9C). In control immunocompetent mice, the implant directly failed to engraft. In mice subjected to the tolerization protocol, we could detect mAb11 plasma concentration for 6 weeks. Unfortunately, implants failed one after each other, as 7 over 9 implants were secreting at week 4 but only 3 were still secreting at week 6.

Figure 4-9. Immune system involvement in the engraftement of C25 encapsulated cells

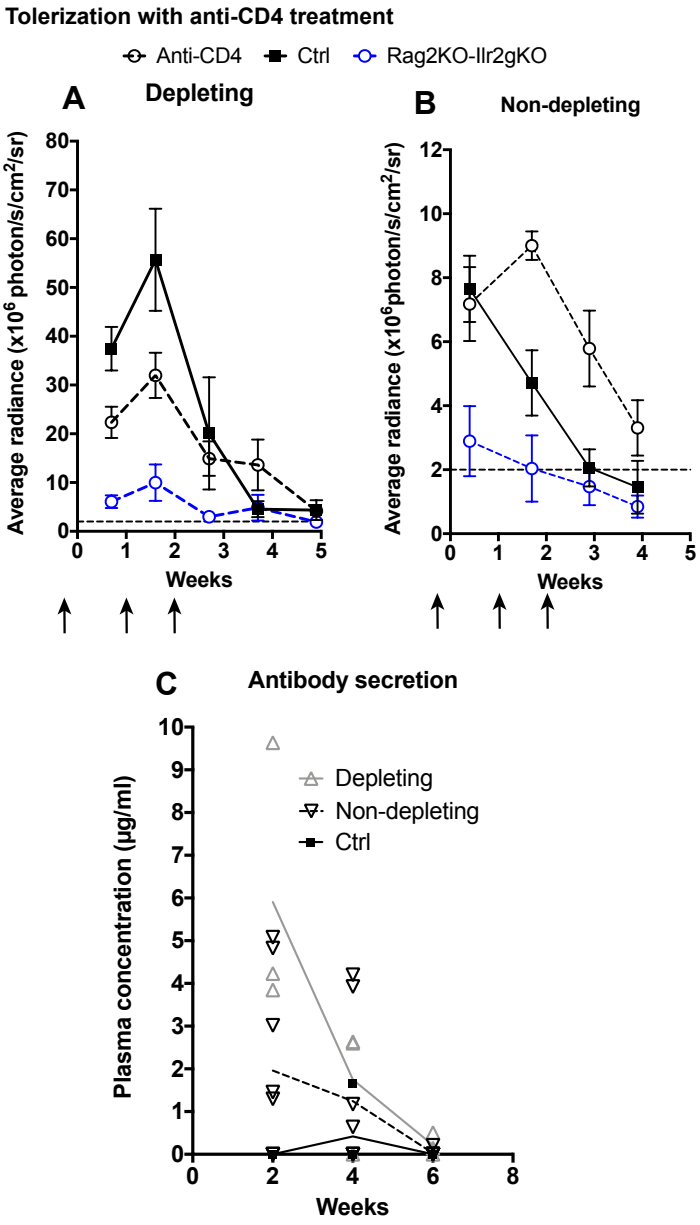

Figure 9: Immune system involvement in the engraftement of C25 encapsulated cells

A-B | Average radiance for animals under tolerizing (A) depleting and (B) non-depleting anti-CD4 antibody protocols compared with control mice receiving saline solution injections and immunodeficient mice Rag2KO-Ilr2gKO. Black arrow shows the injections time for anti-CD4 and saline solutions at -1 day, 7 days and 14 days after device implantation. n = 4 per group. Seeding conditions: (A) 1 million cells in 1.5% PEG hydrogel in PTFE membrane. Implantation after 3 weeks of tissue formation. (B) 1 million cells in 1.5% PEG hydrogel in PP45 membrane. Direct implantation (overnight incubation) after devices loading. Note that beside the very different seeding conditions, the cells behave similarly. Dash line at $2x10^6$ photon/s/cm^2/sr. **C |** Comparison of the mAb11 plasma concentration (µg per ml) in mice receiving injections of anti-CD4 depleting and non-depleting antibodies as well as saline solution (control group). Injections were performed every week. Seeding condition: 1 millions cells in 1.5% PEG hydrogel in PP45 membrane. Implantation after 3 weeks of tissue formation. n = 4 for both anti-CD4 injected groups, n = 3 for the control group. All animals are represented on the graph.

4.4 Discussion

After testing its characteristics *in vitro,* the C25 myoblast cell line appeared to be a promising candidate as a renewable cell source for human applications of ECT. C25 cells are able to grow in 3D in PEG hydrogel. Interestingly, they spontaneously differentiate and form stable myotubes when cultured in 3D in PEG hydrogel. We considered the propensity of C25 myoblasts to differentiate into post-mitotic myotubes as an advantage for cell encapsulation, as rapidly dividing cells tend to form a necrotic cell core inside the device, which may compromise the long-term survival of the implant. On the other hand, dividing cells can self-renew, which can also compensate for the loss of cells in metabolically restrictive conditions such as hypoxia.

In addition, the C25 cell line is highly permissible to lentiviral infection, which facilitates genetic modifications. Using lentiviral vectors to optimize the expression of the IgG light and heavy chains, we engineered a C25 cell line able to secrete the mAb11 antibody at high rate, reaching 13 pg per cell per day. Indeed, the C2C12 myoblast clone selected for the successful proof-of-concept study in the Alzheimer's mouse model was able to secrete 29 pg per cell per day (Lathuilière et al., 2014a). Without selecting clones of C25 cells with high secretion rates, it was possible to reach a mAb11 secretion level in the same order of magnitude, which suggests that C2C12 and C25 myoblasts have similar capacity for antibody production. We demonstrated using the C2C12 secreting cell line that capsules secreting more than 30 µg of mAb11 IgG2a per day could reduce the Aβ plaque load following subcutaneous implantation in different mouse models of Alzheimer's disease (Lathuilière et al., 2016). Consequently, we did set our target for capsule secretion as 30 µg/implant/day, which could be achieved using flat sheet devices loaded with human C25 myoblasts. By testing several seeding conditions in terms of loaded cell density and PEG hydrogel concentration, we reached capsule secretion rates over 100 µg/day. The best condition *in vitro* was to seed only 1 million cells and let the cells grow and settle in the device. We concluded that C25 myoblasts had the proper features for cell encapsulation, and should be considered as a promising candidate to translate the ECT for antibody delivery from mouse to human application.

Based on this *in vitro* study, we tested the ability of the encapsulated C25 cells to undergo long-term survival and antibody secretion *in vivo.* Regardless of the seeding condition or the mouse model, C25 cells survival dropped drastically after implantation within the first 3 weeks. Then the C25 cell number stabilized and remained stable up to 15 weeks. Besides the initial loss of surviving cell inside the device, the stability of the system was a positive result, as it may facilitate the long-term administration of predictable amounts of recombinant antibodies.

The optimizations aimed at minimizing the initial cell survival drop in order to stabilize a number of surviving cells as high as possible within the device. Under the optimal survival conditions, C25 cells stabilized as a thin healthy layer of cells after 3 weeks. Under these conditions, the estimated number of cells in the implant was around half a million, based on the bioluminescence read-out. Unfortunately, this number of cells was not sufficient for *in vivo* antibody secretion. Indeed, even if every single cell inside the device would be secreting 13 pg of antibody per day, the estimated half a million surviving cells is only secreting 6 to 7 µg of antibody per day. Consequently, C25 cell stabilized at a too low density to secrete detectable quantities of antibodies in the plasma. Probably due to the very restrictive conditions *in vivo*, C25 cells were not able to further divide and were found to rapidly differentiate inside the device. Further optimization, such as reducing the thickness of the permeable polymer membrane used in the flat sheet device, with the intent to facilitate the diffusion of oxygen and nutrients, did not improve cell survival or antibody secretion.

An important difficulty in this study was the need for xenogeneic cell implantation. Implantation of mouse C2C12 cell line in mouse animal models previously allowed the engraftment of the implant under normal immune conditions. Unfortunately, ECT allows allogeneic condition as it avoid cell-to-cell interaction but it does not allow xenogeneic implantations (Song and Roy, 2016).

Our results suggested that the immune system might play an important role for cell survival during the first 3 week post-implantation. Indeed, engraftment in tolerized CD4 depleted mice was better than in immunodeficient mice but worst than in immunocompetent mice. Tolerization seemed to delay by about two

weeks the implant failure but eventually did not improve the cell survival. Consequently, we were not able to maintain detectable antibody plasma concentration (above 1 µg/ml) longer than 6 weeks.

4.5 Conclusion

We successfully engrafted encapsulated human myoblast within our ECT device in Rag2KO-Ilr2gKO mice for as long as 4 months. However, we failed to reach long-term continuous antibody secretion *in vivo* using encapsulated human cells despite our optimization efforts.

The successful aspect of this study was that we were able to develop a human cell line secreting sufficient amount of antibody *in vitro* and that we maintain highly stable human cell survival *in vivo* up to 4 months. The drawbacks of this study were that the tested human cells stabilized at low density and were not able to secrete detectable amount of antibody in our mouse models.

It is clear that C25 human myoblasts are no longer a good candidate for translation of our ECT system in human. We are currently using our know-how in order to test other cell line candidates based on human myoblast immortalization.

5

Chapter 5 : Conclusion

5.1 Amyloid beta cascade hypothesis

The amyloid cascade hypothesis has not been engraved in stone. Initially stated in the 90s (Hardy and Higgins, 1992), it was revisited by its authors early 2000, in order to include new discoveries about the toxicity of soluble Aβ at the level of the synapse, or the role of microglia activation (Hardy and Selkoe, 2002). From the simple initial hypothesis, the proposed interpretation of the mechanisms leading to AD became progressively more complex. It was discussed that instead of being linear, the downstream processes, such as synaptotoxicity and tau pathology, could also act in parallel (Karran et al., 2011; Morley and Farr, 2014). Collectively, they were considered to aggravate neuronal impairment and ultimately lead to neurodegeneration.

The role of Aβ in the cascade, however, is by definition among the initial triggering events. The concept that accumulation or aggregation of Aβ is the origin of the cascade is the essence of the hypothesis. The genetic evidence derived from the familial AD cases showed that Aβ accumulation can arise from very different origins: duplication of the *APP* gene (McNaughton et al., 2012), modulation of the Aβ42/Aβ40 balance (Tanzi, 2012), increased levels of oligomeric forms of Aβ (Gessel et al., 2012; Nilsberth et al., 2001), to cite a few.

These different mechanisms very well illustrate the heterogeneity of the possible causes of AD.

Despite these updates, the Aβ cascade hypothesis still fails to convincingly explain the cause of sporadic AD, if we consider Aβ deposition to be the main factor at the origin of the disease. However, the possibility that soluble forms of Aβ (Lacor et al., 2007), but not plaques, are responsible for the onset of sporadic AD remains plausible, although this hypothesis is also very difficult to verify. An increase in the level of soluble Aβ oligomers (Aβo) in the brain parenchyma, which may happen decades before the onset of clinical symptoms, would not necessarily generate pathological alterations detectable years later. However, if Aβo were responsible for the disease, one can think that passive anti-Aβ immunization would have shown significant benefits (Panza et al., 2019).

Passive anti-Aβ immunization

Indeed, among all tested anti-Aβ antibodies in phase III clinical trials, several had the potential to target oligomers. Based on their reported features, Aducanumab (Sevigny et al., 2016) or Gantenerumab (Ostrowitzki et al., 2012) could trigger Aβo phagocytosis and Crenezumab has been shown to induce Aβo de-aggregation (Ultsch et al., 2016). In addition, by inducing microglial cell activation, anti-Aβ antibodies, such as Gantenerumab (Xiang et al., 2016), are able to increase the microglial barrier protection around amyloid plaques, which is expected to prevent Aβo release (Condello et al., 2015). On the other hand, Solanezumab was shown to target Aβ monomers (Siemers et al., 2010), which may also prevent Aβo production and aggregation, by reducing the level of available building blocks. Overall, there were several clinical trials testing the effects of passive anti-Aβ immunization, in which the treatment was expected to impact on the level of Aβo. If Aβo had a major role in the disease, it is legitimate to think that these treatments should have slowed down disease progression and led to cognitive benefits (Panza et al., 2019).

But, as previously discussed, the phase III clinical trials failed to prevent cognitive decline, even though all of them showed target engagement and some of them reduced the Aβ burden (Ostrowitzki et al., 2017).

Mouse models of AD

At this point, it is worth recollecting that passive anti-Aβ immunization was able to reduce cognitive impairments in AD mouse models (Hartman et al., 2005; Lee et al., 2006). However, AD mouse models, as most of the animal models of human diseases, are highly artificial and therefore unlikely to replicate all aspects of the disease. Most of them are based on the overexpression of mutated human genes, such as *APP* and *PSEN1*, in order to cause an overload of Aβ and trigger the progressive accumulation and aggregation of Aβ (Oakley et al., 2006; Radde et al., 2006). The Aβ mouse models do neither exhibit any tau pathology, nor any major brain atrophy. But they show synaptic and neuronal loss as well as cognitive impairments. It is logical to conclude that this cognitive impairment is due to Aβ toxicity. In these models, the use of anti-Aβ antibodies is halting the Aβ cascade by reducing Aβ accumulation and its toxicity, even after the onset of the disease. Then the main question is to understand why AD patients enrolled in clinical trials are not responding to the treatment as expected. Why even though we are now able to reduce Aβ burden in AD patients, it does not translate in cognitive benefit?

Then, why are the clinical trials failing in AD patients?

In humans, tau pathology might be one of the culprits for the failures. Although there is more and more evidence that Aβ alone can be toxic for the surrounding neurons and is able to trigger cognitive dysfunction, it might fail to induce on its own the typical neurodegeneration associated with AD (He et al., 2018; Li et al., 2016). On the other hand, tau pathology appears to induce deleterious events able to cause neurodegeneration (Lewis et al., 2000). Indeed, in its pathological forms, tau increases Aβ-mediated toxicity (Ittner et al., 2010), synapse loss (Brelstaff et al., 2018), and causes microglial cells dysfunction (Streit et al., 2009), which can ultimately trigger neuronal loss and brain atrophy (Lewis et al., 2001, 2000). But WT tau seems unable to aggregate or propagate without the presence of neuritic plaques (Duff et al., 2000; Li et al., 2016), highlighting the importance of the synergistic role of tau and Aβ in AD.

5.2 An analogy to avalanches

Once tau pathology has been initiated, the disease may progress through different pathways involving tau propagation (Braak and Braak, 1991). Tau exhibits prion-like mechanisms of propagation (Frost and Diamond, 2010). Non-pathological tau can be converted into pathological forms by interaction with tau seeds. These tau seeds propagate independently of the initial event (He et al., 2018). Consequently, targeting Aβ once tau pathological conversion has occurred might be useless, as the spreading of the tau pathology may proceed independently of the amyloid pathology (Li et al., 2016). Hence, the answer that was invariably given after each clinical trial failure, stating that treatment was initiated too late, still appears plausible in the light of these recent findings. However, the issue might not be that Aβ accumulation and aggregation were already too advanced, but rather that tau had already undergone its conversion into pathological forms.

The best analogy for the progression of AD after pathological conversion of tau is not a cascade. Once tau becomes a major pathogenic actor, AD is better represented as a self-amplifying avalanche. And like an avalanche, AD needs multiple events to be triggered. Chronic microglia activation, decrease Aβ phagocytosis, aging, impaired APP processing are some of the factors that can lead to the formation of neuritic plaques, coinciding with tau hyperphosphorylation and promoting conditions that might facilitate tau conversion into pathological species. At this point, it has been proposed that a secondary event might be required to cause pathogenic tau conversion. Such a secondary event could include the presence of genetic risks or exposure to environmental factors (Li et al., 2016).

In the case of familial AD, Aβ accumulation caused by dysfunction of APP processing might be so overwhelming that any minor secondary events might suffice to trigger AD. In the case of sporadic AD however, these additional factors might play a crucial role in disease etiology.

In this hypothesis, we do not question the importance of Aβ accumulation in AD, but we rather highlight the fact that AD is a multifactorial disease. Pathological

tau, aberrant microglial activity and aging are all important actors in the disease, in addition to Aβ aggregation.

5.3 A better understanding of passive anti-Aβ immunization

During the past twenty years, passive anti-Aβ immunization has been developed as a treatment, based on experimental evidence mainly obtained in mouse models of amyloid pathology, which did not replicate the pathological interaction between Aβ and tau found in AD. “All models are wrong, but some are useful”, says George Box about statistics (Box and Draper, 1987). This is also the case for mouse models of human diseases, and particularly so in the context of AD. As mice do not naturally develop AD, mouse models are all artificial. Nevertheless, in order to study AD, the presence of tau pathology in addition to Aβ might be of particular importance.

In the context of passive anti-Aβ immunization, tau pathology should be included as the mechanisms leading to cognitive impairments, as well as the clearing mechanisms of AD pathology might be different when the tau pathology is present (Grueninger et al., 2010; Saul et al., 2013; Wilcock et al., 2011). As extensively discussed, microglia activity is affected by the tau pathology (Streit et al., 2009). Hence, microglia may not respond in the same way to passive immunization when exposed to the pathogenic effects of tau (Wilcock et al., 2011). In addition, WT tau should be favored in models of AD, as tau mutations have not been implicated in the disease, and WT tau interacts very differently with Aβ (He et al., 2018; Li et al., 2016).

Conclusion of our work

In line with the idea that WT tau is more relevant in the context of AD, we developed a mouse model combining Aβ and WT tau pathologies. This model was useful to explore Aβ and tau interactions and study the effects of passive immunization in this context. Thanks to its modularity, the model gave us insights into the respective contributions of Aβ and tau pathologies in the hallmarks of the disease. The most interesting observation was that WT tau overexpression decreases microglial cells close interaction with Aβ plaques.

In a previous study of passive anti-Aβ immunization in a combined P301L mutant tau and Aβ mouse model, Oddo et al. (Oddo et al., 2004) demonstrated that anti-Aβ antibody administration before the onset of the disease decreases both Aβ and tau pathologies. In addition, they suggested that early administration was key and also demonstrated that whereas tau pathology was reduced in the somatodendritic neuronal compartment, passive anti-Aβ immunization could not rescue the formation of NFTs. In our prevention study using the TauPS2APP mouse model, we confirmed that the anti-Aβ antibody mAb11 was also able to decrease somatodendritic accumulation of phosphorylated tau species.

Then we investigated administration of passive anti-Aβ immunization in the context of established Aβ and tau pathologies in the combined Aβ and WT tau mouse model. In this context, anti-Aβ antibody mAb11 decreased WT total tau spreading in the neurites, but did neither affect the level of phospho-tau, nor the neuronal degeneration caused by tau overexpression. Confirming the hypothesis that administration of passive immunization after the onset of the disease does not influence tau pathology and its downstream consequences (Oddo et al., 2004).

We also observed that passive anti-Aβ immunization increases microglia clustering around Aβ deposits and increases Aβ plaque compaction. We hypothesized that the observed decrease of WT tau could be linked to changes in microglial activity. This hypothesis is strengthened by the recent work of the group of David Holtzman (Leyns et al., 2019), showing that decreased clustering of microglia in TREM2KO and TREM2 R47H mouse models increases tau seeding pathology at the level of the neuritic plaque. It confirms that microglial cell clustering at the level of the neuritic plaques might play an important role in modulating tau pathology.

Next steps

As a next step, we are currently further analyzing the effects of passive immunization on dystrophic neurites surrounding the neuritic plaques. In terms of further experiments, it would be interesting to assess the involvement of microglia activation in WT tau spreading. Administration of an anti-Aβ antibody

able to bind Aβ deposits, but failing to activate microglial cell clustering, could provide interesting insights.

Looking at the effects of tau pathology on the efficacy of passive anti-Aβ immunization could also be of particular interest. Further studies are still needed to understand the effects of passive immunization against Aβ in the context of the Alzheimer's pathology.

5.4 Improvement of antibody delivery

The last part of the present thesis addresses a different topic also related to the application and optimization of passive immunization against neurodegenerative diseases. In this project, we aimed to further develop ECT for continuous subcutaneous administration of anti-Aβ antibodies in human. We successfully developed a human cell line secreting antibodies. The goal was to adapt the current system using a renewable cell source of human origin.

The immortalized C25 human myoblasts from Vincent Mouly group (Mamchaoui et al., 2011) seemed a very promising cell line during *in vitro* assessment. *In vivo*, the encapsulated myoblasts survived and formed a viable tissue in the implant but failed to secrete detectable amounts of antibodies, which limits their long-term application. We are currently testing another source of immortalized human myoblasts as an alternative cell source for encapsulated cell technology.

6

Chapter 6 : Material and methods

Cells

We used two myoblasts cell lines in the following studies: the murine C2C12 cell line and the human C25 cell line.

The C2C12 cells used for encapsulation were either the C2C12 clone #29 developed in our laboratory and described previously (Lathuilière et al., 2016) or C2C12 wild-type cells purchased from the American Type Culture Collection (ATCC number CRL-1772). Cells were cultured at 37°C with 5% CO_2 in Dulbecco's modified Eagle Medium (DMEM) supplemented with 10% fetal bovine serum (FBS), 100 U/ml penicillin and 100 µg/ml streptomycin.

Human myoblasts C25 were provided by the Myology Institute of Paris. We used the C25cl48 a clonal immortalized myoblast cell line coming from a healthy 25 year old donor and developed by Prof. Vincent Mouly laboratory (Mamchaoui et al., 2011). This cell line was immortalized using lentiviral vector to express human telomerase reverse transcriptase (hTERT) and cyclin-dependent kinase (CDK)-4. C25 cells were cultured in skeletal muscle cell growth medium (PromoCell; C-23160) supplemented with 5% FBS at 37°C with 5% CO_2.

Polyethylene Glycol (PEG) Hydrogel

Cells were seeded in the implants using a polymeric hydrogel biomaterial as extracellular matrix. Detailed characteristic and synthetized process are

described elsewhere (Ehrbar et al., 2007a) (Ehrbar et al., 2007b)(Lathuilière et al., 2014b). We used a 10% mix stoichiometrically balanced of two functionalized polyethylene glycol (PEG) precursors: n-PEG-MMP-Lys (W) with the W mutation allowing enzymatic cell degradation and n-PEG-Gln (NQ) ([Lys]/[Gln] = 1). This 10% NQ/W PEG hydrogel was diluted in Tris buffered saline (TBS 50mM, pH 7.6) at the desired w/v percentage to reach the wanted stiffness. For the batch used in the following experiment, 1.5% w/v PEG hydrogel correspond to a stiffness of 300 Pa and 3% w/v PEG hydrogel to a stiffness of 3 KPa. The PEG mix was supplemented with 100 µM TG-RGD to allow cell adhesion before being mix with cell and cross-linked using thrombin activated Factor XIIIa (FXIIIa).

3D cell culture in PEG Hydrogel

For three dimension cell culture, cells were mixed at the desired density with either 3% w/v or 1.5% w/v PEG hydrogel. After activated FXIII addition (10 U/ml), 30 µl drops of cell/hydrogel mix were quickly casted in the bottom of 24 wells plate. Once the hydrogel polymerized, growth medium was added and cells were kept at 37°C with 5% CO_2. 3D cultured cells were imaged on a Leica DMI 4000 brightfield microscope every week.

C25 cells muscle differentiation

For myosin heavy chain (MHC) immunocytostaining, C25 cells were grew on top of glass coverslips in 24 wells plate. In order to test C25 cells ability to differentiate in skeletal muscle cells, C25 cells were grew at confluence and then exposed to skeletal muscle cell differentiation medium (Zenbio, SKM-D) during 5 days. Cells were then rinsed with PBS and fixed with 4% PFA for 20 min at RT. After fixation, coverslips were incubated with blocking buffer (1% BSA and 5% NGS in 0.1% Triton-X PBS) for 2h at RT. Primary antibody against MHC (mouse IgG2b anti chicken MHC clone MF20 from the developmental studies hybridoma bank) was incubated overnight at 1/20 dilution in blocking buffer. After washing, coverslips were incubated with secondary antibody CY3 goat anti-mouse IgG2b specific (Jackson ImmunoResearch, 11-165-207) diluted 1/500 in PBS. Cell nuclei were then stain with DAPI staining for 10min and coverslips were mounted using moviol.

For immunocytostaining of the 3D culture in the PEG hydrogel, the protocol was the same except that the secondary antibody incubation was performed overnight at 4°C and all washing step were extended in order for the solution to penetrated the hydrogel. Cells in the PEG hydrogel were not exposed to differentiation medium.

mAb-11 antibody

MAb-11 antibody recognized a conformational epitope of Aβ aggregates. It was derived from the human combinatorial antibody library Fab 1 (MorphoSys; HuCAL-Fab1) (Rauchenberger et al., 2003). The sequence is very similar to the anti-Aβ antibody Gantenerumab developed by Roche (Bohrmann et al., 2012). Both antibody shared common binding properties and activate cell-mediated phagocytosis (Xiang et al., 2016)(Lathuilière et al., 2016). Two cDNA encoding the heavy and the light chains of a human mouse chimeric version of mAb-11 (human variable domains, mouse IgG2a constant domains) were synthetized for murine use.

Genetic engineering

C25 cells were genetically modified to express either the firefly luciferase enzyme or the chimeric recombinant mAb-11 IgG2a. For this purpose, cDNA coding for the firefly luciferase, the mAb-11 IgG2a light chain (LC) or the mAb-11 IgG2a heavy chain (HC) were respectively cloned in the pRRLSIN.CPPT.PGK-MCS.WPRE lentiviral shuttle plasmid (Addgene plasmid #12252). Lentivirus containing the plasmid were produced using transient transfection of HEK293T cells as described elsewhere (Zufferey, 2002). The number of infectious particles or transducing units per milliliter (TU/ml) was determined by infecting HeLa cells and quantify the number of integrated vector genome using quantitative polymerase chain reaction (qPCR) (Towers et al., 1999).

To generate C25 cells expressing luciferase, cells were infected with the luciferase lentiviral vector with different lentivirus to cell ratio (multiplicity of infection, MOI). To generate C25 cells expressing mAb-11 antibody, C25 cells were infected simulatenuosly with both lentivirus containing mAb-11 light chain

or mAb-11 heavy chain at different MOI. Single cloning was performed using limiting dilution method (Fuller et al., 2001).

Implant

The implant was designed for continuous subcutaneous antibody delivery. The devices were assembled by the Cell Encapsulation Technology Team at Nestlé Health Science as published previously (Lathuilière et al., 2014b). The device is a flat sheet implants 27 mm long, 12 mm wide and 1.2 mm thick. The internal volume is approximately 40 µl. It is constituted of a semi-permeable membrane made of either polypropylene membrane with 45 µm pore (PP45) or a polytetrafuoroethylene (PTFE) membrane and a polyester mesh. The different sheets are welded together using ultrasonic. Devices were sterilized using ethylene oxide prior cell loading and implantation.

Cell loading in implants

The detailed procedure for cell loading in the implant was already described (Lathuilière et al., 2014b). Quickly, cells were harvested with 0.05% trypsin-EDTA solution (Gibco; 25300-054), counted, centrifuged, rinsed with PBS and resuspended in skeletal muscle cell growth media (PromoCell; C-23160) at the desired seeding concentration. Cells were then mixed with the PEG hydrogel mix at either 3% w/v or 1.5% w/v. After FXIII activation, cells were quickly injected in the inner volume of the implant using the loading port and rocked until polymerization of the PEG hydrogel. Once the cells trapped in the implant, the loading port was cut and the device sealed using photo polymerizing medical-grade glue (Loctite). The devices were then maintained in growth medium changed every 2-3 days at 37°C with 5% CO_2 for *in vitro* studies or kept at 37°C with 5% CO_2 overnight and surgically implanted in mice for *in vivo* studies.

Encapsulation *In vitro* studies

Cells were loaded at the desired cell density either in 3% w/v or 1.5% w/v PEG hydrogel and maintained in growth medium at 37°C with 5% CO2.

For bioluminescence reading, the growth medium was supplemented with 150 µg/ml D-Luciferin Firely, sodium salt monohydrate (Biosynth; L-8240) and images were acquired with an IVIS 100 Imaging system (Xenogen) every 5 min

until de signal reach a plateau and stabilized. The stabilized signal was used to determine the average radiance in photons per cm^2 per second per steradian (photon/cm^2/s/sr) by drawing region of interest (ROI) and integrating the bioluminescent signal using the Living Image Software provided by PerkinElmer.

For mAb-11 quantification, fresh growth medium was added on capsule during 4h, harvested, centrifuged and analyzed with a mAb-11 functional enzyme-linked immunosorbent assay (ELISA) developed by Roche.

At the end of the experiment, implant were fixed with 4% PFA at 4°C overnight, dehydrated and embedded in paraffin until further process.

MAb-11 quantification with ELISA

The ELISA used to quantify mAb-11 was developed by Roche and detailed protocol was already described in previous publication (Lathuilière et al., 2014a). Collected conditioned medium or plasma was diluted in LowCross Buffer (Candor Bioscience, 100 500) and incubated 1h at room temperature (RT) in 96-well plate coated with 7 µg/ml amyloid beta peptide. After PBS/0.05% Tween 20 washing, peroxidase (POD) conjugated goat anti-mouse antibody was incubated for mAb-11 antibody detection. After washing, POD substrate (ABST solution, Roche, 11 684 302 001) was applied for colorimetric read-out at 405 nm using a Versamax plate (Molecular Devices). The standards curved was determined using purified mAb11 IgG2a diluted at known concentration and calculated using a non-linear four parameter fit provided by the SoftMax Pro Softwate (Moelcular Devices).

Transgenic mice

We performed experiment on two different transgenic Alzheimer's mice model. The 5xFAD mice were from the original hybrid B6SJL background (Jackson Laboratory, B6SJL-Tg (APPSwFlLon,PSEN1*M146L*L286V) 6799Vas/Mmjax, stock No 34840-JAX). The animals carried five human transgenes: three transgenes expressing mutated APP, Swedish (K670N/M671L), Florida (I716V), London (V717I), and two transgenes expressing mutated PS1, M146L and L286V (Oakley et al., 2006). We used only heterozygous mice.

The TauPS2APP mice were on congenic C57BL/6N background and express three human mutated proteins: The swedish (K670N/M671L) familial APP, the N141I PSEN2 protein and the P301L human tau mutant (Grueninger et al., 2010). TauPS2APP mice were provided by Roche.

We also used two different immunodeficient mice models: the Rag2KO (Jackson Laboratory, B6(Cg)-Rag2$^{tm1.1Cgn}$/J, stock No: 008449) and the Rag2KO-Il2rgKO mouse model (Jackson Laboratory, C;129S4-Rag2$^{tm1.1Flv}$ Il2rg$^{tm1.1Flv}$ /J, Stock No: 014593). Both are *Rag2* gene double knockout preventing T and B cell maturation. The second model is also missing the *Il2rg* gene preventing natural killer cell development.

In vivo studies

Experiments on mice were performed under the license VD-3130 and VD-3210 according to the Swiss Federal Law for animal protection and animal experimentation (Art.18 LPA, Art. 141 OPAn, Art. 30). All animals were housed according to the EPFL regulation with water and food *ad libitum*, 5 animals maximum per cage (IVC type GM500) with nesting materiel and enrichment. The animal facility was maintained in a 12:12h light:dark cycle.

The experimental groups were aged matched and the number of males and females balanced carefully. Capsules with different features were randomly assigned to littermate mice.

Implantation

The surgery for subcutaneous device implantation was performed under isofluorane anesthesia. During the surgery, the skin of the animals was opened in between the shoulder blades and the skin on the back detached from the muscle using a spatula. Implants were carefully rinsed with sterile PBS before being inserted underneath the skin of the back of the mice. The wound was closed with stiches. After implantation analgesia was provided in drinking water during 5 days (acetaminophen; 2 mg/ml).

In vivo bioluminescence imaging

Bioluminescence imaging was performed using the IVIS Spectrum In Vivo Imaging System (PerkinElmer) every two weeks after implantation of device

containing C25 luciferase cell line. Animals were injected intraperitoneally (IP) with 150 mg/kg D-Luciferin Firely, sodium salt monohydrate (Biosynth; L-8240) resuspended in sterile 0.9% sodium chloride solution (B.Braun; 534534). Animals were imaged under isofluorane anesthesia 45 min after luciferin injection once the bioluminescence signal reached a plateau and stabilized. Average radiance (photon/cm^2/s/sr) was measured by integrating the bioluminescent signal at the capsule position using the Living Image Software provided by PerkinElmer.

Blood draw

Animals implanted with antibody mAb-11 secreting device underwent blood draw every 2 weeks after implantation until the end of the experiemnt. Blood was sampled from the saphenous vein, collected in EDTA-coated tubes (Sarstedt; 16.444, Microvette CB 300 K2E) and centrifuged at 5000 g for 10 min to separate the plasma. The plasma was kept at – 80°C until mAb-11 quantification using the Roche ELISA described previously (Lathuilière et al., 2014a).

Tolerization

For tolerization, depleting and non-depleting monoclonal anti-mouse CD4 antibodies were used (BioXcell, clone GK1.5 BE0003-1, clone YTS 177 BE0003-3). Different tolerization procedures were used:

In order to avoid anti-drug antibody (ADA) response in Alzheimer's mice (5xFAD and TauPS2APP mice) implanted with C2C12 secreting mAb-11, animals were injected intraperitoneally (IP) with 0.5 mg GK1.5/mice one day prior the implantation and three day after. This protocol was already tested and prevented ADA response (Lathuilière et al., 2016).

For xenograft tolerization when encapsulated human cells were implanted in B6SJL wild type mice, depleting antibody (GK1.5; 0.5 mg/mice) was injected IP at day -1, 4 and 7 around the implantation day and non-depleting antibody (YTS 177) was injected intravenously (IV) at 1mg/ at day -1, 4 and 7 around the implantation date.

Stereotaxy

The propagation human tau mice model was developed by stereotaxic injection of adeno-associate virus serotype 8 (AAV8) injection. Recombinant AAV8 particle containing the cDNA 4R0N human wild-type tau under the PGK promotor (AAV8-PGK-4R0NTau-WPRE) were produced according to standard methods.

Animals were anesthetized using xylazine (10mg/kg) and ketamine (100mg/kg) and placed on a stereotaxic framed. The skin was opened and the skull drilled to inject 1 µl of virus ($2.8x10^{10}$ viral genomes) in the right hippocampus (CA3, coordinates antéroposterior -2.1, lateral -2.25, ventral -2.25) using catheters. The skin was closed and analgesia provided in drinking water during 5 days (acetaminophen; 2 mg/ml).

Necropsy

At the end of the experiment, animals were overdosed with pentobarbital. We performed a terminal intracardiac puncture to sample blood and implants were dissected from the subcutaneous tissue. Animals were then perfused with 4% Paraformaldehyde (PFA) in order to fixed the tissues and the brain was dissected out of the skull.

Collected brain were kept at 4°C overnight in 4% PFA and then in sterile filtrated 25% saccharose solution in PBS for minimum 4 days prior tissue processing.

Implant were kept 4 hours at 37°C with 5% CO_2 in growth medium. Growth medium was sampled, centrifuged to remove tissue debris and kept at – 80°C for mAb-11 ex vivo release quantification using ELISA. Implants were then fixed with 4% PFA at 4°C overnight, dehydrated and embedded in paraffin until further process.

Blood was collected in EDTA-coated tube, centrifuged and the separated plasma was kept at -80°C for mAb-11 ELISA quantification.

Histological capsule processing

After paraffin embedding, implants were cut in 4 or 10 µm transversal sections with a microtome. Sections were stained with standard hematoxylin and eosin (HE) (Fischer et al., 2008) or Masson's trichrome stainings (Foot, 1933).

Immunohistochemistry

After cryoprotection in 25% saccharose solution, brains were cut using a cryostat in coronal section and kept at 4°C in PBS azide. Prior immunohistochemistry, sections were mounted in Superfrost plus slide (Thermo Scientific).

For Aβ plaques (mouse IgG1 anti-human amyloid beta antibody clone 6e10, 1/500, Sigma 39320), microglia (Rabbit anti-mouse Iba1, 1/500, Abcam EPR16588), phagolysosome (Rat anti-mouse CD68, 1/500, BioRad MCA1957GA) and synaptophysin (Rabbit synaptophysin, 1/500, Abcam, Ab32127) detection, we followed simple standard immunohistochemistry protocol. Quickly, sections were blocked in 5% normal goat serum (NGS) or 5% normal donkey serum (NDS) in 0.1% Triton-X PBS for at least 2 hours at room temperature (RT). Then primary antibodies were incubated overnight in blocking buffer at 4°C. After incubation, the sections were washed with PBS and incubated with fluorescent conjugated secondary antibody diluted in PBS for 2 hours. After the immunohistochemistry staining, we performed a DAPI staining and mount the slides with fluoromount-G (SouthernBiotech, 0100-01). As secondary, we used AlexaFluor 488 (AF488) goat anti-mouse IgG1 specific (Jackson ImmunoResearch, 1/500, 115-545-305), AF647 Donkey anti-rabbit (1/250), CY3 Donkey anti-rat (1/1000) and CY3 Donkey anti-rabbit (1/1000) respectively.

For Aβ staining, we also used mouse IgG2b anti-amyloid beta antibody clone 4g8 (Biolegend, 1/1000, 800709). In addition of the standard protocol described above, the sections were pre-treated with 70% acid formic for 30 min at RT and antigen retrieval was performed (10mM trisodium citrate buffer at 95°C for 20min). As secondary, we used an AlexaFluor 488 (AF488) Goat anti-mouse, IgG2b specific (Jackson ImmunoReseach, 1/500, 115-545-207). The 4g8 antibody was better than the 6e10 antibody and was used for Aβ quantification but it was difficult to combined with other staining due to the aggressive pre-treatment.

Tau immunohistochemistry all required antigen retrieval (10mM trisodium citrate buffer at 95°C for 20min) prior to the standard protocol. Mouse anti-human misfolded tau MC1 (provided by Peter Davies, Department of Pathology,

Albert Einstein College of Medecine) was incubated overnight at 1/500 dilution and detected using a CY3 goat anti-mouse IgG1 specific secondary antibody (Jackson ImmunoReseach, 1/500, 115-165-205). For total Tau and Phospho-Tau (Ser202, Thr205) detection, we used biotin conjugated primary antibodies HT7 (Mouse anti-human tau biotin-labeled, 1/1000, Pierce MN1000B) and AT8 (Mouse anti-human PHF-Tau biotin labeled, 1/1000, Thermo MN1020B) and we amplified the signal using the AF555 Tyramide SuperBoost Kit (Invitrogen, B40913). All tau immunohistochemistry protocols were compatible with the anti-Aβ 4g8 protocol.

Detection of Aβ plaques immunodecoration by anti-Aβ mAb-11 was performed using goat anti-mouse IgG2a specific antibody directly. To avoid non-specific binding, sections were first treated with Ultra V blocking solution (LabVision) for 5 min followed by PBS 0.01% Tween-20 washing and a second blocking using Power Block Solution 1x (BioGenex) supplemented with 10% normal sheep serum for 2 hours at RT. The section were then incubated for 1 h with CY3 goat anti-mouse IgG2a specific (Jackson Immunoresearch, 115-165-206) at 1/100 dilution in 1% Bovine Serum Albumin (BSA) and PBS.

Image Processing

After immunohistochemistry, brain slices on slides were entirely imaged using the Olympus slide scanner VS120-L100 with a 10x objective. Acquired Olympus virtual slide format images (.vsi) were opened and analyzed using the QuPath software (Bankhead et al., 2017). Region of interests (ROI), usually the ipsilateral and contralateral hippocampus, were drawn by hand based on the DAPI signal using a drawing tablet. Then, detection of the area covered by the fluorescent signal within the ROI was measured using Fiji thresholding algorithms. The algorithm was chosen in order to fit the signal as well as possible. Algorithm fitness depended on signal distribution and intensity but Triangle, Moments and Otsu were usually chosen.

Sorting algorithms for sorting plaques and microglia according to their size were performed on QuPath after signal detection by thresholding algorithms.

For analysis of the plaque surrounding, plaques were detected and a 5 µm thick surrounding was drawn around them. Then the signal of interest (microglia, phagolysosome or tau) area was detected and overlapping signal area with the plaque surrounding was measured.

After QuPath analysis, data were exported as table in Excel (Microsoft Office) to be sorted.

Statistical analysis

Graphs and statistical analysis were performed on Prism (GraphPad). Data are represented as mean +/- standard error of the mean (SEM). Two-tailed unpaired parametric Student's *t*-test was used for comparisons between two groups. For results containing more than two groups, regular one-way or two-way ANOVA were applied. We corrected *post hoc* multiple comparison using Sidak test. Definition of the statistical significance was set at $p < 0.05$ and p values were reported using the GraphPad style: ns ($p > 0.05$), * ($p \leq 0.05$), ** ($p \leq 0.01$), *** ($p \leq 0.001$), **** ($p \leq 0.0001$).

7

Chapter 7 : References

Adolfsson, O., Pihlgren, M., Toni, N., Varisco, Y., Buccarello, A.L., Antoniello, K., Lohmann, S., Piorkowska, K., Gafner, V., Atwal, J.K., Maloney, J., Chen, M., Gogineni, A., Weimer, R.M., Mortensen, D.L., Friesenhahn, M., Ho, C., Paul, R., Pfeifer, A., Muhs, A., Watts, R.J., 2012. An effector-reduced anti-β-amyloid (Aβ) antibody with unique aβ binding properties promotes neuroprotection and glial engulfment of Aβ. J. Neurosci. Off. J. Soc. Neurosci. 32, 9677–9689. https://doi.org/10.1523/JNEUROSCI.4742-11.2012

Aebischer, P., Schluep, M., Déglon, N., Joseph, J.M., Hirt, L., Heyd, B., Goddard, M., Hammang, J.P., Zurn, A.D., Kato, A.C., Regli, F., Baetge, E.E., 1996. Intrathecal delivery of CNTF using encapsulated genetically modified xenogeneic cells in amyotrophic lateral sclerosis patients. Nat. Med. 2, 696–699.

Alzheimer, A., 1911. Uber eine eigenartige Krankheitsfälle des späteren Alters. Z. Für Gesamte Neurol. Psychiatr. 4.

Alzheimer association CH, 2019. Alzheimer association Suisse, des chiffres et des faits [WWW Document]. URL https://www.alzheimer-schweiz.ch/fr/les-demences/article/des-chiffres-et-des-faits-sur-les-demences/ (accessed 5.19.19).

Andorfer, C., Kress, Y., Espinoza, M., de Silva, R., Tucker, K.L., Barde, Y.-A., Duff, K., Davies, P., 2003. Hyperphosphorylation and aggregation of tau in mice expressing normal human tau isoforms. J. Neurochem. 86, 582–590. https://doi.org/10.1046/j.1471-4159.2003.01879.x

Arndt, J.W., Qian, F., Smith, B.A., Quan, C., Kilambi, K.P., Bush, M.W., Walz, T., Pepinsky, R.B., Bussière, T., Hamann, S., Cameron, T.O., Weinreb, P.H., 2018. Structural and kinetic basis for the selectivity of aducanumab for aggregated forms of amyloid-β. Sci. Rep. 8. https://doi.org/10.1038/s41598-018-24501-0

Asai, H., Ikezu, S., Tsunoda, S., Medalla, M., Luebke, J., Haydar, T., Wolozin, B., Butovsky, O., Kügler, S., Ikezu, T., 2015. Depletion of microglia and inhibition of exosome synthesis halt tau propagation. Nat. Neurosci. 18, 1584–1593. https://doi.org/10.1038/nn.4132

Askew, K., Li, K., Olmos-Alonso, A., Garcia-Moreno, F., Liang, Y., Richardson, P., Tipton, T., Chapman, M.A., Riecken, K., Beccari, S., Sierra, A., Molnár, Z., Cragg, M.S., Garaschuk, O., Perry, V.H., Gomez-Nicola, D., 2017. Coupled Proliferation and Apoptosis Maintain the Rapid Turnover of Microglia in the Adult Brain. Cell Rep. 18, 391–405. https://doi.org/10.1016/j.celrep.2016.12.041

Atwood, C.S., Bowen, R.L., Smith, M.A., Perry, G., 2003. Cerebrovascular requirement for sealant, anti-coagulant and remodeling molecules that allow for the maintenance of vascular integrity and blood supply. Brain Res. Brain Res. Rev. 43, 164–178.

Avila, J., 2006. Tau protein, the main component of paired helical filaments. J. Alzheimers Dis. JAD 9, 171–175.

Bacskai, B.J., Kajdasz, S.T., McLellan, M.E., Games, D., Seubert, P., Schenk, D., Hyman, B.T., 2002. Non-Fc-mediated mechanisms are involved in clearance of amyloid-beta in vivo by immunotherapy. J. Neurosci. Off. J. Soc. Neurosci. 22, 7873–7878.

Bae, E.-J., Lee, H.-J., Rockenstein, E., Ho, D.-H., Park, E.-B., Yang, N.-Y., Desplats, P., Masliah, E., Lee, S.-J., 2012. Antibody-aided clearance of extracellular α-synuclein prevents cell-to-cell aggregate transmission. J. Neurosci. Off. J. Soc. Neurosci. 32, 13454–13469. https://doi.org/10.1523/JNEUROSCI.1292-12.2012

Balbás, P., Lorence, A., 2004. Recombinant Gene Expression: Reviews and Protocols. Springer Science & Business Media.

Bankhead, P., Loughrey, M.B., Fernández, J.A., Dombrowski, Y., McArt, D.G., Dunne, P.D., McQuaid, S., Gray, R.T., Murray, L.J., Coleman, H.G., James, J.A., Salto-Tellez, M., Hamilton, P.W., 2017. QuPath: Open source software for digital pathology image analysis. Sci. Rep. 7, 16878. https://doi.org/10.1038/s41598-017-17204-5

Bard, F., Barbour, R., Cannon, C., Carretto, R., Fox, M., Games, D., Guido, T., Hoenow, K., Hu, K., Johnson-Wood, K., Khan, K., Kholodenko, D., Lee, C., Lee, M., Motter, R., Nguyen, M., Reed, A., Schenk, D., Tang, P., Vasquez, N., Seubert, P., Yednock, T., 2003. Epitope and isotype specificities of antibodies to beta -amyloid peptide for protection against Alzheimer's disease-like neuropathology. Proc. Natl. Acad. Sci. U. S. A. 100, 2023–2028. https://doi.org/10.1073/pnas.0436286100

Bard, F., Cannon, C., Barbour, R., Burke, R.L., Games, D., Grajeda, H., Guido, T., Hu, K., Huang, J., Johnson-Wood, K., Khan, K., Kholodenko, D., Lee, M., Lieberburg, I., Motter, R., Nguyen, M., Soriano, F., Vasquez, N., Weiss, K., Welch, B., Seubert, P., Schenk, D., Yednock, T., 2000. Peripherally administered antibodies against amyloid beta-peptide enter the central nervous system and reduce pathology in a mouse model of Alzheimer disease. Nat. Med. 6, 916–919. https://doi.org/10.1038/78682

Bateman, R.J., Benzinger, T.L., Berry, S., Clifford, D.B., Duggan, C., Fagan, A.M., Fanning, K., Farlow, M.R., Hassenstab, J., McDade, E.M., Mills, S., Paumier, K., Quintana, M., Salloway, S.P., Santacruz, A., Schneider, L.S., Wang, G., Xiong, C., 2017. The DIAN-TU Next Generation Alzheimer's prevention trial: adaptive design and disease progression model. Alzheimers Dement. J. Alzheimers Assoc. 13, 8–19. https://doi.org/10.1016/j.jalz.2016.07.005

Belaunzaran, O.M., Cordero, M.I., Setola, V., Bianchi, S., Galli, C., Bouche, N., Mlynarik, V., Gruetter, R., Sandi, C., Bensadoun, J.-C., Molinari, M., Aebischer, P., 2011. Chronic Delivery of Antibody Fragments Using Immunoisolated Cell Implants as a Passive Vaccination Tool. PLOS ONE 6, e18268. https://doi.org/10.1371/journal.pone.0018268

Bemiller, S.M., McCray, T.J., Allan, K., Formica, S.V., Xu, G., Wilson, G., Kokiko-Cochran, O.N., Crish, S.D., Lasagna-Reeves, C.A., Ransohoff, R.M., Landreth, G.E., Lamb, B.T., 2017. TREM2 deficiency exacerbates tau pathology through dysregulated kinase signaling in a mouse model of tauopathy. Mol. Neurodegener. 12, 74. https://doi.org/10.1186/s13024-017-0216-6

Bennett, R.E., DeVos, S.L., Dujardin, S., Corjuc, B., Gor, R., Gonzalez, J., Roe, A.D., Frosch, M.P., Pitstick, R., Carlson, G.A., Hyman, B.T., 2017. Enhanced Tau Aggregation in the Presence of Amyloid β. Am. J. Pathol. 187, 1601–1612. https://doi.org/10.1016/j.ajpath.2017.03.011

Bertram, L., Tanzi, R.E., 2009. Genome-wide association studies in Alzheimer's disease. Hum. Mol. Genet. 18, R137–R145. https://doi.org/10.1093/hmg/ddp406

Bhaskar, K., Konerth, M., Kokiko-Cochran, O.N., Cardona, A., Ransohoff, R.M., Lamb, B.T., 2010. Regulation of Tau Pathology by the Microglial Fractalkine Receptor. Neuron 68, 19–31. https://doi.org/10.1016/j.neuron.2010.08.023

Bhaskar, K., Yen, S.-H., Lee, G., 2005. Disease-related Modifications in Tau Affect the Interaction between Fyn and Tau. J. Biol. Chem. 280, 35119–35125. https://doi.org/10.1074/jbc.M505895200

Bien-Ly, N., Yu, Y.J., Bumbaca, D., Elstrott, J., Boswell, C.A., Zhang, Y., Luk, W., Lu, Y., Dennis, M.S., Weimer, R.M., Chung, I., Watts, R.J., 2014. Transferrin receptor (TfR) trafficking determines brain uptake of TfR antibody affinity variants. J. Exp. Med. 211, 233–244. https://doi.org/10.1084/jem.20131660

Blanchard, V., Moussaoui, S., Czech, C., Touchet, N., Bonici, B., Planche, M., Canton, T., Jedidi, I., Gohin, M., Wirths, O., Bayer, T.A., Langui, D., Duyckaerts, C., Tremp, G., Pradier, L., 2003. Time sequence of maturation of dystrophic neurites associated with Aβ deposits in APP/PS1 transgenic mice. Exp. Neurol. 184, 247–263. https://doi.org/10.1016/S0014-4886(03)00252-8

Boche, D., Donald, J., Love, S., Harris, S., Neal, J.W., Holmes, C., Nicoll, J.A.R., 2010. Reduction of aggregated Tau in neuronal processes but not in the cell bodies after Abeta42 immunisation in Alzheimer's disease. Acta Neuropathol. (Berl.) 120, 13–20. https://doi.org/10.1007/s00401-010-0705-y

Bohrmann, B., Baumann, K., Benz, J., Gerber, F., Huber, W., Knoflach, F., Messer, J., Oroszlan, K., Rauchenberger, R., Richter, W.F., Rothe, C., Urban, M., Bardroff, M., Winter, M., Nordstedt, C., Loetscher, H., 2012. Gantenerumab: a novel human anti-Aβ antibody demonstrates sustained cerebral amyloid-β binding and elicits cell-mediated removal of human amyloid-β. J. Alzheimers Dis. JAD 28, 49–69. https://doi.org/10.3233/JAD-2011-110977

Bolmont, T., Clavaguera, F., Meyer-Luehmann, M., Herzig, M.C., Radde, R., Staufenbiel, M., Lewis, J., Hutton, M., Tolnay, M., Jucker, M., 2007. Induction of Tau Pathology by Intracerebral Infusion of Amyloid-β-Containing Brain Extract and by Amyloid-β Deposition in APP × Tau Transgenic Mice. Am. J. Pathol. 171, 2012–2020. https://doi.org/10.2353/ajpath.2007.070403

Boutajangout, A., Authelet, M., Blanchard, V., Touchet, N., Tremp, G., Pradier, L., Brion, J.-P., 2004. Characterisation of cytoskeletal abnormalities in mice transgenic for wild-type human tau and familial Alzheimer's disease mutants of APP and presenilin-1. Neurobiol. Dis. 15, 47–60. https://doi.org/10.1016/j.nbd.2003.09.007

Box, G.E.P., Draper, N.R., 1987. Empirical model-building and response surfaces, Empirical model-building and response surfaces. John Wiley & Sons, Oxford, England.

Braak, H., Braak, E., 1991. Neuropathological stageing of Alzheimer-related changes. Acta Neuropathol. (Berl.) 82, 239–259.

Bradshaw, E.M., Chibnik, L.B., Keenan, B.T., Ottoboni, L., Raj, T., Tang, A., Rosenkrantz, L.L., Imboywa, S., Lee, M., Von Korff, A., Alzheimer Disease Neuroimaging Initiative, Morris, M.C., Evans, D.A., Johnson, K., Sperling, R.A., Schneider, J.A., Bennett, D.A., De Jager, P.L., 2013. CD33 Alzheimer's disease locus: altered monocyte function and amyloid biology. Nat. Neurosci. 16, 848–850. https://doi.org/10.1038/nn.3435

Brelstaff, J., Tolkovsky, A.M., Ghetti, B., Goedert, M., Spillantini, M.G., 2018. Living Neurons with Tau Filaments Aberrantly Expose Phosphatidylserine and Are Phagocytosed by Microglia. Cell Rep. 24, 1939-1948.e4. https://doi.org/10.1016/j.celrep.2018.07.072

Brion, J.-P., Passareiro, H., Nunez, J., Flament-Durand, J., 1985. Mise en évidence immunologique de la protéine tau au niveau des lésions de dégénérescence neurofibrillaire de la maladie d'Alzheimer. Arch Biol. Arch.Biol.(Brux) 95, 229–235.

Brothers, H.M., Gosztyla, M.L., Robinson, S.R., 2018. The Physiological Roles of Amyloid-β Peptide Hint at New Ways to Treat Alzheimer's Disease. Front. Aging Neurosci. 10. https://doi.org/10.3389/fnagi.2018.00118

Buerger, K., Teipel, S.J., Zinkowski, R., Blennow, K., Arai, H., Engel, R., Hofmann-Kiefer, K., McCulloch, C., Ptok, U., Heun, R., Andreasen, N., DeBernardis, J., Kerkman, D., Moeller, H.-J., Davies, P., Hampel, H., 2002. CSF tau protein phosphorylated at threonine 231 correlates with cognitive decline in MCI subjects. Neurology 59, 627–629. https://doi.org/10.1212/wnl.59.4.627

Buss, N.A., Henderson, S.J., McFarlane, M., Shenton, J.M., de Haan, L., 2012. Monoclonal antibody therapeutics: history and future. Curr. Opin. Pharmacol., Anti-infectives • New technologies 12, 615–622. https://doi.org/10.1016/j.coph.2012.08.001

Bussian, T.J., Aziz, A., Meyer, C.F., Swenson, B.L., van Deursen, J.M., Baker, D.J., 2018. Clearance of senescent glial cells prevents tau-dependent pathology and cognitive decline. Nature 562, 578–582. https://doi.org/10.1038/s41586-018-0543-y

Butler, A.W., Ng, M.Y.M., Hamshere, M.L., Forabosco, P., Wroe, R., Al-Chalabi, A., Lewis, C.M., Powell, J.F., 2009. Meta-analysis of linkage studies for Alzheimer's disease--a web resource. Neurobiol. Aging 30, 1037–1047. https://doi.org/10.1016/j.neurobiolaging.2009.03.013

Butovsky, O., Jedrychowski, M.P., Moore, C.S., Cialic, R., Lanser, A.J., Gabriely, G., Koeglsperger, T., Dake, B., Wu, P.M., Doykan, C.E., Fanek, Z., Liu, L., Chen, Z., Rothstein, J.D., Ransohoff, R.M., Gygi, S.P., Antel, J.P., Weiner, H.L., 2014. Identification of a unique TGF-β-dependent molecular and functional signature in microglia. Nat. Neurosci. 17, 131–143. https://doi.org/10.1038/nn.3599

Butovsky, O., Weiner, H.L., 2018. Microglial signatures and their role in health and disease. Nat. Rev. Neurosci. 19, 622. https://doi.org/10.1038/s41583-018-0057-5

Chabrier, M.A., Blurton-Jones, M., Agazaryan, A.A., Nerhus, J.L., Martinez-Coria, H., LaFerla, F.M., 2012. Soluble Aβ Promotes Wild-Type Tau Pathology in vivo. J. Neurosci. Off. J. Soc. Neurosci. 32, 17345–17350. https://doi.org/10.1523/JNEUROSCI.0172-12.2012

Chen, W., Abud, E.A., Yeung, S.T., Lakatos, A., Nassi, T., Wang, J., Blum, D., Buée, L., Poon, W.W., Blurton-Jones, M., 2016. Increased tauopathy drives microglia-mediated clearance of beta-amyloid. Acta Neuropathol. Commun. 4, 63. https://doi.org/10.1186/s40478-016-0336-1

Cohen, E., Paulsson, J.F., Blinder, P., Burstyn-Cohen, T., Du, D., Estepa, G., Adame, A., Pham, H.M., Holzenberger, M., Kelly, J.W., Masliah, E., Dillin, A., 2009. Reduced IGF-1 signaling delays age-associated proteotoxicity in mice. Cell 139, 1157–1169. https://doi.org/10.1016/j.cell.2009.11.014

Condello, C., Yuan, P., Schain, A., Grutzendler, J., 2015. Microglia constitute a barrier that prevents neurotoxic protofibrillar Aβ42 hotspots around plaques. Nat. Commun. 6, 6176. https://doi.org/10.1038/ncomms7176

Conejero-Goldberg, C., Gomar, J.J., Bobes-Bascaran, T., Hyde, T.M., Kleinman, J.E., Herman, M.M., Chen, S., Davies, P., Goldberg, T.E., 2014. APOE2 enhances neuroprotection against Alzheimer's disease through multiple molecular mechanisms. Mol. Psychiatry 19, 1243–1250. https://doi.org/10.1038/mp.2013.194

Corder, E.H., Saunders, A.M., Risch, N.J., Strittmatter, W.J., Schmechel, D.E., Gaskell, P.C., Rimmler, J.B., Locke, P.A., Conneally, P.M., Schmader, K.E., 1994. Protective effect of apolipoprotein E type 2 allele for late onset Alzheimer disease. Nat. Genet. 7, 180–184. https://doi.org/10.1038/ng0694-180

Corder, E.H., Saunders, A.M., Strittmatter, W.J., Schmechel, D.E., Gaskell, P.C., Small, G.W., Roses, A.D., Haines, J.L., Pericak-Vance, M.A., 1993. Gene dose of apolipoprotein E type 4 allele and the risk of Alzheimer's disease in late onset families. Science 261, 921–923. https://doi.org/10.1126/science.8346443

Coronel, R., Bernabeu-Zornoza, A., Palmer, C., Muñiz-Moreno, M., Zambrano, A., Cano, E., Liste, I., 2018. Role of Amyloid Precursor Protein (APP) and Its Derivatives in the Biology and Cell Fate Specification of Neural Stem Cells. Mol. Neurobiol. 55, 7107–7117. https://doi.org/10.1007/s12035-018-0914-2

Cras, P., Kawai, M., Lowery, D., Gonzalez-DeWhitt, P., Greenberg, B., Perry, G., 1991. Senile plaque neurites in Alzheimer disease accumulate amyloid precursor protein. Proc. Natl. Acad. Sci. U. S. A. 88, 7552–7556.

Crimins, J.L., Pooler, A., Polydoro, M., Luebke, J.I., Spires-Jones, T.L., 2013. The intersection of amyloid beta and tau in glutamatergic synaptic dysfunction and collapse in Alzheimer's disease. Ageing Res. Rev., Synaptic Global positioning systems 12, 757–763. https://doi.org/10.1016/j.arr.2013.03.002

Cummings, J.L., Cohen, S., van Dyck, C.H., Brody, M., Curtis, C., Cho, W., Ward, M., Friesenhahn, M., Rabe, C., Brunstein, F., Quartino, A., Honigberg, L.A., Fuji, R.N., Clayton, D., Mortensen, D., Ho, C., Paul, R., 2018. ABBY: A phase 2 randomized trial of crenezumab in mild to moderate Alzheimer disease. Neurology 90, e1889–e1897. https://doi.org/10.1212/WNL.0000000000005550

Das, P., Murphy, M.P., Younkin, L.H., Younkin, S.G., Golde, T.E., 2001. Reduced effectiveness of Abeta1-42 immunization in APP transgenic mice with significant amyloid deposition. Neurobiol. Aging 22, 721–727.

DeKosky, S.T., Scheff, S.W., 1990. Synapse loss in frontal cortex biopsies in Alzheimer's disease: Correlation with cognitive severity. Ann. Neurol. 27, 457–464. https://doi.org/10.1002/ana.410270502

DeMattos, R.B., Bales, K.R., Cummins, D.J., Dodart, J.C., Paul, S.M., Holtzman, D.M., 2001. Peripheral anti-A beta antibody alters CNS and plasma A beta clearance and decreases brain A beta burden in a mouse model of Alzheimer's disease. Proc. Natl. Acad. Sci. U. S. A. 98, 8850–8855. https://doi.org/10.1073/pnas.151261398

Di Fede, G., Catania, M., Morbin, M., Rossi, G., Suardi, S., Mazzoleni, G., Merlin, M., Giovagnoli, A.R., Prioni, S., Erbetta, A., Falcone, C., Gobbi, M., Colombo, L., Bastone, A., Beeg, M., Manzoni, C., Francescucci, B., Spagnoli, A., Cantù, L., Del Favero, E., Levy, E., Salmona, M., Tagliavini, F., 2009. A recessive mutation in the APP gene with dominant-negative effect on amyloidogenesis. Science 323, 1473–1477. https://doi.org/10.1126/science.1168979

Dickson, D.W., Crystal, H.A., Mattiace, L.A., Masur, D.M., Blau, A.D., Davies, P., Yen, S.-H., Aronson, M.K., 1992. Identification of normal and pathological aging in prospectively studied nondemented elderly humans. Neurobiol. Aging 13, 179–189. https://doi.org/10.1016/0197-4580(92)90027-U

Dickson, T.C., King, C.E., McCormack, G.H., Vickers, J.C., 1999. Neurochemical Diversity of Dystrophic Neurites in the Early and Late Stages of Alzheimer's Disease. Exp. Neurol. 156, 100–110. https://doi.org/10.1006/exnr.1998.7010

Doody, R.S., Thomas, R.G., Farlow, M., Iwatsubo, T., Vellas, B., Joffe, S., Kieburtz, K., Raman, R., Sun, X., Aisen, P.S., Siemers, E., Liu-Seifert, H., Mohs, R., Alzheimer's Disease Cooperative Study Steering Committee, Solanezumab Study Group, 2014. Phase 3 trials of solanezumab for mild-to-moderate Alzheimer's disease. N. Engl. J. Med. 370, 311–321. https://doi.org/10.1056/NEJMoa1312889

Duff, K., Knight, H., Refolo, L.M., Sanders, S., Yu, X., Picciano, M., Malester, B., Hutton, M., Adamson, J., Goedert, M., Burki, K., Davies, P., 2000. Characterization of Pathology in Transgenic Mice Over-Expressing Human Genomic and cDNA Tau Transgenes. Neurobiol. Dis. 7, 87–98. https://doi.org/10.1006/nbdi.1999.0279

Dunn, K.C., Aotaki-Keen, A.E., Putkey, F.R., Hjelmeland, L.M., 1996. ARPE-19, a human retinal pigment epithelial cell line with differentiated properties. Exp. Eye Res. 62, 155–169. https://doi.org/10.1006/exer.1996.0020

Duvivier-Kali, V.F., Omer, A., Parent, R.J., O'Neil, J.J., Weir, G.C., 2001. Complete protection of islets against allorejection and autoimmunity by a simple barium-alginate membrane. Diabetes 50, 1698–1705. https://doi.org/10.2337/diabetes.50.8.1698

Edison, P., Archer, H.A., Hinz, R., Hammers, A., Pavese, N., Tai, Y.F., Hotton, G., Cutler, D., Fox, N., Kennedy, A., Rossor, M., Brooks, D.J., 2007. Amyloid, hypometabolism, and cognition in

Alzheimer disease: an [11C]PIB and [18F]FDG PET study. Neurology 68, 501–508. https://doi.org/10.1212/01.wnl.0000244749.20056.d4

Ehrbar, M., Rizzi, S.C., Hlushchuk, R., Djonov, V., Zisch, A.H., Hubbell, J.A., Weber, F.E., Lutolf, M.P., 2007a. Enzymatic formation of modular cell-instructive fibrin analogs for tissue engineering. Biomaterials 28, 3856–3866. https://doi.org/10.1016/j.biomaterials.2007.03.027

Ehrbar, M., Rizzi, S.C., Schoenmakers, R.G., Miguel, B.S., Hubbell, J.A., Weber, F.E., Lutolf, M.P., 2007b. Biomolecular hydrogels formed and degraded via site-specific enzymatic reactions. Biomacromolecules 8, 3000–3007. https://doi.org/10.1021/bm070228f

Farlow, M., Arnold, S.E., van Dyck, C.H., Aisen, P.S., Snider, B.J., Porsteinsson, A.P., Friedrich, S., Dean, R.A., Gonzales, C., Sethuraman, G., DeMattos, R.B., Mohs, R., Paul, S.M., Siemers, E.R., 2012. Safety and biomarker effects of solanezumab in patients with Alzheimer's disease. Alzheimers Dement. 8, 261–271. https://doi.org/10.1016/j.jalz.2011.09.224

Farlow, M.R., Andreasen, N., Riviere, M.-E., Vostiar, I., Vitaliti, A., Sovago, J., Caputo, A., Winblad, B., Graf, A., 2015. Long-term treatment with active Aβ immunotherapy with CAD106 in mild Alzheimer's disease. Alzheimers Res. Ther. 7, 23. https://doi.org/10.1186/s13195-015-0108-3

Feige, M.J., Hendershot, L.M., Buchner, J., 2010. How antibodies fold. Trends Biochem. Sci. 35, 189–198. https://doi.org/10.1016/j.tibs.2009.11.005

Fernandez, C.G., Hamby, M.E., McReynolds, M.L., Ray, W.J., 2019. The Role of APOE4 in Disrupting the Homeostatic Functions of Astrocytes and Microglia in Aging and Alzheimer's Disease. Front. Aging Neurosci. 11. https://doi.org/10.3389/fnagi.2019.00014

Fischer, A.H., Jacobson, K.A., Rose, J., Zeller, R., 2008. Hematoxylin and Eosin Staining of Tissue and Cell Sections. Cold Spring Harb. Protoc. 2008, pdb.prot4986. https://doi.org/10.1101/pdb.prot4986

Foot, N.C., 1933. The Masson Trichrome Staining Methods in Routine Laboratory Use. Stain Technol. 8, 101–110. https://doi.org/10.3109/10520293309116112

Frost, B., Diamond, M.I., 2010. Prion-like mechanisms in neurodegenerative diseases. Nat. Rev. Neurosci. 11, 155–159. https://doi.org/10.1038/nrn2786

Fuller, J.P., Stavenhagen, J.B., Teeling, J.L., 2014. New roles for Fc receptors in neurodegeneration-the impact on Immunotherapy for Alzheimer's Disease. Front. Neurosci. 8, 235. https://doi.org/10.3389/fnins.2014.00235

Fuller, S.A., Takahashi, M., Hurrell, J.G., 2001. Cloning of hybridoma cell lines by limiting dilution. Curr. Protoc. Mol. Biol. Chapter 11, Unit11.8. https://doi.org/10.1002/0471142727.mb1108s01

Gessel, M.M., Bernstein, S., Kemper, M., Teplow, D.B., Bowers, M.T., 2012. Familial Alzheimer's Disease Mutations Differentially Alter Amyloid β-Protein Oligomerization. ACS Chem. Neurosci. 3, 909–918. https://doi.org/10.1021/cn300050d

Gilman, S., Koller, M., Black, R.S., Jenkins, L., Griffith, S.G., Fox, N.C., Eisner, L., Kirby, L., Rovira, M.B., Forette, F., Orgogozo, J.-M., AN1792(QS-21)-201 Study Team, 2005. Clinical effects of Abeta immunization (AN1792) in patients with AD in an interrupted trial. Neurology 64, 1553–1562. https://doi.org/10.1212/01.WNL.0000159740.16984.3C

Glenner, G.G., Wong, C.W., 1984a. Alzheimer's disease: initial report of the purification and characterization of a novel cerebrovascular amyloid protein. Biochem. Biophys. Res. Commun. 120, 885–890.

Glenner, G.G., Wong, C.W., 1984b. Alzheimer's disease and Down's syndrome: sharing of a unique cerebrovascular amyloid fibril protein. Biochem. Biophys. Res. Commun. 122, 1131–1135.

Goate, A., Chartier-Harlin, M.C., Mullan, M., Brown, J., Crawford, F., Fidani, L., Giuffra, L., Haynes, A., Irving, N., James, L., 1991. Segregation of a missense mutation in the amyloid precursor

protein gene with familial Alzheimer's disease. Nature 349, 704–706. https://doi.org/10.1038/349704a0

Goedert, M., Spillantini, M.G., Jakes, R., Rutherford, D., Crowther, R.A., 1989. Multiple isoforms of human microtubule-associated protein tau: sequences and localization in neurofibrillary tangles of Alzheimer's disease. Neuron 3, 519–526.

Götz, J., Chen, F., van Dorpe, J., Nitsch, R.M., 2001. Formation of neurofibrillary tangles in P301l tau transgenic mice induced by Abeta 42 fibrils. Science 293, 1491–1495. https://doi.org/10.1126/science.1062097

Götz, J., Ittner, L.M., 2008. Animal models of Alzheimer's disease and frontotemporal dementia. Nat. Rev. Neurosci. 9, 532–544. https://doi.org/10.1038/nrn2420

Graeber, M.B., Mehraein, P., 1999. Reanalysis of the first case of Alzheimer's disease. Eur. Arch. Psychiatry Clin. Neurosci. 249 Suppl 3, 10–13.

Griciuc, A., Serrano-Pozo, A., Parrado, A.R., Lesinski, A.N., Asselin, C.N., Mullin, K., Hooli, B., Choi, S.H., Hyman, B.T., Tanzi, R.E., 2013. Alzheimer's disease risk gene CD33 inhibits microglial uptake of amyloid beta. Neuron 78, 631–643. https://doi.org/10.1016/j.neuron.2013.04.014

Gros-Louis, F., Soucy, G., Larivière, R., Julien, J.-P., 2010. Intracerebroventricular infusion of monoclonal antibody or its derived Fab fragment against misfolded forms of SOD1 mutant delays mortality in a mouse model of ALS. J. Neurochem. 113, 1188–1199. https://doi.org/10.1111/j.1471-4159.2010.06683.x

Grueninger, F., Bohrmann, B., Czech, C., Ballard, T.M., Frey, J.R., Weidensteiner, C., von Kienlin, M., Ozmen, L., 2010. Phosphorylation of Tau at S422 is enhanced by Abeta in TauPS2APP triple transgenic mice. Neurobiol. Dis. 37, 294–306. https://doi.org/10.1016/j.nbd.2009.09.004

Grundke-Iqbal, I., Iqbal, K., Quinlan, M., Tung, Y.C., Zaidi, M.S., Wisniewski, H.M., 1986a. Microtubule-associated protein tau. A component of Alzheimer paired helical filaments. J. Biol. Chem. 261, 6084–6089.

Grundke-Iqbal, I., Iqbal, K., Tung, Y.C., Quinlan, M., Wisniewski, H.M., Binder, L.I., 1986b. Abnormal phosphorylation of the microtubule-associated protein tau (tau) in Alzheimer cytoskeletal pathology. Proc. Natl. Acad. Sci. U. S. A. 83, 4913–4917. https://doi.org/10.1073/pnas.83.13.4913

Guerreiro, R., Wojtas, A., Bras, J., Carrasquillo, M., Rogaeva, E., Majounie, E., Cruchaga, C., Sassi, C., Kauwe, J.S.K., Younkin, S., Hazrati, L., Collinge, J., Pocock, J., Lashley, T., Williams, J., Lambert, J.-C., Amouyel, P., Goate, A., Rademakers, R., Morgan, K., Powell, J., St. George-Hyslop, P., Singleton, A., Hardy, J., 2013. TREM2 Variants in Alzheimer's Disease. N. Engl. J. Med. 368, 117–127. https://doi.org/10.1056/NEJMoa1211851

Haass, C., Lemere, C.A., Capell, A., Citron, M., Seubert, P., Schenk, D., Lannfelt, L., Selkoe, D.J., 1995. The Swedish mutation causes early-onset Alzheimer's disease by beta-secretase cleavage within the secretory pathway. Nat. Med. 1, 1291–1296.

Hardy, J., Selkoe, D.J., 2002. The amyloid hypothesis of Alzheimer's disease: progress and problems on the road to therapeutics. Science 297, 353–356. https://doi.org/10.1126/science.1072994

Hardy, J.A., Higgins, G.A., 1992. Alzheimer's Disease: The Amyloid Cascade Hypothesis. Science 256, 184.

Hartman, R.E., Izumi, Y., Bales, K.R., Paul, S.M., Wozniak, D.F., Holtzman, D.M., 2005. Treatment with an amyloid-beta antibody ameliorates plaque load, learning deficits, and hippocampal long-term potentiation in a mouse model of Alzheimer's disease. J. Neurosci. Off. J. Soc. Neurosci. 25, 6213–6220. https://doi.org/10.1523/JNEUROSCI.0664-05.2005

Hassiotis, S., Manavis, J., Blumbergs, P.C., Hattersley, K.J., Carosi, J.M., Kamei, M., Sargeant, T.J., 2018. Lysosomal LAMP1 immunoreactivity exists in both diffuse and neuritic amyloid

plaques in the human hippocampus. Eur. J. Neurosci. 47, 1043–1053. https://doi.org/10.1111/ejn.13913

He, Z., Guo, J.L., McBride, J.D., Narasimhan, S., Kim, H., Changolkar, L., Zhang, B., Gathagan, R.J., Yue, C., Dengler, C., Stieber, A., Nitla, M., Coulter, D.A., Abel, T., Brunden, K.R., Trojanowski, J.Q., Lee, V.M.-Y., 2018. Amyloid-β plaques enhance Alzheimer's brain tau-seeded pathologies by facilitating neuritic plaque tau aggregation. Nat. Med. 24, 29–38. https://doi.org/10.1038/nm.4443

Heneka, M.T., Carson, M.J., El Khoury, J., Landreth, G.E., Brosseron, F., Feinstein, D.L., Jacobs, A.H., Wyss-Coray, T., Vitorica, J., Ransohoff, R.M., Herrup, K., Frautschy, S.A., Finsen, B., Brown, G.C., Verkhratsky, A., Yamanaka, K., Koistinaho, J., Latz, E., Halle, A., Petzold, G.C., Town, T., Morgan, D., Shinohara, M.L., Perry, V.H., Holmes, C., Bazan, N.G., Brooks, D.J., Hunot, S., Joseph, B., Deigendesch, N., Garaschuk, O., Boddeke, E., Dinarello, C.A., Breitner, J.C., Cole, G.M., Golenbock, D.T., Kummer, M.P., 2015. Neuroinflammation in Alzheimer's disease. Lancet Neurol. 14, 388–405. https://doi.org/10.1016/S1474-4422(15)70016-5

Heneka, M.T., Kummer, M.P., Latz, E., 2014. Innate immune activation in neurodegenerative disease. Nat. Rev. Immunol. 14, 463–477. https://doi.org/10.1038/nri3705

Héraud, C., Goufak, D., Ando, K., Leroy, K., Suain, V., Yilmaz, Z., De Decker, R., Authelet, M., Laporte, V., Octave, J.-N., Brion, J.-P., 2014. Increased misfolding and truncation of tau in APP/PS1/tau transgenic mice compared to mutant tau mice. Neurobiol. Dis. 62, 100–112. https://doi.org/10.1016/j.nbd.2013.09.010

Hickman, S.E., Kingery, N.D., Ohsumi, T.K., Borowsky, M.L., Wang, L., Means, T.K., El Khoury, J., 2013. The microglial sensome revealed by direct RNA sequencing. Nat. Neurosci. 16, 1896–1905. https://doi.org/10.1038/nn.3554

Hollingworth, P., Harold, D., Sims, R., Gerrish, A., Lambert, J.-C., Carrasquillo, M.M., Abraham, R., Hamshere, M.L., Pahwa, J.S., Moskvina, V., Dowzell, K., Jones, N., Stretton, A., Thomas, C., Richards, A., Ivanov, D., Widdowson, C., Chapman, J., Lovestone, S., Powell, J., Proitsi, P., Lupton, M.K., Brayne, C., Rubinsztein, D.C., Gill, M., Lawlor, B., Lynch, A., Brown, K.S., Passmore, P.A., Craig, D., McGuinness, B., Todd, S., Holmes, C., Mann, D., Smith, A.D., Beaumont, H., Warden, D., Wilcock, G., Love, S., Kehoe, P.G., Hooper, N.M., Vardy, E.R.L.C., Hardy, J., Mead, S., Fox, N.C., Rossor, M., Collinge, J., Maier, W., Jessen, F., Rüther, E., Schürmann, B., Heun, R., Kölsch, H., van den Bussche, H., Heuser, I., Kornhuber, J., Wiltfang, J., Dichgans, M., Frölich, L., Hampel, H., Gallacher, J., Hüll, M., Rujescu, D., Giegling, I., Goate, A.M., Kauwe, J.S.K., Cruchaga, C., Nowotny, P., Morris, J.C., Mayo, K., Sleegers, K., Bettens, K., Engelborghs, S., De Deyn, P.P., Van Broeckhoven, C., Livingston, G., Bass, N.J., Gurling, H., McQuillin, A., Gwilliam, R., Deloukas, P., Al-Chalabi, A., Shaw, C.E., Tsolaki, M., Singleton, A.B., Guerreiro, R., Mühleisen, T.W., Nöthen, M.M., Moebus, S., Jöckel, K.-H., Klopp, N., Wichmann, H.-E., Pankratz, V.S., Sando, S.B., Aasly, J.O., Barcikowska, M., Wszolek, Z.K., Dickson, D.W., Graff-Radford, N.R., Petersen, R.C., Alzheimer's Disease Neuroimaging Initiative, van Duijn, C.M., Breteler, M.M.B., Ikram, M.A., DeStefano, A.L., Fitzpatrick, A.L., Lopez, O., Launer, L.J., Seshadri, S., CHARGE consortium, Berr, C., Campion, D., Epelbaum, J., Dartigues, J.-F., Tzourio, C., Alpérovitch, A., Lathrop, M., EADI1 consortium, Feulner, T.M., Friedrich, P., Riehle, C., Krawczak, M., Schreiber, S., Mayhaus, M., Nicolhaus, S., Wagenpfeil, S., Steinberg, S., Stefansson, H., Stefansson, K., Snaedal, J., Björnsson, S., Jonsson, P.V., Chouraki, V., Genier-Boley, B., Hiltunen, M., Soininen, H., Combarros, O., Zelenika, D., Delepine, M., Bullido, M.J., Pasquier, F., Mateo, I., Frank-Garcia, A., Porcellini, E., Hanon, O., Coto, E., Alvarez, V., Bosco, P., Siciliano, G., Mancuso, M., Panza, F., Solfrizzi, V., Nacmias, B., Sorbi, S., Bossù, P., Piccardi, P., Arosio, B., Annoni, G., Seripa, D., Pilotto, A., Scarpini, E., Galimberti, D., Brice, A., Hannequin, D., Licastro, F., Jones, L., Holmans, P.A., Jonsson, T., Riemenschneider, M., Morgan, K., Younkin, S.G., Owen, M.J., O'Donovan, M., Amouyel, P., Williams, J., 2011. Common variants at ABCA7, MS4A6A/MS4A4E, EPHA1, CD33 and CD2AP are associated with Alzheimer's disease. Nat. Genet. 43, 429–435. https://doi.org/10.1038/ng.803

Holmes, C., Boche, D., Wilkinson, D., Yadegarfar, G., Hopkins, V., Bayer, A., Jones, R.W., Bullock, R., Love, S., Neal, J.W., Zotova, E., Nicoll, J.A.R., 2008. Long-term effects of Abeta42 immunisation in Alzheimer's disease: follow-up of a randomised, placebo-controlled

phase I trial. Lancet Lond. Engl. 372, 216–223. https://doi.org/10.1016/S0140-6736(08)61075-2

Holtman, I.R., Raj, D.D., Miller, J.A., Schaafsma, W., Yin, Z., Brouwer, N., Wes, P.D., Möller, T., Orre, M., Kamphuis, W., Hol, E.M., Boddeke, E.W.G.M., Eggen, B.J.L., 2015. Induction of a common microglia gene expression signature by aging and neurodegenerative conditions: a co-expression meta-analysis. Acta Neuropathol. Commun. 3, 31. https://doi.org/10.1186/s40478-015-0203-5

Hong, S., Beja-Glasser, V.F., Nfonoyim, B.M., Frouin, A., Li, S., Ramakrishnan, S., Merry, K.M., Shi, Q., Rosenthal, A., Barres, B.A., Lemere, C.A., Selkoe, D.J., Stevens, B., 2016. Complement and microglia mediate early synapse loss in Alzheimer mouse models. Science 352, 712–716. https://doi.org/10.1126/science.aad8373

Honig, L.S., Vellas, B., Woodward, M., Boada, M., Bullock, R., Borrie, M., Hager, K., Andreasen, N., Scarpini, E., Liu-Seifert, H., Case, M., Dean, R.A., Hake, A., Sundell, K., Poole Hoffmann, V., Carlson, C., Khanna, R., Mintun, M., DeMattos, R., Selzler, K.J., Siemers, E., 2018. Trial of Solanezumab for Mild Dementia Due to Alzheimer's Disease. N. Engl. J. Med. 378, 321–330. https://doi.org/10.1056/NEJMoa1705971

Huang, P.L., 2000. Mouse models of nitric oxide synthase deficiency. J. Am. Soc. Nephrol. JASN 11 Suppl 16, S120-123.

Huang, Y.-W.A., Zhou, B., Wernig, M., Südhof, T.C., 2017. ApoE2, ApoE3, and ApoE4 Differentially Stimulate APP Transcription and Aβ Secretion. Cell 168, 427-441.e21. https://doi.org/10.1016/j.cell.2016.12.044

Ittner, L.M., Götz, J., 2011. Amyloid-β and tau — a toxic *pas de deux* in Alzheimer's disease. Nat. Rev. Neurosci. 12, 67–72. https://doi.org/10.1038/nrn2967

Ittner, L.M., Ke, Y.D., Delerue, F., Bi, M., Gladbach, A., van Eersel, J., Wölfing, H., Chieng, B.C., Christie, M.J., Napier, I.A., Eckert, A., Staufenbiel, M., Hardeman, E., Götz, J., 2010. Dendritic function of tau mediates amyloid-beta toxicity in Alzheimer's disease mouse models. Cell 142, 387–397. https://doi.org/10.1016/j.cell.2010.06.036

Jansen, I.E., Savage, J.E., Watanabe, K., Bryois, J., Williams, D.M., Steinberg, S., Sealock, J., Karlsson, I.K., Hägg, S., Athanasiu, L., Voyle, N., Proitsi, P., Witoelar, A., Stringer, S., Aarsland, D., Almdahl, I.S., Andersen, F., Bergh, S., Bettella, F., Bjornsson, S., Brækhus, A., Bråthen, G., Leeuw, C. de, Desikan, R.S., Djurovic, S., Dumitrescu, L., Fladby, T., Hohman, T.J., Jonsson, P.V., Kiddle, S.J., Rongve, A., Saltvedt, I., Sando, S.B., Selbæk, G., Shoai, M., Skene, N.G., Snaedal, J., Stordal, E., Ulstein, I.D., Wang, Y., White, L.R., Hardy, J., Hjerling-Leffler, J., Sullivan, P.F., Flier, W.M. van der, Dobson, R., Davis, L.K., Stefansson, H., Stefansson, K., Pedersen, N.L., Ripke, S., Andreassen, O.A., Posthuma, D., 2019. Genome-wide meta-analysis identifies new loci and functional pathways influencing Alzheimer's disease risk. Nat. Genet. 51, 404. https://doi.org/10.1038/s41588-018-0311-9

Jay, T.R., Hirsch, A.M., Broihier, M.L., Miller, C.M., Neilson, L.E., Ransohoff, R.M., Lamb, B.T., Landreth, G.E., 2017. Disease Progression-Dependent Effects of TREM2 Deficiency in a Mouse Model of Alzheimer's Disease. J. Neurosci. Off. J. Soc. Neurosci. 37, 637–647. https://doi.org/10.1523/JNEUROSCI.2110-16.2016

Jay, T.R., Miller, C.M., Cheng, P.J., Graham, L.C., Bemiller, S., Broihier, M.L., Xu, G., Margevicius, D., Karlo, J.C., Sousa, G.L., Cotleur, A.C., Butovsky, O., Bekris, L., Staugaitis, S.M., Leverenz, J.B., Pimplikar, S.W., Landreth, G.E., Howell, G.R., Ransohoff, R.M., Lamb, B.T., 2015. TREM2 deficiency eliminates TREM2+ inflammatory macrophages and ameliorates pathology in Alzheimer's disease mouse models. J. Exp. Med. 212, 287–295. https://doi.org/10.1084/jem.20142322

Jicha, G.A., 2009. Is passive immunization for Alzheimer's disease 'alive and well' or 'dead and buried'? Expert Opin. Biol. Ther. 9, 481–491. https://doi.org/10.1517/14712590902828285

Jimenez, S., Baglietto-Vargas, D., Caballero, C., Moreno-Gonzalez, I., Torres, M., Sanchez-Varo, R., Ruano, D., Vizuete, M., Gutierrez, A., Vitorica, J., 2008. Inflammatory response in the hippocampus of PS1M146L/APP751SL mouse model of Alzheimer's disease: age-

dependent switch in the microglial phenotype from alternative to classic. J. Neurosci. Off. J. Soc. Neurosci. 28, 11650–11661. https://doi.org/10.1523/JNEUROSCI.3024-08.2008

Jin, M., Shepardson, N., Yang, T., Chen, G., Walsh, D., Selkoe, D.J., 2011. Soluble amyloid beta-protein dimers isolated from Alzheimer cortex directly induce Tau hyperphosphorylation and neuritic degeneration. Proc. Natl. Acad. Sci. U. S. A. 108, 5819–5824. https://doi.org/10.1073/pnas.1017033108

Jonsson, T., Atwal, J.K., Steinberg, S., Snaedal, J., Jonsson, P.V., Bjornsson, S., Stefansson, H., Sulem, P., Gudbjartsson, D., Maloney, J., Hoyte, K., Gustafson, A., Liu, Y., Lu, Y., Bhangale, T., Graham, R.R., Huttenlocher, J., Bjornsdottir, G., Andreassen, O.A., Jönsson, E.G., Palotie, A., Behrens, T.W., Magnusson, O.T., Kong, A., Thorsteinsdottir, U., Watts, R.J., Stefansson, K., 2012. A mutation in *APP* protects against Alzheimer's disease and age-related cognitive decline. Nature 488, 96–99. https://doi.org/10.1038/nature11283

Jonsson, T., Stefansson, H., Steinberg, S., Jonsdottir, I., Jonsson, P.V., Snaedal, J., Bjornsson, S., Huttenlocher, J., Levey, A.I., Lah, J.J., Rujescu, D., Hampel, H., Giegling, I., Andreassen, O.A., Engedal, K., Ulstein, I., Djurovic, S., Ibrahim-Verbaas, C., Hofman, A., Ikram, M.A., van Duijn, C.M., Thorsteinsdottir, U., Kong, A., Stefansson, K., 2013. Variant of TREM2 Associated with the Risk of Alzheimer's Disease. N. Engl. J. Med. 368, 107–116. https://doi.org/10.1056/NEJMoa1211103

Kang, J., Lemaire, H.-G., Unterbeck, A., Salbaum, J.M., Masters, C.L., Grzeschik, K.-H., Multhaup, G., Beyreuther, K., Müller-Hill, B., 1987. The precursor of Alzheimer's disease amyloid A4 protein resembles a cell-surface receptor. Nature 325, 733. https://doi.org/10.1038/325733a0

Karran, E., Mercken, M., Strooper, B.D., 2011. The amyloid cascade hypothesis for Alzheimer's disease: an appraisal for the development of therapeutics. Nat. Rev. Drug Discov. 10, 698–712. https://doi.org/10.1038/nrd3505

Keren-Shaul, H., Spinrad, A., Weiner, A., Matcovitch-Natan, O., Dvir-Szternfeld, R., Ulland, T.K., David, E., Baruch, K., Lara-Astaiso, D., Toth, B., Itzkovitz, S., Colonna, M., Schwartz, M., Amit, I., 2017. A Unique Microglia Type Associated with Restricting Development of Alzheimer's Disease. Cell 169, 1276-1290.e17. https://doi.org/10.1016/j.cell.2017.05.018

Kim, J., Basak, J.M., Holtzman, D.M., 2009. The Role of Apolipoprotein E in Alzheimer's Disease. Neuron 63, 287–303. https://doi.org/10.1016/j.neuron.2009.06.026

Kitazawa, M., Oddo, S., Yamasaki, T.R., Green, K.N., LaFerla, F.M., 2005. Lipopolysaccharide-Induced Inflammation Exacerbates Tau Pathology by a Cyclin-Dependent Kinase 5-Mediated Pathway in a Transgenic Model of Alzheimer's Disease. J. Neurosci. 25, 8843–8853. https://doi.org/10.1523/JNEUROSCI.2868-05.2005

Klein, W.L., Krafft, G.A., Finch, C.E., 2001. Targeting small Aβ oligomers: the solution to an Alzheimer's disease conundrum? Trends Neurosci. 24, 219–224. https://doi.org/10.1016/S0166-2236(00)01749-5

Koffie, R.M., Meyer-Luehmann, M., Hashimoto, T., Adams, K.W., Mielke, M.L., Garcia-Alloza, M., Micheva, K.D., Smith, S.J., Kim, M.L., Lee, V.M., Hyman, B.T., Spires-Jones, T.L., 2009. Oligomeric amyloid β associates with postsynaptic densities and correlates with excitatory synapse loss near senile plaques. Proc. Natl. Acad. Sci. 106, 4012–4017. https://doi.org/10.1073/pnas.0811698106

Köhler, G., Milstein, C., 1975. Continuous cultures of fused cells secreting antibody of predefined specificity. Nature 256, 495. https://doi.org/10.1038/256495a0

Kosik, K.S., Joachim, C.L., Selkoe, D.J., 1986. Microtubule-associated protein tau (tau) is a major antigenic component of paired helical filaments in Alzheimer disease. Proc. Natl. Acad. Sci. U. S. A. 83, 4044–4048. https://doi.org/10.1073/pnas.83.11.4044

Krabbe, G., Halle, A., Matyash, V., Rinnenthal, J.L., Eom, G.D., Bernhardt, U., Miller, K.R., Prokop, S., Kettenmann, H., Heppner, F.L., 2013. Functional impairment of microglia coincides with

Beta-amyloid deposition in mice with Alzheimer-like pathology. PloS One 8, e60921. https://doi.org/10.1371/journal.pone.0060921

Krasemann, S., Madore, C., Cialic, R., Baufeld, C., Calcagno, N., El Fatimy, R., Beckers, L., O'Loughlin, E., Xu, Y., Fanek, Z., Greco, D.J., Smith, S.T., Tweet, G., Humulock, Z., Zrzavy, T., Conde-Sanroman, P., Gacias, M., Weng, Z., Chen, H., Tjon, E., Mazaheri, F., Hartmann, K., Madi, A., Ulrich, J.D., Glatzel, M., Worthmann, A., Heeren, J., Budnik, B., Lemere, C., Ikezu, T., Heppner, F.L., Litvak, V., Holtzman, D.M., Lassmann, H., Weiner, H.L., Ochando, J., Haass, C., Butovsky, O., 2017. The TREM2-APOE Pathway Drives the Transcriptional Phenotype of Dysfunctional Microglia in Neurodegenerative Diseases. Immunity 47, 566-581.e9. https://doi.org/10.1016/j.immuni.2017.08.008

Lacor, P.N., Buniel, M.C., Chang, L., Fernandez, S.J., Gong, Y., Viola, K.L., Lambert, M.P., Velasco, P.T., Bigio, E.H., Finch, C.E., Krafft, G.A., Klein, W.L., 2004. Synaptic targeting by Alzheimer's-related amyloid beta oligomers. J. Neurosci. Off. J. Soc. Neurosci. 24, 10191–10200. https://doi.org/10.1523/JNEUROSCI.3432-04.2004

Lacor, P.N., Buniel, M.C., Furlow, P.W., Clemente, A.S., Velasco, P.T., Wood, M., Viola, K.L., Klein, W.L., 2007. Abeta oligomer-induced aberrations in synapse composition, shape, and density provide a molecular basis for loss of connectivity in Alzheimer's disease. J. Neurosci. Off. J. Soc. Neurosci. 27, 796–807. https://doi.org/10.1523/JNEUROSCI.3501-06.2007

Lasser, R., Ostrowitzki, S., Scheltens, P., Boada, M., Dubois, B., Dorflinger, E., Balas, B., Nikolcheva, T., Volz, D., Ashford, E., Edgar, C., Garibaldi, G., Fontoura, P., Santarelli, L., 2015. Efficacy and safety of gantenerumab in prodromal Alzheimer's disease: Results from scarlet road—a global, multicenter trial. Alzheimers Dement. J. Alzheimers Assoc. 11, P331–P332. https://doi.org/10.1016/j.jalz.2015.08.153

Lathuilière, A., Bohrmann, B., Kopetzki, E., Schweitzer, C., Jacobsen, H., Moniatte, M., Aebischer, P., Schneider, B.L., 2014a. Genetic engineering of cell lines using lentiviral vectors to achieve antibody secretion following encapsulated implantation. Biomaterials 35, 792–802.

Lathuilière, A., Cosson, S., Lutolf, M.P., Schneider, B.L., Aebischer, P., 2014b. A high-capacity cell macroencapsulation system supporting the long-term survival of genetically engineered allogeneic cells. Biomaterials 35, 779–791. https://doi.org/10.1016/j.biomaterials.2013.09.071

Lathuilière, A., Laversenne, V., Astolfo, A., Kopetzki, E., Jacobsen, H., Stampanoni, M., Bohrmann, B., Schneider, B.L., Aebischer, P., 2016. A subcutaneous cellular implant for passive immunization against amyloid-β reduces brain amyloid and tau pathologies. Brain 139, 1587–1604. https://doi.org/10.1093/brain/aww036

Lathuilière, A., Mach, N., Schneider, B.L., 2015. Encapsulated Cellular Implants for Recombinant Protein Delivery and Therapeutic Modulation of the Immune System. Int. J. Mol. Sci. 16, 10578–10600. https://doi.org/10.3390/ijms160510578

Laurén, J., Gimbel, D.A., Nygaard, H.B., Gilbert, J.W., Strittmatter, S.M., 2009. Cellular prion protein mediates impairment of synaptic plasticity by amyloid-β oligomers. Nature 457, 1128–1132. https://doi.org/10.1038/nature07761

Lee, E.B., Leng, L.Z., Zhang, B., Kwong, L., Trojanowski, J.Q., Abel, T., Lee, V.M.-Y., 2006. Targeting Amyloid-β Peptide (Aβ) Oligomers by Passive Immunization with a Conformation-selective Monoclonal Antibody Improves Learning and Memory in Aβ Precursor Protein (APP) Transgenic Mice. J. Biol. Chem. 281, 4292–4299. https://doi.org/10.1074/jbc.M511018200

Lehmann, M., Graser, E., Risch, K., Hancock, W.W., Müller, A., Kuttler, B., Hahn, H.J., Kupiec-Weglinski, J.W., Brock, J., Volk, H.D., 1997. Anti-CD4 monoclonal antibody-induced allograft tolerance in rats despite persistence of donor-reactive T cells. Transplantation 64, 1181–1187.

Levites, Y., Das, P., Price, R.W., Rochette, M.J., Kostura, L.A., McGowan, E.M., Murphy, M.P., Golde, T.E., 2006. Anti-Abeta42- and anti-Abeta40-specific mAbs attenuate amyloid deposition

in an Alzheimer disease mouse model. J. Clin. Invest. 116, 193–201. https://doi.org/10.1172/JCI25410

Levy-Lahad, E., Wasco, W., Poorkaj, P., Romano, D.M., Oshima, J., Pettingell, W.H., Yu, C.E., Jondro, P.D., Schmidt, S.D., Wang, K., 1995. Candidate gene for the chromosome 1 familial Alzheimer's disease locus. Science 269, 973–977.

Lewis, J., Dickson, D.W., Lin, W.-L., Chisholm, L., Corral, A., Jones, G., Yen, S.-H., Sahara, N., Skipper, L., Yager, D., Eckman, C., Hardy, J., Hutton, M., McGowan, E., 2001. Enhanced Neurofibrillary Degeneration in Transgenic Mice Expressing Mutant Tau and APP. Science 293, 1487–1491. https://doi.org/10.1126/science.1058189

Lewis, J., McGowan, E., Rockwood, J., Melrose, H., Nacharaju, P., Slegtenhorst, M.V., Gwinn-Hardy, K., Murphy, M.P., Baker, M., Yu, X., Duff, K., Hardy, J., Corral, A., Lin, W.-L., Yen, S.-H., Dickson, D.W., Davies, P., Hutton, M., 2000. Neurofibrillary tangles, amyotrophy and progressive motor disturbance in mice expressing mutant (P301L) tau protein. Nat. Genet. 25, 402. https://doi.org/10.1038/78078

Leyns, C.E.G., Gratuze, M., Narasimhan, S., Jain, N., Koscal, L.J., Jiang, H., Manis, M., Colonna, M., Lee, V.M.Y., Ulrich, J.D., Holtzman, D.M., 2019. TREM2 function impedes tau seeding in neuritic plaques. Nat. Neurosci. 1. https://doi.org/10.1038/s41593-019-0433-0

Leyns, C.E.G., Ulrich, J.D., Finn, M.B., Stewart, F.R., Koscal, L.J., Serrano, J.R., Robinson, G.O., Anderson, E., Colonna, M., Holtzman, D.M., 2017. TREM2 deficiency attenuates neuroinflammation and protects against neurodegeneration in a mouse model of tauopathy. Proc. Natl. Acad. Sci. 114, 11524–11529. https://doi.org/10.1073/pnas.1710311114

Li, S., Hong, S., Shepardson, N.E., Walsh, D.M., Shankar, G.M., Selkoe, D., 2009. Soluble Oligomers of Amyloid β Protein Facilitate Hippocampal Long-Term Depression by Disrupting Neuronal Glutamate Uptake. Neuron 62, 788–801. https://doi.org/10.1016/j.neuron.2009.05.012

Li, S., Jin, M., Koeglsperger, T., Shepardson, N.E., Shankar, G.M., Selkoe, D.J., 2011. Soluble Aβ Oligomers Inhibit Long-Term Potentiation through a Mechanism Involving Excessive Activation of Extrasynaptic NR2B-Containing NMDA Receptors. J. Neurosci. 31, 6627–6638. https://doi.org/10.1523/JNEUROSCI.0203-11.2011

Li, T., Braunstein, K.E., Zhang, J., Lau, A., Sibener, L., Deeble, C., Wong, P.C., 2016. The neuritic plaque facilitates pathological conversion of tau in an Alzheimer's disease mouse model. Nat. Commun. 7, 12082. https://doi.org/10.1038/ncomms12082

Lin, Y.-T., Seo, J., Gao, F., Feldman, H.M., Wen, H.-L., Penney, J., Cam, H.P., Gjoneska, E., Raja, W.K., Cheng, J., Rueda, R., Kritskiy, O., Abdurrob, F., Peng, Z., Milo, B., Yu, C.J., Elmsaouri, S., Dey, D., Ko, T., Yankner, B.A., Tsai, L.-H., 2018. APOE4 Causes Widespread Molecular and Cellular Alterations Associated with Alzheimer's Disease Phenotypes in Human iPSC-Derived Brain Cell Types. Neuron 98, 1141-1154.e7. https://doi.org/10.1016/j.neuron.2018.05.008

Lindwall, G., Cole, R.D., 1984. Phosphorylation affects the ability of tau protein to promote microtubule assembly. J. Biol. Chem. 259, 5301–5305.

Logovinsky, V., Satlin, A., Lai, R., Swanson, C., Kaplow, J., Osswald, G., Basun, H., Lannfelt, L., 2016. Safety and tolerability of BAN2401--a clinical study in Alzheimer's disease with a protofibril selective Aβ antibody. Alzheimers Res. Ther. 8, 14. https://doi.org/10.1186/s13195-016-0181-2

Lorenzo, A., Yankner, B.A., 1994. Beta-amyloid neurotoxicity requires fibril formation and is inhibited by congo red. Proc. Natl. Acad. Sci. 91, 12243–12247. https://doi.org/10.1073/pnas.91.25.12243

Lull, M.E., Block, M.L., 2010. Microglial activation and chronic neurodegeneration. Neurother. J. Am. Soc. Exp. Neurother. 7, 354–365. https://doi.org/10.1016/j.nurt.2010.05.014

Makin, S., 2018. The amyloid hypothesis on trial. Nature 559, S4. https://doi.org/10.1038/d41586-018-05719-4

Mamchaoui, K., Trollet, C., Bigot, A., Negroni, E., Chaouch, S., Wolff, A., Kandalla, P.K., Marie, S., Di Santo, J., St Guily, J.L., Muntoni, F., Kim, J., Philippi, S., Spuler, S., Levy, N., Blumen, S.C., Voit, T., Wright, W.E., Aamiri, A., Butler-Browne, G., Mouly, V., 2011. Immortalized pathological human myoblasts: towards a universal tool for the study of neuromuscular disorders. Skelet. Muscle 1, 34. https://doi.org/10.1186/2044-5040-1-34

Masters, C.L., Simms, G., Weinman, N.A., Multhaup, G., McDonald, B.L., Beyreuther, K., 1985. Amyloid plaque core protein in Alzheimer disease and Down syndrome. Proc. Natl. Acad. Sci. U. S. A. 82, 4245–4249. https://doi.org/10.1073/pnas.82.12.4245

Maurer, K., Volk, S., Gerbaldo, H., 1997. Auguste D and Alzheimer's disease. Lancet Lond. Engl. 349, 1546–1549. https://doi.org/10.1016/S0140-6736(96)10203-8

Mazaheri, F., Breus, O., Durdu, S., Haas, P., Wittbrodt, J., Gilmour, D., Peri, F., 2014. Distinct roles for BAI1 and TIM-4 in the engulfment of dying neurons by microglia. Nat. Commun. 5, 4046. https://doi.org/10.1038/ncomms5046

Mazaheri, F., Snaidero, N., Kleinberger, G., Madore, C., Daria, A., Werner, G., Krasemann, S., Capell, A., Trümbach, D., Wurst, W., Brunner, B., Bultmann, S., Tahirovic, S., Kerschensteiner, M., Misgeld, T., Butovsky, O., Haass, C., 2017. TREM2 deficiency impairs chemotaxis and microglial responses to neuronal injury. EMBO Rep. 18, 1186–1198. https://doi.org/10.15252/embr.201743922

McNaughton, D., Knight, W., Guerreiro, R., Ryan, N., Lowe, Jessica, Poulter, M., Nicholl, D.J., Hardy, J., Revesz, T., Lowe, James, Rossor, M., Collinge, J., Mead, S., 2012. Duplication of amyloid precursor protein (APP), but not prion protein (PRNP) gene is a significant cause of early onset dementia in a large UK series. Neurobiol. Aging 33, 426.e13-426.e21. https://doi.org/10.1016/j.neurobiolaging.2010.10.010

Mehta, D., Jackson, R., Paul, G., Shi, J., Sabbagh, M., 2017. Why do trials for Alzheimer's disease drugs keep failing? A discontinued drug perspective for 2010–2015. Expert Opin. Investig. Drugs 26, 735–739. https://doi.org/10.1080/13543784.2017.1323868

Meziane, H., Dodart, J.C., Mathis, C., Little, S., Clemens, J., Paul, S.M., Ungerer, A., 1998. Memory-enhancing effects of secreted forms of the beta-amyloid precursor protein in normal and amnestic mice. Proc. Natl. Acad. Sci. U. S. A. 95, 12683–12688. https://doi.org/10.1073/pnas.95.21.12683

Morgan, D., Gordon, M.N., Tan, J., Wilcock, D., Rojiani, A.M., 2005. Dynamic complexity of the microglial activation response in transgenic models of amyloid deposition: implications for Alzheimer therapeutics. J. Neuropathol. Exp. Neurol. 64, 743–753. https://doi.org/10.1097/01.jnen.0000178444.33972.e0

Morley, J.E., Farr, S.A., 2014. The role of amyloid-beta in the regulation of memory. Biochem. Pharmacol., Alzheimer's Disease – Amyloid, Tau and Beyond 88, 479–485. https://doi.org/10.1016/j.bcp.2013.12.018

Navarro, V., Sanchez-Mejias, E., Jimenez, S., Muñoz-Castro, C., Sanchez-Varo, R., Davila, J.C., Vizuete, M., Gutierrez, A., Vitorica, J., 2018. Microglia in Alzheimer's Disease: Activated, Dysfunctional or Degenerative. Front. Aging Neurosci. 10. https://doi.org/10.3389/fnagi.2018.00140

Negroni, E., Riederer, I., Chaouch, S., Belicchi, M., Razini, P., Di Santo, J., Torrente, Y., Butler-Browne, G.S., Mouly, V., 2009. In vivo myogenic potential of human CD133+ muscle-derived stem cells: a quantitative study. Mol. Ther. J. Am. Soc. Gene Ther. 17, 1771–1778. https://doi.org/10.1038/mt.2009.167

Nicodemus, G.D., Bryant, S.J., 2008. Cell Encapsulation in Biodegradable Hydrogels for Tissue Engineering Applications. Tissue Eng. Part B Rev. 14, 149–165. https://doi.org/10.1089/ten.teb.2007.0332

Niewoehner, J., Bohrmann, B., Collin, L., Urich, E., Sade, H., Maier, P., Rueger, P., Stracke, J.O., Lau, W., Tissot, A.C., Loetscher, H., Ghosh, A., Freskgård, P.-O., 2014. Increased brain penetration and potency of a therapeutic antibody using a monovalent molecular shuttle. Neuron 81, 49–60. https://doi.org/10.1016/j.neuron.2013.10.061

Nilsberth, C., Westlind-Danielsson, A., Eckman, C.B., Condron, M.M., Axelman, K., Forsell, C., Stenh, C., Luthman, J., Teplow, D.B., Younkin, S.G., Näslund, J., Lannfelt, L., 2001. The "Arctic" APP mutation (E693G) causes Alzheimer's disease by enhanced Aβ protofibril formation. Nat. Neurosci. 4, 887. https://doi.org/10.1038/nn0901-887

Oakley, H., Cole, S.L., Logan, S., Maus, E., Shao, P., Craft, J., Guillozet-Bongaarts, A., Ohno, M., Disterhoft, J., Van Eldik, L., Berry, R., Vassar, R., 2006. Intraneuronal beta-amyloid aggregates, neurodegeneration, and neuron loss in transgenic mice with five familial Alzheimer's disease mutations: potential factors in amyloid plaque formation. J. Neurosci. Off. J. Soc. Neurosci. 26, 10129–10140. https://doi.org/10.1523/JNEUROSCI.1202-06.2006

O'Brien, R.J., Wong, P.C., 2011. Amyloid Precursor Protein Processing and Alzheimer's Disease. Annu. Rev. Neurosci. 34, 185–204. https://doi.org/10.1146/annurev-neuro-061010-113613

Oddo, S., Billings, L., Kesslak, J.P., Cribbs, D.H., LaFerla, F.M., 2004. Abeta immunotherapy leads to clearance of early, but not late, hyperphosphorylated tau aggregates via the proteasome. Neuron 43, 321–332. https://doi.org/10.1016/j.neuron.2004.07.003

Oddo, S., Caccamo, A., Shepherd, J.D., Murphy, M.P., Golde, T.E., Kayed, R., Metherate, R., Mattson, M.P., Akbari, Y., LaFerla, F.M., 2003. Triple-Transgenic Model of Alzheimer's Disease with Plaques and Tangles: Intracellular Aβ and Synaptic Dysfunction. Neuron 39, 409–421. https://doi.org/10.1016/S0896-6273(03)00434-3

Oh, E.S., Savonenko, A.V., King, J.F., Fangmark Tucker, S.M., Rudow, G.L., Xu, G., Borchelt, D.R., Troncoso, J.C., 2009. Amyloid precursor protein increases cortical neuron size in transgenic mice. Neurobiol. Aging 30, 1238–1244. https://doi.org/10.1016/j.neurobiolaging.2007.12.024

Onorato, M., Mulvihill, P., Connolly, J., Galloway, P., Whitehouse, P., Perry, G., 1989. Alteration of neuritic cytoarchitecture in Alzheimer disease. Prog. Clin. Biol. Res. 317, 781–789.

Orive, G., Santos, E., Poncelet, D., Hernández, R.M., Pedraz, J.L., Wahlberg, L.U., Vos, P.D., Emerich, D., 2015. Cell encapsulation: technical and clinical advances. Trends Pharmacol. Sci. 36, 537–546. https://doi.org/10.1016/j.tips.2015.05.003

Ostrowitzki, S., Deptula, D., Thurfjell, L., Barkhof, F., Bohrmann, B., Brooks, D.J., Klunk, W.E., Ashford, E., Yoo, K., Xu, Z.-X., Loetscher, H., Santarelli, L., 2012. Mechanism of amyloid removal in patients with Alzheimer disease treated with gantenerumab. Arch. Neurol. 69, 198–207. https://doi.org/10.1001/archneurol.2011.1538

Ostrowitzki, S., Lasser, R.A., Dorflinger, E., Scheltens, P., Barkhof, F., Nikolcheva, T., Ashford, E., Retout, S., Hofmann, C., Delmar, P., Klein, G., Andjelkovic, M., Dubois, B., Boada, M., Blennow, K., Santarelli, L., Fontoura, P., SCarlet RoAD Investigators, 2017. A phase III randomized trial of gantenerumab in prodromal Alzheimer's disease. Alzheimers Res. Ther. 9, 95. https://doi.org/10.1186/s13195-017-0318-y

Panza, F., Lozupone, M., Logroscino, G., Imbimbo, B.P., 2019. A critical appraisal of amyloid-β-targeting therapies for Alzheimer disease. Nat. Rev. Neurol. 15, 73–88. https://doi.org/10.1038/s41582-018-0116-6

Parkhurst, C.N., Yang, G., Ninan, I., Savas, J.N., Yates, J.R., Lafaille, J.J., Hempstead, B.L., Littman, D.R., Gan, W.-B., 2013. Microglia promote learning-dependent synapse formation through brain-derived neurotrophic factor. Cell 155, 1596–1609. https://doi.org/10.1016/j.cell.2013.11.030

Pérez, M., Ribe, E., Rubio, A., Lim, F., Morán, M.A., Ramos, P.G., Ferrer, I., Isla, M.T.G., Avila, J., 2005. Characterization of a double (amyloid precursor protein-tau) transgenic: Tau phosphorylation and aggregation. Neuroscience 130, 339–347. https://doi.org/10.1016/j.neuroscience.2004.09.029

Perry, V.H., Teeling, J., 2013. Microglia and macrophages of the central nervous system: the contribution of microglia priming and systemic inflammation to chronic

neurodegeneration. Semin. Immunopathol. 35, 601–612. https://doi.org/10.1007/s00281-013-0382-8

Pike, C.J., Walencewicz, A.J., Glabe, C.G., Cotman, C.W., 1991. Aggregation-related toxicity of synthetic β-amyloid protein in hippocampal cultures. Eur. J. Pharmacol. Mol. Pharmacol. 207, 367–368. https://doi.org/10.1016/0922-4106(91)90014-9

Pinzer, B.R., Cacquevel, M., Modregger, P., McDonald, S.A., Bensadoun, J.C., Thuering, T., Aebischer, P., Stampanoni, M., 2012. Imaging brain amyloid deposition using grating-based differential phase contrast tomography. NeuroImage 61, 1336–1346. https://doi.org/10.1016/j.neuroimage.2012.03.029

Pooler, A.M., Polydoro, M., Maury, E.A., Nicholls, S.B., Reddy, S.M., Wegmann, S., William, C., Saqran, L., Cagsal-Getkin, O., Pitstick, R., Beier, D.R., Carlson, G.A., Spires-Jones, T.L., Hyman, B.T., 2015. Amyloid accelerates tau propagation and toxicity in a model of early Alzheimer's disease. Acta Neuropathol. Commun. 3. https://doi.org/10.1186/s40478-015-0199-x

Puzzo, D., Arancio, O., 2013. Amyloid-β Peptide: Dr. Jekyll or Mr. Hyde? J. Alzheimers Dis. JAD 33, S111–S120. https://doi.org/10.3233/JAD-2012-129033

Radde, R., Bolmont, T., Kaeser, S.A., Coomaraswamy, J., Lindau, D., Stoltze, L., Calhoun, M.E., Jäggi, F., Wolburg, H., Gengler, S., Haass, C., Ghetti, B., Czech, C., Hölscher, C., Mathews, P.M., Jucker, M., 2006. Abeta42-driven cerebral amyloidosis in transgenic mice reveals early and robust pathology. EMBO Rep. 7, 940–946. https://doi.org/10.1038/sj.embor.7400784

Rapoport, M., Dawson, H.N., Binder, L.I., Vitek, M.P., Ferreira, A., 2002. Tau is essential to β-amyloid-induced neurotoxicity. Proc. Natl. Acad. Sci. 99, 6364–6369. https://doi.org/10.1073/pnas.092136199

Rauchenberger, R., Borges, E., Thomassen-Wolf, E., Rom, E., Adar, R., Yaniv, Y., Malka, M., Chumakov, I., Kotzer, S., Resnitzky, D., Knappik, A., Reiffert, S., Prassler, J., Jury, K., Waldherr, D., Bauer, S., Kretzschmar, T., Yayon, A., Rothe, C., 2003. Human combinatorial Fab library yielding specific and functional antibodies against the human fibroblast growth factor receptor 3. J. Biol. Chem. 278, 38194–38205. https://doi.org/10.1074/jbc.M303164200

Rhein, V., Song, X., Wiesner, A., Ittner, L.M., Baysang, G., Meier, F., Ozmen, L., Bluethmann, H., Dröse, S., Brandt, U., Savaskan, E., Czech, C., Götz, J., Eckert, A., 2009. Amyloid-beta and tau synergistically impair the oxidative phosphorylation system in triple transgenic Alzheimer's disease mice. Proc. Natl. Acad. Sci. U. S. A. 106, 20057–20062. https://doi.org/10.1073/pnas.0905529106

Rijn, R.S. van, Simonetti, E.R., Hagenbeek, A., Hogenes, M.C.H., Weger, R.A. de, Dijk, M.R.C., Weijer, K., Spits, H., Storm, G., Bloois, L. van, Rijkers, G., Martens, A.C.M., Ebeling, S.B., 2003. A new xenograft model for graft-versus-host disease by intravenous transfer of human peripheral blood mononuclear cells in RAG2-/- γc-/- double-mutant mice. Blood 102, 2522–2531. https://doi.org/10.1182/blood-2002-10-3241

Robinson, S.R., Bishop, G.M., 2002. Aβ as a bioflocculant: implications for the amyloid hypothesis of Alzheimer's disease. Neurobiol. Aging 23, 1051–1072. https://doi.org/10.1016/S0197-4580(01)00342-6

Roch, J.M., Masliah, E., Roch-Levecq, A.C., Sundsmo, M.P., Otero, D.A., Veinbergs, I., Saitoh, T., 1994. Increase of synaptic density and memory retention by a peptide representing the trophic domain of the amyloid beta/A4 protein precursor. Proc. Natl. Acad. Sci. U. S. A. 91, 7450–7454. https://doi.org/10.1073/pnas.91.16.7450

Rodriguez-Callejas, J.D., Fuchs, E., Perez-Cruz, C., 2016. Evidence of Tau Hyperphosphorylation and Dystrophic Microglia in the Common Marmoset. Front. Aging Neurosci. 8. https://doi.org/10.3389/fnagi.2016.00315

Rosenmann, H., 2013. Immunotherapy for targeting tau pathology in Alzheimer's disease and tauopathies. Curr. Alzheimer Res. 10, 217–228.

Sadleir, K.R., Kandalepas, P.C., Buggia-Prévot, V., Nicholson, D.A., Thinakaran, G., Vassar, R., 2016. Presynaptic dystrophic neurites surrounding amyloid plaques are sites of microtubule disruption, BACE1 elevation, and increased Aβ generation in Alzheimer's disease. Acta Neuropathol. (Berl.) 132, 235–256. https://doi.org/10.1007/s00401-016-1558-9

Saito, T., Matsuba, Y., Mihira, N., Takano, J., Nilsson, P., Itohara, S., Iwata, N., Saido, T.C., 2014. Single App knock-in mouse models of Alzheimer's disease. Nat. Neurosci. 17, 661–663. https://doi.org/10.1038/nn.3697

Salloway, S., Honigberg, L.A., Cho, W., Ward, M., Friesenhahn, M., Brunstein, F., Quartino, A., Clayton, D., Mortensen, D., Bittner, T., Ho, C., Rabe, C., Schauer, S.P., Wildsmith, K.R., Fuji, R.N., Suliman, S., Reiman, E.M., Chen, K., Paul, R., 2018. Amyloid positron emission tomography and cerebrospinal fluid results from a crenezumab anti-amyloid-beta antibody double-blind, placebo-controlled, randomized phase II study in mild-to-moderate Alzheimer's disease (BLAZE). Alzheimers Res. Ther. 10. https://doi.org/10.1186/s13195-018-0424-5

Salloway, S., Sperling, R., Fox, N.C., Blennow, K., Klunk, W., Raskind, M., Sabbagh, M., Honig, L.S., Porsteinsson, A.P., Ferris, S., Reichert, M., Ketter, N., Nejadnik, B., Guenzler, V., Miloslavsky, M., Wang, D., Lu, Y., Lull, J., Tudor, I.C., Liu, E., Grundman, M., Yuen, E., Black, R., Brashear, H.R., 2014. Two Phase 3 Trials of Bapineuzumab in Mild-to-Moderate Alzheimer's Disease. N. Engl. J. Med. 370, 322–333. https://doi.org/10.1056/NEJMoa1304839

Salter, M.W., Kalia, L.V., 2004. Src kinases: a hub for NMDA receptor regulation. Nat. Rev. Neurosci. 5, 317–328. https://doi.org/10.1038/nrn1368

Sarlus, H., Heneka, M.T., 2017. Microglia in Alzheimer's disease. J. Clin. Invest. 127, 3240–3249. https://doi.org/10.1172/JCI90606

Saul, A., Sprenger, F., Bayer, T.A., Wirths, O., 2013. Accelerated tau pathology with synaptic and neuronal loss in a novel triple transgenic mouse model of Alzheimer's disease. Neurobiol. Aging 34, 2564–2573. https://doi.org/10.1016/j.neurobiolaging.2013.05.003

Schafer, D.P., Lehrman, E.K., Kautzman, A.G., Koyama, R., Mardinly, A.R., Yamasaki, R., Ransohoff, R.M., Greenberg, M.E., Barres, B.A., Stevens, B., 2012. Microglia Sculpt Postnatal Neural Circuits in an Activity and Complement-Dependent Manner. Neuron 74, 691–705. https://doi.org/10.1016/j.neuron.2012.03.026

Schenk, D., Barbour, R., Dunn, W., Gordon, G., Grajeda, H., Guido, T., Hu, K., Huang, J., Johnson-Wood, K., Khan, K., Kholodenko, D., Lee, M., Liao, Z., Lieberburg, I., Motter, R., Mutter, L., Soriano, F., Shopp, G., Vasquez, N., Vandevert, C., Walker, S., Wogulis, M., Yednock, T., Games, D., Seubert, P., 1999. Immunization with amyloid-β attenuates Alzheimer-disease-like pathology in the PDAPP mouse. Nature 400, 173. https://doi.org/10.1038/22124

Scheuner, D., Eckman, C., Jensen, M., Song, X., Citron, M., Suzuki, N., Bird, T.D., Hardy, J., Hutton, M., Kukull, W., Larson, E., Levy-Lahad, E., Viitanen, M., Peskind, E., Poorkaj, P., Schellenberg, G., Tanzi, R., Wasco, W., Lannfelt, L., Selkoe, D., Younkin, S., 1996. Secreted amyloid beta-protein similar to that in the senile plaques of Alzheimer's disease is increased in vivo by the presenilin 1 and 2 and APP mutations linked to familial Alzheimer's disease. Nat. Med. 2, 864–870.

Schneider, L.S., Sano, M., 2009. Current Alzheimer's disease clinical trials: Methods and placebo outcomes. Alzheimers Dement. J. Alzheimers Assoc. 5, 388–397. https://doi.org/10.1016/j.jalz.2009.07.038

Selkoe, D.J., 1991. The molecular pathology of Alzheimer's disease. Neuron 6, 487–498. https://doi.org/10.1016/0896-6273(91)90052-2

Serrano-Pozo, A., William, C.M., Ferrer, I., Uro-Coste, E., Delisle, M.-B., Maurage, C.-A., Hock, C., Nitsch, R.M., Masliah, E., Growdon, J.H., Frosch, M.P., Hyman, B.T., 2010. Beneficial effect of human anti-amyloid-beta active immunization on neurite morphology and tau pathology. Brain J. Neurol. 133, 1312–1327. https://doi.org/10.1093/brain/awq056

Sevigny, J., Chiao, P., Bussière, T., Weinreb, P.H., Williams, L., Maier, M., Dunstan, R., Salloway, S., Chen, T., Ling, Y., O'Gorman, J., Qian, F., Arastu, M., Li, M., Chollate, S., Brennan, M.S., Quintero-Monzon, O., Scannevin, R.H., Arnold, H.M., Engber, T., Rhodes, K., Ferrero, J., Hang, Y., Mikulskis, A., Grimm, J., Hock, C., Nitsch, R.M., Sandrock, A., 2016. The antibody aducanumab reduces Aβ plaques in Alzheimer's disease. Nature 537, 50–56. https://doi.org/10.1038/nature19323

Shankar, G.M., Bloodgood, B.L., Townsend, M., Walsh, D.M., Selkoe, D.J., Sabatini, B.L., 2007. Natural Oligomers of the Alzheimer Amyloid-β Protein Induce Reversible Synapse Loss by Modulating an NMDA-Type Glutamate Receptor-Dependent Signaling Pathway. J. Neurosci. 27, 2866–2875. https://doi.org/10.1523/JNEUROSCI.4970-06.2007

Shankar, G.M., Li, S., Mehta, T.H., Garcia-Munoz, A., Shepardson, N.E., Smith, I., Brett, F.M., Farrell, M.A., Rowan, M.J., Lemere, C.A., Regan, C.M., Walsh, D.M., Sabatini, B.L., Selkoe, D.J., 2008. Amyloid-β protein dimers isolated directly from Alzheimer's brains impair synaptic plasticity and memory. Nat. Med. 14, 837–842. https://doi.org/10.1038/nm1782

Sherrington, R., Froelich, S., Sorbi, S., Campion, D., Chi, H., Rogaeva, E.A., Levesque, G., Rogaev, E.I., Lin, C., Liang, Y., Ikeda, M., Mar, L., Brice, A., Agid, Y., Percy, M.E., Clerget-Darpoux, F., Piacentini, S., Marcon, G., Nacmias, B., Amaducci, L., Frebourg, T., Lannfelt, L., Rommens, J.M., St George-Hyslop, P.H., 1996. Alzheimer's Disease Associated with Mutations in Presenilin 2 is Rare and Variably Penetrant. Hum. Mol. Genet. 5, 985–988. https://doi.org/10.1093/hmg/5.7.985

Sherrington, R., Rogaev, E.I., Liang, Y., Rogaeva, E.A., Levesque, G., Ikeda, M., Chi, H., Lin, C., Li, G., Holman, K., Tsuda, T., Mar, L., Foncin, J.F., Bruni, A.C., Montesi, M.P., Sorbi, S., Rainero, I., Pinessi, L., Nee, L., Chumakov, I., Pollen, D., Brookes, A., Sanseau, P., Polinsky, R.J., Wasco, W., Da Silva, H.A., Haines, J.L., Perkicak-Vance, M.A., Tanzi, R.E., Roses, A.D., Fraser, P.E., Rommens, J.M., St George-Hyslop, P.H., 1995. Cloning of a gene bearing missense mutations in early-onset familial Alzheimer's disease. Nature 375, 754–760. https://doi.org/10.1038/375754a0

Shinkai, Y., Rathbun, G., Lam, K.P., Oltz, E.M., Stewart, V., Mendelsohn, M., Charron, J., Datta, M., Young, F., Stall, A.M., 1992. RAG-2-deficient mice lack mature lymphocytes owing to inability to initiate V(D)J rearrangement. Cell 68, 855–867.

Siemers, E.R., Friedrich, S., Dean, R.A., Gonzales, C.R., Farlow, M.R., Paul, S.M., Demattos, R.B., 2010. Safety and changes in plasma and cerebrospinal fluid amyloid beta after a single administration of an amyloid beta monoclonal antibody in subjects with Alzheimer disease. Clin. Neuropharmacol. 33, 67–73. https://doi.org/10.1097/WNF.0b013e3181cb577a

Sierra, A., Encinas, J.M., Deudero, J.J.P., Chancey, J.H., Enikolopov, G., Overstreet-Wadiche, L.S., Tsirka, S.E., Maletic-Savatic, M., 2010. Microglia shape adult hippocampal neurogenesis through apoptosis-coupled phagocytosis. Cell Stem Cell 7, 483–495. https://doi.org/10.1016/j.stem.2010.08.014

Sköldunger, A., Wimo, A., Johnell, K., 2012. Net costs of dementia in Sweden - an incidence based 10 year simulation study. Int. J. Geriatr. Psychiatry 27, 1112–1117. https://doi.org/10.1002/gps.2828

Snowdon, D.A., 2003. Healthy aging and dementia: findings from the Nun Study. Ann. Intern. Med. 139, 450–454. https://doi.org/10.7326/0003-4819-139-5_part_2-200309021-00014

Snowdon, D.A., 1997. Aging and Alzheimer's disease: lessons from the Nun Study. The Gerontologist 37, 150–156.

Snyder, E.M., Nong, Y., Almeida, C.G., Paul, S., Moran, T., Choi, E.Y., Nairn, A.C., Salter, M.W., Lombroso, P.J., Gouras, G.K., Greengard, P., 2005. Regulation of NMDA receptor trafficking by amyloid-β. Nat. Neurosci. 8, 1051. https://doi.org/10.1038/nn1503

Solomon, B., Koppel, R., Hanan, E., Katzav, T., 1996. Monoclonal antibodies inhibit in vitro fibrillar aggregation of the Alzheimer beta-amyloid peptide. Proc. Natl. Acad. Sci. U. S. A. 93, 452–455. https://doi.org/10.1073/pnas.93.1.452

Song, S., Roy, S., 2016. Progress and Challenges in Macroencapsulation Approaches for Type 1 Diabetes (T1D) Treatment: Cells, Biomaterials, and Devices. Biotechnol. Bioeng. 113, 1381–1402. https://doi.org/10.1002/bit.25895

Soscia, S.J., Kirby, J.E., Washicosky, K.J., Tucker, S.M., Ingelsson, M., Hyman, B., Burton, M.A., Goldstein, L.E., Duong, S., Tanzi, R.E., Moir, R.D., 2010. The Alzheimer's disease-associated amyloid beta-protein is an antimicrobial peptide. PloS One 5, e9505. https://doi.org/10.1371/journal.pone.0009505

Sperling, R., Salloway, S., Brooks, D.J., Tampieri, D., Barakos, J., Fox, N.C., Raskind, M., Sabbagh, M., Honig, L.S., Porsteinsson, A.P., Lieberburg, I., Arrighi, H.M., Morris, K.A., Lu, Y., Liu, E., Gregg, K.M., Brashear, H.R., Kinney, G.G., Black, R., Grundman, M., 2012. Amyloid-related imaging abnormalities in patients with Alzheimer's disease treated with bapineuzumab: a retrospective analysis. Lancet Neurol. 11, 241–249. https://doi.org/10.1016/S1474-4422(12)70015-7

Sperling, R.A., Aisen, P.S., Beckett, L.A., Bennett, D.A., Craft, S., Fagan, A.M., Iwatsubo, T., Jack, C.R., Kaye, J., Montine, T.J., Park, D.C., Reiman, E.M., Rowe, C.C., Siemers, E., Stern, Y., Yaffe, K., Carrillo, M.C., Thies, B., Morrison-Bogorad, M., Wagster, M.V., Phelps, C.H., 2011. Toward defining the preclinical stages of Alzheimer's disease: recommendations from the National Institute on Aging-Alzheimer's Association workgroups on diagnostic guidelines for Alzheimer's disease. Alzheimers Dement. J. Alzheimers Assoc. 7, 280–292. https://doi.org/10.1016/j.jalz.2011.03.003

Spires, T.L., Meyer-Luehmann, M., Stern, E.A., McLean, P.J., Skoch, J., Nguyen, P.T., Bacskai, B.J., Hyman, B.T., 2005. Dendritic Spine Abnormalities in Amyloid Precursor Protein Transgenic Mice Demonstrated by Gene Transfer and Intravital Multiphoton Microscopy. J. Neurosci. 25, 7278–7287. https://doi.org/10.1523/JNEUROSCI.1879-05.2005

Stelzmann, R.A., Schnitzlein, H.N., Murtagh, F.R., 1995. An english translation of alzheimer's 1907 paper, "über eine eigenartige erkankung der hirnrinde." Clin. Anat. 8, 429–431. https://doi.org/10.1002/ca.980080612

Streit, W.J., Braak, H., Xue, Q.-S., Bechmann, I., 2009. Dystrophic (senescent) rather than activated microglial cells are associated with tau pathology and likely precede neurodegeneration in Alzheimer's disease. Acta Neuropathol. (Berl.) 118, 475–485. https://doi.org/10.1007/s00401-009-0556-6

Streit, W.J., Sammons, N.W., Kuhns, A.J., Sparks, D.L., 2004. Dystrophic microglia in the aging human brain. Glia 45, 208–212. https://doi.org/10.1002/glia.10319

Sun, B., Banugaria, S.G., Prater, S.N., Patel, T.T., Fredrickson, K., Ringler, D.J., de Fougerolles, A., Rosenberg, A.S., Waldmann, H., Kishnani, P.S., 2014. Non-depleting anti-CD4 monoclonal antibody induces immune tolerance to ERT in a murine model of Pompe disease. Mol. Genet. Metab. Rep. 1, 446–450. https://doi.org/10.1016/j.ymgmr.2014.08.005

Tagarelli, A., Piro, A., Tagarelli, G., Lagonia, P., Quattrone, A., 2006. Alois Alzheimer: A Hundred Years after the Discovery of the Eponymous Disorder. Int. J. Biomed. Sci. IJBS 2, 196–204.

Tanzi, R.E., 2012. The Genetics of Alzheimer Disease. Cold Spring Harb. Perspect. Med. 2. https://doi.org/10.1101/cshperspect.a006296

Tariot, P.N., Lopera, F., Langbaum, J.B., Thomas, R.G., Hendrix, S., Schneider, L.S., Rios-Romenets, S., Giraldo, M., Acosta, N., Tobon, C., Ramos, C., Espinosa, A., Cho, W., Ward, M., Clayton, D., Friesenhahn, M., Mackey, H., Honigberg, L., Sanabria Bohorquez, S., Chen, K., Walsh, T., Langlois, C., Reiman, E.M., 2018. The Alzheimer's Prevention Initiative Autosomal-Dominant Alzheimer's Disease Trial: A study of crenezumab versus placebo in preclinical PSEN1 E280A mutation carriers to evaluate efficacy and safety in the treatment of autosomal-dominant Alzheimer's disease, including a placebo-treated noncarrier cohort. Alzheimers Dement. Transl. Res. Clin. Interv. 4, 150–160. https://doi.org/10.1016/j.trci.2018.02.002

Tharp, W.G., Sarkar, I.N., 2013. Origins of amyloid-β. BMC Genomics 14, 290. https://doi.org/10.1186/1471-2164-14-290

Towers, G.J., Stockholm, D., Labrousse-Najburg, V., Carlier, F., Danos, O., Pagès, J.C., 1999. One step screening of retroviral producer clones by real time quantitative PCR. J. Gene Med. 1, 352–359. https://doi.org/10.1002/(SICI)1521-2254(199909/10)1:5<352::AID-JGM57>3.0.CO;2-I

Uchihara, T., Duyckaerts, C., He, Y., Kobayashi, K., Seilhean, D., Amouyel, P., Hauw, J.J., 1995. ApoE immunoreactivity and microglial cells in Alzheimer's disease brain. Neurosci. Lett. 195, 5–8.

Ulland, T.K., Song, W.M., Huang, S.C.-C., Ulrich, J.D., Sergushichev, A., Beatty, W.L., Loboda, A.A., Zhou, Y., Cairns, N.J., Kambal, A., Loginicheva, E., Gilfillan, S., Cella, M., Virgin, H.W., Unanue, E.R., Wang, Y., Artyomov, M.N., Holtzman, D.M., Colonna, M., 2017. TREM2 Maintains Microglial Metabolic Fitness in Alzheimer's Disease. Cell 170, 649-663.e13. https://doi.org/10.1016/j.cell.2017.07.023

Ulrich, J.D., Ulland, T.K., Mahan, T.E., Nyström, S., Nilsson, K.P., Song, W.M., Zhou, Y., Reinartz, M., Choi, S., Jiang, H., Stewart, F.R., Anderson, E., Wang, Y., Colonna, M., Holtzman, D.M., 2018. ApoE facilitates the microglial response to amyloid plaque pathology. J. Exp. Med. 215, 1047–1058. https://doi.org/10.1084/jem.20171265

Ultsch, M., Li, B., Maurer, T., Mathieu, M., Adolfsson, O., Muhs, A., Pfeifer, A., Pihlgren, M., Bainbridge, T.W., Reichelt, M., Ernst, J.A., Eigenbrot, C., Fuh, G., Atwal, J.K., Watts, R.J., Wang, W., 2016. Structure of Crenezumab Complex with Aβ Shows Loss of β-Hairpin. Sci. Rep. 6, 39374. https://doi.org/10.1038/srep39374

Uludag, H., De Vos, P., Tresco, P.A., 2000. Technology of mammalian cell encapsulation. Adv. Drug Deliv. Rev., Cells as Drug Delivery Platforms 42, 29–64. https://doi.org/10.1016/S0169-409X(00)00053-3

Van Cauwenberghe, C., Van Broeckhoven, C., Sleegers, K., 2016. The genetic landscape of Alzheimer disease: clinical implications and perspectives. Genet. Med. 18, 421–430. https://doi.org/10.1038/gim.2015.117

Vandenberghe, R., Riviere, M.-E., Caputo, A., Sovago, J., Maguire, R.P., Farlow, M., Marotta, G., Sanchez-Valle, R., Scheltens, P., Ryan, J.M., Graf, A., 2016. Active Aβ immunotherapy CAD106 in Alzheimer's disease: A phase 2b study. Alzheimers Dement. Transl. Res. Clin. Interv. 3, 10–22. https://doi.org/10.1016/j.trci.2016.12.003

Venegas, C., Kumar, S., Franklin, B.S., Dierkes, T., Brinkschulte, R., Tejera, D., Vieira-Saecker, A., Schwartz, S., Santarelli, F., Kummer, M.P., Griep, A., Gelpi, E., Beilharz, M., Riedel, D., Golenbock, D.T., Geyer, M., Walter, J., Latz, E., Heneka, M.T., 2017. Microglia-derived ASC specks cross-seed amyloid-β in Alzheimer's disease. Nature 552, 355–361. https://doi.org/10.1038/nature25158

Wang, H.Y., Lee, D.H., D'Andrea, M.R., Peterson, P.A., Shank, R.P., Reitz, A.B., 2000. beta-Amyloid(1-42) binds to alpha7 nicotinic acetylcholine receptor with high affinity. Implications for Alzheimer's disease pathology. J. Biol. Chem. 275, 5626–5632. https://doi.org/10.1074/jbc.275.8.5626

Wang, Y., Ulland, T.K., Ulrich, J.D., Song, W., Tzaferis, J.A., Hole, J.T., Yuan, P., Mahan, T.E., Shi, Y., Gilfillan, S., Cella, M., Grutzendler, J., DeMattos, R.B., Cirrito, J.R., Holtzman, D.M., Colonna, M., 2016. TREM2-mediated early microglial response limits diffusion and toxicity of amyloid plaques. J. Exp. Med. 213, 667–675. https://doi.org/10.1084/jem.20151948

Waring, S.C., Rosenberg, R.N., 2008. Genome-Wide Association Studies in Alzheimer Disease. Arch. Neurol. 65, 329–334. https://doi.org/10.1001/archneur.65.3.329

Weingarten, M.D., Lockwood, A.H., Hwo, S.Y., Kirschner, M.W., 1975. A protein factor essential for microtubule assembly. Proc. Natl. Acad. Sci. U. S. A. 72, 1858–1862.

Weitkamp, T., Diaz, A., David, C., Pfeiffer, F., Stampanoni, M., Cloetens, P., Ziegler, E., 2005. X-ray phase imaging with a grating interferometer. Opt. Express 13, 6296–6304.

Wilcock, D.M., DiCarlo, G., Henderson, D., Jackson, J., Clarke, K., Ugen, K.E., Gordon, M.N., Morgan, D., 2003. Intracranially administered anti-Abeta antibodies reduce beta-amyloid

deposition by mechanisms both independent of and associated with microglial activation. J. Neurosci. Off. J. Soc. Neurosci. 23, 3745–3751.

Wilcock, D.M., Gharkholonarehe, N., Van Nostrand, W.E., Davis, J., Vitek, M.P., Colton, C.A., 2009. Amyloid reduction by amyloid-beta vaccination also reduces mouse tau pathology and protects from neuron loss in two mouse models of Alzheimer's disease. J. Neurosci. Off. J. Soc. Neurosci. 29, 7957–7965. https://doi.org/10.1523/JNEUROSCI.1339-09.2009

Wilcock, D.M., Rojiani, A., Rosenthal, A., Levkowitz, G., Subbarao, S., Alamed, J., Wilson, D., Wilson, N., Freeman, M.J., Gordon, M.N., Morgan, D., 2004a. Passive amyloid immunotherapy clears amyloid and transiently activates microglia in a transgenic mouse model of amyloid deposition. J. Neurosci. Off. J. Soc. Neurosci. 24, 6144–6151. https://doi.org/10.1523/JNEUROSCI.1090-04.2004

Wilcock, D.M., Rojiani, A., Rosenthal, A., Subbarao, S., Freeman, M.J., Gordon, M.N., Morgan, D., 2004b. Passive immunotherapy against Abeta in aged APP-transgenic mice reverses cognitive deficits and depletes parenchymal amyloid deposits in spite of increased vascular amyloid and microhemorrhage. J. Neuroinflammation 1, 24. https://doi.org/10.1186/1742-2094-1-24

Wilcock, D.M., Zhao, Q., Morgan, D., Gordon, M.N., Everhart, A., Wilson, J.G., Lee, J.E., Colton, C.A., 2011. Diverse inflammatory responses in transgenic mouse models of Alzheimer's disease and the effect of immunotherapy on these responses. ASN Neuro 3, 249–258. https://doi.org/10.1042/AN20110018

Willis, B.A., Sundell, K., Lachno, D.R., Ferguson-Sells, L.R., Case, M.G., Holdridge, K., DeMattos, R.B., Raskin, J., Siemers, E.R., Dean, R.A., 2018. Central pharmacodynamic activity of solanezumab in mild Alzheimer's disease dementia. Alzheimers Dement. Transl. Res. Clin. Interv. 4, 652–660. https://doi.org/10.1016/j.trci.2018.10.001

Winblad, B., Andreasen, N., Minthon, L., Floesser, A., Imbert, G., Dumortier, T., Maguire, R.P., Blennow, K., Lundmark, J., Staufenbiel, M., Orgogozo, J.-M., Graf, A., 2012. Safety, tolerability, and antibody response of active Aβ immunotherapy with CAD106 in patients with Alzheimer's disease: randomised, double-blind, placebo-controlled, first-in-human study. Lancet Neurol. 11, 597–604. https://doi.org/10.1016/S1474-4422(12)70140-0

Wisniewski, T., Goñi, F., 2015. Immunotherapeutic approaches for Alzheimer's disease. Neuron 85, 1162–1176. https://doi.org/10.1016/j.neuron.2014.12.064

Xiang, X., Werner, G., Bohrmann, B., Liesz, A., Mazaheri, F., Capell, A., Feederle, R., Knuesel, I., Kleinberger, G., Haass, C., 2016. TREM2 deficiency reduces the efficacy of immunotherapeutic amyloid clearance. EMBO Mol. Med. 8, 992–1004. https://doi.org/10.15252/emmm.201606370

Yaffe, D., Saxel, O., 1977. Serial passaging and differentiation of myogenic cells isolated from dystrophic mouse muscle. Nature 270, 725. https://doi.org/10.1038/270725a0

Yamada, K., Yabuki, C., Seubert, P., Schenk, D., Hori, Y., Ohtsuki, S., Terasaki, T., Hashimoto, T., Iwatsubo, T., 2009. Aβ Immunotherapy: Intracerebral Sequestration of Aβ by an Anti-Aβ Monoclonal Antibody 266 with High Affinity to Soluble Aβ. J. Neurosci. 29, 11393–11398. https://doi.org/10.1523/JNEUROSCI.2021-09.2009

Yin, Z., Raj, D., Saiepour, N., Van Dam, D., Brouwer, N., Holtman, I.R., Eggen, B.J.L., Möller, T., Tamm, J.A., Abdourahman, A., Hol, E.M., Kamphuis, W., Bayer, T.A., De Deyn, P.P., Boddeke, E., 2017. Immune hyperreactivity of Aβ plaque-associated microglia in Alzheimer's disease. Neurobiol. Aging 55, 115–122. https://doi.org/10.1016/j.neurobiolaging.2017.03.021

Yoshiyama, Y., Higuchi, M., Zhang, B., Huang, S.-M., Iwata, N., Saido, T.C., Maeda, J., Suhara, T., Trojanowski, J.Q., Lee, V.M.-Y., 2007. Synapse Loss and Microglial Activation Precede Tangles in a P301S Tauopathy Mouse Model. Neuron 53, 337–351. https://doi.org/10.1016/j.neuron.2007.01.010

Yuan, P., Condello, C., Keene, C.D., Wang, Y., Bird, T.D., Paul, S.M., Luo, W., Colonna, M., Baddeley, D., Grutzendler, J., 2016. TREM2 Haplodeficiency in Mice and Humans Impairs the Microglia Barrier Function Leading to Decreased Amyloid Compaction and Severe Axonal Dystrophy. Neuron 90, 724–739. https://doi.org/10.1016/j.neuron.2016.05.003

Zhang, K., Hopkins, J.J., Heier, J.S., Birch, D.G., Halperin, L.S., Albini, T.A., Brown, D.M., Jaffe, G.J., Tao, W., Williams, G.A., 2011. Ciliary neurotrophic factor delivered by encapsulated cell intraocular implants for treatment of geographic atrophy in age-related macular degeneration. Proc. Natl. Acad. Sci. U. S. A. 108, 6241–6245. https://doi.org/10.1073/pnas.1018987108

Zhao, Y., Wu, X., Li, X., Jiang, L.-L., Gui, X., Liu, Y., Sun, Y., Zhu, B., Piña-Crespo, J.C., Zhang, M., Zhang, N., Chen, X., Bu, G., An, Z., Huang, T.Y., Xu, H., 2018. TREM2 Is a Receptor for β-Amyloid that Mediates Microglial Function. Neuron 97, 1023-1031.e7. https://doi.org/10.1016/j.neuron.2018.01.031

Zinn, K.R., Chaudhuri, T.R., Szafran, A.A., O'Quinn, D., Weaver, C., Dugger, K., Lamar, D., Kesterson, R.A., Wang, X., Frank, S.J., 2008. Noninvasive Bioluminescence Imaging in Small Animals. ILAR J. Natl. Res. Counc. Inst. Lab. Anim. Resour. 49, 103–115.

Zufferey, R., 2002. Production of lentiviral vectors. Curr. Top. Microbiol. Immunol. 261, 107–121.

8

Chapter 8 : Annexes

LAVERSENNE Vanessa

Vanessa.laversenne@epfl.ch

+41788472178

Education

Swiss Federal Institute of Technology in Lausanne,

EPFL (2014 – currently) **Ph.D.**

Bioengineering and Biotechnology

EPFL and Harvard Medical School (2010-2013) **Master**

Bioengineering specialized in Neuroscience

EPFL (2007-2010) **Bachelor**

Engineering in Life Science

Professional Experience

2014 –2019 **Neurodegenerative Disease Laboratory (LEN) headed by Prof. Patrick Aebischer**

Projects

Development of a human cell line suitable for the clinical application of cell encapsulation.
- Collaboration with Dr. Bernd Borhmann, Leader research at Hoffmann-La Roche, pRED, Basel.
- Lentiviral vector
- Human and mammalian cells culture
- Cell encapsulation
- Tissue engineering
- *In Vivo* (mice) surgery

Engineering of a novel antibody with enhanced ability to pass the blood-brain barrier
- Protein engineering

Investigation of the effect of amyloid beta passive immunization on tau pathology
- Stereotaxic brain injection of AAV on mice
- Immunohistochemistry
- Image processing and analysis/ Microscopy

2012-2013 **Laboratory for Drug Discovery in Neurodegeneration (LDDN) Harvard NeuroDiscovery Center**

Supervision by Dr. Justin Boyd and Prof. Marcie Glicksman

Collaboration with Prof.Bradshaw and Prof. De Jager laboratories, Brigham and Women's Hospital

Project

Optimization and validation of drug screening assay based on CD33 expression in peripheral blood mononuclear cells for Alzheimer's disease
- High content imaging on patient peripheral blood mononuclear cells
- Automation for small compound drug discovery / Library screening (3000 compounds)

Publications & Conferences

2017

Macroencapsulation of human cells secreting antibodies for passive immunization against amyloid beta.

Laversenne V, Lathuilière A, Bohrmann B, Mamchaoui K, Aebischer P, Schneider BL. ADPD Vienna, 2017

Small molecule screening of human PBMCS to identify compounds that correct the functional consequences of the CD33 Alzheimer's disease risk allele. Bradshaw EM, Ryan KJ, Boyd JD, **Laversenne V**, Winn P, Frangieh M, Cimpean M, McHenry A, Yung C, Glicksman M, De Jager PL. ADPD Vienna, 2017

2016

A subcutaneous cellular implant for passive immunization against amyloid-β reduces brain amyloid and tau pathologies. Lathuilière A, **Laversenne V**, Astolfo A, Kopetzki E, Jacobsen H, Stampanoni M, Bohrmann B, Schneider BL, Aebischer P. Brain. 2016 May;139(Pt 5):1587-604.

Amyloid-β plaque deposition measured using propagation-based X-ray phase contrast CT imaging. Astolfo A, Lathuilière A, **Laversenne V**, Schneider B, Stampanoni M. J Synchrotron Radiat. 2016 May;23(Pt 3):813-9

2014

The CD33 Alzheimer's disease locus: Correcting the functional consequences of the risk allele using small molecules. Ryan KJ, Boyd JD, **Laversenne V**, Chan G, Winn P, Frangieh M, Cimpean M, McHenry A, Chibnik LB, Glicksman MA, De Jager PL, Bradshaw EM. Journal of Neuroimmunology 2014;275(Pt 1-2):52-53

Awards

Represented EPFL at the GYSS@one-north 2017 (Global Young Scientist Summit, 2017, Singapore) Selected as one of the 5 outstanding Ph.D. or Post-Doc fellow at EPFL all fields united. Requirement was to have strong academic achievements and assessed to be within the top 5-10 percent of cohort.

Winner of the top 5 posters presentation at the GYSS 2017 Selected as top 5 posters presentation. Jury was composed of the best scientist of our century (Nobel prices, field medals).

Bertarelli Fellowship 2012-2013 Fellowship of the Bertarelli program in translational neuroscience and neuroengineering. Selected as one of the most promising EPFL Student in Bioengineering to represent EPFL at the Harvard Medical School.

Winner of the Poster Award Best poster presentation at the EPFL ETHZ joint Summer School in Translational Biology 2015

Best results of the biology-chemistry section High School Graduation, 2007

Projects

Drug Discovery Process for LRRK2 GTPase Activity in Parkinson's Disease Translational Neuroscience project, EPFL, study of the modulation of LRRK2 by small compounds in Parkinson's disease, supervised by Prof. Darren Moore

Helminths and chronic inflammatory diseases. Bachelor Thesis, EPFL, review on the interaction between helminths and Autoimmune diseases, supervised by Prof. Nicola Harris

Formation

RESAL module 1: Swiss mandatory class and continue formation for animal experimentation

Teaching Toolkit I & II: EPFL Teaching Workshops

Languages

French	Mother tongue
English	Fluent (C1 European standard)
German	Beginner (A2 European standard)

doi:10.1093/brain/aww036 BRAIN 2016: 139; 1587–1604 | 1587

BRAIN
A JOURNAL OF NEUROLOGY

A subcutaneous cellular implant for passive immunization against amyloid-β reduces brain amyloid and tau pathologies

Aurélien Lathuilière,[1] Vanessa Laversenne,[1] Alberto Astolfo,[2] Erhard Kopetzki,[3] Helmut Jacobsen,[4] Marco Stampanoni,[2] Bernd Bohrmann,[4] Bernard L. Schneider[1,*] and Patrick Aebischer[1,*]

*These authors contributed equally to this work.

Passive immunization against misfolded toxic proteins is a promising approach to treat neurodegenerative disorders. For effective immunotherapy against Alzheimer's disease, recent clinical data indicate that monoclonal antibodies directed against the amyloid-β peptide should be administered before the onset of symptoms associated with irreversible brain damage. It is therefore critical to develop technologies for continuous antibody delivery applicable to disease prevention. Here, we addressed this question using a bioactive cellular implant to deliver recombinant anti-amyloid-β antibodies in the subcutaneous tissue. An encapsulating device permeable to macromolecules supports the long-term survival of myogenic cells over more than 10 months in immunocompetent allogeneic recipients. The encapsulated cells are genetically engineered to secrete high levels of anti-amyloid-β antibodies. Peripheral implantation leads to continuous antibody delivery to reach plasma levels that exceed 50 μg/ml. In a proof-of-concept study, we show that the recombinant antibodies produced by this system penetrate the brain and bind amyloid plaques in two mouse models of the Alzheimer's pathology. When encapsulated cells are implanted before the onset of amyloid plaque deposition in TauPS2APP mice, chronic exposure to anti-amyloid-β antibodies dramatically reduces amyloid-β_{40} and amyloid-β_{42} levels in the brain, decreases amyloid plaque burden, and most notably, prevents phospho-tau pathology in the hippocampus. These results support the use of encapsulated cell implants for passive immunotherapy against the misfolded proteins, which accumulate in Alzheimer's disease and other neurodegenerative disorders.

1 Neurodegenerative Studies Laboratory, Brain Mind Institute, Ecole Polytechnique Fédérale de Lausanne (EPFL), CH-1015 Lausanne, Switzerland
2 Swiss Light Source, Paul Scherrer Institute (PSI), 5232, Villigen-PSI, Switzerland
3 Pharma Research and Early Development, DTA Neuroscience, Roche Innovation Center Penzberg, F. Hoffmann-La Roche, Switzerland
4 Pharma Research and Early Development, DTA Neuroscience, Roche Innovation Center Basel, F. Hoffmann-La Roche, Switzerland

Correspondence to: Patrick Aebischer,
EPFL-SV-BMI-LEN,
Station 19,
1015 Lausanne,
Switzerland
E-mail: patrick.aebischer@epfl.ch

Correspondence may also be addressed to: Bernard Schneider, EPFL-SV-BMI-LEN, Station 19, 1015 Lausanne, Switzerland
E-mail: bernard.schneider@epfl.ch

Received November 04, 2015. Revised January 06, 2016. Accepted January 19, 2016. Advance Access publication March 8, 2016

Bernd Bohrmann,
Roche Innovation Center Basel,
Grenzacherstrasse 124,
4070 Basel,
F. Hoffmann-La Roche,
Switzerland
E-mail: bernd.bohrmann@roche.com

Keywords: Alzheimer's disease; immunization; encapsulation; cellular implant; antibody

Abbreviations: ECT = encapsulated cell technology; mAb = monoclonal antibody

Introduction

Passive immunization using monoclonal antibodies has recently emerged for the treatment of neurological diseases. In particular, monoclonal antibodies can be administered to target the misfolded proteins that progressively aggregate and propagate in the CNS and contribute to the histopathological signature of neurodegenerative diseases. Alzheimer's disease is the most prevalent proteinopathy, characterized by the deposition of amyloid plaques and neurofibrillary tangles. According to the 'amyloid cascade hypothesis', which is supported by strong genetic evidence (Goate and Hardy, 2012), the primary pathogenic event in Alzheimer's disease is the accumulation and aggregation of amyloid-β into insoluble extracellular plaques in addition to cerebral amyloid angiopathy (Hardy and Selkoe, 2002). High levels of amyloid-β may cause a cascade of deleterious events, including neurofibrillary tangle formation, neuronal dysfunction and death. Anti-amyloid-β antibodies have been developed to interfere with the amyloid-β cascade. Promising data obtained in preclinical studies have validated immunotherapy against Alzheimer's disease, prompting a series of clinical trials (Bard *et al.*, 2000; Bacskai *et al.*, 2002; Oddo *et al.*, 2004; Wilcock *et al.*, 2004*a*; Bohrmann *et al.*, 2012). Phase III trials using monoclonal antibodies directed against soluble amyloid-β (bapineuzumab and solanezumab) in patients with mild-to-moderate Alzheimer's disease showed some effects on biomarkers that are indicative of target engagement. These trials, however, missed the primary endpoints, and it is therefore believed that anti-amyloid-β immunotherapy should be administered at the early presymptomatic stage (secondary prevention) to better potentiate therapeutic effects (Doody *et al.*, 2014; Salloway *et al.*, 2014). For the treatment of Alzheimer's disease, it is likely that long-term treatment using a high dose of monoclonal antibody will be required. However, bolus administration of anti-amyloid-β antibodies may aggravate dose-dependent adverse effects such as amyloid-related imaging abnormalities (ARIA) (Sperling *et al.*, 2012). In addition, the cost of recombinant antibody production and medical burden associated with repeated subcutaneous or intravenous bolus injections may represent significant constraints, especially in the case of preventive immunotherapy initiated years before the onset of clinical symptoms in patients predisposed to develop Alzheimer's disease.

Therefore, alternative methods need to be developed for the continuous, long-term administration of antibodies. Here, we used an implant based on a high-capacity encapsulated cell technology (ECT) (Lathuiliere *et al.*, 2014*b*). The ECT device contains myogenic cells genetically engineered for antibody production. Macromolecules can be exchanged between the implanted cells and the host tissue through a permeable polymer membrane. As the membrane shields the implanted cells from immune rejection in allogeneic conditions, it is possible to use a single donor cell source for multiple recipients. We demonstrate that anti-amyloid immunotherapy using an ECT device implanted in the subcutaneous tissue can achieve therapeutic effects inside the brain. Chronic exposure to anti-amyloid-β monoclonal antibodies produced *in vivo* using the ECT technology leads to a significant reduction of the amyloid brain pathology in two mouse models of Alzheimer's disease.

Materials and methods

Macroencapsulation device

The flat sheet macroencapsulation device was specifically designed for the subcutaneous implantation of cells and was engineered as described elsewhere (Lathuiliere *et al.*, 2014*b*). To guarantee the quality and reproducibility of the device assembly, a process based on ultrasonic welding was implemented. The tight sealing of each device was controlled using an air-leak test. The assembled device was 27-mm long, 12-mm wide and 1.2-mm thick. The distance between the two permeable membranes was between 100 and 300 μm and defined the volume of the inner chamber. A loading port was integrated into the device frame to allow the injection of cells through a 1 ml pipette tip connected to the device. The devices were gas sterilized with ethylene oxide before further use.

MAb-11 monoclonal anti-amyloid-β antibody

MAb-11 is an anti-amyloid-β monoclonal antibody that carries 11 amino acid substitutions compared to gantenerumab (Bohrmann *et al.*, 2012). MAb-11 binds to amyloid-β

aggregates via a conformational epitope with binding properties that are similar to gantenerumab, as demonstrated by equilibrium dissociation constant (K_D) values of 0.14–0.67 nM, which were determined for amyloid-β_{40} and amyloid-β_{42} by surface plasmon resonance (Biacore). MAb-11 was derived from the MorphoSys HuCAL-Fab1 phage display library (Rauchenberger *et al.*, 2003). For the present study, we synthetized two cDNAs, encoding the light and heavy chains of a chimeric version of mAb-11, containing the mouse constant domains of murine IgG2a and the human variable domains of mAb-11. We also used similar chimeric constructs encoding the Fab and F(ab')$_2$ fragments derived from mAb-11 IgG2a and lacking the murine Fc effector domain.

Cell culture and genetic engineering

Cell lines were purchased from the American Type Culture Collection (ATCC) and maintained at 37 °C and 5% CO_2 in medium containing penicillin (100 U/ml) and streptomycin (100 U/ml) (Invitrogen) according to ATCC guidelines. The spontaneously immortalized C8-B4 mouse microglial cell line (ATCC number CRL-2540) (Alliot *et al.*, 1996) was cultured in Dulbecco's modified Eagle medium (DMEM) containing 10% foetal bovine serum (FBS). The C2C12 mouse myoblast cell line (ATCC number CRL-1772), which is derived from the leg skeletal muscles of an adult C3H (H2k) mouse (Yaffe and Saxel, 1977), was grown in similar conditions.

To induce the secretion of the chimeric recombinant mAb-11 IgG2a, C2C12 myoblasts were genetically engineered using a dual lentiviral vector system, as described previously (Lathuiliere *et al.*, 2014*a*). Briefly, cDNAs encoding either the mAb-11 IgG2a light chain or heavy chain were subcloned into the pRRLSIN.cPPT.PGK-GFP.WPRE lentiviral shuttle plasmid (Addgene plasmid #12252). Lentivirus particles were produced using a third-generation system using transient transfection of HEK293T cells with pCMV-dR8.2Δvpr, pMD2.G, pRSV-Rev and the shuttle plasmid (Zufferey, 2002). Viral titres (infectious particles) were determined for each vector by infecting HeLa cells and measuring the number of integrated vector genomes per cell by quantitative polymerase chain reaction (as described in Charrier *et al.*, 2005). A cell population stably expressing mAb-11 was generated by lentiviral transduction of C2C12 myoblasts at a multiplicity of infection (MOI) of 1500 for both the heavy and light chain vectors. From this pool of cells, individual clones were isolated using limiting dilution, expanded and screened according to the measured rate of mAb-11 secretion. For the present study, we used two clonal C2C12 myoblast cell lines, clones #72 and #29, which secrete 13 pg/cell/day and 29 pg/cell/day of the full mAb-11 IgG2a antibody, respectively. In addition, another C2C12 clonal cell line was engineered to produce 11.4 pg/cell/day of a recombinant mAb-11 F(ab')$_2$ fragment (clone #91L). For secretion of the full IgG2a antibody, clone #29 was used in the 5XFAD mouse study and in the second TauPS2APP mouse study. Clone #72 was used in the first TauPS2APP mouse study. For the control ECT devices, capsules were loaded with a population of C2C12 myoblasts transduced with the pRRLSIN.cPPT.PGK-GFP.WPRE lentiviral vector (Addgene plasmid #12252), as described in Lathuiliere *et al.* (2014*a*).

Microglial phagocytosis study

The measurement of antibody-mediated amyloid-β phagocytosis was performed as proposed previously (Webster *et al.*, 2001). In this study, we used either purified preparations of full mAb-11 IgG2a antibody, or a purified Fab antibody fragment. A suspension of 530 μM fluorescent fibrillar amyloid-β_{42} was prepared in 10 mM HEPES (pH 7.4) by stirring overnight at room temperature. The resulting suspension contained 30 μM fluorescein-conjugated amyloid-β_{42} and 500 μM unconjugated amyloid-β_{42} (Bachem). IgG-fibrillar amyloid-β_{42} immune complexes were obtained by preincubating fluorescent fibrillar amyloid-β_{42} at a concentration of 50 μM in phosphate-buffered saline (PBS) with various concentrations of purified mAb-11 IgG2a or Fab antibody fragment for 30 min at 37 °C. The immune complexes were washed twice by centrifugation for 5 min at 14 000*g* and resuspended in the initial volume to obtain a fluorescent fibrillar amyloid-β_{42} solution (total amyloid-β_{42} concentration: 530 μM). The day before the experiment, 8×10^4 C8-B4 cells were plated in 24-well plates. The medium was replaced with serum-free DMEM before the addition of the peptides. The cells were incubated for 30 min with fibrillar amyloid-β_{42} or IgG-fibrillar amyloid-β_{42} added to the culture medium. Next, the cells were washed twice with Hank's Balanced Salt Solution (HBSS) and subsequently detached by trypsinization, which also eliminates surface-bound fibrillar amyloid-β_{42}. The cells were fixed for 10 min in 4% paraformaldehyde and finally resuspended in PBS. The cell fluorescence was determined with a flow cytometer (Accuri C6; BD Biosciences), and the data were analysed using the FlowJo software (TreeStar Inc.). To determine the effect of the anti-amyloid-β antibodies on amyloid-β phagocytosis, the concentration of fluorescent fibrillar amyloid-β_{42} was set at 1.5 μM, which is in the linear region of the dose-response curve depicting fibrillar amyloid-β_{42} phagocytosis in C8-B4 cells (Fig. 2C). All experiments were performed in duplicate.

Transgenic mice

Two different transgenic mouse models were utilized for the present study. The two lines were backcrossed for more than seven generations with C57BL/6N mice. The triple transgenic TauPS2APP mouse line carries transgenes expressing the Swedish (K670N/M671L) mutant of human APP, the N141I mutant of PSEN2 and the P301L mutant of human tau (Grueninger *et al.*, 2010). The 5XFAD mouse line carries two transgenes expressing human APP with three familial mutations [Swedish (K670N/M671L), Florida (I716V) and London (V717I)] and PS1 with two familial mutations (M146L and L286V) (Oakley *et al.*, 2006). The experimental groups were rigorously age-matched. All experiments were performed in accordance with Swiss legislation and with the European Community Council directive (86/609/EEC) for the care and use of laboratory animals. Animals were housed in a controlled temperature room that was maintained in a 12:12 h light:dark cycle and had access to water and food *ad libitum*.

In vivo studies

The devices were loaded with 10^6 mAb-11-expressing C2C12 cells mixed with a hydrogel scaffold composed of 1.5%

polyethylene glycol (PEG) (Ehrbar *et al.*, 2007). Capsules were randomly assigned to individual mice in each group. The detailed procedure for loading and implantation has been previously described (Lathuiliere *et al.*, 2014*b*). Blood was sampled from the facial vein starting at 3 weeks after surgery and then again once every other week until the end of the experiment. The blood was collected in EDTA-coated tubes and centrifuged for 5 min at 1500*g* to separate the plasma. The concentration of mAb-11 was determined by enzyme-linked immunosorbent assay (ELISA) on the same day as collection, and the remaining plasma samples were kept frozen at −80 °C. At the end of the experiment, the animals were sacrificed with an overdose of pentobarbital. Terminal intracardiac puncture was performed to collect the blood samples. The animals were perfused with heparinized PBS. After opening the skull, the brains were carefully dissected and fresh frozen at −80 °C until further use. Implants were dissected from the subcutaneous tissue and incubated overnight in 6-well plates containing DMEM supplemented with 10% FBS. The following day, the mAb-11 secretion level was quantified by incubating the implant in 2.5 ml of fresh culture medium for 1 h. The concentrations of mAb-11 were determined in samples of culture medium by ELISA.

MAb-11 quantification

The mAb-11 concentration was quantified in mouse plasma and culture medium using an ELISA assay, as previously described (Lathuiliere *et al.*, 2014*a*). As standards, we used either purified mAb11 IgG2a or a purified recombinant mAb-11 Fab fragment. The plasma samples were diluted at least 1:100 in Low Cross Buffer (Candor) and loaded in duplicate. The colorimetric reaction was quantified at a wavelength of 405 nm on a Versamax plate reader (Molecular Devices). A standard curve was generated by a non-linear four-parameter fit, and the sample concentration was calculated using SoftMax Pro software (Molecular Devices).

Anti-drug antibody detection assay

To detect antibodies against mAb-11 IgG2a, a direct immunoassay was implemented. Briefly, 96-well microtitre plates were coated with 20 µg/ml of purified mAb-11 and blocked with 2% bovine serum albumin (BSA) in PBS. After incubation with the plasma samples, the presence of bound IgM was measured by incubation with a conjugated goat anti-mouse IgM (Jackson Immunoresearch), followed by a colorimetric reaction with ABTS solution (Roche Applied Science). In a pre-study validation experiment performed with 30 naive plasma samples, the minimal dilution was set to 1:100 and the cut point was determined by calculating the mean plus 1.645 times the standard deviation, corresponding to 5% false positive detection (Geng *et al.*, 2005). For screening, a dynamic cut point was used (Shankar *et al.*, 2008), and the positive samples were serially diluted to determine the anti-drug antibody titre.

Immunohistochemistry

The 10 µm sagittal cryosections were prepared from each mouse brain on Superfrost plus slides (Thermo Scientific). The sections were fixed in −20 °C acetone for 3 min and washed in PBS plus 0.01% Tween-20. For the detection of the mAb-11 IgG2a (plaque immunodecoration), the blocking of non-specific binding sites was performed by incubating the slides in Ultra V blocking solution (LabVision) for 5 min, followed by a wash in PBS plus 0.01% Tween-20 and a subsequent incubation in Power Block solution (BioGenex) with 10% normal sheep serum for 20 min. Cy3-conjugated goat-anti-mouse IgG2a isotype-specific antibody (Jackson Immunoresearch) was diluted to 16 µg/ml in PBS plus 1% BSA and 0.01% Tween-20 and incubated for 1 h at room temperature. For the detection of the $F(ab')_2$ fragment of mAb-11, blocking of endogenous peroxidase was performed using Phenylhydrazine 0.1% in PBS during 1 h at 37 °C. After washing with PBS, brain sections were blocked in 2% NDS, 1% BSA in 0.1% Triton™ X-100 PBS during 2 h at room temperature. Biotin-SP-conjugated goat anti-mouse IgGs recognizing the $F(ab')_2$ fragment (Jackson Immunoresearch) were diluted 1:500 in blocking solution and incubated on slices overnight at 4 °C. For labelling, Alexa Fluor® 568-labelled Tyramide Signal Amplification kit (TSA™, Life technologies) was used according to the manufacturer's instructions. For the detection of amyloid-β plaques, sections were blocked with 2% BSA and 5% normal goat serum in PBS for 1 h at room temperature. Biotinylated 6E10 anti-amyloid-β monoclonal antibody (Covance) was diluted to 1 µg/ml in blocking buffer and incubated overnight at 4 °C. After washing in PBS plus 0.001% Tween-20, an Alexa Fluor® 555 labelled TSA kit was used according to the manufacturer's instructions (Invitrogen). To demonstrate the binding of mAb-11 to amyloid-β plaques, purified mAb-11 at a concentration of 1 µg/ml was incubated overnight at 4 °C on brain sections from the TauPS2APP mice that had not been exposed to any antibody treatment. After three washing steps, the bound mAb-11 antibody was detected with Cy3-conjugated goat anti-mouse IgG2a secondary antibody (Jackson Immunoresearch). Immunodetection of phosphorylated tau with AT8 was performed using the Alexa Fluor® 568-labeled TSA Kit (Life technologies). Biotin-labelled mouse anti-human PHF-Tau monoclonal antibody (AT8, Thermo Scientific) was used at a 1:500 dilution. Immunostaining for phospho-S422 tau was performed as described in (Grueninger *et al.*, 2010). For Iba1 and MC1 immunostainings, mounted sections were fixed for 10 min in 4% paraformaldehyde, washed with PBS and incubated for 1 h at 37 °C in 0.1% phenylhydrazine, followed by blocking in 10% normal goat serum, 1% BSA and 0.3% PBS Triton™ X-100 for 2 h at room temperature. The mouse monoclonal MC1 antibody (provided by P. Davies, 1:500 dilution) and the rabbit anti-Iba1 antibody (Wako, 019-19741, 1:2000 dilution) were incubated with brain sections overnight at 4 °C and revealed with the DAB chromogen. Following Iba1 immunostaining, Congo Red histochemical staining was performed as described in Wilcock *et al.* (2006*b*).

Histological staining

The devices were fixed overnight at 4 °C in 4% paraformaldehyde, dehydrated and processed for embedding in paraffin. Three-micrometre thick sections were prepared on a microtome and stained according to Masson's trichrome protocol. To detect the possible presence of microhaemorrhages in the brain tissue, the Perl's Prussian blue protocol was used to stain the ferric ions present in haemosiderin. An observer blind to

the experimental treatment manually scored the presence of microhaemorrhages on six 25-μm thick sagittal sections chosen at regular intervals across one brain hemisphere of each animal.

Microscopy and image processing

To quantify the amyloid-β plaque load in sections stained with the 6E10 antibody, the slides were scanned using the Virtual Slide System VS120-L100 slide scanner (Olympus) with a 10× objective. For the first two *in vivo* studies, for each mouse, we analysed the presence of amyloid plaques in four sagittal sections, in the medial part of the cortex of one brain hemisphere, with an interval of 100 μm between each section. After manual segmentation of the brain regions of interest, the images were processed by automated thresholding according to Li's minimum cross entropy thresholding method, which is based on an iterative version of the algorithm in ImageJ software. For the last study, for each mouse, we analysed the presence of amyloid plaques in 18 sagittal sections, in the medial part of the cortex of one brain hemisphere, with an inter-slice interval of 60 μm. After manual segmentation of the brain regions of interest, the images were processed by automated thresholding according to Renyi entropy thresholding method.

Representative images of device histology and immunohistological staining of the brain tissue were acquired using a DM 5500 microscope (Leica). For immunodecoration in 5XFAD mouse tissue, high-resolution confocal images were acquired using a 63× NA 1.4 oil immersion objective on a LSM700 Zeiss microscope and deconvoluted with Huygens software (Scientific Volume Imaging). For Immunodecoration on TauPS2APP mice tissue, high-resolution confocal images were acquired using 40× oil immersion objective on a LSM700 Zeiss microscope.

Tau quantification was performed by counting neurons positive for phosphorylated tau (AT8 staining) located in the hippocampal CA1 region (first 600 μm, starting from the subiculum), as described in Collin *et al.* (2014), using an Olympus DP50 microscope equipped with a 10× objective. Six sections located in the medial part of the cortex, with an interslice interval of 60 μm, were counted in each animal.

Microglia quantification was performed by counting Iba1-positive cells within an area of 250 × 250 μm^2 centred on an amyloid plaque stained with Congo Red. If possible, isolated amyloid plaques smaller than 50 μm × 50 μm were preferably considered for the quantification. For control and $F(ab')_2$ treated groups, microglia were counted around two plaques per sections in six sections with an interslice interval of 60 μm. For the IgG2a treated group, considering the very low number of remaining plaques, microglia were counted around 100 plaques distributed as equally as possible among sections and animals. All the quantifications were performed by an observer blind to the experimental groups.

Amyloid-β peptide quantification

The concentration of the amyloid-β_{40} and amyloid-β_{42} peptides was measured using specific commercial ELISA assays (Invitrogen) according to the manufacturer's protocol. Briefly, frozen brain tissue from the lateral part of the cortex was homogenized in 5 M guanidine, 50 mM Tris, pH 8 (at a 1:8 ratio between the wet tissue mass and the buffer mass). Samples were diluted in PBS containing 5% BSA, 0.03% Tween-20 and a complete protease inhibitor cocktail (Roche) before being subjected to the ELISA assay.

Gratings-based X-ray phase contrast tomographic microscopy and quantification of amyloid-β plaques

Whole volume amyloid-β plaque quantifications were performed using grating-based X-ray phase contrast tomographic microscopy as described in Pinzer *et al.* (2012). In brief, the data were collected with a grating interferometer installed at the TOMCAT beamline of the Swiss Light Source with a photon energy of 25 keV (McDonald *et al.*, 2009). The phase grating (pitch of 3.98 μm) and the absorption grating (pitch of 2.00 μm) were placed and aligned at the third Talbot distance (121 mm). A total of 1440 projections were collected over a sample rotation of 180°/7 phase steps of the phase grating. The beam size was 14.6 × 4.2 mm^2 that permitted to scan three half brains at the same time with three vertical scans. The photons were converted in light using a LuAG:Ce scintillator 350-μm thick and subsequently read by a CMOS detector (PCO.Edge) with a pixel size of 6.5 μm. Differential phase contrast slices were reconstructed and filtered accordingly with Pinzer *et al.* (2012). For each sample, a manual segmentation of the brain cortex was done defining our region of interest. The amyloid-β plaques were counted over the region of interest using IDL software (http://www.exelisvis.com) excluding from the result amyloid-β plaques smaller than 10 voxels and larger than 500 voxels (which translate in an equivalent spherical plaque of 17 μm and 64 μm, respectively, in diameter) to avoid the counting of noise signal or artefacts as amyloid-β plaques. The segmentation threshold was carefully decided based on visual investigation on representative samples and kept constant over all the samples. To account for the subjective threshold decision (lower values increase the number of plaques), the counting procedure was run using five different thresholds equally distributed over the initially selected one plus/minus the standard deviation of the background noise [as performed in a similar situation in Astolfo *et al.* (2013)]. The mean (shown in Fig. 7D) and deviation standard calculated over these five total numbers of amyloid-β plaques was used to estimate the plaque density. The number of plaques was determined in individual cubic volumes of 50 × 50 × 50 pixels (50 pixels = 325 μm) and expressed as a density of amyloid-β plaques, colour-coded in Fig. 7B and C.

Statistical analysis

Results were analysed through either one-way or two-way ANOVA, using the Newman-Keuls test for *post hoc* multiple comparisons. For comparisons between two groups, two-tailed heteroscedastic Student's *t*-tests were applied. Correlations were analysed using the Pearson's test. Analyses were performed with the Statistica software (Statsoft). Data are represented as mean ± standard error of the mean (SEM) and the statistical test applied for each dataset is indicated in the

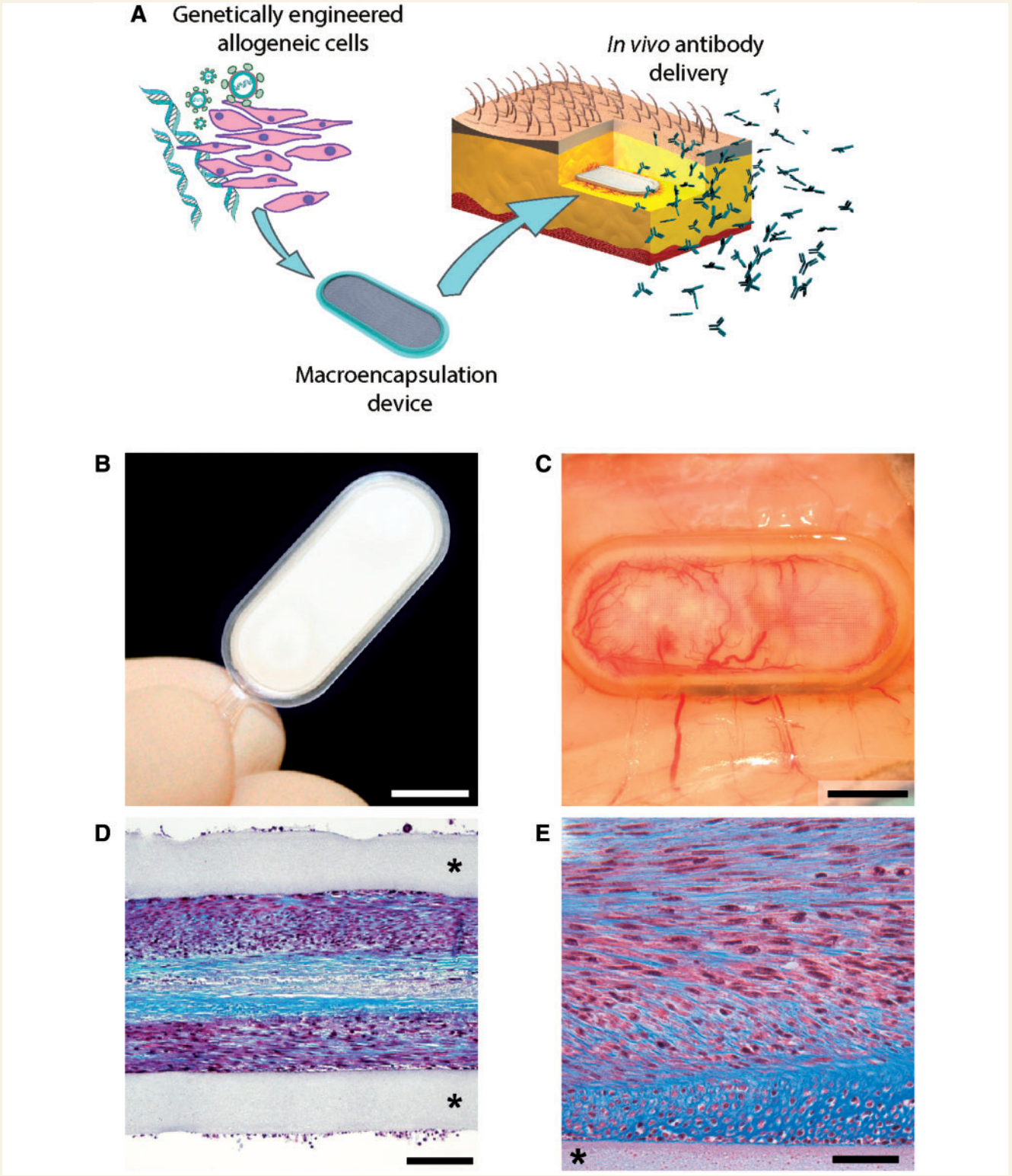

Figure 1 Cell encapsulation device for long-term subcutaneous therapeutic antibody delivery. (**A**) Schematic representation of ECT for passive immunization. Allogeneic cells are genetically engineered using lentiviral vectors to produce a therapeutic antibody. The modified cells are confined in a macroencapsulation 'flat sheet' device and implanted in the subcutaneous tissue for *in vivo* antibody secretion. (**B**) Macroscopic view of the encapsulation device, composed of a transparent frame supporting polymer permeable membranes and reinforced with an outer polyester mesh. (**C**) Dense neovascularization develops around a device containing antibody-secreting C2C12 myoblasts, 8 months after implantation in the mouse subcutaneous tissue. (**D** and **E**) Representative photomicrographs showing encapsulated antibody-secreting C2C12 myoblasts surviving at high density within the flat sheet device 39 weeks after implantation. (**E**) Higher magnification: note that the cells produce a collagen-rich matrix stained in blue with Masson's trichrome protocol. Asterisk: polypropylene porous membrane. Scale bars = 750 μm (**B** and **C**), 100 μm (**D**), 50 μm (**E**).

legend of each figure. The alpha level of significance was set at $P < 0.05$.

Results

Cell encapsulation supports the long-term survival of myoblasts secreting anti-amyloid-β monoclonal antibodies

As an alternative mode for the chronic delivery of therapeutic monoclonal antibodies, we developed a flat sheet ECT device for the subcutaneous implantation of genetically engineered myogenic cells (Fig. 1A) (Lathuiliere *et al.*, 2014*b*). For passive immunization against the amyloid pathology, we genetically modified C2C12 mouse myoblasts using a dual lentiviral vector system to produce a murinized chimeric recombinant IgG2a antibody (mAb-11) directed against both amyloid plaques and amyloid-β oligomers (Lathuiliere *et al.*, 2014*a*). We derived clonal C2C12 cell lines secreting either the full mAb-11 IgG2a antibody, or a recombinant mAb-11 $F(ab')_2$ fragment, which retains the ability to bind amyloid-β but lacks the antibody Fc portion.

The high-capacity flat sheet ECT device developed for subcutaneous implantation was based on a polypropylene frame (1 cm × 2.5 cm) supporting two polypropylene membranes with 0.45 μm pores (Fig. 1B). The device was mechanically reinforced with a polyester mesh apposed on the external face of the porous membrane, which allowed for the development of a dense neovascularization network following implantation in the subcutaneous tissue (Fig. 1C). Prior to device implantation, 10^6 C2C12 myoblasts were mixed with a degradable PEG hydrogel and injected inside the device. After a 9-month implantation in C57BL/6 mice, the C2C12 cells had expanded in the capsule inner space to form a dense cell mass interspersed with a collagen-rich extracellular matrix (Fig. 1D and E). When loaded with mAb-11-secreting myoblasts, this cellular implant was found to continuously produce recombinant anti-amyloid-β antibodies both *in vitro* and *in vivo*.

The plaque-specific mAb-11 antibody enhances fibrillar amyloid-β phagocytosis by microglial cells

We determined *in vitro* if the chimeric recombinant IgG2a mAb-11 was able to bind aggregated amyloid-β and enhance phagocytosis by mouse microglial cells, a mechanism that has been proposed to mediate the clearance of amyloid plaques (Bard *et al.*, 2000; Bohrmann *et al.*, 2012; Demattos *et al.*, 2012). Brain sections from 16-month-old TauPS2APP mice incubated with mAb-11 showed specific binding to brain amyloid deposits (Fig. 2A), consistent with the high affinity of mAb-11 for aggregated amyloid-β. Next, we incubated C8-B4 mouse microglial cells with fluorescent amyloid-β_{42} fibrils, and assessed their ability to internalize fibrillar amyloid-β_{42} by flow cytometry. The cell fluorescence increased as a function of the fibrillar amyloid-β_{42} concentration (Fig. 2B), in a linear relationship at fibrillar amyloid-β_{42} concentrations < 5 μM (Fig. 2C). Internalization of fibrillar amyloid-β_{42} at a concentration of 1.5 μM was significantly increased following preincubation with mAb-11 IgG2a (Fig. 2D). As expected, the increased uptake of fibrillar amyloid-β by microglial cells was mediated by the Fc region, as no effect was found by preincubating fibrillar amyloid-β_{42} with a mAb-11-derived Fab fragment lacking the Fc effector domain ($P = 0.00017$ compared to full IgG2a).

Passive immunization by ECT delivery of mAb-11 decreases amyloid brain pathology in 5XFAD mice

We assessed the efficacy of ECT-mediated immunotherapy in a mouse model of Alzheimer's disease with a rapidly evolving amyloid pathology. 5XFAD mice overexpress mutated forms of the human amyloid precursor protein (APP) and human presenillin 1 (PS1, encoded by *PSEN1*). The induced amyloid-β_{42} production leads to intraneuronal amyloid-β accumulation at 1.5 months and amyloid plaque deposition after only 2 months (Oakley *et al.*, 2006). To model the secondary prevention of Alzheimer's disease, age-matched cohorts of 5XFAD mice were implanted between 5 and 12 weeks of age, after the onset of plaque deposition. Flat sheet devices were loaded with C2C12 myoblasts secreting the full mAb-11 IgG2a (clone #29). Just 7 weeks after implantation, 15.2 ± 3.8 μg/ml of mAb-11 could be detected in the plasma, further increasing to 59.1 ± 6.7 μg/ml at the experimental end-point, 19 weeks post-implantation (Fig. 3A). Explanted devices secreted, on average, 105.5 ± 11.2 μg/day of mAb11 IgG2a (Fig. 3A). Based on the pharmacokinetic parameters measured by injecting recombinant mAb-11 in mice (Supplementary material), the total antibody exposure (3.96 ± 0.43 mg/ml∗day) was estimated to be equivalent to weekly intravenous injections of recombinant mAb-11 IgG2a at a dose of 16.7 ± 1.9 mg/kg for 19 weeks (Supplementary material).

We sought to determine whether the antibodies produced by ECT could be detected inside the brain. Indeed, the blood–brain barrier limits IgG penetration into the brain, with a typical plasma/brain antibody concentration ratio between 100 and 1000 (Wang *et al.*, 2008; Tabrizi *et al.*, 2010). In all mice implanted with a mAb-11 releasing ECT device, brain sections showed antibody immunodecoration localizing to amyloid-β plaques, as indicated by mouse IgG2a immunoreactivity (Fig. 3B). IgG2a

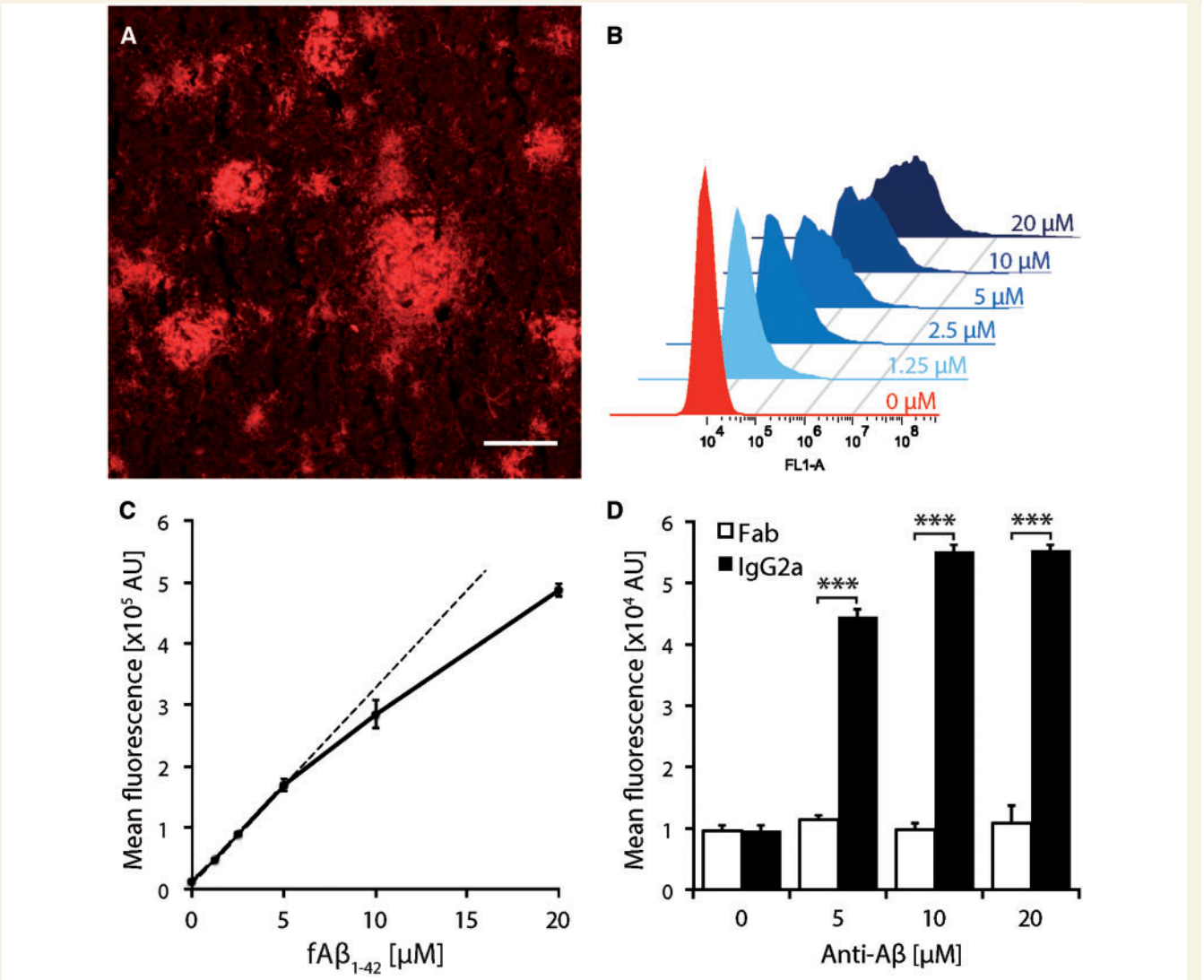

Figure 2 The plaque-specific anti-amyloid-β mAb-11 antibody enhances amyloid phagocytosis by microglial cells. (**A**) Brain section from a 16-month-old TauPS2APP mouse incubated with 1 µg/ml mAb-11 IgG2a antibody. Anti-mouse IgG staining reveals specific binding to diffuse amyloid deposits and the dense cores of amyloid plaques. Scale bar = 50 µm. (**B**) Flow cytometry analysis of C8-B4 microglial cells incubated with increasing concentrations of fluorescent fibrillar amyloid-β_{42} (fAβ_{42}). Histograms of the fluorescence intensity demonstrate the dose-dependent internalization of fibrillar amyloid-β_{42}. (**C**) The mean fluorescence intensity of C8-B4 microglial cells increases as a function of the fibrillar amyloid-β_{42} concentration. Note the linear increase in fluorescence intensity with low fibrillar amyloid-β_{42} concentrations (0–5 µM). Data are expressed as the mean ± SEM; $n = 2$ per condition. (**D**) Preincubation of fluorescent fibrillar amyloid-β_{42} (1.5 µM) with mAb-11 IgG2a enhances internalization in C8-B4 microglial cells. No effect is observed when fibrillar amyloid-β_{42} is pre-incubated with mAb-11 Fab fragments lacking the Fc region. Data are expressed as the mean + SEM; $n = 2$ per condition. Two-way ANOVA with Neuman-Keuls *post hoc* test: $***P < 0.001$; group effect $F(1,14) = 1998.7$, $P = 6.92 \times 10^{-11}$.

immunofluorescence was observed on fibrillar bundles around plaques and on the dense cores of amyloid-β aggregates (Fig. 3C).

To assess the amyloid pathology in 5XFAD mice, we performed anti-amyloid-β immunohistochemistry on brain sections. Dense and widespread amyloidosis, mainly affecting the cortex, hippocampus and thalamus, was found in 5- to 6-month-old animals implanted with devices containing GFP-expressing C2C12 myoblasts (Fig. 4A and B). Amyloid pathology was reduced in the 5XFAD mice treated with the mAb-11 secreting devices (Fig. 4C and D). Quantitative morphometry showed a significant reduction of the percentage of area covered with amyloid-β plaques in the cortex (−31.0%, $P = 0.0069$), hippocampus (−18.1%, $P = 0.018$) and thalamus (−31.7%, $P = 0.013$) (Fig. 4E). Plaque density was decreased in the same brain regions (cortex: −37.8%, $P = 0.00005$; hippocampus: −20.1%, $P = 0.002$; thalamus: −30.3%, $P = 0.007$; Fig. 4F). The median plaque area was significantly increased in the treated mice ($P = 0.012$; Fig. 4G), consistent with a clearance of small amyloid deposits revealed by the shift in the plaque size distribution (Supplementary Fig.

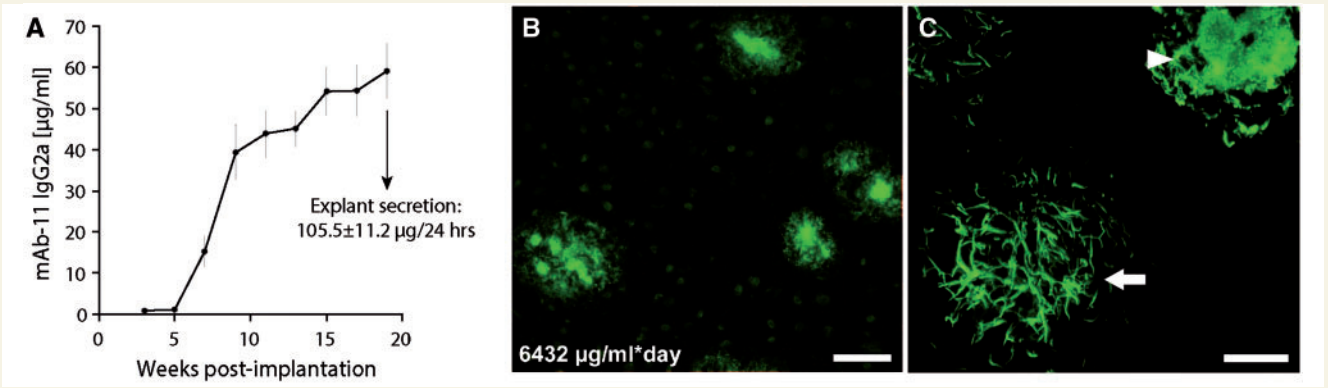

Figure 3 Anti-amyloid-β antibodies delivered by ECT in the subcutaneous tissue bind to amyloid plaques in the brain of 5XFAD mice. (**A**) Plasma levels of mAb-11 in 5XFAD mice implanted for 19 weeks with ECT devices containing mAb-11-secreting C2C12 myoblasts (clone 29, 29 pg mAb-11/cell/day). The bar graph shows the mAb-11 secretion rates of the ECT devices after explantation. Data are expressed as the mean ± SEM; $n = 16$. (**B**) Representative photomicrograph showing mAb-11 immunodecoration (green pseudocoloured IgG2a immunostaining) on amyloid-β plaques in the frontal cortex of a 27-week-old 5XFAD mouse exposed to 6432 µg/ml*day of antibody in the plasma. (**C**) High magnification confocal imaging of mAb-11 immunodecoration on amyloid-β plaques. Note that mAb-11 binds both fibrillar bundles (arrow) and plaques with a dense amyloid core (arrowhead). Scale bars = 100 µm (**B**), 10 µm (**C**).

1). In cortical homogenates, the mAb-11 treatment significantly reduced the levels of total amyloid-β_{42} ($P = 0.0027$) and amyloid-β_{40} ($P = 0.0025$) (Fig. 4H). We found a significant negative correlation between the total amyloid-β_{42} levels and the exposure to mAb-11 in the plasma, indicating that treatment efficacy primarily depends on the amount of antibody delivered (Fig. 4I). Prussian blue staining did not reveal any sign of microhaemorrhages in the mAb-11-treated mice (data not shown). Because mAb-11 IgG2a comprised complementarity-determining regions (CDR) derived from the human antibody, we tested whether the treated animals developed an anti-drug antibody response by measuring the presence of antibodies recognizing mAb-11 in the mouse plasma. Only 1 of 16 animals developed a significant anti-drug antibody response with the detectable presence of anti-mAb-11 IgM (data not shown). Overall, our results demonstrate that ECT-mediated peripheral immunotherapy can partially oppose amyloid pathology in the rapidly developing 5XFAD mouse model.

Preventive mAb-11 immunization by ECT reduces amyloid pathology in the brain of TauPS2APP mice

Immunization against amyloid-β has been shown to be most effective when initiated before the onset of plaque deposition in mouse models of Alzheimer's disease (Das *et al.*, 2001; Levites *et al.*, 2006). To further assess the effect of passive immunization, we next used TauPS2APP mice, a slowly progressing model that develops both amyloid and tau pathologies, and therefore more closely mimics sporadic Alzheimer's disease. The first experiment is described in the Supplementary material and Supplementary Fig. 2. Briefly, ECT devices secreting mAb-11 IgG2a were implanted in 7-month-old TauPS2APP mice, leading to chronic antibody exposure for 39 weeks. Similarly to the previous experiment in 5XFAD mice, ECT-mediated passive immunization led to a significant decrease in amyloid deposition. However, 7 of 15 mAb-11-treated animals had detectable levels of anti-mAb-11 IgM, indicating that this mouse model may be more prone to develop an anti-drug antibody response potentially neutralizing part of the treatment effects.

In a second experiment, ECT devices were subcutaneously implanted in 2-month-old TauPS2APP mice to deliver mAb-11 antibodies 6 months before the onset of amyloid deposition outside the hippocampus. The mice were transiently injected with anti-CD4 antibodies to block the anti-drug antibody response against mAb-11. Three groups of mice received either control GFP-expressing myoblasts, myoblasts secreting the mAb-11 IgG2a antibody (clone #29), or myoblasts producing a mAb-11-derived F(ab')$_2$ fragment. Already 3 weeks after implantation of the antibody-releasing device, both the full mAb-11 IgG2a (16.2 µg/ml, Fig. 5A) and the mAb-11 F(ab')$_2$ fragment (0.5 µg/ml, Fig. 5B) were detectable in the plasma of the respective groups of mice. Plasma levels then stabilized at ~50 µg/ml (mAb-11 IgG2a) and 2 µg/ml [mAb-11 F(ab')$_2$] until the experimental end-point, 41 weeks after implantation. Explanted devices showed secretion rates reaching on average 33.7 ± 9.7 µg/day for the mAb-11 IgG2a (~150 kDa) and 17.7 ± 2.8 µg/day for the mAb-11 F(ab')$_2$ fragment (~110 kDa). Higher secretion rate, higher stability and longer half-life of the full IgG, compared to the F(ab')$_2$ fragment, all contribute to the 25-fold difference seen in the plasma concentration. Total plasma exposure to mAb-11 IgG2a during the 41-week implantation period (14.8 mg/ml*day) was estimated to be equivalent to a regimen of weekly intravenous injections at a dose of 29.5 mg/kg.

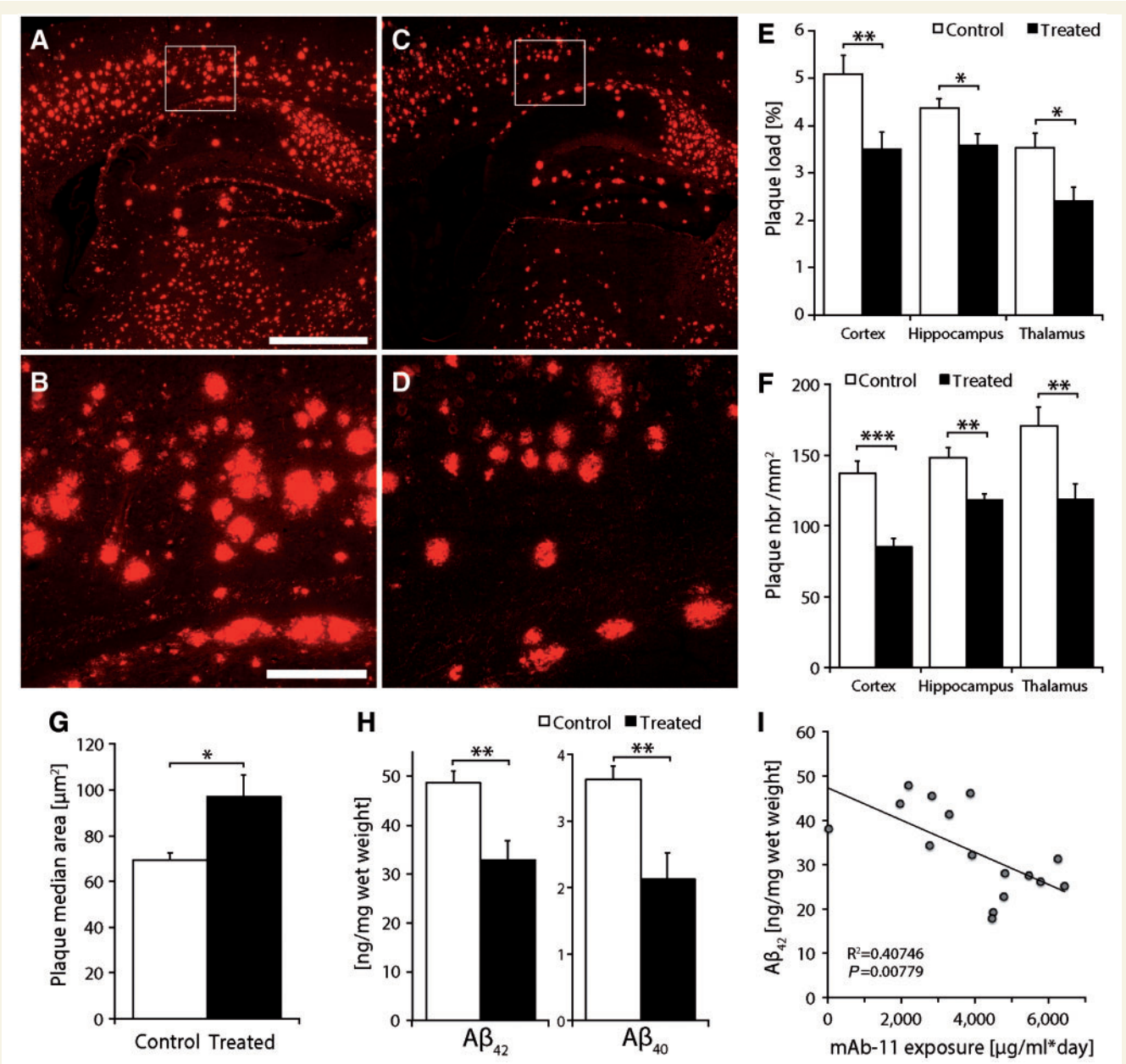

Figure 4 Continuous anti-amyloid-β antibody delivered by ECT reduces amyloid burden in 5XFAD mice. (**A**–**D**) Representative photomicrographs of the amyloid pathology (6E10 immunofluorescence) in 5XFAD mice implanted for 19 weeks with control devices (containing GFP-expressing C2C12 myoblasts) (**A** and **B**) or with devices secreting mAb-11 (**C** and **D**). In these 5- to 6-month-old mice, the staining reveals a robust amyloid pathology that is reduced in the treated animals (**C** and **D**). (**B** and **D**) Higher magnifications of the regions outlined in (**A**) and (**C**), respectively. (**E**) The quantification of amyloid-β burden shows a significant reduction in the plaque load (percentage of the section surface occupied by plaques) in the cortex, hippocampus and thalamus of treated mice. (**F**) The density of amyloid plaques is significantly decreased in these brain regions. (**G**) The median amyloid plaque area is significantly larger in the treated animals. (**H**) The analysis of brain homogenates demonstrates a significant reduction in the amount of amyloid-β_{42} and amyloid-β_{40} peptides in mice implanted with mAb-11-releasing devices. (**I**) The level of amyloid-β_{42} in cortex homogenates is significantly correlated with the total exposure to mAb-11 in the plasma of the treated animals. Data are expressed as the mean + SEM. $n = 15$ per group. Two-tailed heteroscedastic *t*-tests: $^{*}P < 0.05$; $^{**}P < 0.01$; $^{***}P < 0.001$. Correlation is analysed with the Pearson's test. Scale bars = 1 mm (**A**), 200 µm (**C**).

The amyloid pathology was analysed in 1-year-old TauPS2APP mice, 41 weeks after device implantation. The recombinant antibodies produced by ECT were found to immunodecorate amyloid-β plaques in the cortex of the treated mice (Fig. 5C). As expected, detection of mouse IgG F(ab')$_2$ fragments revealed the presence of both the full IgG2a and the F(ab')$_2$ fragment on amyloid plaques in the two groups of treated mice, whereas an Fc region-specific antibody was able to detect plaque immunodecoration only in the IgG2a-treated mice. Next, we

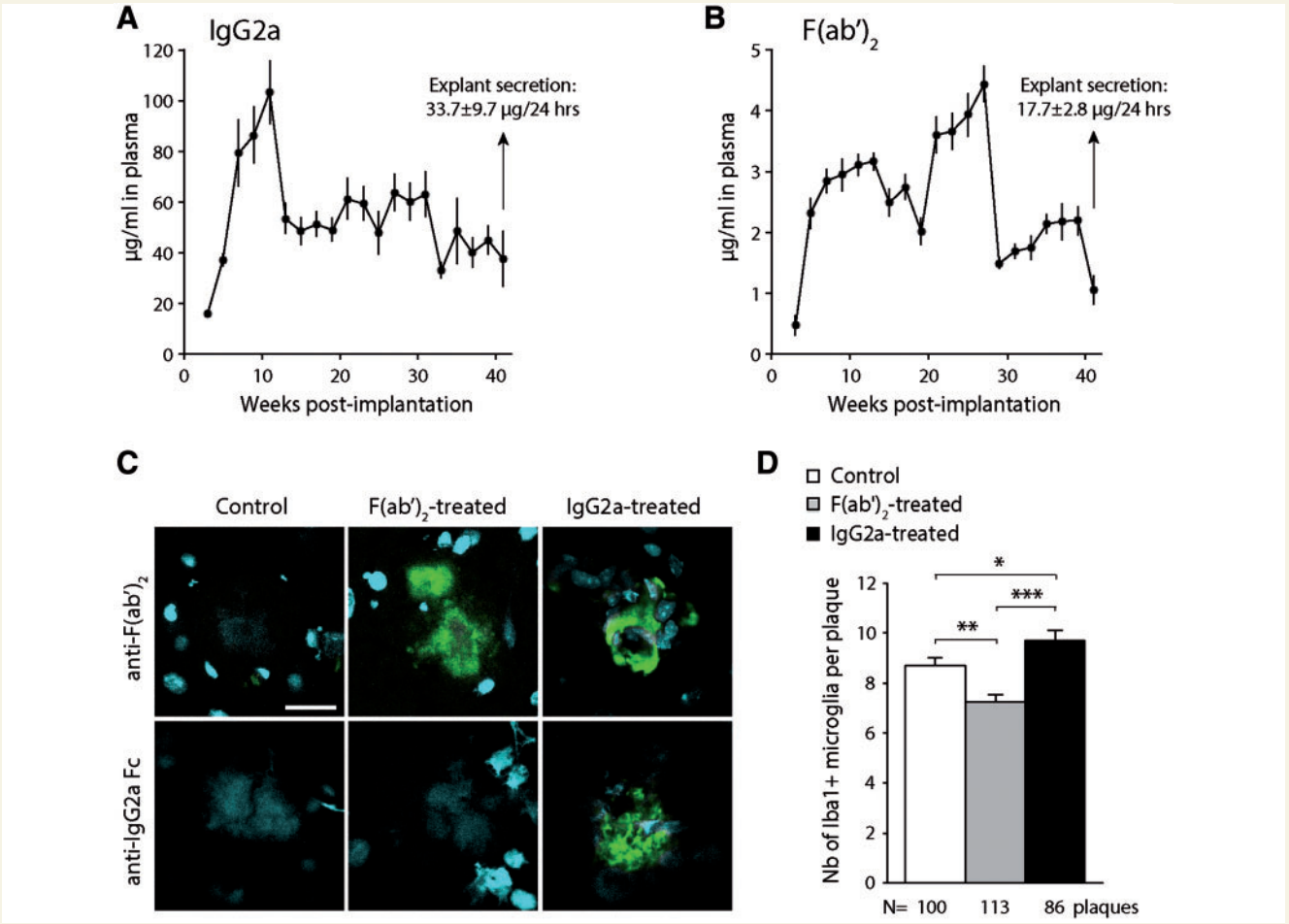

Figure 5 Preventive mAb-11 delivery using ECT affects the local recruitment of microglial cells in TauPS2APP mice. (**A** and **B**) Plasma levels of mAb-11 in TauPS2APP mice implanted for 41 weeks with devices containing either IgG2a-secreting C2C12 myoblasts (**A**), or $F(ab')_2$ fragment-secreting C2C12 myoblasts (**B**). The bar graph shows the mAb-11 secretion rate of the ECT devices after explantation. Data are expressed as the mean ± SEM; $n = 10$. (**C**) Representative photomicrographs showing mAb-11 immunodecoration (green pseudocoloured immunostaining) on amyloid-β plaques in the frontal cortex of a TauPS2APP mice implanted with either control, IgG2a-secreting or $F(ab')_2$-secreting devices. Note that the anti-IgG2a Fc antibody detects only the presence of the full IgG2a antibody, confirming staining specificity. Nuclei are stained with DAPI. (**D**) Quantification of Iba1-positive microglial cells present around amyloid plaques in each group of mice. Note the significant decrease in microglial cell density around plaques in $F(ab')_2$-treated TauPS2APP mice and the increase in IgG2a-treated mice. The number of plaques analysed in each group is indicated. Data are expressed as the mean ± SEM; $F(ab')_2$- and IgG2a-treated groups: $n = 10$. One-way ANOVA with Newman-Keuls *post hoc* test: $^{*}P < 0.05$, $^{**}P < 0.01$, $^{***}P < 0.001$. Scale bar = 20 µm.

assessed if the mAb-11 treatment had any effect on the recruitment of Iba1-positive microglial cells near amyloid deposits (Congo red staining) (Supplementary Fig. 3 and Fig. 5D). In the cortex of control TauPS2APP mice, there were on average 8.7 ± 0.3 Iba1-positive microglial cells neighbouring Congo red-stained individual plaques. The number of microglial cells around plaques was significantly decreased to 7.3 ± 0.3 in the $F(ab')_2$-treated mice, whereas it was increased to 9.7 ± 0.4 in the IgG2a-treated mice. Therefore, the recruitment of microglial cells depends on the presence of the Fc region of the mAb-11 antibody bound to the amyloid plaques.

When initiated before plaque deposition occurred in TauPS2APP mice, the chronic subcutaneous delivery of mAb-11 IgG2a led to a dramatic reduction in amyloid burden detected by anti-amyloid-β immunohistochemistry, compared with the mice implanted with control devices (Fig. 6A). Plaque load was clearly reduced throughout the cortex (−79.9%, $P = 0.004$) and hippocampus (−78.5%, $P = 0.017$) (Fig. 6B). Similarly, the number of plaques was dramatically decreased in both regions (−94.5% and −92.7%, respectively; Fig. 6C). There was minimal deposition of amyloid plaques in the thalamus of 12-month-old TauPS2APP mice. In contrast, the amyloid burden was reduced by only 15–20% with $F(ab')_2$-secreting devices, an effect that was not significant ($P > 0.2$). Compared to the control group, amyloid-β levels were also dramatically reduced in the cortex of IgG2a-treated mice, for both

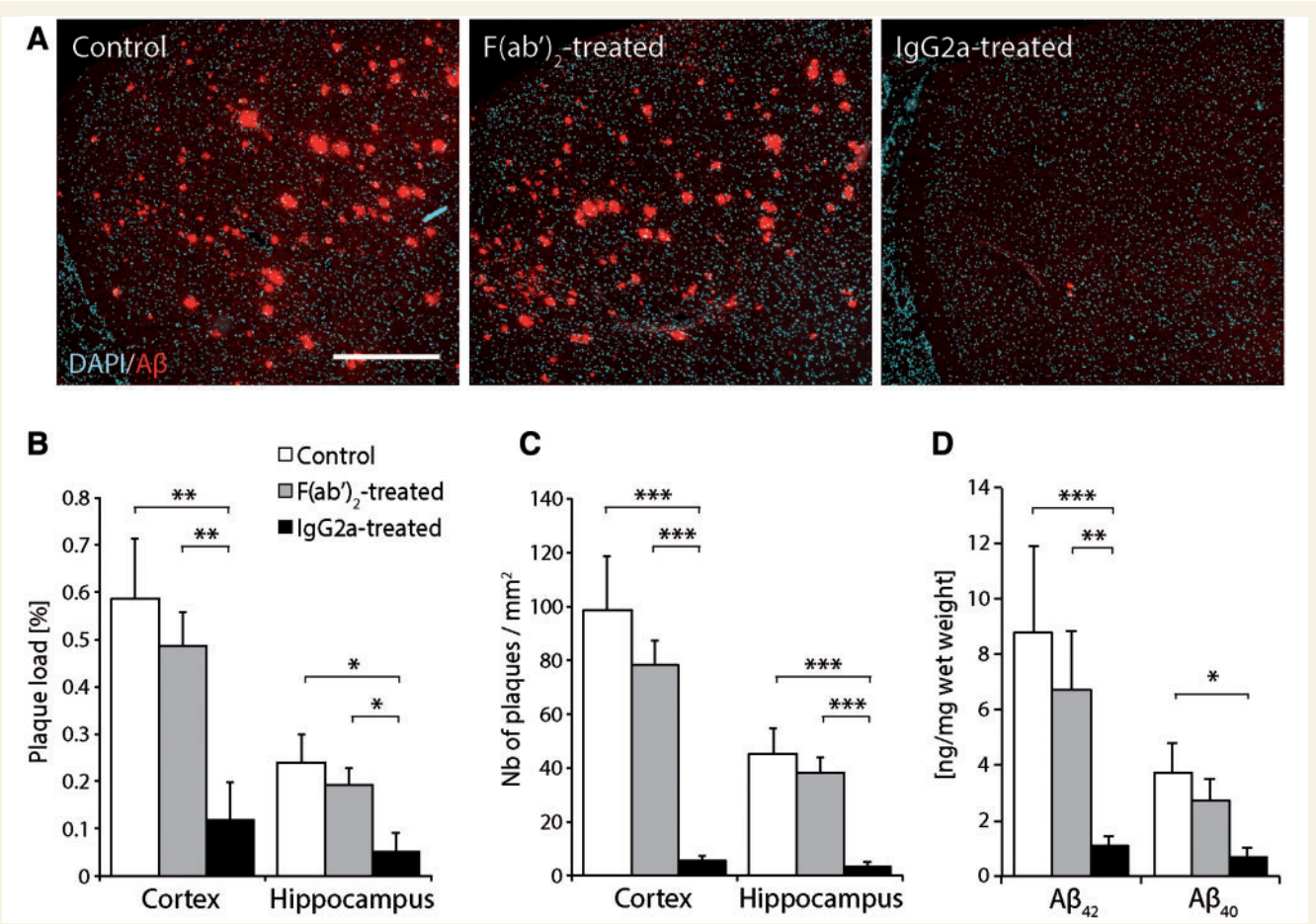

Figure 6 Preventive mAb-11 immunization using ECT delivery strongly reduces amyloid load in the brain of TauPS2APP mice. (**A**) Amyloid burden revealed by anti-amyloid-β immunostaining (6E10) in the frontal cortices of 12-month-old TauPS2APP mice. Note the decreased amyloid pathology in the cortex of the TauPS2APP mouse continuously treated with mAb-11 IgG2a. (**B**) Plaque load, expressed as the percentage of the brain area occupied by amyloid-β-positive plaques, is significantly reduced in the cortex and hippocampus of mice treated with mAb-11 IgG2a. (**C**) The density of amyloid plaques is significantly decreased in these brain regions. (**D**) The amount of amyloid-β_{42} and amyloid-β_{40} is significantly decreased in the cortex of mice treated with mAb-11 IgG2a. Data are expressed as the mean ± SEM; Control group: $n = 8$, $F(ab')_2$- and IgG2a-treated groups: $n = 10$. One-way ANOVA with Newman-Keuls *post hoc* test: $^{*}P < 0.05$, $^{**}P < 0.01$, $^{***}P < 0.001$. Scale bar = 500 μm (**A**).

amyloid-β_{42} (−87.4%, $P = 0.0002$) and amyloid-β_{40} (−82.5%, $P = 0.024$), whereas the effect of the $F(ab')_2$ fragment remained minimal (Fig. 6D). Of note, the level of amyloid-β_{42} in the cortex of 12-month-old TauPS2APP mice was more than 5-fold lower compared to 7-month-old 5XFAD mice (compare Figs 6D and 4H). Altogether, these results indicate that when delivered by ECT, full IgG2a antibodies are more effective than $F(ab')_2$ fragments for the clearing of amyloid pathology, most likely because ECT leads to higher levels of circulating mAb-11 IgG2a in the plasma (Fig. 5A and B).

Strong reduction of plaque density throughout the whole cortex of ECT-mAb-11 treated mice

To further quantify the number of amyloid plaques in ECT-treated mice, the entire contralateral hemicortex of the treated mice was analysed by gratings-based X-ray phase contrast tomographic microscopy (Weitkamp *et al.*, 2005; Pinzer *et al.*, 2012). This technique allows full brain visualization and does not rely on immunodetection methods, which may be subject to interference with the therapeutic antibody bound to amyloid-β. X-ray phase contrast revealed the presence of discrete hyperintense dots throughout the entire cortex of 12-month-old TauPS2APP mice implanted with control devices. These dots were previously shown to correspond to amyloid deposits (Pinzer *et al.*, 2012). The density of plaques in the cortex (plaques/mm^3) was determined following threshold segmentation (Fig. 7A and B and Supplementary Videos 1–3). Coronal maximum-intensity maps show that plaque density was clearly reduced in the entire hemicortex of the mAb-11 IgG2a-treated mice (Fig. 7C). In contrast, the density and distribution of amyloid plaques were similar in

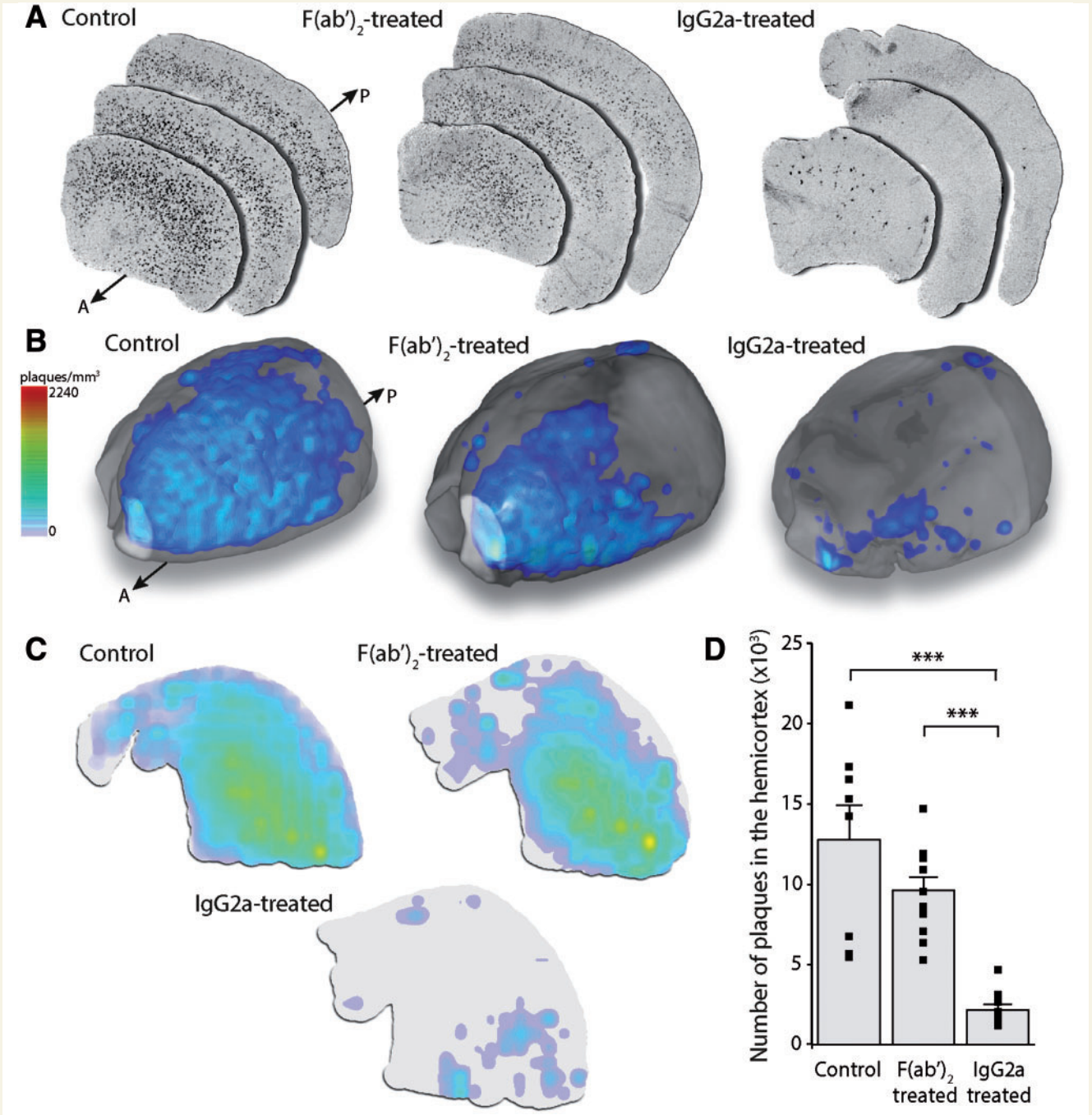

Figure 7 ECT delivery of mAb-11 IgG2a prevents amyloid plaque deposition throughout the entire cortex of TauPS2APP mice. (**A**) Phase-contrast tomographic microscopy of the whole hemicortex reveals hyperintense signals in 12-month-old TauPS2APP mice. The signals are shown on three cortex sections for three representative mice, one from each group, along the anterior (A)–posterior (P) axis. Note the reduction in hyperintense signals in the mAb-11 IgG2a-treated mice. (**B**) Representative hemicortex with superimposed colour-coded density of the hyperintense dots (plaques/mm^3). Note that IgG2a-treated mice have detectable plaques only in the most frontal part of the cortex. (**C**) Coronal maximum-intensity maps of the representative hemicortex. Note the overall reduction in plaque density in the IgG2a-treated mouse. (**D**) Quantification of the total number of plaques in the hemicortex of mice implanted either with control, mAb-11 F(ab')$_2$- and mAb-11 IgG2a-secreting ECT devices. Data are expressed as the mean ± SEM; Control group: $n = 8$, F(ab')$_2$-treated: $n = 11$, IgG2a-treated: $n = 10$. One-way ANOVA with Newman-Keuls *post hoc* test: $^{***}P < 0.001$.

control and F(ab')$_2$-treated mice. Volumetric information from the phase contrast CT datasets was used to determine the total number of plaques in the hemicortex of the mice in each group (Fig. 7D). The mAb-11 IgG2a treatment dramatically reduced the number of detectable plaques (−83%, $P = 0.00013$), whereas the effect of the F(ab')$_2$ treatment was not significant (−25%, $P = 0.0697$).

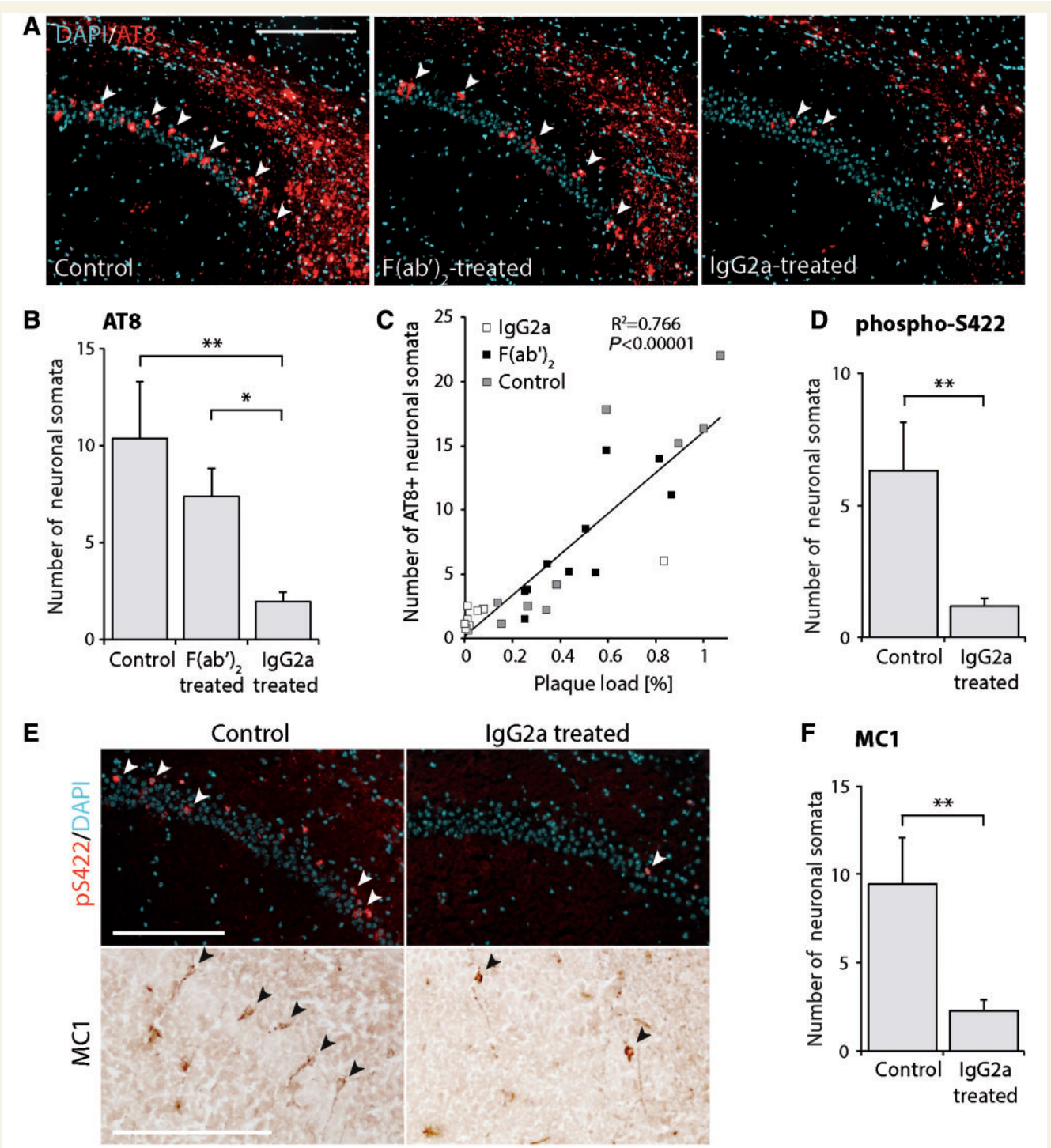

Figure 8 ECT delivery of mAb-11 IgG2a decreases tau pathology in the CA1 region of the hippocampus of TauPS2APP mice. (**A**) Representative photomicrographs of the CA1 region of the hippocampus. Neurons are stained for tau phosphorylated at serine 202 and threonine 205 residues (AT8), and nuclei are stained with DAPI. AT8-positive neuronal somata in the pyramidal layer are indicated with arrowheads. (**B**) Quantification of the number of AT8-positive neurons in the CA1 pyramidal layer of the hippocampus. Note the significant reduction in mAb-11 IgG2a treated mice. (**C**) Correlation between amyloid-β burden and the number of AT8-positive neurons in the CA1 hippocampal region. Individual values from control, mAb-11 F(ab')$_2$-treated and IgG2a-treated mice are shown in the same graph for correlation. (**D**) Quantification of the number of neurons with somatodendritic localization of phospho-S422 tau in the CA1 pyramidal layer of the hippocampus. (**E**) Representative images of phospho-S422 tau and MC1 stainings in the hippocampal CA1 region. Arrowheads indicate neurons with somatodendritic staining. (**F**) Quantification of the number of MC1-positive neuronal somata in the CA1 pyramidal layer. Data are expressed as the mean ± SEM; Control group: $n = 8$, F(ab')$_2$- and IgG2a-treated groups: $n = 10$. One-way ANOVA with Newman-Keuls *post hoc* test (**B**) and two-tailed heteroscedastic *t*-tests (**D** and **F**): $^{*}P < 0.05$, $^{**}P < 0.01$. Correlation in (**C**) is analysed with the Pearson's test. Scale bar = 200 μm (**A** and **E**).

Reduced amyloid-β deposition correlates with decreased tau pathology in the CA1 hippocampus

Next, we analysed the presence of hyperphosphorylated forms of human tau in the CA1 region of the hippocampus of TauPS2APP mice, which overexpress P301L-mutated human tau (Fig. 8A). We assessed the number of neurons located in the CA1 pyramidal layer with an accumulation of AT8-positive phospho-tau (S202/T205) in the somatodendritic compartment (Fig. 8B). In mAb-11 IgG2a-treated mice, the number of AT8-positive neurons was significantly decreased with respect to both control ($P = 0.005$) and F(ab')$_2$-treated mice ($P = 0.035$). However, there was no significant difference between the control and F(ab')$_2$-treated groups ($P = 0.2$). Furthermore, the number of AT8-positive neurons in the CA1 was strongly correlated with amyloid burden in the cortex across all three groups (Fig. 8C), confirming that pathological hyperphosphorylation of tau is linked to amyloid-β deposition in this mouse model (Grueninger *et al.*, 2010).

To confirm the effect of immunotherapy on another tau phosphorylation site, phospho-S422 tau was stained on adjacent sections of the hippocampus. Again, the number of CA1 neurons with a somatodendritic accumulation of phospho-S422 tau was significantly reduced in the mAb-11 IgG2a-treated mice compared to control animals ($P = 0.006$) (Fig. 8D and E). Next, to assess the effect on tau misfolding, we performed a staining with the conformation-dependent MC1 antibody. The number of MC1-positive neuronal cell bodies in CA1 hippocampus was significantly decreased in mAb-11 IgG2a-treated mice ($P = 0.0098$).

Altogether, these results indicate that preventive passive immunization using ECT delivery of recombinant mAb-11 IgG2a antibodies in the periphery is an effective approach to chronically deliver therapeutic antibodies, reduce amyloid deposition throughout the brain and mitigate downstream effects on the tau pathology.

Discussion

The implantation of genetically engineered cells within a retrievable subcutaneous device leads to the continuous production of monoclonal antibodies *in vivo*. This technology achieves steady therapeutic monoclonal antibody levels in the plasma, offering an effective alternative to bolus injections for passive immunization against chronic diseases. Peripheral delivery of anti-amyloid-β monoclonal antibody by ECT leads to a significant reduction of amyloid burden in two mouse models of Alzheimer's disease. The effect of the ECT treatment is more pronounced when passive immunization is preventively administered in TauPS2APP mice, most notably decreasing the phospho-tau pathology.

With the recent development of biomarkers to monitor Alzheimer's pathology, it is recognized that a steady increase in cerebral amyloid over the course of decades precedes the appearance of the first cognitive symptoms (reviewed in Sperling *et al.*, 2011). The current consensus therefore suggests applying anti-amyloid-β immunotherapy during this long asymptomatic phase to avoid the downstream consequences of amyloid deposition and to leverage neuroprotective effects. Several preventive clinical trials have been recently initiated for Alzheimer's disease. The Alzheimer's Prevention Initiative (API) and the Dominantly Inherited Alzheimer Network (DIAN) will test antibody candidates in presymptomatic dominant mutation carriers, while the Anti-Amyloid treatment in the Asymptomatic Alzheimer's disease (A4) trial enrols asymptomatic subjects after risk stratification. If individuals with a high risk of developing Alzheimer's disease can be identified using current biomarker candidates, these patients are the most likely to benefit from chronic long-term anti-amyloid-β immunotherapy. However, such a treatment may pose a challenge to healthcare systems, as the production capacity of the antibody and its related cost would become a challenging issue (Skoldunger *et al.*, 2012). Therefore, the development of alternative technologies to chronically administer anti-amyloid-β antibody is an important aspect for therapeutic interventions at preclinical disease stages.

Here, we show that the ECT technology for the peripheral delivery of anti-amyloid-β monoclonal antibodies can significantly reduce cerebral amyloid pathology in two mouse models of Alzheimer's disease. The subcutaneous tissue is a site of implantation easily accessible and therefore well adapted to preventive treatment. It is, however, challenging to reach therapeutic efficacy, as only a small fraction of the produced anti-amyloid-β monoclonal antibodies are expected to cross the blood–brain barrier, although they can next persist in the brain for several months (Wang *et al.*, 2011; Bohrmann *et al.*, 2012). Our results are consistent with previous reports, which have shown that the systemic administration of anti-amyloid-β antibodies can decrease brain amyloid burden in preclinical Alzheimer's disease models (Bard *et al.*, 2000, 2003; DeMattos *et al.*, 2001; Wilcock *et al.*, 2004*a*, *b*; Buttini *et al.*, 2005; Adolfsson *et al.*, 2012).

Remarkably, striking differences exist among therapeutic anti-amyloid-β antibodies in their ability to clear already existing plaques. Soluble amyloid-β species can saturate the small fraction of pan-amyloid-β antibodies entering the CNS and inhibit further target engagement (Demattos *et al.*, 2012). Therefore, antibodies recognizing soluble amyloid-β may fail to bind and clear insoluble amyloid deposits (Das *et al.*, 2001; Racke *et al.*, 2005; Levites *et al.*, 2006; Bohrmann *et al.*, 2012). Furthermore, antibody-amyloid-β complexes are drained towards blood vessels, promoting cerebral amyloid angiopathy (CAA) and subsequent microhaemorrhages. The mAb-11 antibody used in the present study is similar to gantenerumab, which is highly specific for amyloid plaques and reduces amyloid

burden in patients with Alzheimer's disease (Bohrmann *et al.*, 2012; Demattos *et al.*, 2012; Ostrowitzki *et al.*, 2012). We find that the murine IgG2a mAb-11 antibody efficiently enhances the phagocytosis of amyloid-β fibrils by microglial cells. In addition, ECT administration of the mAb-11 $F(ab')_2$ fragment lacking the Fc region fails to recruit microglial cells, and leads only to a trend towards clearance of the amyloid plaques. Therefore, our results suggest a pivotal role for microglial cells in the clearance of amyloid plaques following mAb-11 delivery by ECT. Importantly, we do not find any evidence that this treatment may cause microhaemorrhages in the mouse models used in this study. It remains entirely possible that direct binding to amyloid plaques of a $F(ab')_2$ fragment lacking effector functionality can contribute to therapeutic efficacy, as suggested by previous studies using antibody fragments (Bacskai *et al.*, 2002; Tamura *et al.*, 2005; Wang *et al.*, 2010; Cattepoel *et al.*, 2011). However, compared to IgG2a, the lower plasma levels achieved with $F(ab')_2$ are likely to limit the efficacy of peripheral ECT-mediated immunization. The exact role of the effector domain and its interaction with immune cells expressing Fc receptors, could be determined by comparing the therapeutic effects of a control antibody carrying a mutated Fc portion, similar to a previous study which addressed this question using deglycosylated anti-amyloid-β antibodies (Wilcock *et al.*, 2006*a*; Fuller *et al.*, 2014).

Remarkably, continuous administration of mAb-11 initiated before plaque deposition had a dramatic effect on the amyloid pathology in TauPS2APP mice, underlining the efficacy of preventive anti-amyloid-β treatments. In this mouse model, where tau hyperphosphorylation is enhanced by amyloid-β (Grueninger *et al.*, 2010), the treatment decreases the number of AT8- and phospho-S422-positive neurons in the hippocampus. Furthermore, the number of MC1-positive hippocampal neurons is significantly reduced, which also indicates an effect of anti-amyloid-β immunotherapy on the accumulation of misfolded tau. These results highlight the effect of amyloid-β clearance on other manifestations of the Alzheimer's pathology. In line with these findings, previous studies have shown evidence for a decrease in tau hyperphosphorylation following immunization against amyloid-β, both in animal models and in patients with Alzheimer's disease (Oddo *et al.*, 2004; Wilcock *et al.*, 2009; Boche *et al.*, 2010; Serrano-Pozo *et al.*, 2010; Salloway *et al.*, 2014).

Similar to the subcutaneous injection of recombinant proteins (Schellekens, 2005), ECT implants can elicit significant immune responses against the secreted recombinant antibody. An anti-drug antibody response was detected in half of the mice treated with the mAb-11-releasing devices, in the absence of any anti-CD4 treatment. The glycosylation profile of the mAb-11 synthesized in C2C12 myoblasts is comparable to standard material produced by myeloma or HEK293 cells (Lathuiliere *et al.*, 2014*a*). Although we cannot exclude that local release by ECT leads to antibody aggregation and denaturation, it is unlikely that this mode of administration further contributes to compound immunogenicity. Because the Fab regions of the chimeric recombinant mAb-11 IgG2a contain human CDRs, it remains to be determined whether the ECT-mediated delivery of antibodies fully matched with the host species would trigger an anti-drug antibody response.

Further developments will be needed to scale up this delivery system to humans. The possibility of using a single allogeneic cell source for all intended recipients is a crucial advantage of the ECT technology to standardize monoclonal antibody delivery. However, the development of renewable cell sources of human origin will be essential to ECT application in the clinic. Although the ARPE-19 cell line has been successfully adapted to ECT and used in clinical trials (Dunn *et al.*, 1996; Zhang *et al.*, 2011), the development of human myogenic cells (Negroni *et al.*, 2009) is an attractive alternative that is worth exploring. Based on the PK analysis of recombinant mAb-11 antibody subcutaneously injected in mice (Supplementary material), we estimate that the flat sheet devices chronically release mAb-11 at a rate of 6.8 and 11.8 μg/h, to reach a plasma level of 50 μg/ml in the implanted animals. In humans, injected IgG1 has a longer half-life (21–25 days), with a volume of distribution of ~100 ml/kg and an estimated clearance of 0.2 ml/h/kg. These values indicate that the predicted antibody exposure in humans, based on the rate of mAb-11 secretion achieved by ECT in mice, would be only 10 to 20-fold lower than the typical regimens based on monthly bolus injection of 1 mg/kg anti-amyloid-β monoclonal antibody. Hence, it is realistic to consider ECT for therapeutic monoclonal antibody delivery in humans, as the flat sheet device could be scaled up to contain higher amounts of cells. Furthermore, recent progress to engineer antibodies for increased penetration into the brain will enable lowering dosing of biotherapeutics to achieve therapeutic efficacy (Bien-Ly *et al.*, 2014; Niewoehner *et al.*, 2014). For some applications, intrathecal implantation could be preferred to chronically deliver monoclonal antibodies directly inside the CNS (Aebischer *et al.*, 1996; Marroquin Belaunzaran *et al.*, 2011).

Overall, ECT provides a novel approach for the local and systemic delivery of recombinant monoclonal antibodies in the CNS. It will expand the possible therapeutic options for immunotherapy against neurodegenerative disorders associated with the accumulation of misfolded proteins, including Alzheimer's and Parkinson's diseases, dementia with Lewy bodies, frontotemporal lobar dementia and amyotrophic lateral sclerosis (Gros-Louis *et al.*, 2010; Bae *et al.*, 2012; Rosenmann, 2013).

Acknowledgements

The authors thank Aline Aebi, Fabienne Pidoux, Vivianne Padrun, Christel Sadeghi and Philippe Colin at EPFL for outstanding technical support, Steffen Cosson and Matthias Lütolf for providing the PEG hydrogel matrix for the

devices. The authors thank Christophe Schweitzer at Roche for technical support to the cloning of the chimeric recombinant mAb-11, Kevin Brady for performing the pharmacokinetic analysis, Kay Stubenrauch for developing mAb-11 detection ELISA, and Hansruedi Loetscher for continuous support to the project. The authors thank Christine Rothe, Margit Urban, Michael Bardroff and Robert Rauchenberger and MorphoSys, Martinsried, Germany for their contributions that led to the identification of mAb-11, as well as P. Davies (Bronx, NY) for providing the MC1 antibody.

Funding

This work was supported by the Swiss Commission for Technology and Innovation (CTI, grant no. 14666.1 PFLS-LS), as well as by F. Hoffmann-La Roche Ltd.

Supplementary material

Supplementary material is available at *Brain* online.

References

Adolfsson O, Pihlgren M, Toni N, Varisco Y, Buccarello AL, Antoniello K, et al. An effector-reduced anti-beta-amyloid (Abeta) antibody with unique abeta binding properties promotes neuroprotection and glial engulfment of Abeta. J Neurosci 2012; 32: 9677–89.

Aebischer P, Schluep M, Deglon N, Joseph JM, Hirt L, Heyd B, et al. Intrathecal delivery of CNTF using encapsulated genetically modified xenogeneic cells in amyotrophic lateral sclerosis patients. Nat Med 1996; 2: 696–9.

Alliot F, Marty MC, Cambier D, Pessac B. A spontaneously immortalized mouse microglial cell line expressing CD4. Brain Res Dev Brain Res 1996; 95: 140–3.

Astolfo A, Arfelli F, Schultke E, James S, Mancini L, Menk RH. A detailed study of gold-nanoparticle loaded cells using X-ray based techniques for cell-tracking applications with single-cell sensitivity. Nanoscale 2013; 5: 3337–45.

Bacskai BJ, Kajdasz ST, McLellan ME, Games D, Seubert P, Schenk D, et al. Non-Fc-mediated mechanisms are involved in clearance of amyloid-beta in vivo by immunotherapy. J Neurosci 2002; 22: 7873–8.

Bae EJ, Lee HJ, Rockenstein E, Ho DH, Park EB, Yang NY, et al. Antibody-aided clearance of extracellular alpha-synuclein prevents cell-to-cell aggregate transmission. J Neurosci 2012; 32: 13454–69.

Bard F, Barbour R, Cannon C, Carretto R, Fox M, Games D, et al. Epitope and isotype specificities of antibodies to beta -amyloid peptide for protection against Alzheimer's disease-like neuropathology. Proc Natl Acad Sci USA 2003; 100: 2023–8.

Bard F, Cannon C, Barbour R, Burke RL, Games D, Grajeda H, et al. Peripherally administered antibodies against amyloid beta-peptide enter the central nervous system and reduce pathology in a mouse model of Alzheimer disease. Nat Med 2000; 6: 916–19.

Bien-Ly N, Yu YJ, Bumbaca D, Elstrott J, Boswell CA, Zhang Y, et al. Transferrin receptor (TfR) trafficking determines brain uptake of TfR antibody affinity variants. J Exp Med 2014; 211: 233–44.

Boche D, Donald J, Love S, Harris S, Neal JW, Holmes C, et al. Reduction of aggregated Tau in neuronal processes but not in the cell bodies after Abeta42 immunisation in Alzheimer's disease. Acta Neuropathol 2010; 120: 13–20.

Bohrmann B, Baumann K, Benz J, Gerber F, Huber W, Knoflach F, et al. Gantenerumab: a novel human anti-Abeta antibody demonstrates sustained cerebral amyloid-beta binding and elicits cell-mediated removal of human amyloid-beta. J Alzheimers Dis 2012; 28: 49–69.

Buttini M, Masliah E, Barbour R, Grajeda H, Motter R, Johnson-Wood K, et al. Beta-amyloid immunotherapy prevents synaptic degeneration in a mouse model of Alzheimer's disease. J Neurosci 2005; 25: 9096–101.

Cattepoel S, Hanenberg M, Kulic L, Nitsch RM. Chronic intranasal treatment with an anti-Abeta(30-42) scFv antibody ameliorates amyloid pathology in a transgenic mouse model of Alzheimer's disease. PLoS ONE 2011; 6: e18296

Charrier S, Stockholm D, Seye K, Opolon P, Taveau M, Gross DA, et al. A lentiviral vector encoding the human Wiskott-Aldrich syndrome protein corrects immune and cytoskeletal defects in WASP knockout mice. Gene Ther 2005; 12: 597–606.

Collin L, Bohrmann B, Gopfert U, Oroszlan-Szovik K, Ozmen L, Gruninger F. Neuronal uptake of tau/pS422 antibody and reduced progression of tau pathology in a mouse model of Alzheimer's disease. Brain 2014; 137: 2834–46.

Das P, Murphy MP, Younkin LH, Younkin SG, Golde TE. Reduced effectiveness of Abeta1-42 immunization in APP transgenic mice with significant amyloid deposition. Neurobiol Aging 2001; 22: 721–7.

DeMattos RB, Bales KR, Cummins DJ, Dodart JC, Paul SM, Holtzman DM. Peripheral anti-A beta antibody alters CNS and plasma A beta clearance and decreases brain A beta burden in a mouse model of Alzheimer's disease. Proc Natl Acad Sci USA 2001; 98: 8850–5.

Demattos RB, Lu J, Tang Y, Racke MM, Delong CA, Tzaferis JA, et al. A plaque-specific antibody clears existing beta-amyloid plaques in Alzheimer's disease mice. Neuron 2012; 76: 908–20.

Doody RS, Thomas RG, Farlow M, Iwatsubo T, Vellas B, Joffe S, et al. Phase 3 trials of solanezumab for mild-to-moderate Alzheimer's disease. N Engl J Med 2014; 370: 311–21.

Dunn KC, Aotaki-Keen AE, Putkey FR, Hjelmeland LM. ARPE-19, a human retinal pigment epithelial cell line with differentiated properties. Exp Eye Res 1996; 62: 155–69.

Ehrbar M, Rizzi SC, Schoenmakers RG, Miguel BS, Hubbell JA, Weber FE, et al. Biomolecular hydrogels formed and degraded via site-specific enzymatic reactions. Biomacromolecules 2007; 8: 3000–7.

Fuller JP, Stavenhagen JB, Teeling JL. New roles for Fc receptors in neurodegeneration-the impact on Immunotherapy for Alzheimer's Disease. Front Neurosci 2014; 8: 235

Geng D, Shankar G, Schantz A, Rajadhyaksha M, Davis H, Wagner C. Validation of immunoassays used to assess immunogenicity to therapeutic monoclonal antibodies. J Pharm Biomed Anal 2005; 39: 364–75.

Goate A, Hardy J. Twenty years of Alzheimer's disease-causing mutations. J Neurochem 2012; 120: 3–8.

Gros-Louis F, Soucy G, Lariviere R, Julien JP. Intracerebroventricular infusion of monoclonal antibody or its derived Fab fragment against misfolded forms of SOD1 mutant delays mortality in a mouse model of ALS. J Neurochem 2010; 113: 1188–99.

Grueninger F, Bohrmann B, Czech C, Ballard TM, Frey JR, Weidensteiner C, et al. Phosphorylation of Tau at S422 is enhanced by Abeta in TauPS2APP triple transgenic mice. Neurobiol Dis 2010; 37: 294–306.

Hardy J, Selkoe DJ. The amyloid hypothesis of Alzheimer's disease: progress and problems on the road to therapeutics. Science 2002; 297: 353–6.

Lathuiliere A, Bohrmann B, Kopetzki E, Schweitzer C, Jacobsen H, Moniatte M, et al. Genetic engineering of cell lines using lentiviral

vectors to achieve antibody secretion following encapsulated implantation. Biomaterials 2014a; 35: 792–802.
Lathuiliere A, Cosson S, Lutolf MP, Schneider BL, Aebischer P. A high-capacity cell macroencapsulation system supporting the long-term survival of genetically engineered allogeneic cells. Biomaterials 2014b; 35: 779–91.
Levites Y, Das P, Price RW, Rochette MJ, Kostura LA, McGowan EM, et al. Anti-Abeta42- and anti-Abeta40-specific mAbs attenuate amyloid deposition in an Alzheimer disease mouse model. J Clin Invest 2006; 116: 193–201.
Marroquin Belaunzaran O, Cordero MI, Setola V, Bianchi S, Galli C, Bouche N, et al. Chronic delivery of antibody fragments using immunoisolated cell implants as a passive vaccination tool. PLoS ONE 2011; 6: e18268
McDonald SA, Marone F, Hintermuller C, Mikuljan G, David C, Pfeiffer F, et al. Advanced phase-contrast imaging using a grating interferometer. J Synchrotron Radiat 2009; 16: 562–72.
Negroni E, Riederer I, Chaouch S, Belicchi M, Razini P, Di Santo J, et al. In vivo myogenic potential of human CD133 + muscle-derived stem cells: a quantitative study. Mol Ther 2009; 17: 1771–8.
Niewoehner J, Bohrmann B, Collin L, Urich E, Sade H, Maier P, et al. Increased brain penetration and potency of a therapeutic antibody using a monovalent molecular shuttle. Neuron 2014; 81: 49–60.
Oakley H, Cole SL, Logan S, Maus E, Shao P, Craft J, et al. Intraneuronal beta-amyloid aggregates, neurodegeneration, and neuron loss in transgenic mice with five familial Alzheimer's disease mutations: potential factors in amyloid plaque formation. J Neurosci 2006; 26: 10129–40
Oddo S, Billings L, Kesslak JP, Cribbs DH, LaFerla FM. Abeta immunotherapy leads to clearance of early, but not late, hyperphosphorylated tau aggregates via the proteasome. Neuron 2004; 43: 321–32.
Ostrowitzki S, Deptula D, Thurfjell L, Barkhof F, Bohrmann B, Brooks DJ, et al. Mechanism of amyloid removal in patients with Alzheimer disease treated with gantenerumab. Arch Neurol 2012; 69: 198–207.
Pinzer BR, Cacquevel M, Modregger P, McDonald SA, Bensadoun JC, Thuering T, et al. Imaging brain amyloid deposition using grating--based differential phase contrast tomography. Neuroimage 2012; 61: 1336–46.
Racke MM, Boone LI, Hepburn DL, Parsadainian M, Bryan MT, Ness DK, et al. Exacerbation of cerebral amyloid angiopathy-associated microhemorrhage in amyloid precursor protein transgenic mice by immunotherapy is dependent on antibody recognition of deposited forms of amyloid beta. J Neurosci 2005; 25: 629–36.
Rauchenberger R, Borges E, Thomassen-Wolf E, Rom E, Adar R, Yaniv Y, et al. Human combinatorial Fab library yielding specific and functional antibodies against the human fibroblast growth factor receptor 3. J Biol Chem 2003; 278: 38194–205.
Rosenmann H. Immunotherapy for targeting tau pathology in Alzheimer's disease and tauopathies. Curr Alzheimer Res 2013; 10: 217–28.
Salloway S, Sperling R, Fox NC, Blennow K, Klunk W, Raskind M, et al. Two phase 3 trials of bapineuzumab in mild-to-moderate Alzheimer's disease. New Eng J Med 2014; 370: 322–33.
Schellekens H. Factors influencing the immunogenicity of therapeutic proteins. Nephrol Dial Transplant 2005; 20: vi3–9.
Serrano-Pozo A, William CM, Ferrer I, Uro-Coste E, Delisle MB, Maurage CA, et al. Beneficial effect of human anti-amyloid- active immunization on neurite morphology and tau pathology. Brain 2010; 133: 1312–27.
Shankar G, Devanarayan V, Amaravadi L, Barrett YC, Bowsher R, Finco-Kent D, et al. Recommendations for the validation of immunoassays used for detection of host antibodies against biotechnology products. J Pharm Biomed Anal 2008; 48: 1267–81.
Skoldunger A, Wimo A, Johnell K. Net costs of dementia in Sweden - an incidence based 10 year simulation study. Int J Geriatr Psychiatry 2012; 27: 1112–17.
Sperling R, Salloway S, Brooks DJ, Tampieri D, Barakos J, Fox NC, et al. Amyloid-related imaging abnormalities in patients with Alzheimer's disease treated with bapineuzumab: a retrospective analysis. Lancet Neurol 2012; 11: 241–9.
Sperling RA, Aisen PS, Beckett LA, Bennett DA, Craft S, Fagan AM, et al. Toward defining the preclinical stages of Alzheimer's disease: recommendations from the National Institute on Aging-Alzheimer's Association workgroups on diagnostic guidelines for Alzheimer's disease. Alzheimers Dement 2011; 7: 280–92.
Tabrizi M, Bornstein GG, Suria H. Biodistribution mechanisms of therapeutic monoclonal antibodies in health and disease. AAPS J 2010; 12: 33–43.
Tamura Y, Hamajima K, Matsui K, Yanoma S, Narita M, Tajima N, et al. The F(ab)'2 fragment of an Abeta-specific monoclonal antibody reduces Abeta deposits in the brain. Neurobiol Dis 2005; 20: 541–9.
Wang A, Das P, Switzer RC, 3rd, Golde TE, Jankowsky JL. Robust amyloid clearance in a mouse model of Alzheimer's disease provides novel insights into the mechanism of amyloid-beta immunotherapy. J Neurosci 2011; 31: 4124–36.
Wang W, Wang EQ, Balthasar JP. Monoclonal antibody pharmacokinetics and pharmacodynamics. Clin Pharmacol Ther 2008; 84: 548–58.
Wang YJ, Gao CY, Yang M, Liu XH, Sun Y, Pollard A, et al. Intramuscular delivery of a single chain antibody gene prevents brain Abeta deposition and cognitive impairment in a mouse model of Alzheimer's disease. Brain Behav Immun 2010; 24: 1281–93.
Webster SD, Galvan MD, Ferran E, Garzon-Rodriguez W, Glabe CG, Tenner AJ. Antibody-mediated phagocytosis of the amyloid beta-peptide in microglia is differentially modulated by C1q. J Immunol 2001; 166: 7496–503.
Weitkamp T, Diaz A, David C, Pfeiffer F, Stampanoni M, Cloetens P, et al. X-ray phase imaging with a grating interferometer. Opt Express 2005; 13: 6296–304.
Wilcock DM, Alamed J, Gottschall PE, Grimm J, Rosenthal A, Pons J, et al. Deglycosylated anti-amyloid-beta antibodies eliminate cognitive deficits and reduce parenchymal amyloid with minimal vascular consequences in aged amyloid precursor protein transgenic mice. J Neurosci 2006a; 26: 5340–6.
Wilcock DM, Gharkholonarehe N, Van Nostrand WE, Davis J, Vitek MP, Colton CA. Amyloid reduction by amyloid-beta vaccination also reduces mouse tau pathology and protects from neuron loss in two mouse models of Alzheimer's disease. J Neurosci 2009; 29: 7957–65.
Wilcock DM, Gordon MN, Morgan D. Quantification of cerebral amyloid angiopathy and parenchymal amyloid plaques with Congo red histochemical stain. Nat Protoc 2006b; 1: 1591–5.
Wilcock DM, Rojiani A, Rosenthal A, Levkowitz G, Subbarao S, Alamed J, et al. Passive amyloid immunotherapy clears amyloid and transiently activates microglia in a transgenic mouse model of amyloid deposition. J Neurosci 2004a; 24: 6144–51.
Wilcock DM, Rojiani A, Rosenthal A, Subbarao S, Freeman MJ, Gordon MN, et al. Passive immunotherapy against Abeta in aged APP-transgenic mice reverses cognitive deficits and depletes parenchymal amyloid deposits in spite of increased vascular amyloid and microhemorrhage. J Neuroinflammation 2004b; 1: 24.
Yaffe D, Saxel O. Serial passaging and differentiation of myogenic cells isolated from dystrophic mouse muscle. Nature 1977; 270: 725–7.
Zhang K, Hopkins JJ, Heier JS, Birch DG, Halperin LS, Albini TA, et al. Ciliary neurotrophic factor delivered by encapsulated cell intraocular implants for treatment of geographic atrophy in age-related macular degeneration. Proc Natl Acad Sci USA 2011; 108: 6241–5.
Zufferey R. Production of lentiviral vectors. Curr Top Microbiol Immunol 2002; 261: 107–21.

**Ce document a été imprimé au Centre d'impression EPFL,
imprimerie climatiquement neutre, certifiée myClimate.**